UNIVERSIDAD DE CÓRDOBA

Programa de doctorado:

Química Fina

Título de la tesis:

Nanomateriales multifuncionales mesoporosos del tipo SBA-15 y MCM-41 aplicados a procesos de química fina.

Mesoporous multifunctional nanomaterials SBA-15 and MCM-41 type applied to fine chemical processes

Directores:

Antonio Ángel Romero Reyes

Alina Mariana Balu Balu

Autor de la tesis

Mª Dolores Márquez Medina

Fecha de depósito tesis en el Idep: 13 de Mayo de 2019

TITULO: *Nanomateriales multifuncionales mesoporosos del tipo SBA-15 y MCM-41 aplicados a procesos de química fina*

AUTOR: *Mª Dolores Márquez Medina*

Campus de Rabanales
Ctra. Nacional IV, Km. 396 A
14071 Córdoba

https://www.uco.es/ucopress/index.php/es/
ucopress@uco.es

TÍTULO DE LA TESIS:
Nanomateriales multifuncionales mesoporosos del tipo SBA-15 y MCM-41 aplicados a procesos de química fina.

DOCTORANDA:

María Dolores Márquez Medina

INFORME RAZONADO DE LOS DIRECTORES DE LA TESIS

(se hará mención a la evolución y desarrollo de la tesis, así como a trabajos y publicaciones derivados de la misma).

La presente Memoria de Tesis Doctoral se fundamenta en la transición a una química más verde, con procesos de fabricación más sostenibles que utilicen eficientemente las materias primas, eliminen residuos y eviten usar materiales tóxicos y peligrosos. En este aspecto, la Tesis Doctoral afronta el estudio de diversos nanocatalizadores empleados en reacciones redox, desde el punto de vista de una Química Verde, para la obtención de productos con alto valor añadido.

De este modo, se ha llevado a cabo la síntesis de nanomateriales multifuncionales incorporando nanopartículas metálicas sobre materiales del tipo SBA-15 y MCM-41, empleando metodologías post-sintéticas como la molienda mecanoquímica, el flujo continuo o la impregnación hasta humedad incipiente. Además, el doctorando ha conseguido la incorporación estructural del aluminio en silicatos SBA-15 y MCM-41, utilizando por primera vez materiales MOFs conteniendo Al como fuente de dicho metal.

Como resultado de las investigaciones realizadas y demostrando la calidad de éstas, Dña. Mª Dolores Márquez Medina ha participado como primer autor en 3 publicaciones científicas en revistas dentro del primer y segundo cuartil (Q1 y Q2) del "Journal Citation Reports".

1. **Autores:** María Dolores Márquez Medina, Pepijn Prinsen, Hangkong Li, Kaimin Shih, Antonio Ángel Romero y Rafael Luque.
   Título: Continuous flow synthesis of supported magnetic iron oxide nanoparticles for efficient isoeugenol conversion to vanillin.
   Revista: ChemSusChem.
   Indicios de Calidad:
   Categoría: Chemistry, Multidisciplinary. Índice de impacto: 7.411
   Posición dentro de la categoría: 24 de 171; primer cuartil (Q1)
   Volumen: 11; Página inicial: 389; Año: 2018.

2. **Autores:** María Dolores Márquez Medina, Daily Rodríguez-Padrón, Alina M. Balu, Antonio A. Romero, Mario J. Muñoz-Batista y Rafael Luque.
   Título: Mechanochemically synthesized supported magnetic Fe-nanoparticles as catalysts for efficient vanillin production.
   Revista: Catalysts.
   Indicios de Calidad:
   Categoría: Chemistry, Physical. Índice de impacto: 3,465
   Posición dentro de la categoría: 55 de 147; segundo cuartil (Q2)
   Volumen: 9; Página inicial: 290; Año: 2019.

3. **Autores:** María Dolores Márquez Medina, Sareena Mhadmha, Alina M. Balu, Antonio A. Romero, Rafael Luque.
   Título: Post-synthetic mechanochemical incorporation of Al-species into the framework of porous materials: catalytic implications for more sustainable redox chemistries
   Revista: ACS Sustainable Chemistry & Engineering
   Indicios de Calidad:
   Categoría: Engineering, Chemical. Índice de impacto: 6,14
   Posición dentro de la categoría: 10 de 137; primer cuartil (Q1)
   Aceptado para publicación; Año: 2019.

Por todo ello, se autoriza la presentación de la tesis doctoral.

Córdoba, 13 de MAYO de 2019

Firma de los directores

Fdo.: Antonio Ángel Romero Reyes Fdo.: Alina Mariana Balu Balu

Agradecimientos

Tras finalizar un trabajo tan arduo y lleno de dificultades como es el desarrollo de la Tesis Doctoral, un análisis objetivo te muestra inmediatamente que la magnitud de ese aporte hubiese sido imposible sin la participación de personas e instituciones que han facilitado las cosas para que este trabajo llegue a un feliz término. Por ello, es para mí un verdadero placer utilizar este espacio para ser justo y consecuente con ellas, expresándoles mis agradecimientos.

Debo agradecer de manera especial y sincera los Profesores Alina Mariana Balu Balu y Antonio Ángel Romero Reyes por aceptarme para realizar esta Tesis Doctoral bajo su dirección. Su apoyo y confianza en mi trabajo y su capacidad para guiarme ha sido un aporte invaluable, no

solamente en el desarrollo de esta tesis, sino también en mi formación como investigador. Las ideas propias, siempre enmarcadas en su orientación y rigurosidad, han sido la clave del buen trabajo que hemos realizado juntos, el cual no se puede concebir sin su siempre oportuna participación.

Quiero expresar también mi más sincero agradecimiento a el Profesor Rafael Luque Álvarez de Sotomayor, por ayudarme y guiarme en numerosas actividades que se han desarrollado a lo largo de la presente Tesis Doctoral que me han ayudado a formarme como la investigadora que soy hoy en día.

A todos los miembros pertenecientes al departamento de Química Orgánica de la Universidad de Córdoba, ya sea personal técnico y administrativo como profesores y becarios. A todos los miembros del Grupo de investigación FQM-383, Araceli, Antonio Pineda, Alfonso, Kenneth, Daily, Mario, Alain, Ana, Noelia, etc. Y en especial a Layla, Camilla y Alessio ese grupo de italianos que siempre ha estado presente durante toda la Tesis mostrándome su apoyo y ayudándome cuando lo necesitaba. A mis pilares del grupo tanto dentro como fuera del laboratorio Esther y Soledad, gracias por hacerme los días más llevaderos, os deseo lo mejor. A aquellas personas que han pasado a lo largo de mi periodo en el laboratorio por aquí y han dejado una gran huella: Valerina, Gab, Viki, BruBru…

También quiero dar las gracias especialmente al Profesor Joseph Samec, quien me acogió en su grupo durante mi estancia en Estocolmo y me hizo sentir como en casa, brindándome su apoyo y enseñándome un campo completamente nuevo para mí. De este periodo en el extranjero no quiero finalizar sin agradecer a todo el grupo: Elena, Jessica, Hongji, Anon, Rabia, con los cuales he pasado grades momentos viajando, jugando a mikado, etc. Y a mi grupo de españoles que me hacían más amenos los

días con los breaks de las 11 y las Melody quedadas (Samuel, Elisa, Ferran, etc.).

En estos agradecimientos no podía olvidarme de todos mis amigos, aquellos que han estado tanto dentro como fuera del laboratorio aguantando mis momentos, dándome consejo y motivándome cuando más lo necesitaba… Juan, por estar ahí siempre desde que nuestros caminos se cruzaran hace 10 años dándome sus consejos y ayuda de maquetación; Solete, Andrés, Amina, Peter, por seguir siendo esa piña que creamos del Grado en Química y ayudarme en cada momento, Nabila, Sandra, etc. Y en especial a Sergio, por estar siempre a mi lado, a las duras y maduras y brindándome su apoyo incondicional en cada momento y aguantar tantos ensayos.

Y por último, a lo más importante, MI FAMILIA; mis padres porque con su apoyo y cariño incondicional me han permitido alcanzar mis metas y convertirme en lo que soy hoy. A mi hermana, por sacarme una sonrisa cuando más lo necesitaba y celebrar juntas los logros, por ser mi vía de escape en tantos momentos, gracias. Y en general a toda mi familia, mis abuelos, incluidos aquellos que ya no están o no son conscientes pues sé que estarían orgullosos; a mis tías Toñi, Mª Jesús, Julia, Rodo, etc. por estar siempre a mi lado, y a todos aquellos que me han arropado, GRACIAS.

“En medio del invierno, me pareció que había, dentro de mí, un invencible verano”

Albert Camus

Índice General

Capítulo I. Introducción…….…….…….1

I. 1. Catálisis en la Química Verde...……...…….9

I. 2. Materiales porosos nanoestructurados...……..……15

I. 3. Funcionalización de los materiales mesoporosos…...…….27

I. 4. Catálisis heterogénea…...……...…….39

Capítulo II. Hipótesis y Objetivos…….……...…….67

II. 1. Hipótesis y Objetivos…….……69

II. 2. Hypotheses and Objectives…….……...75

Capítulo III. Resultados y Discusión……..……..…….81

III. 1. Continuous flow synthesis of supported magnetic iron oxide nanoparticles for efficient isoeugenol conversion to vanillin …...…..…..…….……...83

III. 2. Mechanochemically synthesized supported magnetic Fe-nanoparticles as catalysts for efficient vanillin production.……..……..……116

III. 3. Post-synthetic mechanochemical incorporation of Al species into the framework of porous materials: towards more sustainable redox chemistries...……...……...…150

Capítulo IV. Conclusiones……..……..……....179

IV. 1. Conclusiones……...……181

IV. 2. Conclusions……...……..185

Capítulo V. Resumen ….…….……..……..….189

V. 1. Resumen……...……191

V. 2. Summary……..……197

Capítulo VI. Indicios de Calidad...…… ……..…201

Capítulo VII. Otras Aportaciones Científicas……207

Anexo I. Materiales y Métodos……...……..211

Preámbulo……..……...215

A. I. 1. Métodos de síntesis de nanopartículas soportadas…...217

A. I. 2. Técnicas de caracterización……..……..…..225

A. I. 3. Actividad catalítica…….……..…...245

Anexo II. Compendio de publicaciones....……..…….253

CAPÍTULO I

Introducción

Capítulo 1. Introducción.

Preámbulo **.....5**

I. 1. Catálisis en la Química Verde 9

I. 2. Materiales porosos nanoestructurados.....15

I. 2. 1. Introducción.....15

I. 2. 2. Materiales M41S.....17

I. 2. 3. Materiales de tipo HMS.....19

I. 2. 4. Materiales de tipo SBA.....21

I. 2. 5. Materiales mesoporosos desarrollados recientemente.....24

I. 3. Funcionalización de los materiales mesoporosos.....27

I. 3. 1. Funcionalización por síntesis directa de materiales silíceos mesoporosos.....28

I. 3. 2. Modificación de los materiales silíceos mesoporosos mediante tratamientos post-síntesis.....30

I. 4. Catálisis heterogénea.....39

Bibliografía 43

Preámbulo

Los aspectos medioambientales como el cambio climático, la contaminación o las energías renovables toman mayor importancia en la concienciación de la sociedad. Por ello, actualmente se producen mayores avances con esta temática en el ámbito científico, y las investigaciones llevadas a cabo en el campo de la química, permiten desarrollar materiales y aplicaciones que son menos perjudiciales con el medioambiente [1] proporcionando una calidad y estilo de vida deseados de acuerdo a los principios de una Química Sostenible [2].

El gran reto al que se enfrenta la química y las industrias relacionadas en el siglo XXI es la transición a una química más sostenible, con procesos de fabricación más sostenibles que utilicen eficientemente las materias

primas, eliminen residuos y eviten usar materiales tóxicos y peligrosos. Se requiere, por tanto, un cambio del concepto tradicional de eficiencia de un proceso, centrado en el rendimiento químico, a otro que asigne valor económico a la sustitución de recursos fósiles por materias primas renovables, eliminando residuos y evitando el uso de sustancias tóxicas y peligrosas [3].

La biomasa posee en principio un ciclo de emisiones cerrado compatible con la economía circular, debido a la posibilidad de las plantas/biomasa de recapturar la mayor parte de dichas emisiones mediante el ciclo fotosintético, en comparación con el ciclo abierto de los combustibles fósiles (Figura I.1).

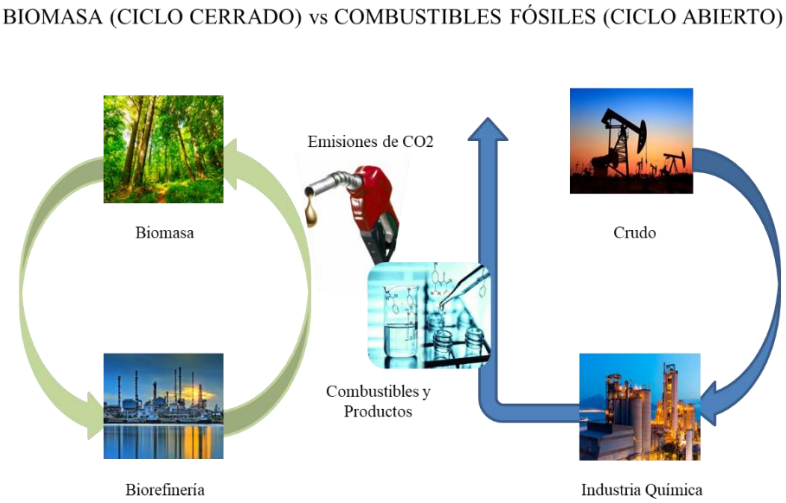

Figura I. 1. Ciclo CO_2: Biomasa vs Combustibles Fósiles.

Uno de los modos de alcanzar ese estado de bienestar deseado, respetando el medio ambiente, es la reutilización de catalizadores empleados en la industria química. Debido a ello, la catálisis heterogénea desarrollará un papel trascendental en el crecimiento de la Industria Química en la primera mitad del siglo XXI, convirtiéndose así en un área

en auge en la actualidad, pues posibilita el uso de materiales más eficientes y procesos más selectivos en comparación con el uso de reactivos estequiométricos y catalizadores en fase homogénea, los cuales requieren de procesos complejos de separación y de etapas adicionales para llevar a cabo tal separación.

Con el diseño de catalizadores heterogéneos, se pretende desarrollar nuevos procesos y metodologías que sean eficientes y benignas con el medio ambiente, así como renovar y mejorar procesos químicos, en cuanto a la economía de éstos y la actividad y selectividad de los catalizadores [4–6]. En este sentido, el uso de nanopartículas soportadas (NPS) posee un elevado interés gracias a su demostrada alta actividad y especificidad. El inconveniente que presentan estas nanopartículas es su tendencia a agregarse y coalescer para estabilizarse. El empleo de materiales porosos, con elevadas áreas superficiales, como por ejemplo zeolitas, SBA, M41S, HMS, etc. han supuesto una opción interesante para estabilizar y dispersar de forma homogénea nanopartículas metálicas de tamaño controlado. De entre todos los materiales porosos mencionados destacan los silicatos SBA-15, los cuales poseen un elevado ordenamiento de grandes canales mesoporosos uniformes con paredes mesoporosas gruesas (3,0-7,0 nm de grosor de pared) que los hace térmica e hidrotérmicamente más estables respecto a los materiales M41S y HMS. Una de las ventajas de estas paredes gruesas estriba en la posibilidad de incorporar núcleos estables de cristales del óxido metálico en la estructura de las mismas [7].

En la presente Tesis Doctoral se ha llevado a cabo la obtención de nanocatalizadores heterogéneos con nanopartículas soportadas mediante distintas metodologías, aplicando los principios de la Química Verde siendo respetuosos con el medio ambiente, evitando el uso de disolventes

o en su caso empleando aquellos que son benignos, según los “12 Principios de la Química Sostenible” [2].

I.1. Catálisis en la Química Verde.

La Química Sostenible o Química Verde, se basa en la eliminación o reducción, de compuestos que sean perjudiciales para el medio ambiente en el diseño de materiales, productos y procesos químicos. Los impulsores de la Química Sostenible, Anastas y Warner, fueron los encargados de enumerar los 12 principios por los que ésta se rige [2]. De estos principios reciben especial importancia la eliminación de disolventes que afecten de forma negativa al medio ambiente y el uso de catalizadores. En concreto, el noveno enunciado se refiere al empleo de catalizadores como una alternativa eficiente, la catálisis se ve implicada en la mayoría de los principios.

Por todo esto, son innumerables los procesos químicos en los que hoy en día la catálisis está presente, tanto a escala industrial como de laboratorio,

para la obtención de productos como medicamentos, plásticos, pinturas, perfumes, combustibles, etc.

Existen dos tipos principales de catálisis: (I) catálisis homogénea donde los reactivos se encuentran en la misma fase que el catalizador y (II) catálisis heterogénea donde el catalizador se encuentra en una fase distinta a los reactivos. En el caso de la primera, encontramos como principal obstáculo la complicada separación del catalizador del medio de reacción, dificultando el aislamiento de éste de los productos obtenidos. En consecuencia, y a pesar de las ventajas que presenta, la catálisis homogénea se está viendo desplazada por la catálisis heterogénea como principal alternativa que nos permite emplear materiales sustitutos de ácidos o bases tipo Brönsted o Lewis (H_2SO_4, H_3PO_4, $AlCl_3$, NaOH, etc.), así como el diseño de materiales con la características deseadas para una serie de procesos/reacciones determinadas, haciéndolos así ideales para su aplicación en la química industrial gracias a [8–12]:

1. Fácil separación del catalizador de los reactivos y/o productos.
2. Fácil reciclado del catalizador.
3. Mayor selectividad a los productos deseados.
4. Menor contaminación del producto por el catalizador.
5. Fácil adaptabilidad a procesos químicos continuos.

En la actualidad, se están buscando catalizadores que reúnan estas características, haciendo que los procesos industriales posean un mayor rendimiento y sean más eficientes y benignos con el entorno que nos rodea. De estas características y requerimientos es de donde está naciendo el diseño de materiales que se adapten a una estructura determinada, posean una buena dispersión de los centros activos, etc. Materiales tales como zeolitas, ALPO, SAPO, materiales mesoporosos

(M41S, HMS, SBA, etc.), materiales híbridos orgánicos/inorgánicos (MOFs), etc., nos permiten tener la posibilidad de controlar las características estructurales de los catalizadores, así como dotarlos de propiedades ácidas, básicas, redox, etc. Asimismo, estos materiales, además de emplearse como catalizadores heterogéneos en sí, se pueden emplear como soportes para distintos metales, enzimas, compuestos orgánicos, etc., pudiendo mejorar las características que presentan inicialmente y haciéndolos más acordes a nuestras necesidades. La IUPAC clasifica estos materiales en tres grandes grupos como: (a) microporosos con tamaños de poro < 2 nm, en los que encontramos materiales como las zeolitas, (b) mesoporosos, los cuales presentan un diámetro de poro entre 2 y 50 nm donde se encuentran materiales tipo SBA-15 y (c) macroporosos, alcanzando diámetros de poro superiores a los 50 nm [13].

Atendiendo a este requerimiento de modificar las propiedades de los materiales a pequeña escala, se ha desarrollado la nanociencia o nanotecnología, la cual se define como la "síntesis, manipulación y visualización de nanomateriales, así como el estudio y la explotación de las diferencias entre el material másico y el nanomaterial y la comprensión y utilización de las leyes interdisciplinares que rigen la nanoescala", considerándose como nanomaterial aquel que posee al menos una de sus fases dentro de la escala de los nanómetros (1-100 nm) [12].

La heterogenización de nanocatalizadores altamente activos sobre diferentes soportes orgánicos o inorgánicos es probablemente la estrategia más eficiente, permitiendo incrementar el área superficial expuesta de la fase activa y el contacto entre los reactivos y el catalizador [14], consiguiendo progresos significativos para la recuperación eficaz

del catalizador. Además, las nanopartículas metálicas incorporadas en los soportes presentan estados degenerados discretos de energía, en comparación con el estado convencional de energía que suelen presentar por ejemplo los metales, aumentando éste conforme desciende el tamaño de las nanopartículas (Figura I.2).

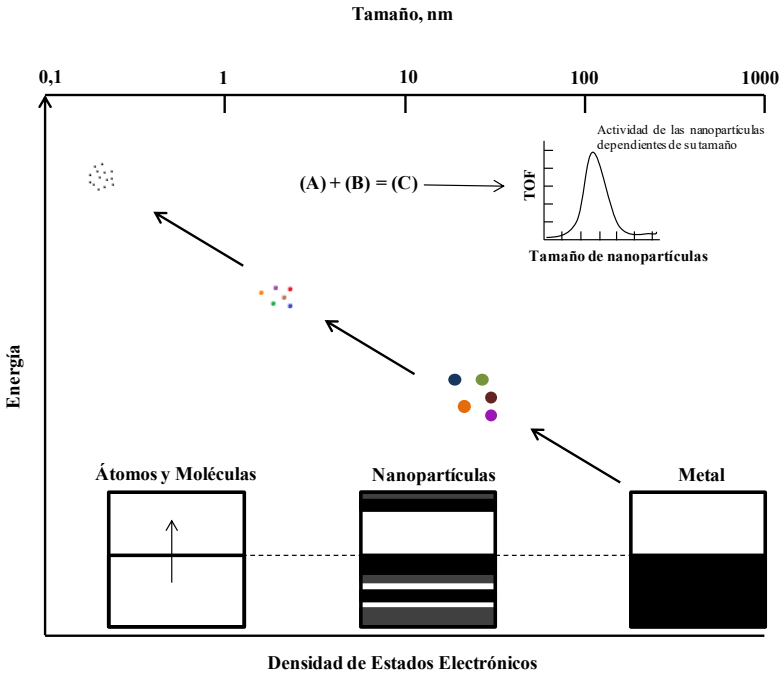

Figura I. 2. Propiedades diferenciales de las nanopartículas con respecto a los metales [4].

Estos materiales en los cuáles se incorporan nanopartículas sobre soportes porosos reciben el nombre de nanopartículas soportadas (NPS). El control sobre propiedades como el tamaño de partícula, la dispersión homogénea y la estabilización de las mismas, los ha hecho ideales para su aplicación en sensores [15], biomedicina [16] y catálisis [12].

En la presente Memoria de Tesis Doctoral, se encuentran presentes trabajos de investigación donde se pretende explicar el desarrollo de nuevas estrategias de síntesis de catalizadores soportados nanoestructurados de manera simple y reproducible. Además, los materiales obtenidos han mostrado rendimientos catalíticos mejorados y sostenibles en procesos de obtención de compuestos químicos de alto valor añadido, permitiéndonos proponer estos materiales para su aplicación a escala industrial.

I. 2. Materiales porosos nanoestructurados.

I. 2. 1. Introducción.

En el transcurso de los últimos años, los materiales microporosos, que comprenden desde las sílices amorfas y los geles inorgánicos hasta materiales cristalinos como zeolitas, aluminofosfatos, galofosfatos, y otros materiales relacionados, se han empleado como catalizadores en una amplia variedad de procesos químicos, entre los que cabe destacar la industria petroquímica.

Dentro de la gran variedad de materiales microporosos, los más populares son las zeolitas. Estos materiales son aluminosilicatos, cuya estructura forma una red tridimensional gracias al ordenamiento de tetraedros MO_4, donde M = Al o Si unidos mediante átomos de oxígeno.

Gracias a su sistema poroso determinado por su estructura cristalina, las zeolitas poseen una distribución de tamaño de poro estrecha y uniforme. Las zeolitas destacan por su utilización como catalizadores ácidos, pero además pueden diseñarse con características básicas y redox, haciéndolas idóneas para su empleo en la industria para llevar a cabo reacciones con moléculas pequeñas que requieren una determinada selectividad, permitiendo que dichas moléculas de interés tecnológico, gracias a que el diámetro cinético de las mismas es menor al del catalizador, puedan difundirse, adsorberse y transformarse catalíticamente en el interior del material microporoso.

No obstante, las zeolitas presentan grandes restricciones con respecto a reacciones en las que existe la presencia de moléculas de reactivos y/o productos que poseen un elevado peso molecular ("voluminosas"). Especialmente en reacciones en fase líquida, comunes en reacciones de obtención de productos de alto valor añadido ("Fine Chemicals"), dichas limitaciones difusionales condicionan una aplicación más generalizada de estos materiales microporosos [8].

Debido a esto, el hallazgo de materiales que poseen tamaños de poro en el intervalo de los mesoporos y bien definidos junto con áreas superficiales elevadas, ha supuesto un nuevo impulso con amplias posibilidades, para la química fina o la industria farmacéutica, relacionado con sus aplicaciones en catálisis y adsorción [17].

En los siguientes apartados, se describirán las distintas rutas sintéticas y las características principales de los materiales mesoporosos, empleados en los trabajos que componen la presente Memoria de Tesis Doctoral.

I. 2. 2. Materiales M41S.

En el año 1969, se describió por primera vez la síntesis de un material mesoporoso, bajo patente, pero debido a una caracterización poco detallada del material, las propiedades más significativas no fueron reconocidas [18]. Con el transcurso de los años, investigadores de la corporación "Mobil Oil R & D" llevaron a cabo la síntesis de M41S, un conjunto de materiales mesoporosos sintetizados con surfactantes del tipo alquiltrimetlamonio, ampliando el campo de investigación de los materiales mesoporosos [19,20].

La familia de tamices moleculares mesoporosos M41S se ha sintetizado, en términos generales, atendiendo a la combinación conveniente entre una fuente de silicio [tetraetilortosilicato (TEOS), sílice fumante o silicato sódico], un surfactante (haluro de alquiltrimetilamonio) y una disolución básica de agua con hidróxido de sodio (NaOH) / hidróxido de tetrametilamonio (TMAOH). En el caso de tratarse de la síntesis de aluminosilicatos se incluye la adición de una fuente de aluminio. Dicha mezcla de síntesis permanece entre 24 a 144 horas a una temperatura superior a 100 ºC, obteniéndose un precipitado sólido con estructura mesoporosa. Tras la etapa de filtrado, lavado y secado en aire, el material sólido se calcina a 500 ºC aproximadamente para eliminar el surfactante obteniéndose, finalmente, el silicato/aluminosilicato M41S [21].

Los investigadores de la "Mobil Oil R & D" propusieron un mecanismo en el cul se forma un cristal líquido que actúa de agente director de la estructura, basado en el ordenamiento de los surfactantes en sus distintas fases alotrópicas. En el caso de los materiales con estructura hexagonal en los mesoporos, MCM-41, esta corporación propuso dos mecanismos (Figura I. 3):

a) Los precursores del aluminosilicato ocupan el espacio existente entre las fases líquido-cristalinas de estructura hexagonal, depositándose sobre las micelas cilíndricas alargadas de ésta. Adquiriendo el comportamiento de "plantilla" dicha red supramolecular para la formación de la red inorgánica.
b) La presencia de los precursores inorgánicos condiciona, de alguna forma, el ordenamiento del surfactante en una disposición hexagonal.

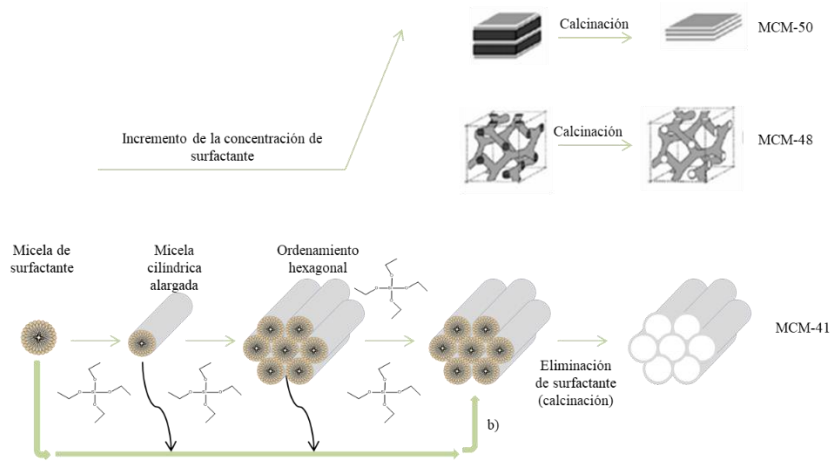

Figura I. 3. Materiales mesoporosos M41S. Mecanismos de formación propuestos inicialmente (parte inferior): a) modelo de cristal líquido y b) mecanismo de cristal líquido cooperativo [19].

La estructura mesoporosa se puede considerar como ordenamientos hexagonales de micelas (cilíndricas alargadas) de surfactante recubiertas por una matriz de sílice. La eliminación del surfactante genera la estructura mesoporosa MCM-41.

La familia M41S se encuentra formada por los materiales MCM-41, MCM-48 y MCM-50, con estructuras caracterizadas por sus respectivos diagramas de difracción de rayos X (Figura I. 4). De todas ellas, la fase

más frecuente, debido a su estabilidad a bajas concentraciones de surfactante, es la forma hexagonal (MCM-41). Por otro lado, la fase MCM-48 o fase cúbica, presenta una estructura más compleja formada por dos sistemas de canales tridimensionales que se acomodan entre sí, la superficie curvada divide el espacio en dos compartimentos iguales pero sin intersección, lo que significa que dos moléculas, cada una en un lado de una superficie, no se encontrarán. El sistema poroso de la MCM-48 puede representarse, por tanto, mediante canales entrecruzados en tres dimensiones que no se interceptan (Figura I.4. b). Cuando el medio de síntesis posee elevadas concentraciones de surfactante tiene lugar la formación de la fase laminar (MCM-50), la cual carece de estabilidad térmica y colapsa al eliminar el surfactante.

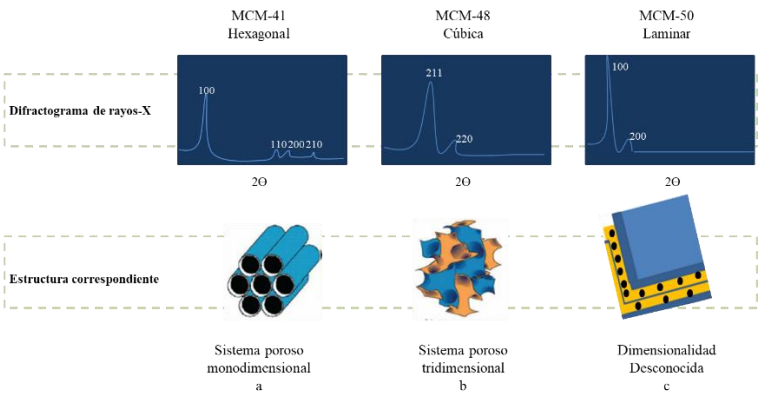

Figura I. 4. Diferentes estructuras de la familia M41S: a) MCM-41 (hexagonal), b) MCM-48 (cúbica) y MCM-50 (laminar) [19].

I. 2. 3. Materiales de tipo HMS.

El mecanismo de autoensamblaje de surfactantes neutros (tipo S_0I_0) permitió a Tanev y Pinnavaia [22] obtener silicatos mesoporosos hexagonales (tipo HMS). La síntesis consiste esencialmente en añadir tetraetil ortosilicato (TEOS) con fuente de silicio a una disolución básica

(etanol y agua desionizada) de una amina primaria como la dodecilamina (DDA). La mezcla da lugar a la formación de un gel, tras agitarse durante 18 horas a temperatura ambiente, y el silicato mesoporoso se obtiene tras filtrado y calcinado. El tamaño de poro de los materiales del tipo HMS es ligeramente superior al de los materiales MCM-41 [23,24].

Los materiales HMS presentan una estructura característica tipo "gusano" en contraposición a los canales hexagonales ordenados que se encuentran presentes en los materiales MCM-41[23,24]. Sin embargo, ambas familias, M41S y HMS, poseen áreas superficiales y volúmenes de poro similares, junto a una distribución de tamaño de poro uniforme. La diferencia principal, radica en el grado de condensación que presentan los materiales HMS, con paredes de mayor grosor que les permiten ser térmicamente más estables.

Además, Tanev y Pinnavaia [22] han propuesto un mecanismo en el cual la hidrólisis del TEOS en una disolución acuosa de DDA da lugar a un precursor inorgánico neutro [$Si(OC_2H_5)_{4-x}(OH)_x$] que, posteriormente, se une a través de puentes de hidrógeno al grupo amino del surfactante, dando lugar a la obtención de micelas cilíndricas alargadas y un empaquetamiento hexagonal de corto alcance de los grupos silanoles (Figura I. 5).

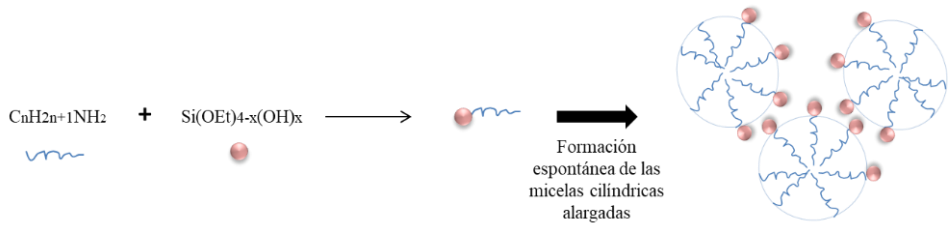

Figura I. 5. Propuesta de mecanismo de síntesis de materiales HMS, vía interacción por puentes de hidrógeno [25].

Los difractogramas de rayos-X característicos de las sílices mesoporosas hexagonales del tipo HMS (Figura I. 6.), muestran picos de difracción a ángulos bajos de 2θ con un pequeño hombro cercano a 5º.

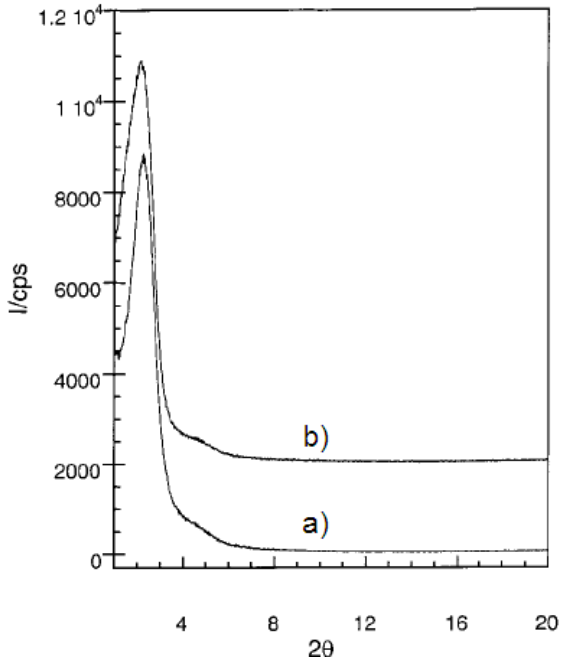

Figura I. 6. Difractogramas de rayos-X de la familia HMS obtenidos mediante a) emulsión heterogénea y b) solución homogénea del surfactante en co-disolventes conteniendo etanol [23].

I. 2. 4. Materiales de tipo SBA.

En la síntesis de la familia de materiales mesoporosos SBA (denominados Santa Barbara Amorphous por el centro donde se descubrieron) se utilizan copolímeros como agentes directores de la estructura bajo condiciones fuertemente ácidas. Así, se han descrito silicatos mesoporosos con estructura cúbica SBA-11 (Pm3m) obtenidos

utilizando el copolímero $C_{16}H_{33}(OCH_2CH_2)_{10}OH$, mientras que el silicato mesoporoso SBA-12, con una estructura tridimensional (P6/mmc), se obtiene a partir del copolímero $C_{18}H_{37}(OCH_2CH_2)_{10}OH$ [26]. Además, el silicato SBA-15 (p6mm) posee una estructura similar a la MCM-41, conteniendo poros hexagonales ordenados. Los materiales SBA-15 se sintetizan utilizando un copolímero tribloque como agente director de la estructura en un medio de síntesis fuertemente ácido, obteniéndose materiales con tamaños de poro mayores respecto a los M41S y con estabilidades hidrotérmica y térmica más elevadas respecto a la MCM-41, debido al mayor grosor de pared del poro [20,21,26–30].

Por otra parte, el material SBA-1 (pm3n), con estructura cúbica, se sintetiza a baja temperatura y en condiciones fuertemente ácidas, utilizando surfactantes con grupos de cabeza "head groups" voluminosos tales como los bromuros de alquiltrimetilamonio $C_{11}H_{2n+1}N(C_2H_5)_3Br$ (n= 12-18) [31–33]. Las condiciones de reacción a temperatura baja dan lugar a un grado de condensación muy bajo en la estructura del silicato, obteniéndose materiales SBA-1 con una pobre estabilidad hidrotérmica. Cuando la síntesis se lleva a cabo a temperaturas por encima de los 55 ºC, tiene lugar la transformación de la fase cúbica SBA-1 a la fase hexagonal SBA-3 (p6mm) [34,35].

El principal obstáculo que presentan los materiales del tipo SBA está relacionado con las condiciones fuertemente ácidas que requiere su síntesis y que dificulta la incorporación de heteroátomos en la estructura mesoporosa del silicato. Esto es debido a que, en tales condiciones fuertemente ácidas, los metales están presentes sólo en forma catiónica en lugar de la correspondiente especie oxigenada y, por tanto, el heteroátomo no puede introducirse en cantidades suficientes en las paredes mesoporosas a través de un proceso de condensación con especies de silicio.

Recientemente, Chaudhary y Sharma [36] han publicado una visión general de los materiales SBA-15 en la que destacan sus características fundamentales como son su alta superficie específica, paredes gruesas en su estructura y poros cilíndricos en todo el silicato mesoporoso [37,38]. El tamaño de poro de la SBA-15 varia de 4 a 12 nm y puede incrementarse hasta 30 nm con la adición de aditivos orgánicos como el trimetilbenceno. La SBA-15 se sintetiza mediante un mecanismo cooperativo de auto-ensamblaje con el copolímero tribloque no iónico consistente en unidades de óxido de etileno y óxido de propileno ($EO_{20}PO_{70}EO_{20}$) como agente director de la estructura, conocido como Pluronic P123 y TEOS o tetrametilortosilicato (TMOS) como fuentes de silicio [39–41].

Debido a su síntesis con Pluronic P123 como agente director de la estructura, se generan microporos perpendiculares al canal hexagonal, que penetran en la pared de sílice durante la síntesis (Figura I. 7). El tamaño de los microporos y mesoporos es cambiante, dependiendo de la temperatura a la que se trabaja durante su síntesis. Los microporos en las paredes de los mesoporos de la SBA-15 se crean a partir de la cadena más hidrofílica del EO del copolimero, que se abre camino en la pared del silicato durante la síntesis y genera la microporosidad tras la calcinación [42–45]. Este sistema de porosidad dual hace del material SBA-15 una elección perfecta para aplicaciones en adsorción y en catálisis.

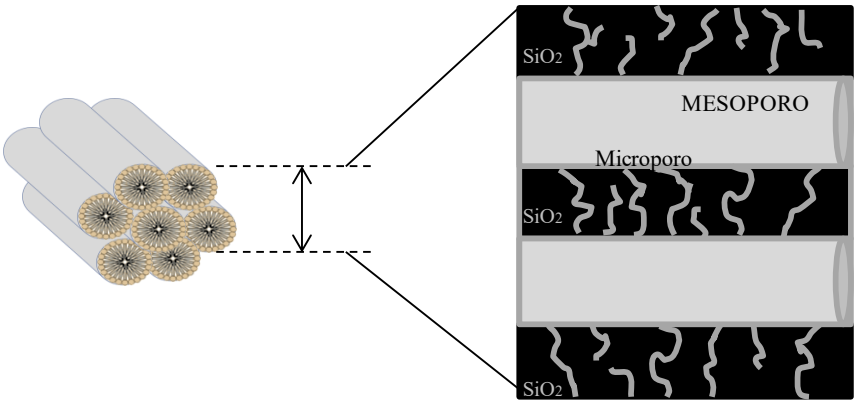

Figura I. 7. Esquema de la distribución de los canales meso- y microporosos presentes en un silicato con estructura tipo SBA-15 [46].

I. 2. 5. Materiales mesoporosos desarrollados recientemente.

Debido a su gran potencial para la conversión y almacenamiento de energía, catálisis, fotocatálisis, adsorción, separación y aplicaciones a las ciencias de la vida, la síntesis de materiales porosos jerarquizados ha despertado un interés significativo en la comunidad científica, concretamente ejemplarizado, en más de 40000 publicaciones científicas sobre materiales mesoporosos en los últimos cinco años y alrededor de 1.388 revisiones [47]. En la última década, se han hecho progresos significativos en el uso de materiales porosos ordenados en áreas desde la nanociencia a la catálisis, separación, energía, ciencias de la vida y otras aplicaciones industriales. Estos materiales están constituidos de una estructura porosa jerarquizada multimodal hecha de poros interconectados con diferentes longitudes en el intervalo de los micro- (< 2 nm), meso- (2-50 nm) a macroporos (> 50 nm) [48].

Son numerosas las estrategias de síntesis que han sido ideadas para la obtención de materiales porosos ordenados incluyendo agentes directores de la estructura formados por surfactantes, cristales coloidales,

polímeros, procesos bioinspirados, emulsiones, secado en frío, separación de fases, lixiviado selectivo, replicación, zeolitización, control sol-gel y post-tratamientos [49–57].

Una relación detallada de los numerosos materiales mesoestructurados sintetizados hasta la actualidad [58–71] resultaría poco útil, ya que el número de materiales mesoporosos que se están desarrollando está en continuo crecimiento y este campo está abierto a la incorporación adicional de nuevos materiales.

I. 3. Funcionalización de los materiales mesoporosos.

Los silicatos mesoporosos han sido un tema de investigación muy popular en el campo de la ciencia de los materiales, ya que pueden modificarse tanto desde la perspectiva de su morfología como de sus propiedades químicas superficiales. Hay una gran variedad de métodos de funcionalización de los sílices mesoporosos y se han desarrollado con la finalidad de mejorar tanto su capacidad de adsorción, propiedades catalíticas y selectividad del material [72]. Para ello, se pueden seguir dos vías: (I) síntesis directa, añadiendo los elementos deseados en la etapa de síntesis del sólido precursor mesofásico; o (II) mediante procesos de post-síntesis.

I. 3. 1. Funcionalización por síntesis directa de materiales silíceos mesoporosos.

Los procedimientos seguidos para la incorporación de múltiples grupos orgánicos e inorgánicos en materiales mesoporosos de sílice son muy variados [73,74]. Por lo general, la síntesis directa es un procedimiento mediante el cual se consigue modificar la estructura del material mediante la incorporación de diferentes elementos en las paredes del silicato y no en la superficie, gracias a las interacciones que tienen lugar durante el procedimiento de síntesis. De esta forma, al encontrarse insertados los grupos funcionales, se evitan perdidas por lixiviación y/o aglomeración (Figura I. 10).

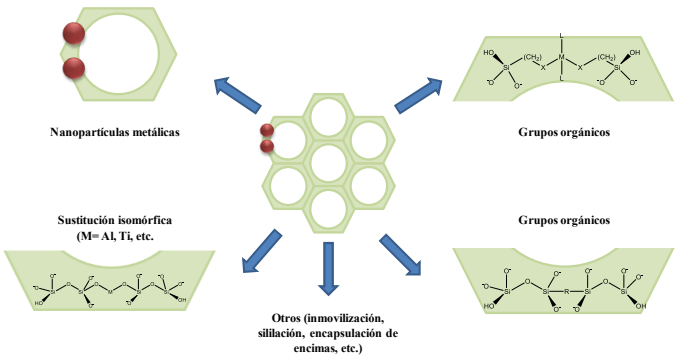

Figura I. 10. Diferentes estrategias de funcionalización in situ de materiales silíceos mesoporosos [75].

Hay un gran número de publicaciones que versan sobre la síntesis hidrotermal directa de materiales mesoporosos ordenados en los que se ha sustituido el silicio por aluminio, siendo este el primer metal en incorporarse a la estructura mesoporosa [76–80]. Sin embargo, las publicaciones sobre la incorporación directa en la estructura de materiales silíceos mesoporosos ordenados de otros metales de transición como por ejemplo, cobalto, vanadio, etc. son mucho más limitadas

[81,82]. Las condiciones fuertemente ácidas requeridas para la síntesis de materiales SBA-15 dificultan la incorporación directa de los metales. En medio ácido, los metales están presentes solo en forma catiónica, en lugar de la correspondiente forma oxigenada, lo que hace que el heteroátomo no pueda introducirse adecuadamente en las paredes mesoporosas a través del proceso de condensación con las especies de silicio. Sin embargo, se ha descrito en bibliografía (Tabla I. 2) la incorporación de diferentes metales mediante síntesis directa variando ligeramente las condiciones de síntesis ácida.

Tabla I. 2. Incorporación de distintos metales en la síntesis directa de SBA-15.

Material	Comentario	Referencia
Al-SBA-15	pH= 1,5	[83]
Al-Cr-SBA-15	pH= 0-3	[84]
Cr-SBA-15	Uso de NH_4F y método de ajuste de pH	[85]
Ga-SBA-15	Método de ajuste de pH	[86]
Ti-SBA-15	Tratamiento hidrotermal usando microondas	[87,88]
Zr-SBA-15		
Fe-SBA-15	Eliminación de surfactante mediante solución etanólica conteniendo sal de Fe	[89]
Cu-SBA-15	pH= 1,5	[90]
Co-SBA-15		
Ni-SBA-15		
Mn-SBA-15		

I. 3. 2. Modificación de los materiales silíceos mesoporosos mediante tratamientos post-síntesis.

Las técnicas de preparación post-sintéticas, como la impregnación hasta humedad incipiente, se han utilizado, generalmente, para la síntesis de catalizadores metálicos soportados. Sin embargo, estos métodos raramente generan partículas metálicas distribuidas uniformemente en la superficie del catalizador y esta falta de control hace poco probable que la distribución de las partículas metálicas sea exclusivamente en el interior de los poros (o en la superficie externa) del material utilizado como soporte.

Por otra parte, las sílices mesoporosas funcionalizadas ofrecen posibilidades prometedoras para numerosas aplicaciones, incluyendo, por ejemplo, la distribución de fármacos, la catálisis y la adsorción. Además, las posibilidades de preparar materiales mesoporosos con funcionalidades específicas son enormes.

Estos procesos se llevan a cabo primeramente por reacción de organosilanos [$(R'O)_3SiR$, $ClSiR_3$] o silozanos [$HN(SiR_3)_3$], con los grupos silanoles [≡Si-OH] sobre la superficie. Las variedades de grupos funcionales que pueden inmovilizarse fácilmente sobre la superficie del silicato está íntimamente relacionado con la capacidad con la que el organosilano puede difundirse en el interior de los mesoporos.

La ventaja de este método es que la estructura mesoporosa del silicato inicial se retiene, generalmente, bajo las condiciones de síntesis, no obstante, el tamaño de poro puede reducirse en cierto grado dependiendo del tamaño del grupo orgánico funcional (-R) y del grado de ocupación [91,92].

Sin embargo, el principal inconveniente de estos métodos de modificación es que los organosilanos pueden reaccionar preferentemente en la apertura de los poros y sobre la superficie externa durante la etapa inicial del proceso de síntesis, perjudicando la difusión de otras moléculas hacia el interior de los poros y produciendo una distribución no homogénea de los grupos funcionales orgánicos [91]. Además, en el caso de grupos funcionales orgánicos (-R) voluminosos o altas concentraciones de organosilanos, los mesoporos pueden bloquearse y dar lugar a una baja accesibilidad de los grupos funcionales.

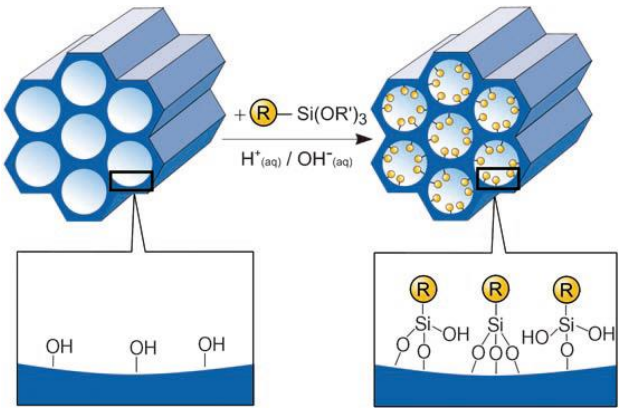

Figura I. 11. Funcionalización post-sintética para modificación orgánica de fases de sílice pura mesoporosa con organosilanos terminales del tipo $(R'O)_3SiR$ (R= grupo funcional orgánico) [91].

Frente a la incorporación de metales *in situ*, las nanopartículas soportadas (NPS) incorporadas mediante procedimientos post-síntesis suelen interaccionar débilmente con el soporte, lo que puede conllevar una deficiente dispersión en los materiales, especialmente si el tamaño de los poros es similar o menor al tamaño de las nanopartículas (NP). Incluso en el caso de las NP que se encuentran homogéneamente dispersas en el

soporte, según las condiciones de reacción, pueden aglomerarse (sinterizar) y/o lixiviar (Figura I.12).

Algunas limitaciones de las metodologías tradicionales para estabilizar nanopartículas, como la prevención de la aglomeración, han tratado de ser resueltas mediante el uso de varias técnicas alternativas mejorando así su gestión y reutilización [4,93–98].

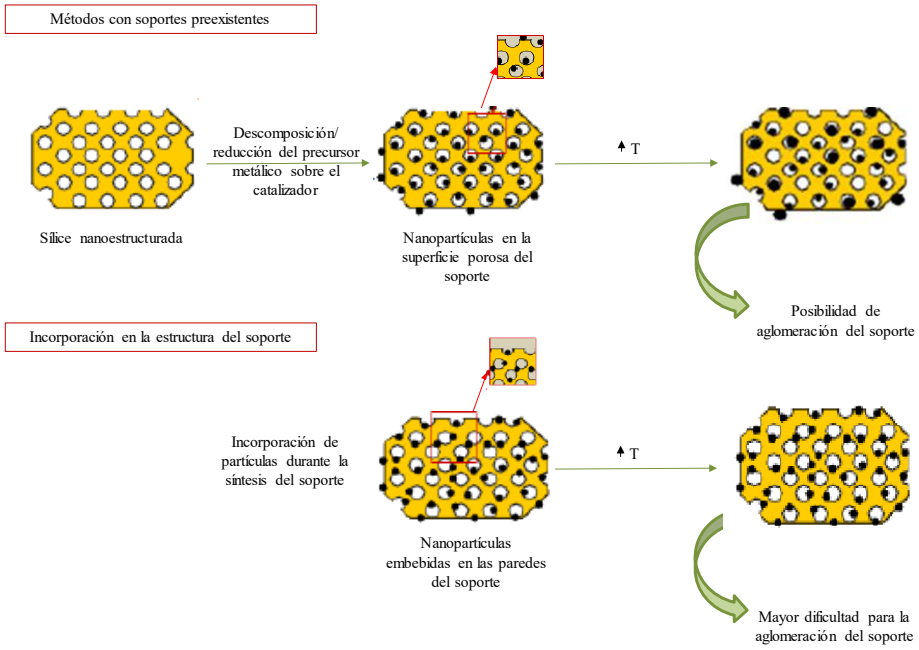

Figura I. 12. Comparación del efecto de la temperatura en NPS en silicatos mesoporosos mediante el método post- síntesis (arriba) e in situ (abajo) en la estructura del soporte [99].

La elevada actividad y especificidad de las nanopartículas metálicas han hecho que sean objeto de numerosos estudios, además del atractivo de las propiedades que poseen al compararlas con los metales, como la elevada relación superficie/volumen combinada con sus pequeños

tamaños. Las NP son catalíticamente activas, aunque inestables termodinámicamente.

La utilización de soportes mesoporosos es una alternativa atractiva que permite estabilizar, dispersar homogéneamente y controlar el tamaño de NP. Dichas nanopartículas soportadas sobre materiales mesoporosos reciben el nombre de NPS, y presentan propiedades relacionadas de forma directa con la morfología y el tamaño de las nanopartículas, la dispersión del metal o del óxido metálico sobre el soporte, la carga del metal y las propiedades electrónicas de las NP en el material.

No obstante, gracias al ajuste y selección de las propiedades texturales del soporte poroso (a veces al unísono con el empleo de un agente reductor), se podría controlar el tamaño y forma de las NP obtenidas. Esta conducta nos permitiría obtener una selectividad de tamaño y catalizadores heterogéneos reusables basados más en el tamaño de NP que en el tamaño de poro.

La preparación de dichas NPS se está llevando a cabo atendiendo a los criterios de sostenibilidad en los cuales se basan los "Principios de la Química Verde" [2], tanto a la hora de la síntesis de las mismas como en su empleo. Las nanopartículas metálicas por tanto deben ser preparadas empleando como precursor metálico aquel que sea lo menos tóxico posible y como disolventes agua o en su caso aquellos que sean benignos con el medio ambiente (como es el caso del etanol), utilizando el menor número de reactivos posibles y temperaturas de reacción cercanas a la temperatura ambiente, empleando el menor número de pasos y minimizando la producción de subproductos y residuos a lo largo del proceso [100,101]. Así mismo, se pretende establecer el objetivo de

obtener una dispersión homogénea sobre el soporte y elevada actividad catalítica.

Cabe destacar, de entre los diversos *procedimientos clásicos*, el método de deposición/reducción convencional (Figura I. 12). Este procedimiento consiste en la impregnación con una sal del del precursor metálico, tras el cual se lleva a cabo la reducción en corriente de H_2 o bien empleando agentes reductores como el borohidruro de sodio, hidracina, etc.

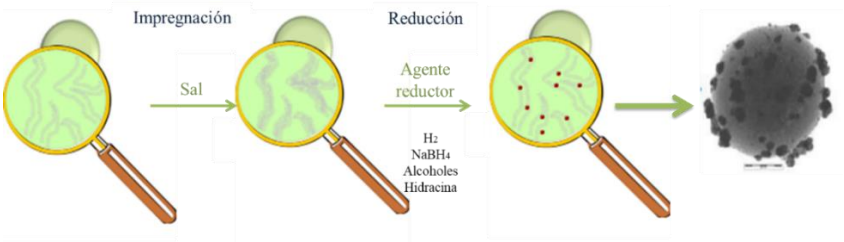

Figura I. 12. Representación esquemática del método de deposición/reducción convencional para la preparación de NPS [102].

Nuestro grupo de investigación FQM-383 está muy comprometido con el desarrollo, optimización y aplicación de nuevas técnicas alternativas como la síntesis de NPS mediante irradiación con microondas [103–106], molienda mecanoquímica [83,107–116], síntesis en flujo continuo [117–120] y, más recientemente la integración de las técnicas de molienda mecanoquímica y la irradiación con microondas [121].

Como prueba de la repercusión actual de estas nuevas técnicas, puede afirmarse que el número de publicaciones relacionas con estos novedosos procedimientos ha crecido exponencialmente en toda la comunidad investigadora a nivel mundial. Así, por ejemplo, la técnica de irradiación con microondas ha sido utilizada en la síntesis de NPS de diferentes óxidos Fe_2O_3, TiO_2, ZnO, CdS, CdSe [122–124], NPS nanometálicas de Au, Ag, Pt, Pd, Ru, Ir, Rh, Fe, Co, Ni, etc. [125–128], polímeros de

coordinación basados en aluminio o estructuras organometálicas (Al-MOFs) [129], etc.

Las publicaciones citadas anteriormente ponen de manifiesto que la irradiación mediante microondas para la obtención de NPS nos permite controlar la dispersión de las nanopartículas sobre el soporte, así como la estabilización de estas. Este hecho, es debido al control que se posee, durante el proceso de síntesis, de parámetros tales como el tiempo y la potencia de irradiación con microondas pudiendo controlar la morfología y tamaño de nanopartículas que presentarán los materiales, como se ha demostrado en investigaciones previas de nuestro grupo. Así mismo, esta metodología permite obtener nanopartículas soportadas en cortos intervalos de tiempo (varios minutos) y con una elevada pureza. Atendiendo a cuestiones medioambientales, el empleo de disolventes no tóxicos (agua o etanol), hacen de esta metodología una técnica con un bajo impacto ambiental.

Además, la irradiación microondas, gracias al calentamiento instantáneo y homogéneo del medio de síntesis, junto con la elección adecuada de los disolventes, permite la deposición e incluso reducción de los precursores metálicos sobre la superficie del soporte sin requerir ningún tipo de agente reductor como la hidracina, $NaBH_4$, etc. [130–132].

Por otra parte, la técnica de molienda mecanoquímica tal y como describen De Borggraeve y col. [133], también es compatible con tecnologías sostenibles para la preparación y funcionalización de derivados de la nanocelulosa.

El método mecanoquímico para la obtención de NPS se puede considerar un procedimiento físico-químico, donde se somete a molienda la sal precursora del óxido metálico o del metal y el soporte mesoporoso,

generalmente ambos en estado sólido. James y col. [134], han puesto de manifiesto la aplicabilidad que puede alcanzar dicha técnica debido a dos de sus características:

i. Efectividad y reproducibilidad del procedimiento en cualquier tipo de síntesis.
ii. Eludir el empleo de disolventes, evitando así problemas de tipo medioambiental.

Este método ha sido empleado con éxito para la síntesis de NPS no solo por nuestro grupo de investigación como hemos indicado anteriormente, sino también por investigadores como Suwanboon y col. [135] demostrando la aplicabilidad y versatilidad para la producción de nanopartículas soportadas con los tamaños y formas deseados gracias a las condiciones empleadas en la molienda mecanoquímica.

Por último, el grupo FQM-383, es pionero en el desarrollo del novedoso procedimiento que utiliza un sistema de flujo continuo [117], el cual implica la deposición de las NPS (Figura I. 13). Este método cumple los requisitos de la química verde al emplear disolventes benignos con el medio ambiente como es el caso del etanol. La disolución de etanol con el precursor metálico/óxido metálico se hace fluir a través del soporte mesoporoso, previamente empaquetado en un reactor. Finalmente, se ajustan la temperatura del reactor, la velocidad de flujo y el tiempo de residencia deseados, para obtener finalmente las NPS.

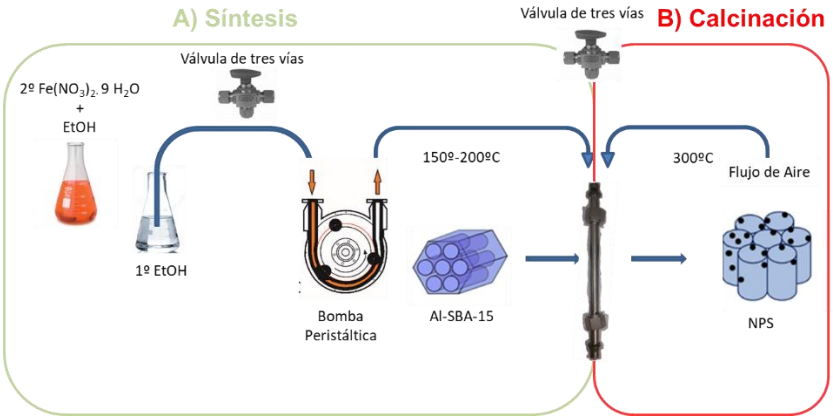

Figura I. 13. Esquema de síntesis de NPS mediante el método de flujo continuo para la deposición de nanopartículas de Fe [117].

Los beneficios de los métodos de flujo continuo son numerosos en el caso de procesos de síntesis/reacción de los nanomateriales en comparación con las tecnologías convencionales que se han descrito anteriormente. De este modo, se pueden alcanzar ventajas como la simple preparación y operación, control del proceso (velocidad de flujo, temperatura de trabajo, etc.), flexibilidad, mayor productividad y condiciones de reacción controlables, proporcionando un enfoque alternativo comparativamente práctico para la síntesis de NPS a escala industrial en comparación con protocolos tradicionales [136–139].

Otra línea de investigación que aborda la presente Memoria de Tesis Doctoral es el desarrollo de silicatos mesoporosos magnéticos, bajo el punto de vista de una química verde y sostenible. La utilización de nanocatalizadores magnéticos en catálisis heterogénea para la síntesis de productos farmacéuticos ha despertado un gran interés tanto académico como industrial [140,141]. Actualmente, los catalizadores nanoestructurados conllevan medios de reacción con partículas en

suspensión de tamaños inferiores a los 100 nm, donde las técnicas convencionales de separación como por ejemplo la filtración y centrifugación, llegan a ser muy laboriosas e incapaces de separar por completo el catalizador. Los nanocatalizadores magnéticos son candidatos excelentes debido a su característica única, "separación del medio de reacción aplicando fuerzas magnéticas" [142–155].

En nuestro grupo de investigación, la incorporación de estas partículas magnéticas soportadas se lleva a cabo mediante métodos post-sintéticos, que conllevan una etapa de reducción y la consecuente obtención del "nanocatalizador magnético" [106,109,119,156–158]. El esquema abreviado de síntesis se muestra en la Figura I. 14.

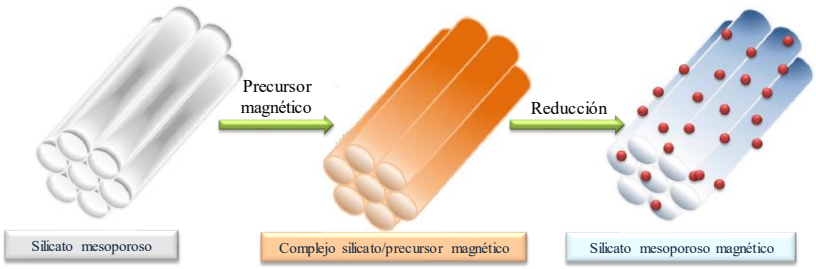

Figura I. 14. Esquema de síntesis de "*nanocomposites*" magnéticos.

I. 4. Catálisis heterogénea.

Unos de los pilares de la Química Verde es la catálisis, pues disminuye la producción de residuos, así como el gasto energético debido a que el tiempo necesario para llevar a cabo los tratamientos químicos deseados se ve acortado, reduciendo de esta forma el impacto ambiental. Así, los catalizadores, son una herramienta crucial en numerosos procesos convirtiéndose en una parte indispensable de la industria, con más del 90% de los procesos empleando algún tipo de catalizador [159,160].

Los catalizadores son sustancias/materiales que incrementan las velocidades de reacción facilitando una ruta alternativa para romper y formar enlaces. La clave de este mecanismo o ruta alternativa es una energía de activación más baja que la necesaria para dicha reacción en

ausencia de catalizador. Frecuentemente, los catalizadores son específicos para una reacción particular.

Muchas investigaciones fundamentales y aplicadas se han llevado a cabo por laboratorios de investigación universitarios y por compañías industriales para conocer cómo funcionan los catalizadores y mejorar su efectividad y hacer posible, además, reducir las cantidades de reactivos que son consumidos en productos de desecho no desecados.

Por otra parte, un catalizador heterogéneo está en una fase diferente a la de los reactivos y productos de reacción, siendo fácilmente separable del medio de reacción. Consecuentemente, son muy numerosas las revisiones bibliográficas y libros que versan sobre aplicaciones de catalizadores heterogéneos sintetizados por diferentes protocolos a todo tipo de reacciones [65,159–165].

Un resumen de algunas de estas reacciones se muestra en la Tabla I. 3, para procesos catalizados sobre centros ácidos y básicos; y en la tabla I. 4, para procesos catalizados sobre centros redox.

Tabla I. 3. Procesos catalizados por compuestos silíceo mesoporosos del tipo M-SBA-15 (M= metal).

Material	Procesos catalizados por centros ácidos	Referencia
Zr-SBA-15	Isomerización de parafinas	[166]
	Reducción de Meerwein-Ponndorf-Verley	[167]
	Esterificación y transesterificación	[168]
	Alquilación/acilación Friedel-Crafts	[169]
Al-SBA-15	Craqueo de cumeno	[170]
	Alquilación de Friedel-Crafts	[171]
	Oligomerización del 1-hexeno	[172]
	Conversión de dipenteno	[173]
Ga-SBA-15	Alquilación de Friedel-Crafts	[174]
	Reacción de isomerización	[175]
Fe- SBA-15	Alquilación de Friedel-Crafts	[176]
	Oxidación de Isoeugenol	[119]
Material	Procesos catalizados por centros básicos	Referencia
Fe- SBA-15	Reacción de Knoevenagel	[177–179]
Mg-SBA-15	Reacción de Kumada	[180]
Zn-SBA-15	Reacción de Negishi	[181]
Sn-SBA-15	Reacción de Migita-Stille	[182]
Si--SBA-15	Reacción de Hivama	[183]
B-SBA-15	Reacción de Suzuki-Miyaura	[184]

Tabla I. 4. Procesos de oxidación catalizados por metalosilicatos del tipo SBA-15.

Material	Procesos catalizados sobre centros redox	Referencia
Ti-SBA-15	Oxidación del alcohol bencílico	[185]
	Epoxidación del propileno	[186]
	Epoxidación del ciclobenceno	[187]
	Epoxidación de olefinas	[188]
Co-SBA-15	Epoxidación del estireno	[189]
	Oxidación del tolueno	[190]
Ce-SBA-15	Epoxidación de olefinas	[36]
Fe- SBA-15	Oxidación de Isoeugenol	[119]

La búsqueda de nuevos catalizadores va a continuar en el futuro como una de las prioridades más fundamentales para la industria química, buscando procesos a temperaturas y presiones tan bajas como sea posible con una velocidad de reacción aceptable. Los beneficios de estos catalizadores sintetizados, especialmente, mediante técnicas alternativas son tanto económicos como medioambientales.

Bibliografía

1. Clark, J.H. Green chemistry: Today (and tomorrow). *Green Chem.* **2006**, *8*, 17–21.
2. Anastas, P.T.; Warner, J.C. Green Chemistry: Theory and Practice. *Oxford Univ. Press. New York.* **1998**.
3. Sheldon, R.A. Engineering a more sustainable world through catalysis and green chemistry. *R. Soc.* **2016**, *1*, 1–7.
4. White, R.J.; Luque, R.; Budarin, V.L.; Clark, J.H.; MacQuarrie, D.J. Supported metal nanoparticles on porous materials. Methods and applications. *Chem. Soc. Rev.* **2009**, *38*, 481–494.
5. Grunes, J.; Zhu, J.; Somorjai, G.A. Catalysis and nanoscience. *Chem. Commun.* **2003**, *3*, 2257–2260.
6. Astruc, D.; Lu, F.; Aranzaes, J.R. Nanoparticles as recyclable catalysts: The frontier between homogeneous and heterogeneous

catalysis. *Angew. Chemie - Int. Ed.* **2005**, *44*, 7852–7872.

7. Khodakov, A.Y.; Zholobenko, V.L.; Impéror-Clerc, M.; Durand, D. Characterization of the initial stages of SBA-15 synthesis by in situ time resolved small angle X-ray scattering. *J. Phys. Chem. B.* **2005**, *109*, 22780–22790.
8. Taguchi, A.; Schüth, F. Ordered mesoporous materials in catalysis. *Microporous and mesoporous materials*. **2005**, *77*, 1-45.
9. Blaser, H.U. Heterogeneous catalysis for fine chemicals production. *Catal. Today* **2000**, *60*, 161–165.
10. Mallat, T.; Baiker, A.; Feng, X.; Lv, P.; Sun, W.; Han, X.; Gao, L.; Zheng, G.; Oliveira, A.A.S.; Costa, D.S.; et al. Gold and gold–palladium alloy nanoparticles on heterostructured TiO_2 nanobelts as plasmonic photocatalysts for benzyl alcohol oxidation. *Catal. Commun.* **2017**, *7*, 209–217.
11. Corma, A.; García, H. Lewis Acid: From convetional homogeneous to green homogeneous and heterogeneous catalysis. *Chemical Rewie*. **2003**, *103*, 4307-4365.
12. Campelo, J.M.; Luna, D.; Luque, R.; Marinas, J.M.; Romero, A.A. Sustainable preparation of supported metal nanoparticles and their applications in catalysis. *ChemSusChem.* **2009**, *2*, 18-45.
13. Sing, K.S.W.; Everett, D.H.; Haul, W.; Moscou, L, Pierotti, R.A.; Rouquerol, J.; Siemieniewska, T. Reporting physisorption dato for Gas/Solid systems with special reference to the determination of surface area and porosity. *Pure and Appl. Chem.* **1985**, 57, 603–619.
14. Polshettiwar, V.; Varma, R.S. Green chemistry by nano-catalysis. *Green Chem.* **2010**, *12*, 743–754.
15. Jain, P.K.; Huang, X.; El-Sayed, I.H.; El-Sayed, M.A. Noble

metals on the nanoscale: Optical and photothermal properties and some applications in imaging, sensing, biology, and medicine. *Acc. Chem. Res.* **2008**, *41*, 1578–1586.

16. Thanh, N.T.K.; Green, L.A.W. Functionalisation of nanoparticles for biomedical applications. *Nano Today*. **2010**, *5*, 213–230.
17. Maschmeyer, T.; Raimondi, M.E.; Seddon, J.M. Mesoporous molecular sieves - M41S and related families. *Encyclopedia of materials : science and technology*; Buschow, Ed.; Elsevier. **2001**, 5342–5346.
18. Di Renzo, F.; Cambon, H.; Dutartre, R. A 28 year old synthesis of micelle-templated mesoporous silica. *Microporous Mater*. **1997**, *10*, 283–286.
19. Kresge, C.T.; Roth, W.J. The discovery of mesoporous molecular sieves from the twenty year perspective. *Chem. Soc. Rev.* **2013**, *42*, 3663–3670.
20. Beck, J.S.; Vartuli, J.C.; Roth, W.J.; Leonowicz, M.E.; Kresge, C.T.; Schmitt, K.D.; Chu, C.T.W.; Olson, D.H.; Sheppard, E.W.; McCullen, S.B.; Higgins, J.B.; Schlenker, J.L. A New Family of Mesoporous Molecular Sieves Prepared with Liquid Crystal Templates. *J. Am. Chem. Soc.* **1992**, *114*, 10834–10843.
21. Kresge, C.T.; Leonowicz, M.E.; Roth, W.J.; Vartuli, J.C.; Beck, J.S. Ordered mesoporous molecular sieves synthesized by a liquid-crystal template mechanism. *Nature*. **1992**, *359*, 710–712.
22. Pinnavaia, T.J.; Tanev, P.T. A neutral templating route to mesoporous molecular sieves. *Science*. **1995**, *267*, 865–867.
23. Pauly, T.R.; Liu, Y.; Pinnavaia, T.J.; Billinge, S.J.L.; Rieker, T.P. Textural mesoporosity and the catalytic activity of mesoporous molecular sieves with wormhole framework structures. *J. Am. Chem. Soc.* **1999**, *121*, 8835–8842.

24. Prouzet, E. Assembly of Mesoporous Molecular Sieves Containing Wormhole Motifs by a. *Angew. Chemie Int. Ed.* **1997**, *36*, 516–518.

25. Tanev, P.T.; Pinnavaia, T.J. Recent advances in synthesis and catalytic applications of mesoporous molecular sieves. *Nanoporous Materials*. **1995**, 13-27.

26. Zhao, D.; Huo, Q.; Feng, J.; Chmelka, B.F.; Stucky, G.D. Nonionic triblock and star diblock copolymer and oligomeric surfactant syntheses of highly ordered, hydrothermally stable, mesoporous silica structures. *J. Am. Chem. Soc.* **1998**, *120*, 6024-6036.

27. Zhao, D.; Feng, J.; Huo, Q.; Melosh, N.; Fredrickson, G.H.; Chmelka, B.F.; Stucky, G.D. Triblock copolymer syntheses of mesoporous silica with periodic 50 to 300 angstrom pores. *Science*. **1998**, *279*, 548–552.

28. Ryoo, R.; Kim, J.M.; Ko, C.H.; Shin, C.H. Disordered molecular sieve with branched mesoporous channel network. *J. Phys. Chem.* **1996**, *100*, 17718–17721.

29. Yang, P.; Zhao, D.; Margolese, D.I.; Chmelka, B.F.; Stucky, G.D. Block copolymer templating syntheses of mesoporous metal oxides with large ordering lengths and semicrystalline framework. *Chem. Mater.* **1999**, *11*, 2813–2826.

30. Yang, P.; Zhao, D.; Margolese, D.I.; Chmelka, B.F.; Stucky, G.D. Generalized syntheses of large-pore mesoporous metal oxides with semicrystalline frameworks. *Nature.* **1998**, *396*, 152.

31. Huo, Q.; Margolese, D.I.; Ciesla, U.; Demuth, D.G.; Feng, P.; Gier, T.E.; Sieger, P.; Firouzi, A.; Chmelka, B.F. Organization of organic molecules with inorganic molecular species into nanocomposite biphase arrays. *Chem. Mater.* **1994**, *6*, 1176-1191.

32. Huo, Q.; Margolese, D.I.; Stucky, G.D. Surfactant control of phases in the synthesis of mesoporous silica-based materials. *Chem. Mater.* **1996**, *8*, 1147–1160.

33. Huo, Q.; Margolese, D.I.; Ciesla, U.; Feng, P.; Gier, T.E.; Sieger, P.; Leon, R.; Petroff, P.M.; Schüth, F.; Stucky, G.D. Generalized synthesis of periodic surfactant/inorganic composite materials. *Nature.* **1994**, *368*, 317.

34. Kim, M.J.; Ryoo, R. Synthesis and pore size control of cubic mesoporous silica SBA-1. *Chem. Mater.* **1999**, *11*, 487–491.

35. Vinu, A.; Murugesan, V.; Hartmann, M. Pore Size Engineering and Mechanical Stability of the Cubic Mesoporous Molecular Sieve SBA-1. *Chemistry of materials*. **2003**, 1385–1393.

36. Chaudhary, V.; Sharma, S. An overview of ordered mesoporous material SBA-15: synthesis, functionalization and application in oxidation reactions. *J. Porous Mater.* **2017**, *24*, 741–749.

37. Huirache-Acuña, R.; Nava, R.; Peza-Ledesma, C.; Lara-Romero, J.; Alonso-Núez, G.; Pawelec, B.; Rivera-Muñoz, E. SBA-15 mesoporous silica as catalytic support for hydrodesulfurization catalysts. *Materials (Basel).* **2013**, *6*, 4139–4167.

38. Zhao, D.; Sun, J.; Li, Q.; Stucky, G.D.; Barbara, S. Morphological Control of Highly Ordered Mesoporous Silica SBA-15 Mesoporous materials are of great interest to the materials community because their pore structures as well as catalytic , adsorbed , conductive and magnetic ordered large mesoporous silica. *Chem. Mater.* **2000**, *12*, 275–279.

39. Ulrich, K.; Galvosas, P.; Kärger, J.; Grinberg, F.; Vernimmen, J.; Meynen, V.; Cool, P. Self-assembly and diffusion of block copolymer templates in SBA-15 nanochannels. *J. Phys. Chem. B.* **2010**, *114*, 4223–4229.

40. Fuertes, A.B. Synthesis of ordered nanoporous carbons of tunable mesopore size by templating SBA-15 silica materials. *Microporous Mesoporous Mater.* **2004**, *67*, 273–281.
41. Fulvio, P.F.; Pikus, S.; Jaroniec, M. Short-time synthesis of SBA-15 using various silica sources. *J. Colloid Interface Sci.* **2005**, *287*, 717–720.
42. Fan, J.; Yu, C.; Wang, L.; Tu, B.; Zhao, D.; Sakamoto, Y.; Terasaki, O. Mesotunnels on the silica wall of ordered SBA-15 to generate three-dimensional large-pore mesoporous networks. *J. Am. Chem. Soc.* **2001**, *123*, 12113–12114.
43. Fan, J.; Yu, C.; Lei, J.; Tu, B.; Zhang, Q.; Li, T.; Zhou, W. Low temperature strategy to synthesize highly ordered mesoporous silicas with very large pores. *J. Am. Chem. Soc*. **2005**, 127, 10794-10795.
44. Galarneau, A.; Cambon, H.; Di Renzo, F.; Ryoo, R.; Choi, M.; Fajula, F. Microporosity and connections between pores in SBA-15 mesostructured silicas as a function of the temperature of synthesis. *New J. Chem.* **2003**, *27*, 73–79.
45. Benamor, T.; Vidal, L.; Lebeau, B.; Marichal, C. Influence of synthesis parameters on the physico-chemical characteristics of SBA-15 type ordered mesoporous silica. *Microporous Mesoporous Mater.* **2012**, *153*, 100–114.
46. Sainz-Pardo, J. Tesis Doctoral "Incorporación de titanio y molibdeno en materiales mesoestructurados para su aplicación en procesos de epoxidación de olefinas". **2007**. hdl.handle.net
47. Suib, S.L. A Review of Recent Developments of Mesoporous Materials. *Chem. Rec.* **2017**, *17*, 1169–1183.
48. Yang, X.Y.; Chen, L.H.; Li, Y.; Rooke, J.C.; Sanchez, C.; Su, B.L. Hierarchically porous materials: Synthesis strategies and structure design. *Chem. Soc. Rev.* **2017**, *46*, 481–558.

49. Aizenberg, J.; Fratzl, P. Biological and Biomimetic Materials. *Adv. Mater.* **2009**, *21*, 387–388.

50. Fratzl, P. Biomimetic materials research: What can we really learn from nature's structural materials? *J. R. Soc. Interface*. **2007**, *4*, 637–642.

51. Fratzl, P.; Weinkamer, R. Nature's hierarchical materials. *Prog. Mater. Sci.* **2007**, *52*, 1263–1334.

52. Lakes, R. Materials with structural hierarchy. *Nature.* **1993**, *361*, 511.

53. Mann, S. Biomineralization: principles and concepts in bioinorganic materials chemistry. *Oxford University Press on Demand*. **2001**.

54. Messersmith, P.B. Materials science. Multitasking in tissues and materials. *Science.* **2008**, *319*, 1767–1768.

55. Munch, E.; Launey, M.E.; Alsem, D.H.; Saiz, E.; Tomsia, A.P.; Ritchie, R.O. Tough, bio-inspired hybrid materials. *Science.* **2008**, *322*, 1516–1520.

56. Sánchez, C.; Arribart, H.; Guille, M.M.G. Biomimetism and bioinspiration as tools for the design of innovative materials and systems. *Nat. Mater.* **2005**, *4*, 277–288.

57. Su, B.L.; Sánchez, C.; Yang, X.Y. Hierarchically structured porous materials: from nanoscience to catalysis, separation, optics, energy, and life science. *John Wiley & Sons*. **2012**.

58. Sun, Q.; Xie, Z.; Yu, J. The state of the art synthetic strategies for SAPO-34 zeolite catalysts in methanol to olefin conversion. *National Science Review*. **2017**, *5*, 1–17.

59. Liu, B.; Xu, D.; Lv, H. Mesoporous Zeolites and Their Enhanced Catalytic Performances : A Review. *Frontiers in Chemistry*. **2018**, *6,* 550.

60. Liang, J.; Liang, Z.; Zou, R.; Zhao, Y. Heterogeneous catalysis in zeolites, mesoporous silica, and metal–organic frameworks. *Adv. Mater.* **2017**, *29*, 1701139.

61. Wang, Y.; Arandiyan, H.; Scott, J.; Bagheri, A.; Dai, H.; Amal, R. Recent advances in ordered meso/macroporous metal oxides for heterogeneous catalysis: A review. *J. Mater. Chem. A.* **2017**, *5*, 8825–8846.

62. Sun, B.; Zhou, G.; Zhang, H. Synthesis, functionalization, and applications of morphology controllable silica-based nanostructures: A review. *Prog. Solid State Chem.* **2016**, *44*, 1-19.

63. Xin, W.; Song, Y. Mesoporous carbons: recent advances in synthesis and typical applications. *RSC Adv.* **2015**, *5*, 83239–83285.

64. Xu, W.; Bahadur, K.; Ju, Q.; Fang, Z.; Huang, W. Heterogeneous catalysts based on mesoporous metal – organic frameworks. *Coord. Chem. Rev.* **2018**, *373*, 199–232.

65. Liu, B.; Xu, D.; Lv, H. Encapsulation of Metal Nanoparticle Catalysts Within Mesoporous Zeolites and Their Enhanced Catalytic Performances: A Review. *Front. Chem.* **2018**, *6*, 550.

66. Doustkhah, E.; Lin, J.; Rostamnia, S.; Len, C.; Luque, R. Development of Sulfonic Acid Functionalized Mesoporous Materials : Synthesis and Catalytic Applications. *Chemistry A European Journal*. **2018**, *25*, 1–23.

67. Wang, J.; Ma, Q.; Wang, Y.; Li, Z.; Li, Z.; Yuan, Q. New insights into the structure–performance relationships of mesoporous materials in analytical science. *Chem. Soc. Rev.* **2018**, *47*, 8766–8803.

68. Shi, S.; Sun, Z.; Hu, Y.H. Synthesis, stabilization and applications of 2-dimensional 1T metallic MoS 2. *J. Mater.*

Chem. A. **2018**, *6*, 23932–23977.

69. Chen, K.; Wu, C.-D. Designed fabrication of biomimetic metal–organic frameworks for catalytic applications. *Coord. Chem. Rev.* **2018**, *378*, 445-465.
70. Tanimu, A.; Jaenicke, S.; Alhooshani, K. Heterogeneous catalysis in continuous flow microreactors: A review of methods and applications. *Chem. Eng. J.* **2017**, *327*, 792–821.
71. Wang, L.Y.; Yu, X.H.; Zhao, Z. Synthesis of Inorganic Porous Materials and Their Applications in the Field of Environmental Catalysis. *Acta Physico-Chimica Sin.* **2017**, *33*, 2359–2376.
72. Huang, L.; Kruk, M. Versatile surfactant/swelling-agent template for synthesis of large-pore ordered mesoporous silicas and related hollow nanoparticles. *Chem. Mater.* **2015**, *27*, 679–689.
73. Linares, N.; Serrano, E.; Rico, M.; Balu, A.M.; Losada, E.; Luque, R.; García-Martínez, J. Incorporation of chemical functionalities in the framework of mesoporous silica. *Chem. Commun.* **2011**, *47*, 9024–9035.
74. Trewyn, B.G.; Slowing, I.I.; Giri, S.; Chen, H.-T.; Lin, V.S.-Y. Synthesis and functionalization of a mesoporous silica nanoparticle based on the sol–gel process and applications in controlled release. *Acc. Chem. Res.* **2007**, *40*, 846–853.
75. Kim, S.S.; Karkamkar, A.; Pinnavaia, T.J.; Kruk, M.; Jaroniec, M. Synthesis and characterization of ordered, very large pore MSU-H silicas assembled from water-oluble Silicates. **2001**, *105*, 7663–7670.
76. Corma, A.; Fornes, V.; Navarro, M.T.; Perezpariente, J. Acidity and stability of MCM-41 crystalline aluminosilicates. *J. Catal.* **1994**, *148*, 569–574.
77. Ryoo, R.; Ko, C.H.; Howe, R.F. Imaging the distribution of

framework aluminum in mesoporous molecular sieve MCM-41. *Chem. Mater.* **1997**, *9*, 1607–1613.

78. Corma, A.; Navarro, M.T.; Pérez-Pariente, J. Synthesis of an ultralarge pore titanium silicate isomorphous to MCM-41 and its application as a catalyst for selective oxidation of hydrocarbons. *J. Chem. Soc. Chem. Commun.* **1994**, *2*, 147–148.
79. Lourenço, J.P.; Fernandes, A.; Henriques, C.; Ribeiro, M.F. Al-containing MCM-41 type materials prepared by different synthesis methods: Hydrothermal stability and catalytic properties. *Microporous mesoporous Mater.* **2006**, *94*, 56–65.
80. Carrillo, A.I.; Serrano, E.; Luque, R.; García-Martínez, J. Microwave-assisted catalysis by iron oxide nanoparticles on MCM-41: effect of the support morphology. *Appl. Catal. A Gen.* **2013**, *453*, 383–390.
81. Ramanathan, A.; Subramaniam, B. Metal incorporated mesoporous silicates: tunable catalytic properties and applications. *Molecules* **2018**, *23*, 263.
82. Glomm, W.R.; Vrålstad, T.; Øye, G.; Stöcker, M.; Sjöblom, J. A Direct Sol-Gel Synthesis Method for Incorporation of Transition Metals into the Framework of Ordered Mesoporous Materials. *J. Dispers. Sci. Technol.* **2005**, *26*, 95–104.
83. Pineda, A.; Balu, A.M.; Campelo, J.M.; Luque, R.; Romero, A.A.; Serrano-Ruiz, J.C. High alkylation activities of ball-milled synthesized low-load supported iron oxide nanoparticles on mesoporous aluminosilicates. *Catal. Today* **2012**, *187*, 65–69.
84. Aguado, J.; Calleja, G.; Carrero, A.; Moreno, J. One-step synthesis of chromium and aluminium containing SBA-15 materials New phillips catalysts for ethylene polymerization. *Chem. Eng. J.* **2008**, *137*, 443–452.
85. Selvaraj, M.; Kawi, S. Direct synthesis of mesoporous CrSBA-15

catalyst and its high activity and selectivity for oxidation of anthracene. *Microporous and Mesoporous materials*. **2007**, *101*, 240–249.

86. Gracía, M.J.; Losada, E.; Luque, R.; Campelo, J.M.; Luna, D.; Marinas, J.M.; Romero, A.A. Activity of Gallium and Aluminum SBA-15 materials in the Friedel–Crafts alkylation of toluene with benzyl chloride and benzyl alcohol. *Appl. Catal. A Gen.* **2008**, *349*, 148–155.
87. Newalkar, B.L.; Olanrewaju, J.; Komarneni, S. Microwave-Hydrothermal Synthesis and Characterization of Zirconium Substituted SBA-15 Mesoporous Silica. *The journal of physical chemistry*. **2001**, *105*, 8356–8360.
88. Iglesias, J.; Melero, J.A.; Sainz-Pardo, J. Direct synthesis of organically modified Ti-SBA-15 materials. *J. Mol. Catal. A Chem.* **2008**, *291*, 75–84.
89. Vinu, A.; Ariga, K.; Mori, T.; Nakanishi, T.; Hishita, S.; Golberg, D.; Bando, Y. Preparation and characterization of well ordered hexagonal mesoporous carbon nitride. *Adv. Mater.* **2005**, *17*, 1648–1652.
90. Prathap, M.U.A.; Kaur, B.; Srivastava, R. Direct synthesis of metal oxide incorporated mesoporous SBA-15, and their applications in non-enzymatic sensing of glucose. *J. Colloid Interface Sci.* **2012**, *381*, 143–151.
91. Hoffmann, F.; Cornelius, M.; Morell, J.; Fröba, M. Silica-based mesoporous organic-inorganic hybrid materials. *Angew. Chemie - Int. Ed.* **2006**, *45*, 3216-3251.
92. Sayari, A.; Hamoudi, S. Periodic mesoporous silica-based organic−inorganic nanocomposite materials. *Chem. Mater.* **2001**, *13*, 3151–3168.

93. Yin, Y.; Alivisatos, A.P. Colloidal nanocrystal synthesis and the organic-inorganic interface. *Nature*. **2005**, *437,* 664-670.

94. Wang, X.; Zhuang, J.; Peng, Q.; Li, Y. A general strategy for nanocrystal synthesis. *Nature*. **2005**, *437*, 121–124.

95. Huang, M.H.; Mao, S.; Feick, H.; Yan, H.; Wu, Y.; Kind, H.; Weber, E.; Russo, R. Room-Temperature Ultraviolet Nanowire Nanolasers. *Science*. **2001**, *292*, 1897–1900.

96. Morales, A.M.; Lieber, C.M. A Laser Ablation Method for the Synthesis of Crystalline Semiconductor Nanowires. *Science*. **1998**, *279,* 208-211.

97. Koo, I.G.; Cho, J.H.; Lee, W.M. Influence of the Gas Humidity on the Uniformity of RF-Powered DBD Plasmas. *Plasma Process and Pol*. **2008**, *5*, 161-167.

98. Daniel, M.; Astruc, D. Gold Nanoparticles : Assembly, Supramolecular Chemistry, Quantum-Size-Related Properties, and Applications toward Biology, Catalysis and Nanotechnology. *Chemical Reviews*. **2004**, *104*, 293-346.

99. Luque, R. Supported metal nanoparticles in catalysis. Progress in Heterogeneous Catalysis. *Nova Science Publishers Inc*. **2008**.

100. Anastas, P.T.; Kirchhoff, M.M. Origins, current status, and future challenges of green chemistry. *Acc. Chem. Res.* **2002**, *35*, 686-694.

101. Dahl, J.A.; Maddux, B.L.S.; Hutchison, J.E. Toward Greener Nanosynthesis. *Chemical reviews*. **2007**, *107*, 2228–2269.

102. Balu, Alina M. Tesis Doctoral. "Nanopartículas soportadas sobre materiales porosos para la síntesis de productos de alto valor añadido." Córdoba. **2012**. http://hdl.handle.net/10396/7660.

103. Balu, A.M.; Dallinger, D.; Obermayer, D.; Campelo, J.M.; Romero, A.A.; Carmona, D.; Balas, F.; Yohida, K.; Gai, P.L.; Vargas, C. Insights into the microwave-assisted preparation of

supported iron oxide nanoparticles on silica-type mesoporous materials. *Green Chem.* **2012**, *14*, 393–402.

104. Ojeda, M.; Budarin, V.; Shuttleworth, P.S.; Clark, J.H.; Pineda, A.; Balu, A.M.; Romero, A.A.; Luque, R. Simple preparation of novel metal-containing mesoporous starches. *Materials.* **2013**, *6*, 1891–1902.
105. Yépez, A.; De, S.; Climent, M.S.; Romero, A.A.; Luque, R. Microwave-assisted conversion of levulinic acid to γ-valerolactone using low loaded supported iron oxide nanoparticles on porous silicates. *Appl. Sci.* **2015**, *5*, 532–543.
106. Zuliani, A.; Balu, A.M.; Luque, R. Efficient and environmentally friendly microwave assisted synthesis of catalytically active magnetic metallic Ni nanoparticles. *ACS Sustain. Chem. Eng.* **2017**, *5*, 11584–11587.
107. Pineda, A.; Balu, A.M.; Campelo, J.M.; Romero, A.A.; Carmona, D.; Balas, F.; Santamaria, J.; Luque, R. A Dry Milling Approach for the Synthesis of Highly Active Nanoparticles Supported on Porous Materials. *ChemSusChem*. **2011**, *4*, 1561–1565.
108. Samu, G.F.; Veres, Á.; Tallósy, S.P.; Janovák, L.; Dékány, I.; Yépez, A.; Luque, R.; Janáky, C. Photocatalytic, photoelectrochemical, and antibacterial activity of benign-by-design mechanochemically synthesized metal oxide nanomaterials. *Catal. Today*. **2017**, *284*, 3–10.
109. Rodríguez-Padrón, D.; Puente-Santiago, A.R.; Balu, A.M.; Romero, A.A.; Luque, R. Solventless mechanochemical preparation of novel magnetic bioconjugates. *Chem. Commun.* **2017**, *53*, 7635–7637.
110. Hidalgo, J.M.; Pineda, A.; Arancon, R.A.D.; Černý, R.; Climent, M.S.; Romero, A.A.; Luque, R. Continuous Flow

Hydroisomerization of C5–C7 Alkanes Using Mechanochemically Synthesized Supported Pt and Pd-SBA-15 Materials. *J. Flow Chem.* **2015**, *5*, 11–16.

111. Jodlowski, A.D.; Yépez, A.; Luque, R.; Camacho, L.; de Miguel, G. Benign by Design Solventless Mechanochemical Synthesis of Three-, Two-, and One-Dimensional Hybrid Perovskites. *Angew. Chemie Int. Ed.* **2016**, *55*, 14972–14977.
112. Rodríguez-Padrón, D.; Puente-Santiago, A.R.; Caballero, A.; Benítez, A.; Balu, A.M.; Romero, A.A.; Luque, R. Mechanochemical design of hemoglobin-functionalised magnetic nanomaterials for energy storage devices. *J. Mater. Chem. A.* **2017**, *5*, 16404–16411.
113. Arancon, R.A.D.; Balu, A.M.; Romero, A.A.; Ojeda, M.; Gómez, M.; Blanco, J.; Domingo, J.L.; Luque, R. Mechanochemically synthesized Ag-based nanohybrids with unprecedented low toxicity in biomedical applications. *Environ. Res.* **2017**, *154*, 204–211.
114. Franco, A.; De, S.; Balu, A.M.; García, A.; Luque, R. Mechanochemical synthesis of graphene oxide-supported transition metal catalysts for the oxidation of isoeugenol to vanillin. *Beilstein J. Org. Chem.* **2017**, *13*, 1439.
115. Franco, A.; De, S.; Balu, A.M.; Romero, A.A.; Luque, R. Selective oxidation of isoeugenol to vanillin over mechanochemically synthesized aluminosilicate supported transition metal catalysts. *ChemistrySelect.* **2017**, *2*, 9546–9551.
116. Yépez, A.; Hidalgo, J.M.; Pineda, A.; Černý, R.; Jíša, P.; García, A.; Romero, A.A.; Luque, R. Mechanistic insights into the hydroconversion of cinnamaldehyde using mechanochemically synthesized Pd/Al-SBA-15 catalysts. *Green Chem.* **2015**, *17*, 565–572.

117. Yépez, A.; Lam, F.L.Y.; Romero, A.A.; Kappe, C.O.; Luque, R. Continuous flow preparation of iron oxide nanoparticles supported on porous silicates. *ChemCatChem.* **2015**, *7*, 276–282.

118. García-Olmo, A.J.; Yépez, A.; Balu, A.M.; Prinsen, P.; García, A.; Maziere, A.; Len, C.; Luque, R. Activity of continuous flow synthesized Pd-based nanocatalysts in the flow hydroconversion of furfural. *Tetrahedron.* **2017**, *73*, 5599–5604.

119. Márquez-Medina, M.D.; Prinsen, P.; Li, H.; Shih, K.; Romero, A.A.; Luque, R. Continuous-Flow Synthesis of Supported Magnetic Iron Oxide Nanoparticles for Efficient Isoeugenol Conversion into Vanillin. *ChemSusChem.* **2018**, *11*, 389–396.

120. Yépez, A.; Prinsen, P.; Pineda, A.; Balu, A.M.; García, A.; Lam, F.L.Y.; Luque, R. A comprehensive study on the continuous flow synthesis of supported iron oxide nanoparticles on porous silicates and their catalytic applications. *React. Chem. Eng.* **2018**, *3*, 757–768.

121. Franco, A.; De, S.; Balu, A.M.; Romero, A.A.; Luque, R. Integrated Mechanochemical/Microwave-Assisted Approach for the Synthesis of Biogenic Silica-Based Catalysts from Rice Husk Waste. *ACS Sustain. Chem. Eng.* **2018**, *6*, 11555–11562.

122. Aivazoglou, E.; Metaxa, E.; Hristoforou, E. Microwave-assisted synthesis of iron oxide nanoparticles in biocompatible organic environment. *AIP Adv.* **2018**, *8*, 48201.

123. Motshekga, S.C.; Pillai, S.K.; Ray, S.S.; Jalama, K.; Krause, R.W.M. Recent trends in the microwave-assisted synthesis of metal oxide nanoparticles supported on carbon nanotubes and their applications. *J. Nanomater.* **2012**, *2012*, 51.

124. Nabiyouni, G.; Ghanbari, D.; Ghasemi, J.; Yousofnejad, A. Microwave-assisted synthesis of $MgFe_2O_4$-ZnO nanocomposite

and its photo-catalyst investigation in methyl orange degradation. *J. Nanostructures.* **2015**, *5*, 289–295.

125. García, S.; Piburn, G.W.; Humphrey, S.M. Microwave-assisted synthesis of metallic nanoparticles. *Microw. Eng. Nanomater. From Mesoscale to Nanoscale* **2016**, 263.
126. Tsuji, M. Microwave-Assisted Synthesis of Metallic Nanomaterials in Liquid Phase. *ChemistrySelect.* **2017**, *2*, 805–819.
127. Guo, Z.; Zhu, H.; Zhang, X.; Wang, F.; Guo, Y.; Wei, Y. Microwave-assisted synthesis of high-loading, highly dispersed Pt/carbon aerogel catalyst for direct methanol fuel cell. *Bull. Mater. Sci.* **2011**, *34*, 577–581.
128. Elazab, H.A.; Sadek, M.A.; El-Idreesy, T.T. Microwave-assisted synthesis of palladium nanoparticles supported on copper oxide in aqueous medium as an efficient catalyst for Suzuki cross-coupling reaction. *Adsorpt. Sci. Technol.* **2018**, *36*, 1352-1365.
129. Vinu, M.; Lin, W.C.; Senthil Raja, D.; Han, J.L.; Lin, C.H. Microwave-Assisted Synthesis of Nanoporous Aluminum-Based Coordination Polymers as Catalysts for Selective Sulfoxidation Reaction. *Polymers.* **2017**, *9*, 498.
130. Campelo, J.M.; Conesa, T.D.; Gracia, M.J.; Jurado, M.J.; Luque, R.; Marinas, J.M.; Romero, A.A. Microwave facile preparation of highly active and dispersed SBA-12 supported metal nanoparticles. *Green Chemistry*. **2008**, *10*, 853-858.
131. Luque, R.; Clark, J.H.; Gai, P.L. Efficient aqueous hydrogenation of biomass platform molecules using supported metal nanoparticles on Starbons®. *Chem. Commun*. **2009**, 5305–5307.
132. Yoshida, K.; Gonzalez-arellano, C.; Luque, R.; Gai, P.L. Efficient hydrogenation of carbonyl compounds using low-loaded supported copper nanoparticles under microwave

irradiation. *Applied Catal. A, Gen.* **2010**, *379*, 38–44.

133. Piras, C.C.; Fernández-Prieto, S.; De Borggraeve, W.M. Ball milling: a green technology for the preparation and functionalisation of nanocellulose derivatives. *Nanoscale Adv.* **2019**, *1*, 937-947.
134. James, S.L.; Adams, C.J.; Bolm, C.; Braga, D.; Collier, P.; Friščić, T.; Grepioni, F.; Harris, K.D.M.; Hyett, G.; Jones, W. Mechanochemistry: opportunities for new and cleaner synthesis. *Chem. Soc. Rev.* **2012**, *41*, 413–447.
135. Suwanboon, S.; Amornpitoksuk, P. Preparation and characterization of nanocrystalline La-doped ZnO powders through a mechanical milling and their optical properties. *Ceramics I.* **2011**, *37*, 3515–3521.
136. Song, Y.; Hormes, J.; Kumar, C.S.S.R. reviews Microfluidic Synthesis of Nanomaterials. *Small*. **2008**, *4*, 698–711.
137. Marre, S.; Jensen, K.F. Synthesis of micro and nanostructures in microfluidic systems. *Chem. Soc. Rev.* **2010**, *39*, 1183–1202.
138. Zhao, C.; He, L.; Zhang, S.; Middelberg, A.P.J. Nanoparticle synthesis in microreactors. *Chem. Eng. Sci.* **2011**, *66*, 1463–1479.
139. Pumera, M. Nanomaterials meet microfluidics. *Chem. Commun*. **2011**, *47*, 5671-5680.
140. Chen, M.N.; Mo, L.P.; Cui, Z.S.; Zhang, Z.H. Magnetic nanocatalysts: Synthesis and application in multicomponent reactions. *Curr. Opin. Green Sustain. Chem.* **2019**, *15*, 27-37.
141. Sharma, S.; Verma, A.; Kumar, A.; Kamyab, H. Magnetic Nano-Composites and their Industrial Applications. *Proceedings of the Nano Hybrids and Composites; Trans Tech Pub*l. **2018,** *20*, 149-172.
142. Gawande, M.B.; Luque, R.; Zboril, R. The Rise of Magnetically

Recyclable Nanocatalysts. *ChemCatChem* **2014**, *6*, 3312–3313.

143. Baig, R.B.N.; Nadagouda, M.N.; Varma, R.S. Magnetically retrievable catalysts for asymmetric synthesis. *Coord. Chem. Rev.* **2015**, *287*, 137–156.
144. Ma, C.; Wang, J.; Zhao, A.; Wang, Q.; Zhang, Z. Magnetic copper ferrite catalyzed homo and cross-coupling reaction of terminal alkynes under ambient atmosphere. *Appl. Organomet. Chem.* **2017**, *31*, e3888.
145. Zhao, X.N.; Hu, H.C.; Zhang, F.J.; Zhang, Z.H. Magnetic $CoFe_2O_4$ nanoparticle immobilized N-propyl diethylenetriamine sulfamic acid as an efficient and recyclable catalyst for the synthesis of amides via the Ritter reaction. *Appl. Catal. A Gen.* **2014**, *482*, 258–265.
146. Li, B.L.; Zhang, M.; Hu, H.C.; Du, X.; Zhang, Z.H. Nano-$CoFe_2O_4$ supported molybdenum as an efficient and magnetically recoverable catalyst for a one-pot, four component synthesis of functionalized pyrroles. *New J. Chem.* **2014**, *38*, 2435–2442.
147. Ma, F.P.; Li, P.H.; Li, B.L.; Mo, L.P.; Liu, N.; Kang, H.J.; Liu, Y.N.; Zhang, Z.H. A recyclable magnetic nanoparticles supported antimony catalyst for the synthesis of N-substituted pyrroles in water. *Appl. Catal. A Gen.* **2013**, *457*, 34-41.
148. Wang, D.; Astruc, D. Fast growing field of magnetically recyclable nanocatalysts. *Chem. Rev.* **2014**, *114*, 6949–6985.
149. Cheng, T.; Zhang, D.; Li, H.; Liu, G. Magnetically recoverable nanoparticles as efficient catalysts for organic transformations in aqueous medium. *Green Chem.* **2014**, *16*, 3401–3427.
150. Baig, R.B.N.; Verma, S.; Varma, R.S.; Nadagouda, M.N. Magnetic Fe@ g-C_3N_4: a photoactive catalyst for the hydrogenation of alkenes and alkynes. *ACS Sustain. Chem. Eng.* **2016**, *4*, 1661–1664.

151. García-Garrido, S.E.; Francos, J.; Cadierno, V.; Basset, J.; Polshettiwar, V. Chemistry by Nanocatalysis: First Example of a Solid-Supported RAPTA Complex for Organic Reactions in Aqueous Medium. *ChemSusChem* **2011**, *4*, 104–111.

152. Polshettiwar, V.; Luque, R.; Fihri, A.; Zhu, H.; Bouhrara, M.; Basset, J.M. Magnetically recoverable nanocatalysts. *Chem. Rev.* **2011**, *111*, 3036–3075.

153. Verma, S.; Baig, R.B.N.; Nadagouda, M.N.; Varma, R.S. Oxidative CH activation of amines using protuberant lychee-like goethite. *Sci. Rep.* **2018**, *8*, 2024.

154. Polshettiwar, V.; Varma, R.S. Nano-organocatalyst: magnetically retrievable ferrite-anchored glutathione for microwave-assisted Paal–Knorr reaction, aza-Michael addition, and pyrazole synthesis. *Tetrahedron* **2010**, *66*, 1091–1097.

155. Tadele, K.; Verma, S.; Nadagouda, M.N.; González, M.A.; Varma, R.S. A rapid flow strategy for the oxidative cyanation of secondary and tertiary amines via CH activation. *Sci. Rep.* **2017**, *7*, 16311.

156. Ostovar, S.; Prinsen, P.; Yépez, A.; Shaterian, H.R.; Luque, R. Catalytic Versatility of Novel Sulfonamide Functionalized Magnetic Composites. *ACS Sustain. Chem. Eng.* **2018**, *6*, 4586-4593.

157. Rodríguez-Padrón, D.; Jodlowski, A.D.; de Miguel, G.; Puente-Santiago, A.R.; Balu, A.M.; Luque, R. Synthesis of carbon-based fluorescent polymers driven by catalytically active magnetic bioconjugates. *Green Chem.* **2018**, *20*, 225–229.

158. Doustkhah, E.; Rostamnia, S.; Gholipour, B.; Zeynizadeh, B.; Baghban, A.; Luque, R. Design of chitosan-dithiocarbamate magnetically separable catalytic nanocomposites for greener

aqueous oxidations at room temperature. *Mol. Catal.* **2017**, *434*, 7–15.

159. Schmal, M. Heterogeneous catalysis and its industrial applications. *Springer*. **2016**.
160. Tao, F.F.; Schneider, W.F.; Kamat, P. V. Heterogeneous catalysis at nanoscale for energy applications. *John Wiley & Sons*. **2015**.
161. Ralphs, K.; Hardacre, C.; James, S.L. Application of heterogeneous catalysts prepared by mechanochemical synthesis. *Chem. Soc. Rev.* **2013**, *42*, 7701–7718.
162. Védrine, J. Heterogeneous catalysis on metal oxides. *Catalysts.* **2017**, *7*, 341.
163. Arancon, R.A.D.; Romero, A.A.; Luque, R. Applications of Microwave Chemistry in Various Catalyzed Organic Reactions. *Microwaves Catal. Methodol. Appl.* **2015**.
164. Rathi, A.K.; Gawande, M.B.; Zboril, R.; Varma, R.S. Microwave-assisted synthesis–Catalytic applications in aqueous media. *Coord. Chem. Rev.* **2015**, *291*, 68–94.
165. Kokel, A.; Schäfer, C.; Török, B. Application of microwave-assisted heterogeneous catalysis in sustainable synthesis design. *Green Chem.* **2017**, *19*, 3729–3751.
166. Cruz-Rodríguez, K.; García-Alamilla, R.; Paraguay-Delgado, F.; Cárdenas-Galindo, M.-G.; Handy, B.E.; Reyes-Gómez, J. Lewis-Brønsted induction acidity in SBA-15 modified with Zr and P. *Int. J. Mater. Res.* **2018**, *109*, 957-963.
167. Li, G.; Jiao, W.; Sun, Z.; Zhao, Y.; Shi, Z.; Yan, Y.; Feng, L.; Zhang, Y.; Tang, Y. A Scalable Upgrading of Concentrated Furfural in Ethanol: Combining Meerwein-Ponndorf-Verley Reduction with in Situ Cross Aldol Condensation. *ACS Sustain. Chem. Eng.* **2018**, *6*, 4316–4320.
168. Thunyaratchatanon, C.; Luengnaruemitchai, A.; Chollacoop, N.;

Chen, S.Y.; Yoshimura, Y. Catalytic hydrogenation of soybean oil-derived fatty acid methyl esters over Pd supported on Zr-SBA-15 with various Zr loading levels for enhanced oxidative stability. *Fuel Process. Technol.* **2018**, *179*, 422–435.

169. Skoda, D.; Styskalik, A.; Moravec, Z.; Bezdicka, P.; Pinkas, J. Templated non-hydrolytic synthesis of mesoporous zirconium silicates and their catalytic properties. *J. Mater. Sci.* **2015**, *50*, 3371–3382.
170. Socci, J.; Osatiashtiani, A.; Kyriakou, G.; Bridgwater, T. The catalytic cracking of sterically challenging plastic feedstocks over high acid density Al-SBA-15 catalysts. *Appl. Catal. A Gen.* **2019**, *570*, 218–227.
171. Kocík, J.; Samikannu, A.; Bourajoini, H.; Pham, T.N.; Mikkola, J.P.; Hájek, M.; Čapek, L. Screening of active solid catalysts for esterification of tall oil fatty acids with methanol. *J. Clean. Prod.* **2017**, *155*, 34–38.
172. Kwon, M.H.; Chae, H.J.; Park, M.B. Oligomerization of 1-hexene over designed SBA-15 acid catalysts. *J. Ind. Eng. Chem.* **2018**, *65*, 397–405.
173. Sanahuja-Parejo, O.; Veses, A.; Navarro, M. V.; López, J.M.; Murillo, R.; Callén, M.S.; García, T. Catalytic co-pyrolysis of grape seeds and waste tyres for the production of drop-in biofuels. *Energy Convers. Manag.* **2018**, *171*, 1202-1212.
174. Ledesma, B.C.; Martínez, M.L.; Beltramone, A.R. Iridium-supported SBA-15 modified with Ga and Al as a highly active catalyst in the hydrodenitrogenation of quinoline. *Catal. Today.* **2018**.
175. Zepeda, T.A.; Pawelec, B.; Infantes-Molina, A.; Yocupicio, R.I.; Alonso-Núñez, G.; Fuentes, S.; Díaz De León, J.N.; Fierro, J.L.G.

Ortho-xylene hydroisomerization under pressure on HMS-Ti mesoporous silica decorated with Ga_2O_3 nanoparticles. *Fuel.* **2015**, *158*, 405–415.

176. Zhang, T.M.; Li, D.Y.; Liu, W. Catalytic Activity of Fe-SBA-15 Prepared by Evaporation-Induced Self-Assembly (EISA) Method. *Mater. Sci. Forum.* **2017**, *898*, 1916–1922.
177. Gilanizadeh, M.; Zeynizadeh, B. Binary copper and iron oxides immobilized on silica-layered magnetite as a new reusable heterogeneous nanostructure catalyst for the Knoevenagel condensation in water. *Res. Chem. Intermed.* **2018**, *44*, 6053-6070.
178. Almáši, M.; Zeleňák, V.; Opanasenko, M.; Čejka, J. A novel nickel metal-organic framework with fluorite-like structure: Gas adsorption properties and catalytic activity in Knoevenagel condensation. *Dalt. Trans.* **2014**, *43*, 3730–3738.
179. Krishnan, R.; Panicker, G.; Krishnapillai, S. Synthesis of on resin poly (propylene imine) dendrimer and its use as organocatalyst. *Tetrahedron Lett.* **2014**, *55*, 2352–2354.
180. Huang, J.; Nolan, S.P. Efficient cross-coupling of aryl chlorides with aryl grignard reagents (Kumada reaction) mediated by a palladium/imidazolium chloride system. *J. Am. Chem. Soc.* **1999**, *121*, 9889–9890.
181. Casares, J.A.; Espinet, P.; Fuentes, B.; Salas, G. Insights into the mechanism of the Negishi reaction: ZnRX versus ZnR_2 reagents. *J. Am. Chem. Soc.* **2007**, *129*, 3508–3509.
182. Tsuji, J. Palladium reagents and catalysts: new perspectives for the 21st century. *John Wiley & Sons*. **2006**.
183. Pierrat, P.; Gros, P.; Fort, Y. Hiyama cross-coupling of chloro-, fluoro-, and methoxypyridyltrimethylsilanes: Room-temperature novel access to functional bi(het)aryl. *Org. Lett.* **2005**, *7*,

697-700.

184. García-Suárez, E.J.; Lara, P.; García, A.B.; Ojeda, M.; Luque, R.; Philippot, K. Efficient and recyclable carbon-supported Pd nanocatalysts for the Suzuki-Miyaura reaction in aqueous-based media: Microwave vs conventional heating. *Appl. Catal. A Gen.* **2013**, *468*, 59–67.

185. Elhamifar, D.; Yari, O.; Karimi, B. Highly ordered mesoporous organosilica–titania with ionic liquid framework as very efficient nanocatalyst for green oxidation of alcohols. *J. Colloid Interface Sci.* **2017**, *500*, 212–219.

186. Zhang, X.; Huang, Y.; Guo, Y.; Yuan, X.; Jiao, F. Catalytic performance of surface-silylated and phenyl-bridged Ti-containing mesoporous silica for epoxidation of propylene. *Microporous Mesoporous Mater.* **2018**, *262*, 251–257.

187. Charbonneau, L.; Kaliaguine, S. Epoxidation of limonene over low coordination Ti in Ti- SBA-16. *Appl. Catal. A Gen.* **2017**, *533*, 1–8.

188. Kang, K.K.; Rhee, H.K. Synthesis and characterization of hierarchical titanium-containing mesoporous materials with MFI crystalline structure using the gas phase recrystallization for the improvement of olefins epoxidation activity. *Microporous Mesoporous Mater.* **2018**, *257*, 202–211.

189. Li, Y.; Zhao, S.; Hu, Q.; Gao, Z.; Liu, Y.; Zhang, J.; Qin, Y. Highly efficient CoOx/SBA-15 catalysts prepared by atomic layer deposition for the epoxidation reaction of styrene. *Catal. Sci. Technol.* **2017**, *7*, 2032–2038.

190. Wu, Z.; Zhang, L.; Guan, Q.; Fu, M.; Ye, D.; Wu, T. Catalytic oxidation of toluene over Au-Co supported on SBA-15. *Mater. Res. Bull.* **2015**, *70*, 567–572.

CAPÍTULO II

Hipótesis y Objetivos

II.1. Hipótesis y objetivos.

El grupo PAIDI FQM-383 "Nanoquímica y valorización de biomasa y residuos" (NANOVAL), está desarrollando actualmente nuevos protocolos para optimizar técnicas alternativas para la síntesis de nanopartículas soportadas y su aplicación a procesos de valorización de biomasa y residuos, para la obtención de compuestos de alto valor añadido con métodos medioambientales sostenibles. Esta Tesis Doctoral se integra en su totalidad en las diferentes líneas de investigación del grupo FQM-383 (NANOVAL).

De forma clara y precisa las distintas hipótesis y objetivos a desarrollar en la presente Memoria de Tesis Doctoral se describen a continuación:

Hipótesis I:

Los procesos de flujo continuo pueden otorgar una serie de ventajas importantes en la síntesis de nanomateriales si lo comparamos con procesos de síntesis de nanomateriales tradicionales descritos en la bibliografía. Éstos nos permiten alcanzar numerosos beneficios como son la simplicidad de preparación y operación, control del proceso (velocidad de flujo, temperatura de trabajo, etc.), flexibilidad, mayor productividad y condiciones de reacción controlables, proporcionándonos un enfoque alternativo comparativamente práctico para la síntesis de nanopartículas soportadas a escala industrial.

Los materiales magnéticos suponen un gran avance debido a la eficiente separación de estos del medio de reacción, favoreciendo un fácil reciclado del material y su posterior reutilización tras la reacción catalítica.

Objetivo I:

Desarrollo de nanocatalizadores magnéticos mediante procesos de flujo continuo, soportando nanopartículas de hierro sobre el aluminosilicato Al-SBA-15. Posteriormente, se caracterizan mediante las técnicas de difracción de rayos-X (DRX), microscopia electrónica de barrido (SEM-EDX), microscopia electrónica de transmisión (TEM), susceptibilidad magnética, espectrometría de masas con acoplamiento inductivo (ICP-MS) y la técnica cromatográfica de pulsos para determinar su acidez superficial utilizando como moléculas sonda piridina y 2,6-dimetilpiridina. Así mismo, la actividad catalítica de los nanomateriales se lleva a cabo en la reacción de oxidación del isoeugenol a vainillina.

Todos estos objetivos se han alcanzado y han sido descritos de forma específica en el trabajo "Continuous flow synthesis of supported magnetic iron oxide nanoparticles for efficient isoeugenol conversion to vanillin" (ChemSusChem, 2018, 11, 389-396, Apartado III. 1.).

Hipótesis II:

El desarrollo de una química más benigna con el medio ambiente ha impulsado la búsqueda de nuevos materiales que puedan ser empleados en catálisis a través de una preparación rápida, económica y eficiente, sustituyendo así los catalizadores tradicionales, que requieren de procesos tediosos y caros. La combinación de nanopartículas metálicas y materiales mesoporosos es una alternativa para obtener materiales que cumplan los requisitos de la Química Verde y remplacen procesos catalíticos homogéneos tradicionales.

Las metodologías empleadas para la síntesis y estabilización de nanopartículas metálicas soportadas sobre materiales mesoporosos han sido muy variadas, destacando la irradiación en microondas, la ablación por láser y la utilización de metodologías de sonicación asistidas por ultrasonidos, así como, el empleo de procesos de molienda mecanoquímica para la preparación de dichos nanomateriales. No obstante, la demostración y/o naturaleza de los procesos mecanoquímicos ha sido cuestionada debido a la dificultad que presenta dicho procedimiento para explicar con datos críticos y/o mecanismos propuestos dichos procesos mecanoquímicos.

Objetivo II:

Obtención de materiales magnéticos con nanopartículas de hierro soportadas sobre aluminosilicatos mesoporosos del tipo Al-SBA-15 sirviéndonos de la técnica de molienda mecanoquímica en un solo paso "*one-pot*", en el que se ha sustituido el ácido propiónico (disolvente orgánico tóxico) por residuos de biomasa (residuos lignocelulósicos) que nos permiten obtener las fases de óxido de hierro magnéticos, representando una alternativa más sostenible para la síntesis de estos materiales. Tras la preparación de dichos nanomateriales se ha realizado la caracterización de sus propiedades texturales y estructurales empleando la técnica de adsorción/desorción de N_2, difracción de rayos-X (XRD), espectroscopía fotoelectrónica de rayos-X (XPS), microscopía electrónica de barrido (SEM-EDX), susceptibilidad magnética, etc.

Se han utilizado los nanomateriales magnéticos como catalizadores en las reacciones de oxidación del isoeugenol y alcohol vainillínico para contrastar sus propiedades catalíticas. Toda esta temática ha sido abordada en el trabajo "*Mechanochemically synthesized supported magnetic Fe-nanoparticles as catalysts for efficient vanillin production"* (Catalysts, 2019, 9, 290, Apartado III. 2.).

Hipótesis III:

La incorporación de centros funcionales y activos en materiales mesoporosos para aplicaciones catalíticas sigue siendo un desafío en catálisis heterogénea, especialmente para sistemas altamente activos y estables con cargas de metal bajas. Las metodologías convencionales (por ejemplo, la impregnación hasta humedad incipiente, la deposición-

precipitación, el anclaje/inmovilización, etc.), generalmente, han demostrado proporcionar materiales activos, pero la posibilidad de controlar la carga y la localización de los centros activos, así como su estabilidad, a menudo se ve comprometida. La mecanoquímica surgió como una metodología alternativa prometedora para incorporar centros activos de forma simple, rápida y eficiente, dando lugar a un procedimiento de síntesis de nanomateriales altamente activos, estables y reproducibles, obteniéndose finalmente catalizadores multifuncionales avanzados para diversas aplicaciones en Química Fina.

Sin embargo, hasta la fecha no se ha explorado la posibilidad de utilizar MOFs ("Metal-Organic Frameworks") en pequeñas cantidades como precursores para generar especies activas en materiales porosos. En principio, la presencia de ligandos orgánicos y la variedad de metales que pueden estar presentes en los MOFs los convierte en un material de partida potencialmente interesante para diseñar nanopartículas altamente dispersas y activas en distintos soportes mesoporosos.

Objetivo III:

Incorporación de aluminio a partir de diferentes fuentes (Al-MOFs e isopropóxido de aluminio) en silicatos mesoporosos del tipo SBA-15 y MCM-41 mediante técnicas de molienda mecanoquímica e impregnación. Una vez obtenidos dichos materiales se ha procedido al estudio de sus propiedades químico-físicas mediante las técnicas de resonancia magnética nuclear (RMN), difracción de rayos-X (XRD), microscopía electrónica de barrido (SEM-EDX), espectrometría de masas con acoplamiento inductivo (ICP-MS), técnica cromatográfica de pulsos empleando piridina y dimetilpiridina como moléculas sonda, adsorción/desorción de N_2, etc.

Además, se ha investigado la utilización como catalizadores de los nanomateriales sintetizados en las reacciones de oxidación del isoeugenol, alcohol bencílico y sulfuro de difenilo. Todos estos aspectos se encuentran desarrollados en el artículo "*Post-synthetic mechanochemical incorporation of Al species into the framework of porous materials: towards more sustainable redox chemistries*" (ACS Sustainable Chemistry and Engineering, 2019, Aceptado para su publicación, Apartado III. 3.).

II.2. Hypotheses and Objectives

The PAIDI group FQM-383 Nanochemistry and biomass and waste valorisation (NANOVAL), is currently developing new protocols to optimize alternative techniques for the synthesis of supported nanoparticles and their application to biomass and waste valorisation processes, to obtain high-added value compounds using low impact environmental technologies. This PhD Thesis is integrated in its entirety in the different research lines of the FQM-383 group (NANOVAL).

Clearly and precisely the different hypotheses and objectives to be pursued in this PhD Thesis are described in this section:

Hypotheses I:

The continuous flow processes can give us important advantages in the nanomaterials syntheses in comparison with traditional syntheses processes described in the literature. The continuous flow processes allow us to achieve many benefits such as the simplicity of preparation and operation, process control (flow rate, working temperature, etc.), flexibility, increased productivity and controllable reaction conditions, providing a practical approach for the synthesis of supported nanoparticles at industrial scale.

The magnetic materials have made a breakthrough due to the efficient separation of these from the reaction medium, favoring easy recycling of the material and its subsequent reuse after the catalytic reaction.

Objective I:

Development of magnetic nanocatalysts under continuous flow processes, supporting iron oxide nanoparticles over aluminium silicate Al-SBA-15. Subsequently, their characterization using X-ray diffraction techniques (XRD), scanning electron microscopy (SEM-EDX), transmission electron microscopy (TEM), magnetic susceptibility, inductive coupling plasma-mass spectrometry (ICP-MS) and pulsed chromatographic technique, to determinate the superficial acidity, using pyridine and 2,6-dimethylpyridine as probe molecules. Furthermore, the catalytic activity of the nanomaterials is tested in the oxidation reaction of isoeugenol to vanillin.

This objective has been achieved and described in detail in the scientific publication "*Continuous flow synthesis of supported magnetic iron oxide nanoparticles for efficient isoeugenol conversion to vanillin*" (ChemSusChem, 2018, 11, 389-396, Chapter III. 1.).

Hypotheses II:

The development of more benign chemistry with the environment has driven the search for new materials that can be used in catalysis through a fast, economic and efficient preparation, thus replacing the traditional catalysts, which require tedious and expensive processes. The combination of metal nanoparticles and mesoporous materials is an attractive alternative to obtain materials following the Green Chemistry principles that can replace traditional homogeneous catalytic processes.

The methodologies used for the synthesis and stabilization of metal nanoparticles have been very diverse, highlighting microwave irradiation, laser ablation and the use of ultrasonic-assisted sonication methodologies, as well as the use of grinding processes mechanochemistry for the preparation of above mentioned. However, the demonstration and/or nature of the mechanochemical processes has been questioned due to it is difficulty to be explained with critical data and/or proposed mechanisms.

Objective II:

Obtention of magnetic materials with iron supported nanoparticles on mesoporous aluminosilicates materials such as Al-SBA-15, using the one-pot mechanochemical milling technique, in which propionic acid (toxic organic solvent) has been replaced by biomass residues (lignocellulosic residues), that allows us to obtain the magnetic iron oxide phases, representing a more sustainable route for the synthesis of these materials. After the preparation of above mentioned materials, the characterization of the textural and structural properties was performed using techniques such as adsorption/desorption of N_2, X-ray diffraction

(XRD), X-ray photoelectron spectroscopy (XPS), scanning electron microscopy (SEM-EDX), magnetic susceptibility, etc.

After their characterization, the magnetic nanocomposites were tested in oxidation reactions of isoeugenol and vanillin alcohol to investigate their catalytic activity. All this thematic is developed in the scientific paper "*Mechanochemically synthesized supported magnetic Fe-nanoparticles as catalysts for efficient vanillin production*" (Catalysts, 2019, 9, 290, chapter III. 2.).

Hypotheses III:

The incorporation of functionalities and active sites in mesoporous materials for catalytic applications remains a challenge in the field, especially for highly active and stable systems with low metal loading. Conventional methodologies (impregnation, deposition-precipitation, anchoring/immobilization, etc.) generally proved to provide active materials, but the possibility of controlling the loading and location of the active sites, as well as their stability, it is often compromised. Mechanochemistry emerged as one of those promising alternative methodologies to provide a simple and fast but efficient process, highly active, stable and reproducible to advanced functional materials for diverse applications in Fine Chemistry.

However, until now the possibility to use MOFs ("Metal-Organic Frameworks") at low weight % as a precursor to generate active species in porous materials it is unexplored. In principle, the presence of organic linkers and the variety of metals that can be present in the MOF makes them a potentially interesting platform to design highly dispersed nanoparticles over a wide range of mesoporous supports.

Objective III:

Incorporation of aluminium from different sources (AlMOFs and aluminium isopropoxide) in mesoporous material as SBA-15 and MCM-41 by mechanochemical grinding and impregnation. Once these materials have been obtained, we proceeded to study their structural properties using techniques such as nuclear magnetic resonance (NMR), X-ray diffraction (XRD), scanning electron microscopy (SEM-EDX), inductive coupling mass spectroscopy (ICP-MS), pulsed chromatographic technique using pyridine and 2,6-dimethylpyridine as probe molecules, adsorption/ desorption of N_2, etc.

Furthermore, the use as catalysts of synthesized nanomaterials in the oxidation reactions of isoeugenol, benzyl alcohol and diphenyle sulfide has been investigated. All these aspects are developed in the scientific publication entitle "*Post-synthetic mechanochemical incorporation of Al species into the framework of porous materials: towards more sustainable redox chemistries*" (ACS Sustainable Chemistry and Engineering, 2019, Accepted for publication, Chapter III. 3.).

CAPÍTULO III

Resultados y Discusión

III. 1. Continuous flow synthesis of supported magnetic iron oxide nanoparticles for efficient isoeugenol conversion to vanillin.

Abstract.....85

Introduction.....85

Results and Discussion.....88

Conclusions.....103

Experimental Section.....104

Acknowledgements 108

References.....108

Supporting Information……112

CHEMISTRY & SUSTAINABILITY
CHEMSUSCHEM
ENERGY & MATERIALS

ChemPubSoc Europe

Continuous flow synthesis of supported magnetic iron oxide nanoparticles for efficient isoeugenol conversion to vanillin

María Dolores Márquez-Medina,[a] Pepijn Prinsen,[a] Hangkong Li,[b] Kaimin Shih,[b] Antonio Ángel Romero,[a] and Rafael Luque*,[a]

[a] Departamento de Química Orgánica, Universidad de Córdoba, Campus de Rabanales, Edificio Marie Curie (C-3), Ctra Nnal IV, km. 396, E-14014 Córdoba, Spain.

[b] Department of Civil Engineering, The University of Hong Kong, Haking Wong Building, Pokfulam Road, Hong Kong HK 852, China.

* Correspondence to: q62alsor@uco.es (RL)

DOI: 10.1002/cssc.201701884

Magnetic iron oxide nanoparticles supported on Al-SBA-15, prepared in continuous flow mode, are highly active and selective for the disruptive oxidation of isoeugenol to vanillin using hydrogen peroxide as the oxidant.

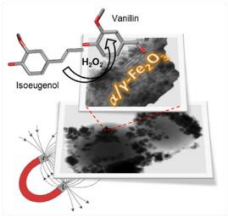

*María Dolores Márquez-Medina, Pepijn Prinsen, Hangkong Li, Kaimin Shih, Antonio Ángel Romero, Rafael Luque**
Page No. – Page No.
Continuous flow synthesis of supported magnetic iron oxide nanoparticles for efficient isoeugenol conversion to vanillin.

Abstract

This work presents the simple synthesis of iron oxide nanocatalysts supported on mesoporous Al-SBA-15 using a continuous flow set-up. The magnetic nanomaterials were tested as catalysts in the oxidative disruption of isoeugenol by using hydrogen peroxide as a green oxidant, featuring high activity (63-88% conversion) and good selectivity to vanillin (44-68%). The catalytic systems exhibited good magnetic properties when synthesised under continuous-flow conditions at temperatures not exceeding 190 °C, which is important to enable their efficient separation from reaction mixtures. The use of microwave irradiation reduced the times of reaction drastically but exerted negative effects on the catalyst reusability.

Introduction

An important part of current research in green chemistry focus on the transition towards more sustainable manufacturing processes that efficiently utilize resources and raw feedstocks, reduce waste streams and avoid the use of toxic and hazardous materials. To bring this into practice, the use of recyclable catalysts has proven to be very useful for a wide range of chemical processes. [1-3] The deposition of highly active catalytic particles onto various organic or inorganic supports is probably the most efficient strategy to recover catalysts. In this context, nanocatalysts recovery by magnetic fields could enable more efficient separation compared with conventional decantation and filtration, especially when nanocatalysts are expensive (i.e., noble metal) and difficult to separate. [4-5]

The incorporation of an iron oxide core in the nanocatalysts increases its density and thus also its recovery efficiency by conventional separation

methods. The synthesis of magnetic nanoparticles (MNPs) was proposed for several applications and is currently a hot topic in future catalyst design practices.[6-10] However, highly active MNPs are rather difficult to synthesize owing to their tendency to aggregate and/or coalesce (sintering). This is important, because the nanosized of iron particles can have a significant impact on their catalytic activities. One method to overcome this problem is to support MNPs on mesoporous solids, which in turn also improves the stability of the metal or metal oxide nanoparticles.[11] In particular, mesoporous SBA-15 materials are attractive porous materials thanks to their well-ordered characteristic structure of hexagonal mesopores with large specific surface area (> 900 m^2 g^{-1}).[12,13] Recently, Gawande et al. reported a relatively simple protocol for the synthesis of MNPs, using a continuous flow process in which Fe_2O_3 nanoparticles are deposited on aluminosilicates in a single step. This setup can provide greater process control, flexibility and productivity and has practical potential as an alternative to industrial scale synthesis processes based on traditional procedures.

Vanillin can be isolated from natural source derived extracts, including vanillin beans and pods, pine woods (e.g. Pinus tabuliformis) and roasted coffee. [16] It can also be obtained from lignins through depolymerization and subsequent conversion and/or isolation. The increasing global demand of vanillin can be not be met anymore by the supply of vanilla orchid pods as the sole source. [17] Nowadays, only *ca.* 1 % of the global production of vanillin is derived from vanilla pods; the majority is produced synthetically using, e.g. lignin[18] and (iso)eugenol[19] as starting materials. The commercial value of vanillin extracted from vanilla pod varies between 1200-4000 USD kg^{-1}, excluding inflation.[20] Although the oxidative disruption of isoeugenol (Scheme 1) was already reported in several occasions before the year 2000, significant results were reported after 2000 by Shimoni et al. using *Bacillus subtilis* sp.

strains as biocatalysts,[21] resulting in vanillin production with 12-14 mol% yields (0.6-0.9 g L^{-1} after 24-48 h at 30 °C). Enzymatic conversion by lipoxygenases was also reported by Markus et al., [22] with yields varying between 10 and 15 mol%. Major improvements (32.5 g L^{-1} vanillin after 72 h at 37 °C) were reported in 2005 by Zhao et al. using *Bacillus fusiformis* strains.[23] Although these biocatalytic transformations are very attractive from an environmental point of view, they present some constrains such as limited selectivity and stability, along with rather long reaction times and the need for nutrient media. Other catalytic systems were proposed by Herrmann et al. using 1 mol% methyltrioxorhenium with short reaction times (10 min.), however, anhydrous hydrogen peroxide was required in 3:1 molar excess and MnO_2 was added to prevent further oxidation to vanillic acid.[24] More recently, Gusevskaya et al. reported the catalytic conversion of isoeugenol, with H_2O_2 as the oxidant in combination with $(n\text{-butyl})_4NVO_3$ and pyrazine-2-carboxylic acid, reaching 50 mol% yields in acetonitrile at 40 °C after 2 h.[25]

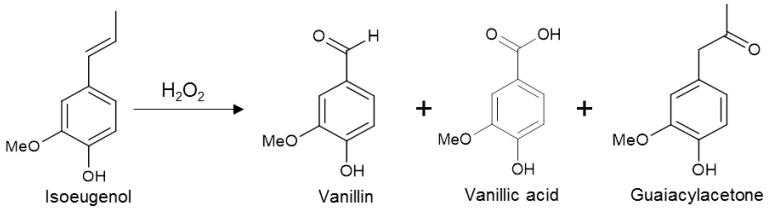

Scheme 1. Oxidative disruption of isoeugenol to vanillin and side products.

Results and Discussion

A series of magnetic nanoparticle (MNPs) catalysts was synthesized in a continuous flow set up (Scheme 2) using iron oxide and Al-SBA-15 as the support.

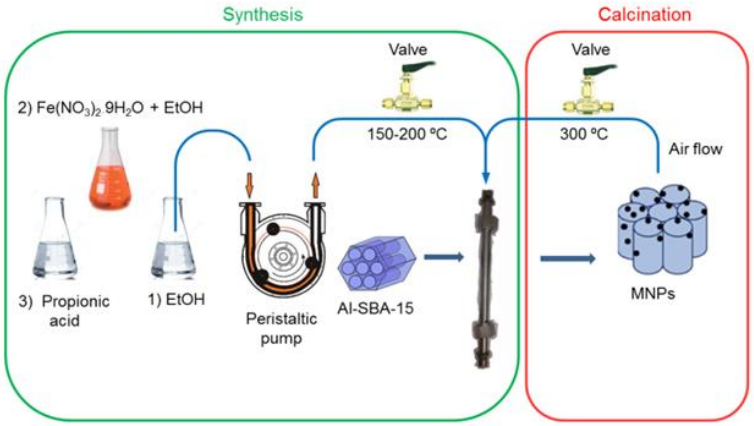

Scheme 2. Continuous flow synthesis of magnetic nanoparticles (MNPs).

This synthesis method promotes the deposition of iron oxide particles on the outer surface of Al-SBA-15 and promotes a close interaction of Fe with Al rather than forming iron oxide particles within Al-SBA-15 pores. A catalyst prepared through deposition of iron oxide on Al-SBA-15 by classic wet impregnation (FeNMag-WI) was additionally synthesized for comparative purposes. The MNP synthesis temperature was varied between 150 and 210 ºC to study its effect on the magnetic properties (Table 1) and the incorporation of iron (Table 2) into the final materials. FeNMag-WI was comparably non-magnetic (on a macroscopic basis) as classic wet impregnation proceeds at room temperature. The largest magnetic susceptibility was reached when the synthesis temperature was set at 170 ºC, whereas magnetic properties were lost at an apparent cut-off temperature of 195 ºC.

Table 1. Magnetic properties of the synthesized MNPs.

Catalyst	Synthesis temperature (ºC)	Magnetic susceptibility χ_m ($\times 10^{-6}$ m^3 kg^{-1})
FeMag-150	150	73
FeMag-160	160	140
FeMag-170	170	206
FeMag-180	180	161
FeMag-190	190	190
FeNMag-195	195	[a]
FeNMag-200	200	[a]
FeNMag-205	205	[a]

[a] Non-magnetic.

Table 2. Elemental analysis according to SEM/EDX and ICP-MS.

Catalyst	SEM/EDX (%)			ICP-MS (%)		
	Al	Si	Fe	Al	Si	Fe
FeMag-150	-	-	-	0.8	28.2	8.4
FeMag-160	1.0	23.6	21.4	0.8	22.2	11.7
FeMag-170	1.3	30.3	18.2	0.8	22.3	13.3
FeMag-180	1.1	28.9	17.1	-	-	-
FeMag-190	1.2	29.3	19.8	-	-	-
FeNMag-195	1.1	28.3	18.2	0.7	17.4	19.0
FeNMag-200	0.5	16.7	48.1	-	-	-

The elemental composition results showed an iron (Fe) content in the whole materials in the range of 8 to 19 wt% (inductively coupled plasma mass spectrometry, ICP-MS), whereas the Fe content at the surface was higher, with values ranging from 17 to 48 wt% (SEM/energy-dispersive X-ray, EDX). The Fe content in the material prepared by classic wet impregnation (FeNMag-WI), in contrast, did not show this surface enrichment effect. On the other hand, it was observed that the Fe content increased with higher synthesis temperatures, coinciding with the collapse of the SBA-15 structure in the materials synthesized at temperatures above 195 ºC.

The structure of the synthesized materials was studied by XRD (Figure 1), shows the whide- and low-angles diffraction patternesog samples synthesized at different temperatures. Low angle diffractograms despict the presence of three peaks, one intense peak at low 2Θ values (reflection line d_{100}) and two weaker peaks at higher angles (reflection lines d_{110} and d_{200}), characteristic of the SBA-15 structures.[26] The decrease in the intensity of these lines in FeNMag-200 indicates that the Al-SBA-15 support underwent structural deterioration upon Fe incorporation. The high iron content in FeNMag-200 (Table 2) was most probably related to a partial collapse of the aluminosilicate SBA-15 as a mesopores could be partly blocked by the high amount of iron oxide deposited on the aluminosilicate surface. These hypotheses were in good agreement with the wide angle XRD pattern in the materials in which the broad peak around 22° almost completely disappeared. Next to Al-SBA-15, peaks from Fe_2O_3 were also visible. Diffraction lines from iron oxide in FeNMag-WI (Figure S1 in the Supporting Information) were comparably hardly detectable, a most plausible indication of a highly dispersed iron oxide nanoparticles.

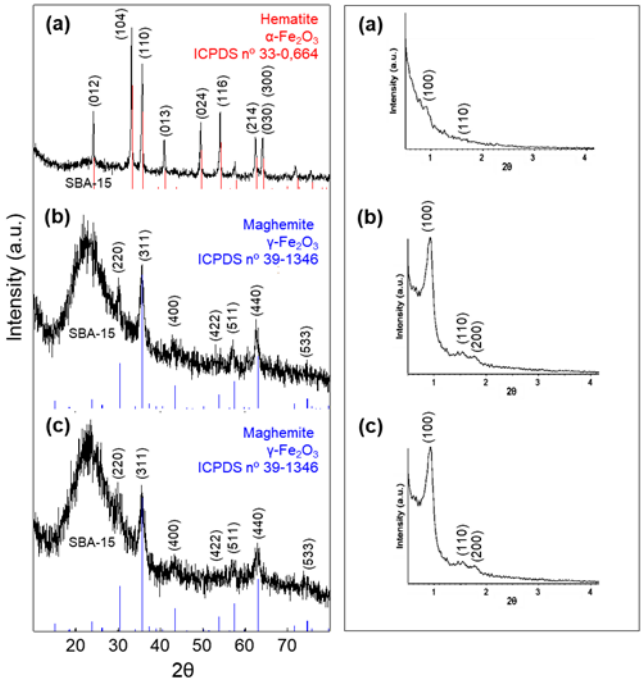

Figure 1. XRD patterns of (a) FeNMag-200, (b) FeMag-190 and (c) FeMag-170.

The iron oxide diffraction pattern of the FeNMag-200 could be indexed as a hematite crystal structure (α-Fe_2O_3, ICPDS No. 33-0,664) (Figure 1a), whereas XRD patterns of the FeMag-190 and FeMag-170 are more difficult to assign. All diffraction peaks of maghemite and magnetite crystals are located within 1° difference. [27] The diffraction patterns of iron oxide FeMag-190 and FeMag-170 samples (Figures 1b and 1c) are likely to be maghemite crystal (γ-Fe_2O_3, JCPDS No. 39-1346). However, the absence of magnetite cannot be excluded at the present signal-to-noise ratio and resolution since iron oxide nanoparticles typically exhibit noisy diffractograms, [28]. Crystal sizes of the non-magnetic (FeNMag-200) versus magnetic samples (FeMag-190 and FeMag-170) were measured to be 30-40 nm and < 10 nm, respectively. FeNMag-200 and FeMag-170 samples were analysed by using a quantitative XRD technique, allowing the quantification of the amorphous material

content. The content of the hematite phase in the FeNMag-200 sample was 50 % by weight, whereas the content of the magnetic phase was less than 10 % by weight in FeMag-170. The adsorption-desorption isotherms of the SBA-15 aluminosilicate support and those of the most representative synthesized nanocatalysts are of type IV (see Figure 2 in the Supporting Information), characteristic of mesoporous materials. All synthetized solids exhibited relatively high specific surface area (≥ 300 m^2 g^{-1}), with pore sizes in the 7-8 nm range (Table 3). FeNMag-WI prepared by wet impregnation showed a similar specific surface area and pore volume, but with a significantly reduced pore diameter. These results pointed to the deposition of a large part of the iron oxide nanoparticles into the pores of Al-SBA-15. Importantly, both the specific surface area and pore volume decreased with an increase of the temperature employed in the continuous-flow synthesis, whereas the pore diameter was retained. This fact can be explained by the increasing iron oxide content (see Table 2), which contributes in weight and partially obstructs the entrance to micropores in mesoporous void spaces.

Table 3. Porosity and acidity analysis of the synthesized (magnetic) nanoparticles.

Catalyst	S_{BET} (m^2 g^{-1})	Average pore diameter (nm)	Average pore volume (mL g^{-1})	Surface acidity (μmol g^{-1})	
				Brønsted	Total
AlSBA-15	800	7.6	0.9	85	61
FeMag-150	470	7.3	0.5	58	39
FeMag-160	470	7.8	0.5	36	30
FeMag-170	350	7.7	0.4	52	35
FeMag-180	310	7.5	0.4	40	40
FeMag-190	300	6.9	0.3	48	45
FeNMag-195	320	7.6	0.4	31	35

Surface acidity properties (Table 3), as studied by the chromatographic pulse technique, pointed out no drastic differences in total acidity for the different synthesized nanocatalysts, whether magnetic or non-magnetic. In some cases, the number of Brønsted acid centers exceeded the number of total acid centers, as 2,6-dimethylpyridine (DMPY) is more basic than pyridine (PY; pK_b= 7.4 and 8.8, respectively). The measured magnetic susceptibility ranged between 70×10^{-6} and 210×10^{-6} m^3 kg^{-1} for magnetic nanocatalysts, consistent with the maghemite content in the materials (10-15 wt%). Pure magnetite nanoparticles generally show larger magnetic susceptibilities, approximately 500×10^{-6} m^3 kg^{-1}.[29] These susceptibility values were large enough for the magnetic nanocatalysts to be magnetically recovered from the reaction mixtures after reaction.

Yepez et al. previously reported TEM images of pure Al-SBA-15 nanoparticles.[30] In comparison, the TEM images (Figure 2) of

representative catalysts synthetized in the present study show that the ordered porous structure of the Al-SBA-15 support was preserved upon Fe incorporation in continuous flow. Hematite (FeNMag-200) and maghemite (FeMag-170) nanoparticles were homogeneously distributed on the aluminosilicate support. High resolution images of a single particle in the FeNMag-200 material along the plane zone (010) depict a periodic spacing of 0.368 nm, consistent with the *d* spacing corresponding to α-Fe_2O_3 plane, indicative of single crystal with good crystallinity The periodic spacing between the 0.489 nm bands is also consistent with the corresponding *d* spacing of the {111} plane of γ-Fe_2O_3.

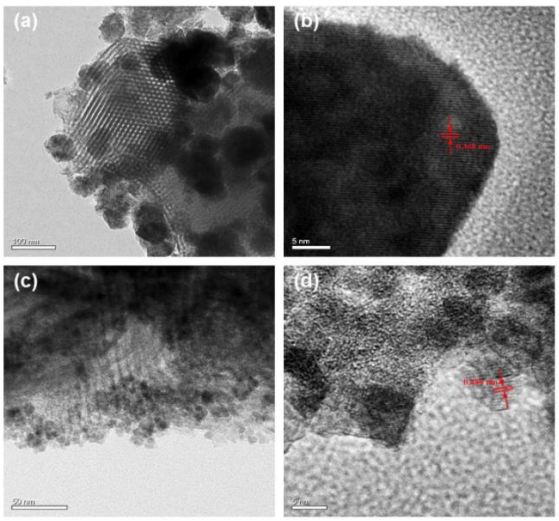

Figure 2. TEM & HRTEM images of FeNMag-200 (a-b) and FeMag-170 (c-d) catalysts.

The synthesized MNPs were employed as heterogeneous catalyst in the selective oxidative disruption of isoeugenol in liquid phase by using aqueous hydrogen peroxide as a green oxidant, both at room temperature and at 90 ºC (conventional heating). Figure 3 depicts the conversion of

isoeugenol and vanillin selectivity observed after 40 min. and after 24 h. Blank runs (no catalyst) and using Al-SBA-15 provide a very low total conversion (<20 %). The use of pure iron oxide nanoparticles (Fe) or a mixture of Fe with Al-SBA-15 comparatively led to significant conversions in the system, pointing to iron oxide as catalytically active phase. The presence of Al-SBA-15 did not significantly influence the final result compared with Fe alone, with exception of a higher selectivity to vanillin achieved at room temperature after 24 h. This may be the result of a caging effect of iron oxide and isoeugenol inside the Al-SBA-15 pores, leading to lower amounts of side products.

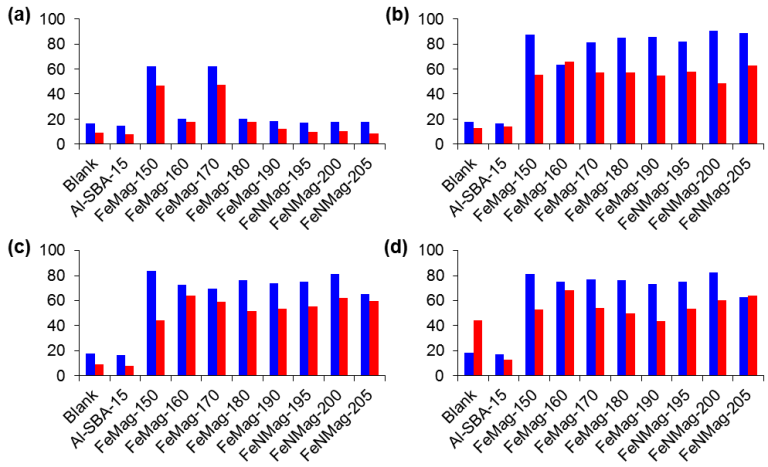

Figure 3. Isoeugenol conversion (blue, mol%) and selectivity to vanillin (red, mol%) using Fe(N)Mag catalysts at 20 °C after (a) 40 min. and (b) 24 h and at 90 °C after (c) 40 min. and (d) 24 h.

GC/MS analysis of the products showed the presence of a diphenyl ether structure as the main side product in all the experiments, produced by oxidative radical coupling of quinone methide tautomers of isoeugenol (or derivates).

As opposed to room temperature experiments, the advantage of heating related to an already close to the equilibrium conversion and selectivity after 40 min. (compared with data after 24 h). Still, interesting results were obtained at room temperature after 24 h, with conversions ranging between 63 and 91 % at vanillin selectivities of approximately ≥ 50 %. Whereas the conversions increased consistently with reaction time up to 24 h, vanillin selectivity increased during the first 8 h of reaction, to then remain practically constant at approximately 50 %. At high temperature, the selectivity was slightly reduced after 24 h compared with 40 min., an indication that further oxidation to vanillic acid or other undesired processes took place. FeNMag-WI catalyst in contrast, prepared by wet impregnation, yielded vanillin amounts in the range of the results obtained with pure iron oxide (Fe) or with mixed Fe + Al-SBA-15 (Figure 3). No clear relationship was found between Fe content and Fe_2O_3 phases present in materials (maghemite or hematite) when comparing conversion and selectivity obtained with all synthesized nanocatalysts under continuous flow conditions at different temperatures. The catalytic activity was more related to their Brønsted acidity. The fact that there was no direct relationship between catalytic activity and Fe_2O_3 phase together with the low selectivity to vanillin observed for Al-SBA-15 leads us to propose active centers similar to those described previously by our research group, [31] which showed a Fe-Al synergistic effect on Fe_2O_3 nanoparticles supported on SBA-15 type aluminosilicates, with excellent catalytic activities in oxidations of benzyl alcohol to benzaldehyde. This effect is most appreciable (Figure 3) when comparing vanillin yields obtained for FeMag-170 and those obtained with physical mixtures of both compounds separately (Fe + Al-SBA-15) as catalyst. In addition to conventional heating, microwave irradiation was also employed, showing beneficial effects (apart from faster and homogeneous heating). Outstandingly, the

equilibrium seemed to be reached almost completely already after 5 min. when microwave heating was utilised (Table 4), giving 60-80 % conversion and 54-65 % selectivity. The differences with conventional heating after 24 h were small (< 10 %). Somewhat lower selectivity was observed after 15 min. owing to possible side reactions.

Table 4. Fe(N)Mag catalyzed isoeugenol conversion and selectivity to vanillin using microwave irradiation.

Catalyst	Conversion (mol%)		Selectivity (mol%)	
	5 min.	15 min.	5 min.	15 min.
Blank	18	19	10	17
Al-SBA-15	15	16	10	9
FeMag-150	73	75	59	58
FeMag-160	77	75	65	64
FeMag-170	80	81	56	57
FeMag-180	69	70	61	57
FeMag-190	68	70	58	54
FeNMag-195	68	67	62	56
FeNMag-200	60	61	59	65
FeNMag-205	62	57	54	55

Table 5. Comparison of catalytic performance of FeMag200 catalyst with previously reported ones for the selective oxidation of isoeugenol to vanillin.

Catalyst	Conversion (mol%)	Selectivity (mol%)	Yield (mol)	Ref.
$PhI(OAc)_2$-NaY[a]	-	-	43	[32]
Nocardia iowensis whole cells[b]	-	-	60	[33]
TiO_2 (P25 Degussa)[c]	84	9	8	[34]
CoTPyP/TN[d]	99	72	71	[35]
$(n\text{-Bu})_4NVO_3$ + PCA[e]	71	70	50	[25]
FeMag-180[f]	85	57	49	This work

[a] 0.3 M isoeugenol in 6 mL acetonitrile, 2 eq. of catalyst, 130 °C, 5 min. [b] 0.01 M isoeugenol in 2 mL aqueous buffer, 40 g L^{-1} cells, 130 °C 32 h. [c] 0.5 mM isoeugenol in 150 mL aqueous phase, 0.8 g L^{-1} catalyst, 20 °C, 2 h. [d] 0.03 mM isoeugenol in 10 mL acetonitrile, 1 mol% cobalt (as cobalt porphyrin/lithium taeniolite), 50 °C, 24 h, 3 bars pure O_2. [e] 0.2 M isoeugenol in 0.9 mL acetonitrile, 2 eq. H_2O_2, 0.025 mol% $(n\text{-Bu})_4NVO_3$ + 0.05 mol% PCA, 80 °C, 2 h. [f] 0.5 M isoeugenol in 8 mL acetonitrile, 2.3 eq. H_2O_2, 12.5 mol% catalyst, 20 °C, 24 h.

Nanocatalysts presented in this work outperform previously reported results, at least in cost-effectiveness, when comparing results with previously reported data on the catalytic oxidation of vanillin by using oxygen or hydrogen peroxide as oxidants (Table 5). Still, the high

amount of operational variables makes the comparison not straightforward. Gusevskaya et al. obtained similar vanillin yields (50 mol%) under comparable conditions, although they used a homogeneous and environmentally unfriendly catalyst in aproximatly 50 times less quantity (mol% of (n-Bu)$_4$NVO$_3$ + pyrazine-2-carboxylic acid (PCA)). [25]

Finally, as the iron nanoparticles were recovered efficiently by activation in an external magnetic field, the re-usability of the magnetic catalysts was assessed (Figure 4). Although the magnetic properties were retained in the recovered catalysts, both conversion and selectivity significantly dropped, particularly after 4-5 uses. The spent FeMag-190 recovered after 4 cycles of 24 h at room temperature exhibited significantly lower porosity than the fresh catalyst (Table 3), 150 m^2g^{-1} specific surface area, 0.4 nm pore diameter and 0.3 mLg^{-1} pore volume. Comparably, vanillin yield was stable over three reutilization experiments using conventional heating (90 ºC) whereas the yield dropped drastically when using microwave irradiation. This indicates that, although beneficial for the reactions kinetics, microwave irradiation had detrimental effects on catalyst performance (both activity and selectivity).

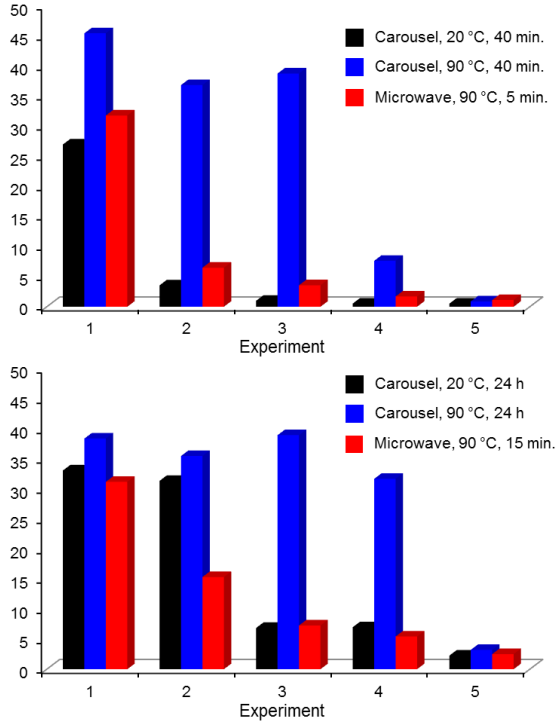

Figure 4. Vanillin yield (mol%) obtained with FeMag-190 catalyst over 5 re-utilization experiments for the catalytic oxidation of isoeugenol at 20 ºC and at 90 ºC (using both conventional heating and microwave irradiation).

In an attempt to provide further insights into catalyst deactivation, the reused catalyst was analyzed by thermogravimetric/differential thermal analysis (TG-DTA) and attenuated total reflection (ATR, Figure 5). The ATR spectrum showed absorption bands characteristic of vanillin-like aromatics including O-H stretching (3330 cm^{-1}), C=O stretching (1675 cm^{-1}), and the characteristic stretching vibration absorption of benzene ring corresponding to three bands at 1513, 1432 and 797 cm^{-1}. The band originated from the bending vibrations of phenolic OH around 1250 cm^{-1}

was more difficult to identify as it was partially overlapped with the broad band from Si-O bonds (1062 cm^{-1}) in Al-SBA-15. Although the small band at 1600 cm^{-1} is representative of C=C stretching in isoeugenol, the amount adsorbed is negligible as any other bands arising from isoeugenol are hardly observable. In addition to these results, TG/DTA experiments (Figure 5a, see also supporting information) showed a significant mass loss (ca. 4-10%) in the 200-400ºC range accompanied by an endothermic peak in the DTA spectra, possibly related to the observed aromatic compounds in ATR experiments. Importantly, a second small mass loss at higher temperatures (400-500ºC, Figure S3 in the supporting information) is also present and likely to be caused by the formation of heavier molecular weight aromatics as side products from the oxidation reaction.

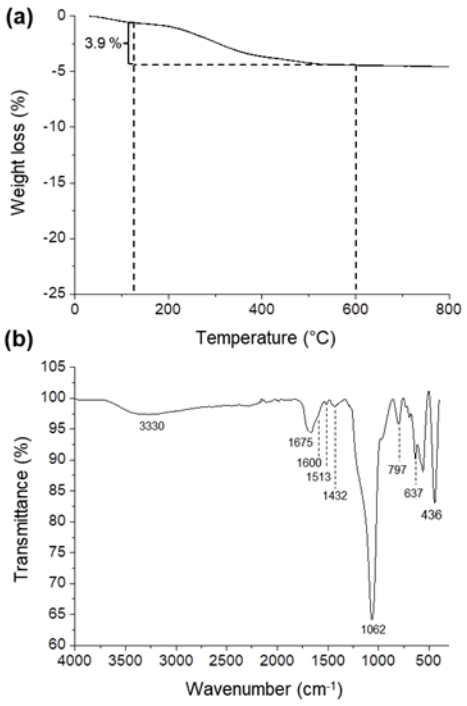

Figure 5. (a) TGA analysis and (b) ATR analysis of deactivated FeMag-190 catalyst recovered after 5 catalytic reuses.

It can be thus concluded that the observed deactivation in the catalytic experiments is mostly attributable to adsorption of aromatics-including vanillin and heavier molecular weight compounds-on the catalyst surface (fouling). The FeMag-190 spent catalyst (after five reuses) was regenerated by recalcination at 300 ºC (in air, 2 h). XRD analysis (Figure S4 in the supporting information) pointed out the presence of the key diffraction lines corresponding to the iron oxide phase with the inherently amorphous nature of the aluminosilicate material. Interestingly, catalytic experiments of regenerated spent catalysts at 300ºC (e.g. FeMag-190) showed a remarkable recovery in the initial catalytic activity after regeneration (Figure 4), which in principle may be fully recovered upon thermal treatment at 550-600ºC (according to

TG/DTA results, Figure 5a, a temperature at which all organics are fully removed). However, thermal regeneration was not conducted at such a high temperature to preserve the magnetic properties of the materials. Nevertheless, the regeneration studies clearly showed that the catalytic activity drop owing to surface fouling could be solved by thermal treatment of the catalysts (300ºC) after which most of the initial catalytic activity in the systems was recovered. These findings also pointed out the strong deactivating role of adsorbed aromatic compounds on the surface after subsequent reuses, a phenomenon that also supports the observed strong deactivation of Fe-containing systems under microwave irradiation.

Conclusions

The synthesis of iron nanoparticles supported on Al-SBA-15 has been successfully performed using a simple and reproducible continuous flow method. Synthesized nanomaterials exhibited suitable good magnetic properties when the synthesis temperature stayed below an apparent cut-off temperature of 195 °C. Nanocatalysts obtained provided excellent catalytic activities and promising selectivities (>50%) to vanillin in the selective oxidation of isoeugenol using hydrogen peroxide as green oxidant. Optimum results pointed to an 85% conversion of 0.5 M isoeugenol with 57% selectivity to vanillin after 24 h at room temperature. Reaction times were drastically reduced to 5-15 min under microwave irradiation, however with negative effects on catalyst re-usability. The catalyst deactivation was related to surface fouling, with thermally treated regenerated catalysts (300ºC) able to recover over 80% of the initial catalytic activity of fresh catalysts.

Experimental Section

The synthesis of the mesoporous aluminosilicate Al-SBA-15 was carried out following the procedure described by Stucky and co-workers. [36] The triblock co-polymer Pluronic P123 was used as directing agent and dissolved in aqueous HCl (2M, pH 1.5) for 2 h at room temperature. After complete dissolution, tetraethyl orthosilicate (25 mmol) was used as the silica source and the corresponding amount of aluminum isopropoxide (10 mmol) was slowly added. The mixture was stirred for 24 h at room temperature. Subsequently, the mixture was submitted to hydrothermal treatment in an oven at 100 °C for 24 h. The obtained solid was filtered off, dried and subsequently calcined under nitrogen atmosphere at 600 °C for 2 h, and then under air atmosphere for 4 h. The obtained SBA solids (Si/Al molar ratio 20) were recovered and stored.

The preparation of magnetic nanoparticles (MNPs) was carried by using a continuous flow setup (Scheme 2). First, a stainless steel reactor (15 cm × 1 cm i.d.) was filled with Al-SBA-15 support (ca. 3.0 g) and fixed between two quartz wool stoppers above and beneath to prevent the displacement of the solids. The reactor was equipped with two stainless steel filters, one at the entrance and another one at the exit to avoid obstructions. The synthesis started by injecting ethanol at 0.5 mL $min.^{-1}$ over 45 min. while reaching the desired synthesis temperature. Subsequently, the ethanol flow was changed to a saturated solution of $Fe(NO_3)_2.9H_2O$ (precursor salt, Sigma Aldrich) in ethanol, at 0.5 mL $min.^{-1}$ over 1 h. After completion, propionic acid was pumped at a flow of 0.5 mL$min.^{-1}$ for 45 min. Then, after closing the valve in this loop, an air flow of 30 mL $min.^{-1}$ was injected for approximately 3 h while the reactor was submitted to a programmed temperature ramp of 1 °C $min.^{-1}$ to reach a final temperature of 300 °C, which then was kept constant for 1 h. FeNMag-WI was prepared by wet impregnation at room temperature using an Fe_2O_3 load corresponding to the same Fe content as determined

by ICP-MS analysis in the FeMag-170 catalyst. We assumed that in wet impregnation 100 % of the iron was retained in the FeNMag-WI material. The Fe_2O_3, Al-SBA-15 and the FeNMag-WI materials were also treated with propionic acid which was added dropwise in batch, followed by calcination in air using an oven with the same temperature program as MNP solid in the continuous flow synthesis.

MNP solids obtained were characterized by X-ray diffraction (XRD), nitrogen adsorption-desorption porosimetry, magnetic susceptibility, scanning electron microscopy (SEM), inductively coupled plasma mass spectroscopy (ICP-MS), (high resolution) transmission electron microscopy and pulse chromatography (to study the surface acid properties). XRD spectra were recorded on a Bruker D8 X-ray diffractometer (2θ range= 10-80°) in the Bragg-Brentano geometry and in reflection mode, using a Cu Xray tube, a rotating platform, a monochromatic primary beam and a high sensitivity detector. In addition, some samples were analyzed using an advanced D8 X-ray diffractometer (Bruker AXS GmbH, Germany) with a LYNXEYE detector and Cu Kα irradiation at 40 kV and 40 mA, using a count time of 1 second for phase identification and 1 second for phase quantification. The quantitative analysis (QXRD) was carried out using TOPAS 4.2 software (Bruker AXS). All samples were mixed with 20 wt% CaF_2 (Merck, Germany) as internal standard for the quantification of the amorphous content. The elemental composition of the synthesized materials was studied in two ways. First, the surface of the solids was analyzed with an Inca Energy 250 microanalysis system using an JEOL JSM 6300 Scanning Electron Microscope equipped with a window type Si/Li detector (ATW2), in the boron to uranium detection range (137 eV to 5.9 keV). Secondly, the quantitative elemental analysis of the solids was determined with ICP-MS, using an Elan DRC-e

equipment (Perkin Elmer SCIEX, Waltham, USA). The surface morphologies of the particles were examined by TEM and HRTEM using FEI Tecnai G2 20 S-TWIN and 2010F JEOL electron microscopes, respectively. The nitrogen adsorption-desorption isotherms were recorded at -196 °C using a Micromeritics ASAP 2000 automatic analyzer. The samples were degassed for 24 h at 100 °C under vacuum ($p < 10\text{-}20$ Pa) prior to analysis. The linear part of the Brunauer-Emmett-Teller (BET) equation (relative pressure between 0.05 and 0.30) was used to determine the specific surface area. The pore size distribution was calculated by using the adsorption branch of the adsorption/desorption isotherm, applying the method of Barrett-Joyner-Halenda (BJH).[37] The magnetic susceptibility χm was determined at room temperature using an MS2 magnetic susceptibility meter (Bartington Instruments Ltd., UK) equipped with a MS2B dual-frequency (470 and 4700 Hz) laboratory sensor. χm is equal to the ratio of the magnetization M within the material to the applied magnetic field strength H. This ratio, strictly speaking, is the volumetric susceptibility, because magnetization essentially involves a certain measure of magnetism (dipole moment) per unit volume. It is a measure of the magnetic response of a material to an external magnetic field. The determination of the surface acidity was carried out at 250 °C, with pyridine (PY) and 2,6-dimethylpyridine (DMPY) as titration bases for total and Brønsted acidity, respectively. The bases were introduced (2, 3, 4, 5 and 6 μL) in a GC injector coupled to a stainless steel column (10 cm × i.d. 2 mm) packed with the analyte (40-70 mg), which in turn was coupled to a 50 cm chromatographic column containing 5 wt% polyphenylether in Chromosorb AW-MCS 80/100. The bases remaining after elution through the packed column were quantified by gas chromatography equipped with a flame ionization detector (GCFID). Thermogravimetric analysis (TGA) was carried out in equipment using

approximately 15 mg sample under dynamic air atmosphere (10 mL min^{-1}). Attenuated total reflectance infrared Fourier transform spectroscopy (ATR-IR) spectra were recorded by using a Spectrum TwoTM instrument (Perkin Elmer, Waltham, USA), from 4000 to 450 cm^{-1} with a resolution of 4 cm^{-1}.

The reactions with isoeugenol were carried out by conventional heating on the one hand and by microwave heating at the other hand. The conventional heated reactions were performed using a multiple parallel synthesis system (Carrusel Reaction Station™, Radleys Discovery Technologies Ltd., UK) equipped with magnetic stirring at 1000 rpm. The experiments were run at 20 and at 90 °C, using 5 mmol isoeugenol and 11.7 mmol hydrogen peroxide (1.2 mL of 33 % w/v H_2O_2 in water) in 8 mL acetonitrile with catalyst (100 mg), which were added when the desired reaction temperature was reached (time = 0). For the experiments with Al-SBA-15+Fe_2O_3-170, the corresponding amounts of Al-SBA-15 (56.7 mg) and Fe_2O_3-170 (43.3 mg) were used (to reach an equal Fe content in the reaction as compared to the experiment with FeMag-170 catalyst, based on the Fe content according to the ICP-MS analysis in Table 2). The experiments with FeNMag-WI were carried out with 100 mg catalyst, as it contained the same amount of Fe as in FeMag-170. The reactions using microwave heating were carried out in a CEM-Discover focused microwave, controlled and monitored by a computer in standard mode ("Discover") under pressure which allows control of the irradiation power, temperature and pressure. The reactants used were isoeugenol (1.25 mmol) and H_2O_2 (2.9 mmol) in acetonitrile (2 mL), with catalyst (25 mg) at 90 °C, by using 300 W irradiation power. In all experiments, the reaction temperature was reached after approximately 1 min without any significant overheating. The reaction mixture was analyzed before, during and after the reaction by gas chromatography on an Agilent

Technologies 7890 A GC System equipped with a Petrocol™ DH column (100 m x 0.25 mm x 0.50 μm i.d.) and a FID detector. The temperature of the column was set at 200 ºC (70 min. hold time) and the temperature of the injector and detector at 300 ºC. The nitrogen gas flow was set at 3 mL min^{-1}. The retention times of isoeugenol and vanillin were 33.4 and 30.2 min., respectively. Isoeugenol calibration was carried out in the 2.00-60.00 g L^{-1} range (R^2= 0.98). The reaction mixture was also analyzed with GC/MS. The standard deviation on conversion and selectivity, as determined from two independent experiments with catalyst FeNMag-200 at 90 ºC was 7 and 2 % after 40 min. and 24 h, respectively. The corresponding deviations on selectivity were 3 and 8 %, respectively. The recycle experiments were carried out identically. The catalyst was recovered with a hand magnet, washed with acetonitrile and dried at 100 ºC. Regeneration of the spent catalyst was performed by recalcination under identical conditions as used in their synthesis (300 ºC, air, 2 h).

Acknowledgements

R.L. gratefully acknowledges MINECO as well as FEDER funds for funding under project CTQ2016-78289-P and finanacial support from the University of Cordoba (Spain).

References

[1] F. Lu, J. Ruiz, D. Astruc, *Tetrahedron Lett.* **2004**, *45*, 9443–9445.

[2] D. Astruc, F. Lu, J. Ruiz, *Angew. Chem. Int. Ed.* **2005**, *44*, 7852-7872.

[3] D. Astruc, *Transition-metal nanoparticles in catalysis*, Wiley-VCH, Weinheim, Germany**, 2008**.

[4] M. Iranmanesha J. Hulliger, *Chem. Soc. Rev.* **2017**, Advance Article, DOI: 10.1039/C7CS00230K.

[5] Q. M. Kainz, O. Reiser, *Acc. Chem. Res.* **2014**, *47*(2), 667–677.

[6] A. H. Lu, E. L. Salabas, F. Schüth, *Angew. Chem. Int. Ed*. **2007**, *46*, 1222-1244.

[7] S. Shylesh, V. Schünemann, W. R. Thiel, *Angew. Chem. Int. Ed.* **2010**, *49*, 3428–3459.

[8] Y. Zhu, L. P. Stubbs, F. Ho, R. Liu, C. P. Ship, J. A. Maguire, N. S. Hosmane, *ChemCatChem* **2010**, *2*, 365–374.

[9] V. Polshettiwar, R. Luque, A. Fihri, H. Zhu, M. Bouhrara, J. M. Basset, *Chem. Rev.* **2011**, *111*, 3036–3075.

[10] R. B. N. Baig, R. S. Varma, *Chem. Commun*. **2013**, *49*, 752–770.

[11] N. I. Cuello, V. R. Elías, E. Winkler, G. Pozo-López, M. I. Oliva, G. A. Eimer, *J. Magn. Magn. Mater.* **2016**, *407*, 299–307.

[12] C. T. Kresge, M. E. Leonowicz, W. J. Roth, J. C. Vartuli, J. S. Beck, *Nature* **1992**, *359*, 710–712.

[13] J. S. Beck, J. C. Vartuli, W. J. Roth, M. E. Leonowicz, C. T. Kresge, K. D. Schmitt, C. T.-W. Chu, D. H. Olson, E. W. Sheppard, S. B. McCullen, J. B. Higgins, J. L. Schlenkert, *J. Am. Chem. Soc.* **1992**, *114*, 10834–10843.

[14] M. B. Gawande, Y. Monga, R. Zboril, R. K. Sharma, *Coord. Chem. Rev.* **2015**, *288*, 118–143.

[15] M. B. Gawande, R. Luque, R. Zboril, *ChemCatChem* **2014**, *6*, 3312–3313.

[16] M. J. W. Dignum, J. Kerler, R. Verpoorte, *Food Rev. Int.* **2001**, *17*, 119-120.

[17] N. J. Walton, A. Narbad, C. B. Faulds, G. Williamson, *Curr. Opin. Biotechnol.* **2000**, *11*, 490–496.

[18] M. Fache, B. Boutevin, S. Caillol, *ACS Sustainable Chem. Eng.* **2016,** *4*(1), 35–46.

[19] A. Franco, S. De, A. M. Balu, A. Garcia, R. Luque, *Beilstein J Org. Chem.* **2017**, *13*, 1439-1445.

[20] N. J. Walton, M. J. Mayer, A. Narbad, *Phytochemistry* **2003**, *63*, 505–515.

[21] E. Shimoni, U. Ravid, Y. Shoham, *J. Biotechnol*. **2000**, *78*, 1-9.

[22] P. H. Markus, A. L. J. Peters, R. Roos, Process for the preparation of phenylaldehydes. European patent EP 542348 (1992).

[23] L. Q. Zhao, Z. -H. Sun, P. Zheng, L. -L. Zhu, *Biotechnol. Lett.* **2005**, *27*, 1505–1509.

[24] W. A. Herrmann, T. Weskamp, J. P. Zoller, R. W. Fischer, *J. Mol. Catal. A.-Chem.* **2012**, *363-364*, 140-147.

[25] E. V. Gusevskaya, L. Menini, L. A. Parreira, R. A. Mesquita, Y. N. Kozlov, G. B. Shul'pin, *J. Mol. Catal. A.-Chem.* **2012**, *363-364*, 140-147.

[26] L. Y. Shi, Y. M. Wang, A. Ji, L. Gao, Y. Wang, *J. Mater. Chem.* **2005**, *15*, 1392–1396.

[27] F. Fajaroh, H. Setyawan, A. Nur, I. W. Lenggor, *Adv. Powder Technol.* **2013**, *24*, 507-511.

[28] G. C. Papaefthymou, E. Devlin, A. Simopoulos, D. K. Yi, S. N. Riduan, S. S. Lee, J. Y. Ying, J. Physical Review B **2009**, *80*, 024406, 1-9.

[29] C. Peters, M. J. Dekkers, *Phys. Chem. Earth* **2003**, *28*, 659-665.

[30] A. Yepez, J. M. Hidalgo, A. Pineda, R. Černý, P. Jíša, A. Garcia, A. A. Romero, R. Luque, *Green Chem.* **2015**, 17, 565-572.

[31] A. M. Balu, A. Pineda, K. Yoshida, J. M. Campelo, P. L. Gai, R. Luque, A. A. Romero, *Chem. Commun.* **2010**, *46*, 7825–7827.

[32] H. Marquez Alvarez, D. P. Barbosa, A. Tinoco Fricks, D. A. G. Aranda, R. H. Valdés, O. A. C. Antunes, *Org. Process Res. Dev.* **2006**, *10*, 941-943.

[33] R. Seshadri, A. S. Lamm, A. Khare, J. P.N. Rosazza, *Enzyme Microb. Technol.* **2008**, *43*, 486–494.

[34] V. Augugliaro, G. Camera-Roda, V. Loddo, G. Palmisano, L. Palmisano, F. Parrino, M. A. Puma, *Appl. Catal., B* **2012**, *111–112*, 555– 561.

[35] I. Badria Adilina, T. Hara, N. Ichikuni, S. Shimazu, *J. Mol. Catal. A: Chem.* **2012**, *361–362*, 72–79.

[36] D. Zhao, J. Feng, Q. Huo, N. Melosh, G. H. Fredrickson, B. F. Chmelka, G. D. Stucky, *Science* **1998**, *279*, 548-542.

[37] E. P. Barrett, L. G. Joyner, P. P. Halenda, *J. Am. Chem. Soc.* **1951**, *73*, 373-380.

CHEMISTRY & SUSTAINABILITY
CHEMSUSCHEM
ENERGY & MATERIALS

Supporting Information

Continuous flow synthesis of supported magnetic iron oxide nanoparticles for efficient isoeugenol conversion to vanillin

María Dolores Marquez,[a] Pepijn Prinsen,[a] Hangkong Li,[b] Kaimin Shih,[b] Antonio Angel Romero,[a] and Rafael Luque*,[a]

cssc_20170884_sm_miscellaneous_information.pdf

Figure S1 shows the XRD pattern of FeWI, prepared by wet impregnation of Fe on Al-SBA-15 at room temperature

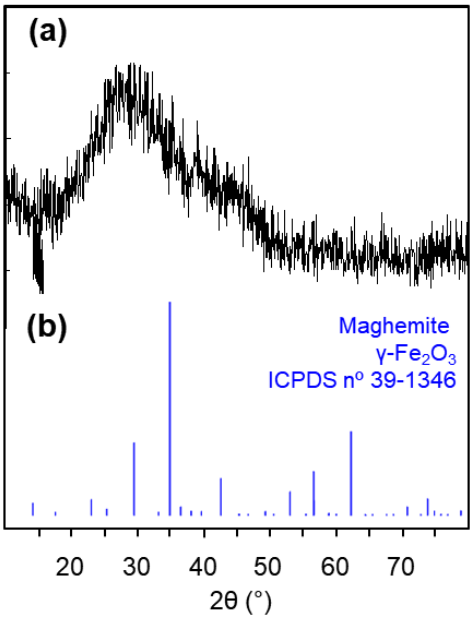

Figure S1. XRD patterns of (a) FeWI and (b) pure maghemite.

Figure S2 show the nitrogen adsorption-desorption isotherms of the mesoporous support (Al-SBA-15) and the samples FeMag-150, FeMag-180 and FeMag-195 (iron oxide particles supported on Al-SBA-15 synthesized at 150, 180 and 195 °C).

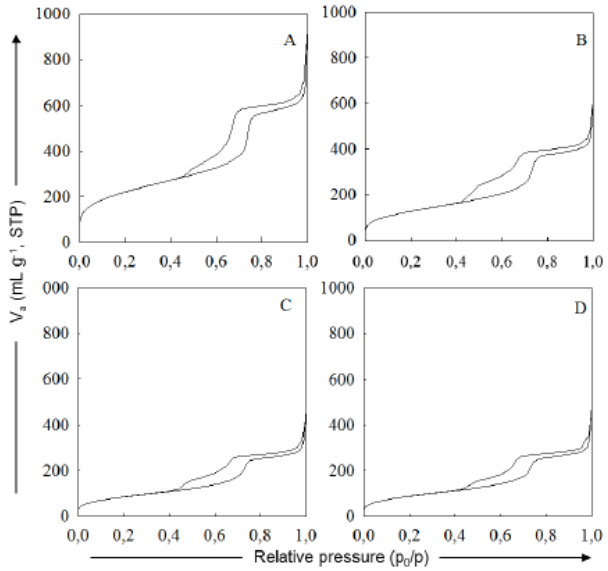

Figure S2. Nitrogen adsorption-desorption isotherms of (a) Al-SBA-15, (b) FeMag-150, (c) FeMag-180 and (d) FeMag-195.

Figure S3 Shows a detailed TG-DTA spectra of FeMag-190 where the corresponding mass losses explained in the manuscript can be clearly seen.

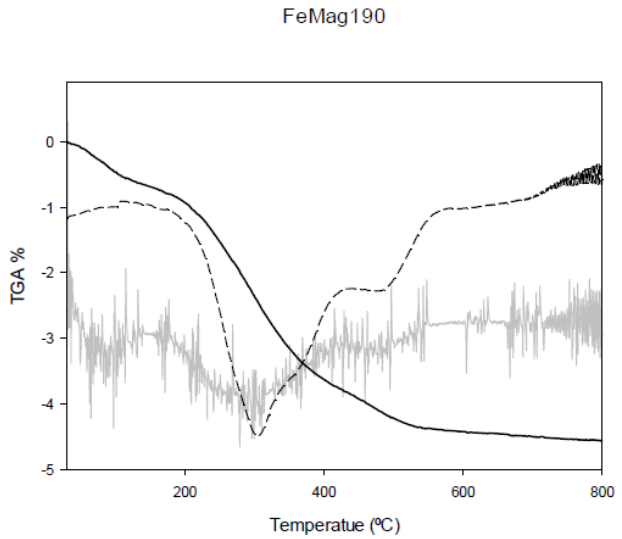

Figure S3. TG-DTA patterm of FeMag-190.

Figure S4 despicts the XRD pattern of the FeMag-190 catalyst recovered after 24 h reaction at 90 °C and regenerated by recalcination at 300° C.

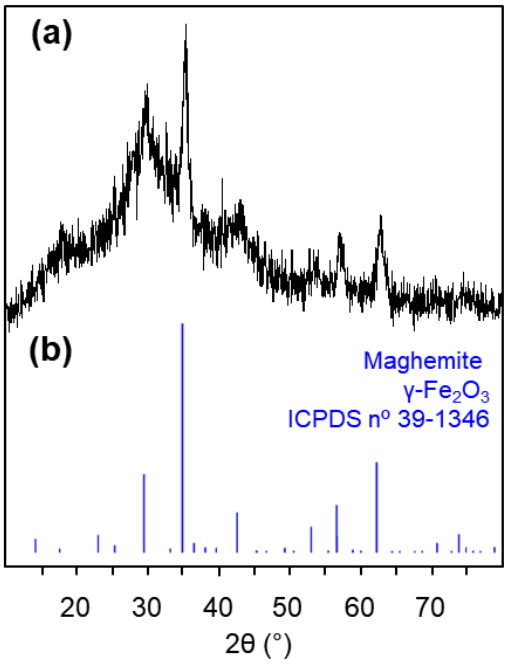

Figure S4. XRD patterns of (a) regenerated FMag-190 catalyst and (b) pure maghemite.

III. 2. Mechanochemically synthesized supported magnetic Fe-nanoparticles as catalysts for efficient vanillin production.

Abstract. 118

Introduction. 118

Results and discussion. 121

Experimental. 133

Conclusions 137

Acknowledgments. 137

References 138

Supporting Information 145

catalysts

MDPI

Mechanochemically synthesized supported magnetic Fe-nanoparticles as catalysts for efficient vanillin production.

M. Dolores Márquez-Medina [1], Daily Rodríguez-Padrón [1], Alina M. Balu [1], Antonio A. Romero [1], Mario J. Muñoz-Batista [1]*, Rafael Luque [1,2,]*

[1] Departamento de Química Orgánica, Universidad de Córdoba, Campus de Rabanales, Edificio Marie Curie (C-3), Ctra Nnal IV, km. 396, E-14014 Córdoba, Spain.

[2] Scientific Center for Molecular Design and Synthesis of Innovative Compounds for the Medical Industry, People's Friendship University of Russia (RUDN University), 6 Miklukho-Maklaya str., 117198 Moscow, Russia.

* Correspondence to: q62alsor@uco.es (RL)

DOI: 10.3390/catal9030290

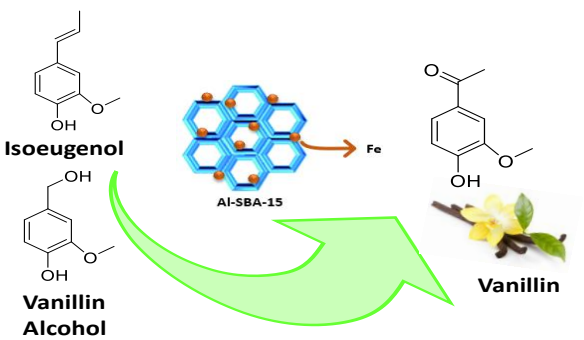

Abstract.

Magnetically separable nanocatalysts were synthesized by incorporating iron nanoparticles on a mesoporous aluminosilicate (Al-SBA-15) through a mechanochemical grinding pathway in a single step. Noticeable, magnetic features were achieved by employing biomass waste as carbon source, which additionally may confer high oxygen functionalities to the resulting material. The resulting catalysts were characterized using X-ray diffraction, X-ray Photoelectron Spectroscopy, Transmission electron microscopy, Scanning electron microscopy, porosimetry and magnetic susceptibility. The magnetic nanocatalysts have been tested in both the selective oxidative cleavage reaction of isoeugenol and vanillyl alcohol to vanillin. As a result, magnetic nanocatalysts have demonstrated high catalytic activity, chemical stability and enormous separation/reusability qualities. The origin of catalytic properties behaviours and its relationship with the iron oxide precursor were analysed in terms of the chemical, morphological and structural properties of the samples. Such analysis allows thus to highlight, superficial concentration of the iron entities and the interaction with Al as key factors to obtain a good catalytic response.

Introduction.

Currently, environmental issues related to the global warming [1], which can have a negative impact on human safety, together with the limited reserves of crude oil have motivated the scientific community in the design of sustainable alternatives for materials, chemicals, energy and fuels production [2,3]. A change is required from the traditional concept of process efficiency focused on chemical performance, considering the premises of sustainable development for the replacement of fossil resources by renewable raw materials. In this regard, biomass

valorization represents an attractive option to supply the chemicals demand by using an abundant and renewable source [4,5]. Lignocellulosic biomass, mainly composed of lignin, cellulose and hemicellulose, can lead to terpenes, carbohydrates, fatty esters and aromatics. In this sense, biomass has recently been subject of numerous studies, attracting great interest as most abundant renewable raw material of organic carbon available on the planet and as a perfect substitute for oil in the production of fuels and chemical products [6–8]. These facts represent at the same time an interesting and challenging topic for the chemical industry [9]. Therefore, the use of catalytic systems can pave the way for an optimum biomass valorization [10,11].

Particularly, the catalytic valorization of biomass-derived compounds such as eugenol, isoeugenol and ferulic acid has been broadly studied through the past years [12–15]. The molecules may replace petrol-based intermediates, such as guaiacol and glyoxylic acid, for the synthesis of vanillin [16]. The latter compound is a well-known flavoring agent, popular in the food, cosmetic and pharmaceutical industries. Several catalytic strategies, employing different transition metal oxides have been explored for the conversion of isoeugenol and vanillyl alcohol to vanillin [17,18]. In particular, supported and non-supported iron oxides have been extensively applied to isoeugenol valorization [19–21]. However, much more efforts should be devoted in order to optimize the catalytic systems and in turn to enhance the catalytic performance in terms of conversion, selectivity and stability.

Nanostructured heterogeneous catalysts possess advantages related to the recovery and reuse thus contributing to increase the sustainable credentials of chemical processes [22,23]. In this regard, the use of stable, active and recyclable materials has proven to be very useful for a wide range of chemical processes [24–26]. The deposition of highly

active nanoparticles on various organic or inorganic supports is probably the most effective strategy for the reuse of nanocatalysts [27]. The design of magnetic nanocatalyts facilitates a more efficient separation by using a magnetic field, compared to conventional decanting and filtration techniques [28–34].

Iron oxide based nanomaterials may possess different magnetic features depending on their crystalline phase (e.g. hematite, maghemite and magnetite) [35]. Magnetic iron oxides are generally obtained by liquid phase methods, which involve additional solvents and reagents [36]. A novel technique for the synthesis of magnetic nanocatalysts is mechanical grinding (mechanochemistry). In general, this method can avoid the use of toxic organic solvents that could be released to the environment and increase the effectiveness and reproducibility in the synthesis of the materials. Mechanochemistry has become a promising alternative for the synthesis of heterogeneous catalysts [37]. Regarding the synthesis of magnetic iron oxide, mechanochemical methods require the use of propionic acid, as previously described by our research group [38,39]. Propionic acid together with the iron precursor gives rise to an iron carboxylate compound, which can be further converted by calcination into crystalline magnetic iron oxide phases. Replacement of such reagent by a lignocellulosic residue, not only results in the desired iron oxide phase but also could represent a sustainable alternative for these type of materials. Also, textural properties constitute a key factor for a good catalytic performance, such as porosity. Therefore, employing mesoporous supports including MCM-41, MCM-48, SBA-15 and Al-SBA-15 for transition metal oxides can provide access to advanced systems with optimum porosity for catalytic applications [40-42]. Through this work, two strategies will be explored for biomass valorization, namely, towards chemical and materials, revealing the

underexploited potential of such type of residues to ameliorate the environmental impact of chemical processes.

Results and discussion.

The proposed methodology resulted to be effective for the preparation of such catalytic systems, pointing out that mechanochemical protocols represent a green and remarkable pathway to synthesize advanced nanomaterials. Table S1 (Supplementary Materials) summarize the materials synthesized. Particularly, the employment of a biomass residue as carbon source present outstanding advantages, since it allows the formation of a magnetic phase without employing other chemicals, such as propionic acid, commonly used for the synthesis of magnetic iron oxide [17]. Nanomaterials synthesized employing iron perchlorate and iron chloride did not show magnetic susceptibility. On the other hand, concentrations higher than 40% for iron citrate and higher than 30% for iron nitrate showed remarkable magnetic features. Magnetic susceptibility values were found in the range of $70\text{-}210 \cdot 10^{-6} m^3 Kg^{-1}$ (Table S1, Supplementary Materials). These values are consistent with the content of maghemite in the support since the pure maghemite nanoparticles generally show magnetic susceptibilities of approximately $500 \cdot 10^{-6} m^3 Kg^{-1}$ [43]. These susceptibility values allow the magnetic separation from the reaction mixture.

After functionalization with iron oxide, XRD analysis of the samples prepared with iron citrate (FeMagC) showed a typical diffraction pattern that could be correlated with a mixture of hematite (as the major component) and maghemite phases (Figure 1). The diffraction peaks at 2θ = 30.2°, 33.2º, 35.7°, 40.9º, 49.5°, 54.1°, 57.3°, 62.4° and 64.1º correspond to (200), (104), (110), (113), (024), (116), (112), (214) and

(300) crystallographic planes of hematite phase, respectively [41]. In addition, maghemite related peaks were observed at 2θ = 24.2º, 43.3º, suggesting the presence of both crystalline phases with a marked hematite prominence. Remarkably, the employment of iron nitrate (FeMagN) resulted in a) formation of pure maghemite (2θ = 30.2º, 35.5º, 43.5º, 57.5º and 63.0º associated with (200), (311), (400), (511) and (440)) and b) loss of crystallinity [44,45]. The presence maghemite phase in the samples facilitate further recovery and reuse of the synthesized catalytic systems.

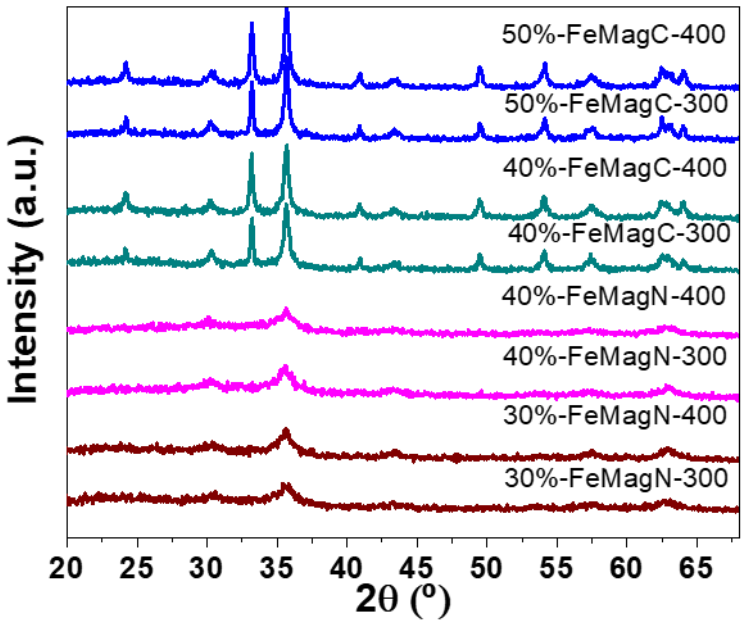

Figure 1. X-ray diffraction (XRD) patterns of selected samples.

Nitrogen adsorption-desorption analysis of selected materials displayed a mesoporous structure in all the cases, as can be observed in Figure 2A and 2B, corresponding with the type IV isotherms, according to the International of Pure and Applied Chemistry (IUPAC) classification,

showing an acute inflection in the P/P_0 range of 0.5-0.8 [46]. A decrease of surface area was observed after incorporation of iron oxide nanoparticles. Brunauer-Emmett-Teller (BET) surface areas around 240-340 m^2g^{-1} were obtained (Table 1). Such values are in good agreement with those previously reported for functionalized Al-SBA-15 samples [47]. In addition, pore diameters and pore volume also showed a decrease of around 50% after functionalization (Table 1). These results can be understood from a partial occlusion of Al-SBA-15 pores in presence of the Fe-oxide co-catalyst. Elemental information about the components of samples was obtained with the help of SEM-EDX and energy-dispersive X-ray spectroscopy (EDX). EDX analysis (Table 1) corroborated the presence of the expected elements Al, Si and Fe and no significant differences were observed among the studied samples, as may be envisaged by their similar chemical composition (for same iron salt concentration) when different precursors were used. EDX analysis also allowed the identification of bulk N concentration in the samples, however, very low concentrations (in comparison to superficial concentration obtained by X-ray photoelectron spectroscopy (XPS)) and, consequently, high standard errors prevented the analysis of this data. This is an expected result considering that a sacrificial template mechanochemical-based method was used, in which the waste feedstock is almost completely removed during the calcination process.

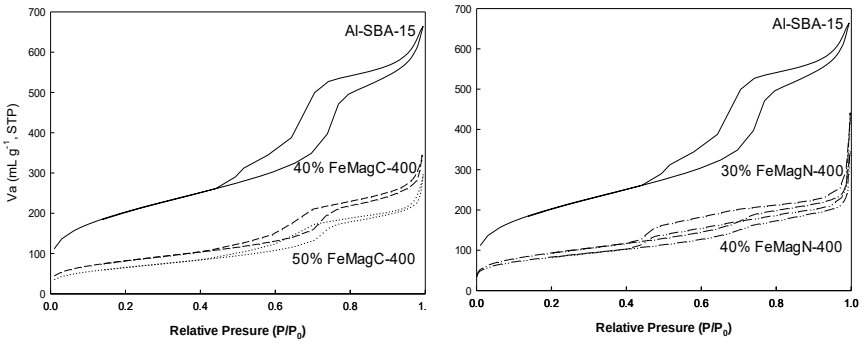

Figure 2. N_2 adsorption-desorption isotherms of (A) FeMagC at 400 ºC, and (B) FeMagN at 400 ºC.

Table 1. Textural properties of the obtained materials. Brunauer-Emmet-Teller; EDX-energy-dispersive X-ray spectroscopy.

Catalyst	S_{BET} (m^2g^{-1})	Average Pore diameter (nm)*	Average pore volume (mLg^{-1})	SEM-EDX		
				%Al	%Si	%Fe
Al-SBA-15	736	8.5	0.8	-	-	-
40% FeMagC-400	297	7.5	0.4	3.0	76.1	20.9
50% FeMagC-400	242	7.6	0.3	2.5	70.7	26.8
30% FeMagN-400	339	6.3	0.2	2.6	72.3	25.1
40% FeMagN-400	300	6.4	0.2	2.3	70.6	27.1

Morphological differences between the samples obtained using iron citrate and iron nitrate were further investigated through a TEM study and using 40%FeMagC-400ºC and 30%FeMagN-400ºC as representative samples. TEM images of 40%FeMagC-400ºC and 30%FeMagN-400ºC (Figure 3 A, B) depicted that iron oxide nanoparticles were successfully incorporated on the Al-SBA-15 surface. In both cases, the Al-SBA-15 support displays its characteristic well crystallized and porous structure [48]. Also, in both examples, several

darker areas, which can be clearly associated with the iron oxide counterpart, were observed. EDX and TEM analysis support the idea that very close contact between the Al-SBA-15 support and iron oxide component both at the surface and trapped in the porous structure was generated; however, a heterogeneous distribution of iron-oxide agglomerates also seemed to be present.

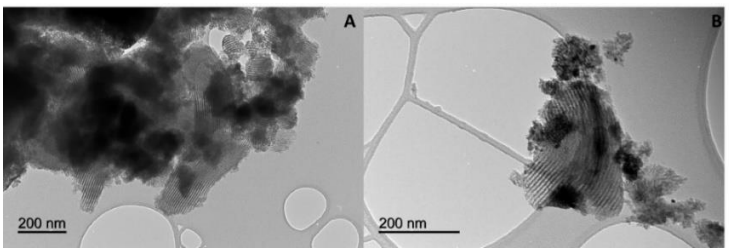

Figure 3. TEM images of (A) 40%FeMagC-400ºC, and (B) 40%FeMagN-400ºC.

In order to provide insight into species at the surface of the material and elucidate their relationship with the precursor used, as well as their influence into the reactions, XPS analysis of same representative samples (40%FeMAGC at 400 ºC and 40%FeMAGN at 400 ºC) were performed. Curve fitting was carried out using carbon C 1s peak (284.6 eV) as reference for binding energy calibration. The deconvoluted C 1s XPS spectra of the obtained materials exhibited three different contributions associated to the presence of C–C/C=C, C-N and C–O bonds. In particularly, C-N signal detected can be understood most likely due to the presence of nitrogen-containing compounds in the utilized biomass source. In both samples, the presence of Fe^{3+} species could be also inferred from the Fe 2p3/2 and Fe 2p1/2 peaks around 710 eV and 725 eV, respectively (Figure 4A, D). XPS spectra did not show the characteristic peaks associated with Fe (II), 709.6 eV or Fe (0), 706.7 eV species [49]. The absence of Fe(II) in the samples, especially, confirmed the formation of maghemite as magnetic phase instead of magnetite,

where both Fe(III) and Fe(II) species are presented [50,51]. Additionally, O1s XPS spectra displayed three different peaks attributed to O–C, O-Fe and O-Si. In addition, the typical signals of Si2p in SiO2 were observed at 103.0 eV for both materials. Calculation of Fe/Si ratio was carried out using XPS (Table 2). Interesting, comparison with the Fe/Si ratio obtained by EDX (bulk) provides evidence that remarkable superficial differences were obtained using nitrate and citrate precursors. While Fe/Si ratios of the bulk obtained by EDX ware essentially unchanged (enhancement factor of 1.4: (Fe/Si)EDX, 40% FeMagN-400/(Fe/Si)EDX, 40% FeMagC-400), the superficial ratio calculated by XPS shows an enhancement factor of 6.2 (Fe/Si)XPS, 40% FeMagN-400/(Fe/Si)XPS, 40% FeMagC-400).

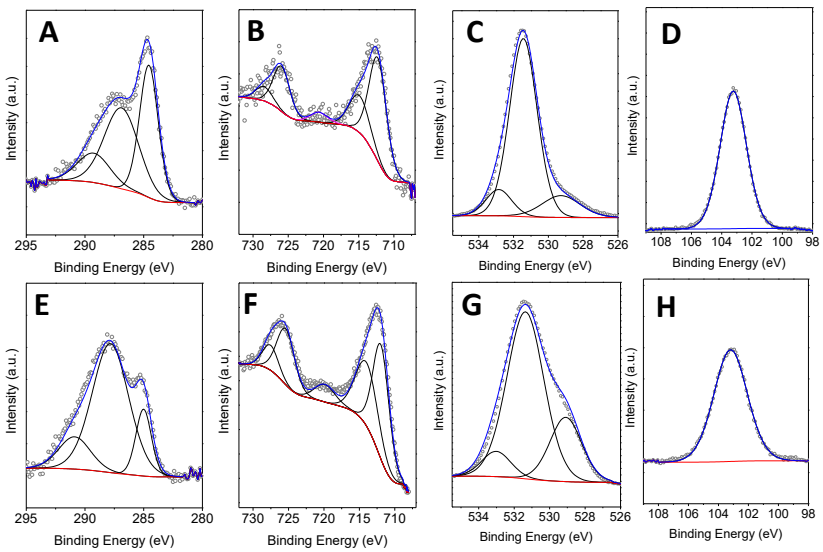

Figure 4. Deconvoluted X-ray photoelectron spectroscopy (XPS) spectra of 40%FeMagC at 400 ºC and 40%FeMagN at 400 ºC for (A,E) C1s, (B, F) Fe2p, (C, G) O1s and (D, H) Si2p.

Table 2. Fe/Si atomic ratio obtained by chemical analysis and X-ray photoelectron spectroscopy (XPS).

Sample	$(Fe/Si)_{XPS}$	$(Fe/Si)_{EDX}$	$(Fe/Si)_{XPS}/(Fe/Si)_{EDX}$
40% FeMagC at 400ºC	0.03	0.3	0.1
40%FeMagN at 400ºC	0.19	0.4	0.5

The catalytic properties of the samples were investigated during the oxidation of isoeugenol and vanillyl alcohol toward selective production of vanillin (Scheme 1).

Scheme 1. Reaction scheme. (A) oxidation of isoeugenol; (B) oxidation of vanillyl alcohol.

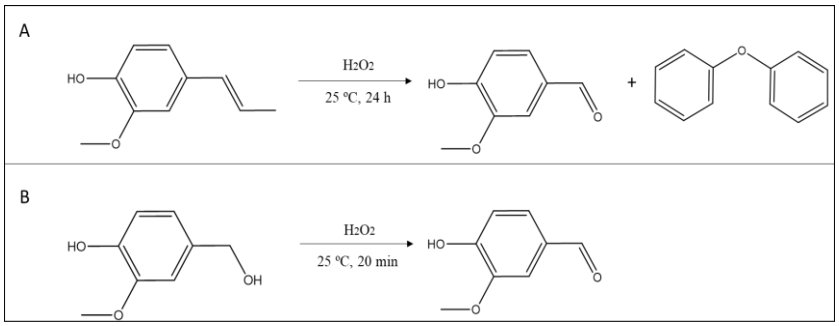

Firstly, control experiments were performed in the absence of the catalysts (blank) and employing Al-SBA-15 as a reference. These control reactions showed negligible activity in the absence of an effective catalytic system (See blank vs. Al-SBA-15 in Figure 5A) for isoeugenol oxidation, obtaining diphenyl structures as main product. In addition, vanillyl alcohol oxidation reaction to vanillin show fair conversions after 2 h of reaction without catalyst and relatively low values when the reference support Al-SBA-15 were used (Figure 5B). The Al-SBA-15 reference is active in the vanillyl alcohol oxidation reaction under used experimental conditions but displays a rather modest activity in comparison with samples containing iron oxide. Under optimized

reaction conditions for isoeugenol oxidation [17], prepared nanomaterials showed remarkable differences as a function of the iron precursor. A similar situation was acquired using vanillyl alcohol as regent, for which 20 minutes was settled on as the final reaction time. In both reactions, samples obtained using iron nitrate provided significantly improved conversions in comparison to the series of samples synthesised from iron citrate. In the case of isoeugenol oxidation, the addition of the iron oxide obtained from iron (III) nitrate drove to the highest positive impact in the conversion (more than 80 %) regardless of the calcination temperature. As can be seen in Figure 5A, the optimum value of activity was reached using the 40%FeMagN-400 sample. On the other hand, significantly lower conversion values were obtained using ammonium iron (III) citrate as iron source (~ 40 %). Focusing on selectivity, higher selectivity towards the desired vanillin product was detected for the series FeMagN which confirms the advantages of the use of nitrate instead of the other inorganic salt (Figure 5A). Note that selectivity to vanillin is higher than 70 % for the catalyst 30MagN at 300 ºC and higher than 50 % for all samples prepared from nitrate, being higher than previously reported for Fe-containing samples and similar SBA-15 based samples (See Table S2, Supplementary Materials) [19,20]. Diphenylether was the other dominant product of this reaction from which a carbon balance above 95 % was obtained for all runs. As is presented in Figure 5B, rather similar behaviour in terms of activity as a function of the iron precursor was obtained during the vanillyl alcohol oxidation. In this case, full selectivity to vanillin was achieved. Catalysts obtained from nitrate salt showed conversions greater than 99% in the reaction while a worsening of activity was detected using citrate. In addition, calcination temperature modulated the catalytic response of the solid, causing more activity at higher calcination temperature, which does not seem related to the crystallinity of samples (Figure 1). No easy

comparison between sample obtained using nitrate or citrate is possible. We, however, have previously demonstrated by ^{27}Al NMR that this Al-SBA-15 suffer a considerable transformation in contact with Fe_2O_3 entities which clearly indicates a strong interaction between Fe and Al elements [52]. In fact, the enhancement of surface acidities presented in Table 3 for Fe-containing samples, measured by using pyridine and 2,6-dimethylpyridine, could be associated to Al-Fe interaction. Note that a siliceous sample (Si-SBA-15) did not show measurable acidity properties. Just as important, higher Lewis acidity was obtained when iron nitrate was used as iron source (while both catalysts synthesized, 40%FeMagN at 400 ºC and 40%FeMagN at 400 ºC, presented similar Brønsted acid sites), which would be favouring an enhanced activity.

Table 3. Surface acidity measured at 250 ºC as μmol adsorbed of PY: pyridine or DMPY: 2,6-dimethylpyridine per gram of sample.

Sample	Surface acidity at 250 ºC/μmol g^{-1}	
	PY (total acidity)	DMPY (Bronsted acidity)
Si-SBA-15	-	-
Al-SBA-15	82	61
40%FeMagN at 400ºC	290	143
40%FeMagC at 400ºC	155	164

In fact, the Al/Fe reduce the binding energy of the Fe–O bond, which, as has been demonstrated [53], generates more flexible lattice oxygen and reactivity during oxidation reactions [52]. To further analyse the activity of the samples and its relationship with the iron precursor, differences of Fe/Si bulk and superficial ratios can be compared. Data presented in Table 2, clearly describe a correlation in the behaviour of the activity (See activity data for 40% FeMagC at 400 ºC and 40% FeMagN at 400 ºC in Figure 5A and B) and superficial iron entities exposed (measured as

Fe/Si ratio obtained by XPS) for the catalytic process using the 40% FeMagC at 400 ºC and 40% FeMagN at 400 ºC samples. This means that, although the use of nitrate instead of citrate seems to produce slightly better interaction with the porous structure of the Al-SBA-15, these differences cannot be considered significative (See Table 1 and 2). On the other hand, Fe/Si ratio obtained by XPS indicate a significant increase of the superficial concentration of iron oxide of the nitrate serie in comparison with samples obtained from citrate, which according to activity data of Figure 4, would be defining the differences between both groups of catalysts (FeMagN vs FeMagC).

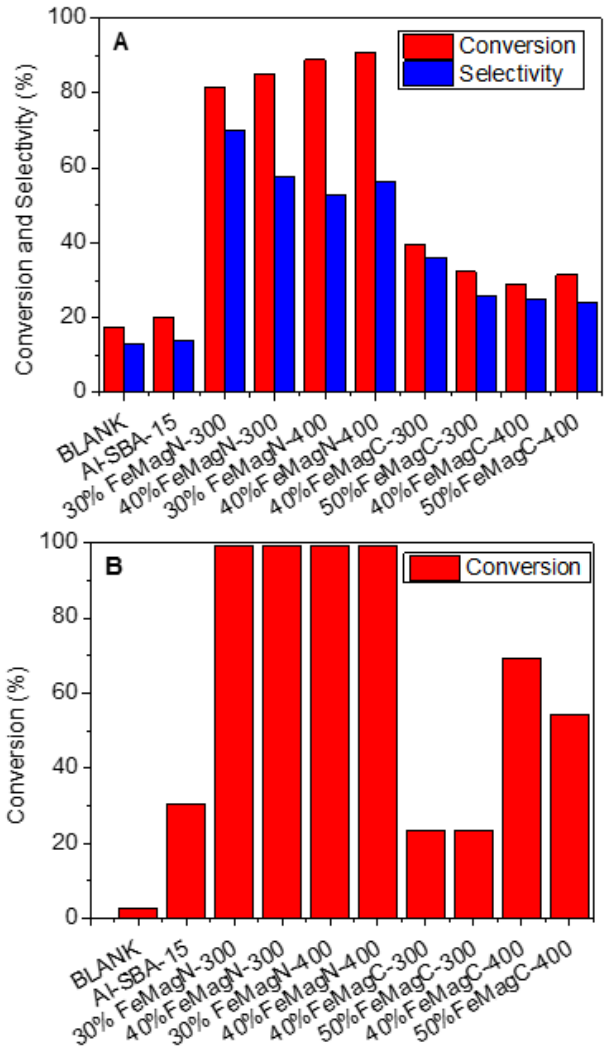

Figure 5. Catalytic conversion and vanillin selectivity (for isoeugenol reaction) for both oxidation reaction at 25 ºC, 1 atm. (A) Oxidation of isoeugenol at 24 h, (B) Oxidation of vanillyl alcohol at 20 min. The blank was measured after 2 h of reaction.

A reusability study of representative samples suggested a relatively high stability of the synthesized catalysts obtained by mechanochemistry. These measurements were performed employing one of the most active catalytic system, namely 30%FeMagN at 400 ºC (Figure 6 A-B) and

cycles of 24 h and 20 min for isoeugenol and vanillyl alcohol, respectively. For isoeugenol oxidation reaction (Figure 6A), after a decrease of the activity (from 77 to 53 % of conversion), the catalytic properties remained essentially unchanged. As shown in Figure 6A, after the first cycle (24 h of reaction), approximately 25% conversion was lost. However, a reactivation of the activity can be easily obtained by calcinating the catalyst at 400 ºC. A very similar conversion and selectivity, in comparison with the first use of the catalyst, were obtained after the calcination treatment (80 and 60 % of conversion and selectivity to vanillin, respectively), suggesting that deactivation of the sample was not due to potential iron-oxide leaching, but to the presence of poisoning surface compounds, which is a common phenomenon under batch condition and long reaction times. Furthermore, much less catalytic deactivation was observed during the oxidation of vanillyl alcohol under the used experimental conditions (Figure 6B, see caption for details) which can be also understood taking into account that significantly shorter reaction times were used. Similarly, a simple calcination post-treatment (400 ºC) demonstrated to be an effective process to reactivate the catalyst (Figure 6B).

Figure 6. Reuses of the 30%FeMagN at 400 ºC for both oxidation reaction at 25 ºC, 1 atm. (A) Oxidation of isoeugenol; each cycle was 24 h of reaction, (B) Oxidation of vanillyl alcohol; each cycle was 20 min of reaction. A.C: reused catalyst after calcination.

Experimental.

Synthesis of Al-SBA-15.

The preparation of the mesoporous aluminosilicate (Al-SBA-15, molar ratio Si/Al = 20) was carried out according to a procedure reported by Stucky et al. [42]. In particular, Pluronic P123 triblock copolymer, Sigma-Aldrich, Madrid, Spain (20.6 g) was dissolved in 750 mL of HCl (Panreac, Barcelona, Spain) solution (0.2 M, pH= 1.5), by stirring at 40°C for 2h. Tetraethyl orthosilicate (TEOS), Sigma-Aldrich, Madrid, Spain (25 mmol) and aluminium isopropoxide, Sigma-Aldrich, Madrid, Spain (10 mmol) were then added to the mixture and further stirred for 24 h at 40°C. Subsequently, the solution was transferred to a 100 mL

autoclave at 100 °C for 24 h. The obtained material was filtered, dried at 60 °C and finally calcined at 600 ºC for 2 h.

Synthesis of catalysts.

The synthesis of the nanocatalysts was carried out by means of a mechanochemical milling process using Al-SBA-15 as support, biomass (a lignocellulosic-derived residue) as carbon source and different iron precursors (ammonium iron (III) citrate (Sigma-Aldrich, Madrid, Spain), iron (III) nitrate (Sigma-Aldrich, Madrid, Spain), iron (III) perchlorate hydrate (Panreac, Barcelona, Spain) and iron (III) chloride, (Sigma-Aldrich, Madrid, Spain)). For the catalyst preparation, Al-SBA-15 support (2 g) and organic waste (1 g) are introduced into the planetary ball mill jar where the different iron salts used in percentages by weight of 10, 20, 30, 40 and 50 were introduced. The synthesis mixture is ground for 10 min at 350 rpm using of 18 stainless steel balls of 10 mm x 1 cm. The material obtained after the grinding process is calcined at three different temperatures, namely 300, 400 and 500 °C. The nanomaterials obtained have been denoted as X-FeMagY-Z, where X = theoretical content by weight of iron present, Y = iron precursor salt (C = ammonium iron (III) citrate, N = iron (III) nitrate, P = iron (III) perchlorate hydrate and Cl = iron (III) chloride) and Z= calcination temperature.

Characterization techniques.

Nanocatalysts were characterized by several techniques, including X-ray diffraction (XRD), X-ray Photoelectron Spectroscopy (XPS), Scanning electron–energy dispersive X-ray microscope (SEM-EDX), Transmission electron microscopy (TEM), N_2 Physisorption. Additionally, magnetic susceptibility values were additionally determined, in order to confirm the magnetic properties of the prepared materials. X-ray diffraction analysis was carried out on a Bruker

D8-Advanced Diffractometer (40kV, 40 mA) with a Cu X-ray tube (λ= 0.15406) and a goniometer Bragg Bretano θ/θ (Bruker AXS, Karlsruhe, Germany). XRD patterns were acquired in a 10 to 80º range, at a step size of 0.02° with a counting time per step of 20 s.

XPS experiments were carried out in an ultrahigh vacuum (UHV) multipurpose surface analysis system SpecsTM, equipped with the Phoibos 150-MCD energy detector (Berlin, Germany). The samples was previously evacuated overnight under vacuum ($<10^{-6}$ Torr). The measurement was accomplished at pressures $<10^{-10}$ mbar, employing a conventional X-ray source (XR-50, Specs (Berlin, Germany), Mg-Kα, hv=1253.6 eV, 1 eV = 1.603 x 10^{-19} J) in a "stop and go" mode. The XPS CASA program (Casa Software Ltd., Cheshire, Uk) was used to obtain the deconvolution of the curves and the element quantification. TEM micrographs were acquired in a FEI Tecnai G2 system, equipped with a charge-coupling device (CCD) camera. Samples were previously suspended in ethanol and subsequently deposited on a copper grid. Element quantification of the catalysts was obtained using a JEOL JSM 7800F (JEOL Ltd., Akishima, Tokyo, Japan) scanning electron microscope equipped with an Inca Energy 250 microanalysis system, Si/Li type window detector (ATW2), detection range from boron to uranium, and resolution of 137 eV to 5.9 KeV. The adsorption/desorption isotherms of N_2 were determined in the Micromeritics automatic analyzer ASAP 2000 (Micrometrics Instrument Corp., Norcross, GA, USA) at -196ºC. Samples were previously degassed overnight at 130 ºC under vacuum (P $<10^{-2}$ Pa). The linear determination of the BET equation was carried out to obtain specific surface areas. Magnetic susceptibility of samples was determined by using a MS2 magnetic susceptibiliter, (Bartington Instruments Ltd., Witney, UK) at room temperature using the dual frequency MS2B (Bartington Instruments Ltd., Witney, UK) laboratory sensor (470 and 4700 Hz). Surface acidity of the samples were

measured using pyridine (PY) and 2,6-dimethylpyridine (DMPY) as titrant bases, since they are essentially adsorbed on both types of acidic sites, Brönsted and Lewis, and Brönsted acid sites, respectively at 250 °C (50 °C below of calcination temperature during the synthesis of the samples). The pulses were carried out by means of a microinjector, in the catalytic bed, from a cyclohexane solution of the titrant (0.989 M in PY and 0.686 M in DMPY). The catalyst is standardized at each titration in a dehydrated and deoxygenated nitrogen flow (50 mL min^{-1}) (99.999% purity) at 250 °C. The catalyst used (~ 0.03 g) is fixed by means of Pyrex glass wool stoppers, inside a stainless-steel tubular microreactor of 4 mm internal diameter. The injected base was analysed by gas chromatography with flame ionization detector (FID), using an analytical column of 0.5 m in length, containing 5% by weight of polyphenylether in Chromosorb AW-MCS 80/100 (Supelco Analytical, Bellefonte, PA, USA).

Catalytic activity.

The production of vanillin was carried out by conventional heating using isoeugenol and vanillyl alcohol as reagents. The selective oxidative cleavage of isoeugenol to vanillin was carried out using a multiple parallel reaction system (Carrusel Reaction Station ™, Radleys Discovery Technologies Ltd., Saffron Walden, United Kingdom) at 25 ºC, employing isoeugenol (0.8 g, 5 mmol), 33 % hydrogen peroxide (1.2 mL, 11.7 mmol) as oxidant agent, acetonitrile as solvent (8 mL, 153 mmol) and 10 mol% of catalyst. In addition, oxidation of vanillyl alcohol to vanillin was carried out, using vanillyl alcohol (0.8 g, 5 mmol), hydrogen peroxide, 30 wt. % in water (1.2 mL, 11.7 mmol), acetonitrile (8 mL, 153 mmol) and 10 mol% of catalyst.

The progress of the reaction was evaluated by gas chromatography (GC) employing an Agilent Technologies 7890 A GC System (Madrid, Spain)

equipped with a Petrocol^{TM} DH column (100m x 0.25mm x 0.5 μm) and a flame ionization detector (FID).

Conclusions

A simple and reproducible process for the synthesis of iron nanoparticles deposited on Al-SBA-15 using biomass waste has been developed. The nanomaterials possess suitable structural and textural properties, for their subsequent use as catalysts, as well as magnetic properties that allow its easy separation from the reaction media. The catalytic performance of such noncatalytic systems has shown promising results for the selective production of vanillin toward isoeugenol and vanillyl alcohol oxidation at room temperature in conventional liquid phase. Conversions in the range of 80 to 90% molar, with selectivities ≥ 50% molar have been achieved. Results suggested that Al-Fe interaction and subsequent enhancement of Lewis acid sites, as well as more iron-oxide species superficially available for the oxidation process, are most important factors to obtain high activity and vanillin selectivity using the nitrate salt.

Acknowledgments.

The authors gratefully acknowledge support from MINECO under project CTQ2016-78289-P, co-financed with FEDER funds. Mario J. Munoz-Batista gratefully acknowledges MINECO for a JdC contract (Ref. FJCI-2016-29014). This publication has been prepared with support from RUDN University Program 5-100.

References

1. Sang, W.; Bai, F. Vascular diversity patterns of forest ecosystem before and after a 43-year interval under changing climate conditions in the Changbaishan Nature Reserve, northeastern China. In *Forest Ecology*; Springer. **2008**, *201*, 115–130.
2. Clark, J.H.; Luque, R.; Matharu, A.S. Green chemistry, biofuels, and biorefinery. *Annu. Rev. Chem. Biomol. Eng.* **2012**, *3*, 183–207.
3. Liao, S.; Wang, F.; Wu, T.; Pan, W. Crude oil price decision under considering emergency and release of strategic petroleum reserves. *Energy*. **2016**, *102*, 436–443.
4. Tuck, C.O.; Pérez, E.; Horváth, I.T.; Sheldon, R.A.; Poliakoff, M. Valorization of biomass: deriving more value from waste. *Science.* **2012**, *337*, 695–699.
5. Ragauskas, A.J.; Beckham, G.T.; Biddy, M.J.; Chandra, R.; Chen, F.; Davis, M.F.; Davison, B.H.; Dixon, R.A.; Gilna, P.; Keller, M. Lignin valorization: improving lignin processing in the biorefinery. *Science.* **2014**, *344*, 1246843.
6. Corma, A.; Iborra, S.; Velty, A. Chemical routes for the transformation of biomass into chemicals. *Chem. Rev.* **2007**, *107*, 2411–2502.
7. Ragauskas, A.J.; Williams, C.K.; Davison, B.H.; Britovsek, G.; Cairney, J.; Eckert, C.A.; Frederick, W.J.; Hallett, J.P.; Leak, D.J.; Liotta, C.L. The path forward for biofuels and biomaterials. *Science.* **2006**, *311*, 484–489.
8. Stöcker, M. Biofuels and biomass to liquid fuels in the biorefinery: Catalytic conversion of lignocellulosic biomass using porous materials. *Angew. Chemie Int. Ed.* **2008**, *47*, 9200–9211.
9. Filiciotto, L.; Luque, R. Biomass Promises: A Bumpy Road to a Renewable Economy. *Curr. Green Chem.* **2018**, *5*, 47–59.

10. Rodríguez-Padrón, D.; Puente-Santiago, A.R.; Balu, A.M.; Muñoz-Batista, M.J.; Luque, R. Environmental Catalysis: Present and Future. *ChemCatChem*. **2018**, *11*, 18-38.
11. Polshettiwar, V.; Varma, R.S. Green chemistry by nano-catalysis. *Green Chem.* **2010**, *12*, 743–754.
12. Franco, A.; De, S.; Balu, A.M.; Romero, A.A.; Luque, R. Selective oxidation of isoeugenol to vanillin over mechanochemically synthesized aluminosilicate supported transition metal catalysts. *ChemistrySelect.* **2017**, *2*, 9546–9551.
13. Filiciotto, L.; Balu, A.M.; Romero, A.A.; Rodríguez-Castellón, E.; van der Waal, J.C.; Luque, R. Benign by design preparation of humin-based iron oxide catalytic nanocomposites. *Green Chem.* **2017**, *19*, 4423–4434.
14. Chen, C.L.; Chang, H.M.; Kirk, T.K. Aromatic acids produced during degradation of lignin in spruce wood by Phanerochaete chrysosporium. *Holzforschung-International J. Biol. Chem. Phys. Technol. Wood.* **1982**, *36*, 3–9.
15. Gallage, N.J.; Møller, B.L. Vanillin–bioconversion and bioengineering of the most popular plant flavor and its de novo biosynthesis in the vanilla orchid. *Mol. Plant.* **2015**, *8*, 40–57.
16. Lampman, G.M.; Sharpe, S.D. A phase transfer catalyzed permanganate oxidation: Preparation of vanillin from isoeugenol acetate. *J. Chem. Educ.* **1983**, *60*, 503.
17. Márquez-Medina, M.D.; Prinsen, P.; Li, H.; Shih, K.; Romero, A.A.; Luque, R. Continuous-Flow Synthesis of Supported Magnetic Iron Oxide Nanoparticles for Efficient Isoeugenol Conversion into Vanillin. *ChemSusChem.* **2018**, *11*, 389–396.
18. Geng, L.; Zheng, B.; Wang, X.; Zhang, W.; Wu, S.; Jia, M.; Yan, W.; Liu, G. Fe_3O_4 nanoparticles anchored on carbon serve the dual

role of catalyst and magnetically recoverable entity in the aerobic oxidation of alcohols. *ChemCatChem.* **2016**, *8*, 805–811.

19. Saberi, F.; Rodríguez-Padrón, D.; Doustkhah, E.; Ostovar, S.; Franco, A.; Shaterian, H.R.; Luque, R. Mechanochemically modified aluminosilicates for efficient oxidation of vanillyl alcohol. *Catal. Commun.* **2019**, *118*, 65–69.
20. Saberi, F.; Rodriguez-Padrón, D.; Garcia, A.; Shaterian, H.R.; Luque, R. Unprecedented Proline-Based Heterogeneous Organocatalyst for Selective Production of Vanillin. *Catalysts.* **2018**, *8*, 167.
21. Fache, M.; Boutevin, B.; Caillol, S. Vanillin production from lignin and its use as a renewable chemical. *ACS Sustain. Chem. Eng.* **2015**, *4*, 35–46.
22. Zhang, K.; Hong, K.; Suh, J.M.; Lee, T.H.; Kwon, O.; Shokouhimehr, M.; Jang, H.W. Facile synthesis of monodispersed Pd nanocatalysts decorated on graphene oxide for reduction of nitroaromatics in aqueous solution. *Res. Chem. Intermed.* **2019**, *45*, 599–611.
23. Zhang, K., Suh, J. M., Choi, J. W., Jang, H. W., Shokouhimehr, M., Varma, R. S. Recent Advances in the Nanocatalyst-Assisted NaBH4 Reduction of Nitroaromatics in Water. *ACS Omega*. **2019**, *4*, 483-495.
24. Lu, F.; Ruiz, J.; Astruc, D. Palladium-dodecanethiolate nanoparticles as stable and recyclable catalysts for the Suzuki-Miyaura reaction of aryl halides under ambient conditions. *Tetrahedron Lett.* **2004**, *45*, 9443–9445.
25. Astruc, D. Transition - metal Nanoparticles in Catalysis : From Historical Background to the State of the Art. *Wiley-VCH Verlag Gmbh & Co*. **2008**, *1*, 1-48.

26. Shokouhimehr, M.; Shin, K.-Y.; Lee, J.S.; Hackett, M.J.; Jun, S.W.; Oh, M.H.; Jang, J.; Hyeon, T. Magnetically recyclable core–shell nanocatalysts for efficient heterogeneous oxidation of alcohols. *J. Mater. Chem. A* **2014**, *2*, 7593–7599.
27. Alamgholiloo, H., Zhang, S., Ahadi, A., Rostamnia, S., Banaei, R., Li, Z., Liu, Xiao.; Shokouhimehr, M. Synthesis of bimetallic 4-PySI-Pd@ Cu (BDC) via open metal site Cu-MOF: Effect of metal and support of Pd@ Cu-MOFs in H_2 generation from formic acid. *Molecular Catalysis*. **2019**, *467*, 30-37.
28. Iranmanesh, M.; Hulliger, J. Magnetic separation: Its application in mining, waste purification, medicine, biochemistry and chemistry. *Chem. Soc. Rev.* **2017**, *46*, 5925–5934.
29. Kainz, Q.M.; Reiser, O. Polymer and dendrimer coated magnetic nanoparticles as versatile supports for catalysts, scavengers, and reagents. *Acc. Chem. Res.* **2014**, *47*, 667–677.
30. Shokouhimehr, M. Magnetically separable and sustainable nanostructured catalysts for heterogeneous reduction of nitroaromatics. *Catalysts.* **2015**, *5*, 534–560.
31. Choi, K.H.; Shokouhimehr, M.; Sung, Y.E. Heterogeneous Suzuki cross-coupling reaction catalyzed by magnetically recyclable nanocatalyst. *Bull. Korean Chem. Soc.* **2013**, *34*, 1477–1480.
32. Jun, S.W.; Shokouhimehr, M.; Lee, D.J.; Jang, Y.; Park, J.; Hyeon, T. One-pot synthesis of magnetically recyclable mesoporous silica supported acid–base catalysts for tandem reactions. *Chem. Commun.* **2013**, *49*, 7821–7823.
33. Shokouhimehr, M.; Lee, J.E.; Han, S.I.; Hyeon, T. Magnetically recyclable hollow nanocomposite catalysts for heterogeneous reduction of nitroarenes and Suzuki reactions. *Chem. Commun.* **2013**, *49*, 4779–4781.

34. Rafiaei, S. M., Kim, A., & Shokouhimehr, M. Gadolinium triflate immobilized on magnetic nanocomposites as recyclable Lewis acid catalyst for acetylation of phenols. *Nanoscience and Nanotechnology Letters*. **2014**, *6*, 309-313.
35. Rodríguez-Padrón, D.; Balu, A.M.; Romero, A.A.; Luque, R. New bio-nanocomposites based on iron oxides and polysaccharides applied to oxidation and alkylation reactions. Beilstein J. Org. Chem. 2017, 13, 1982.
36. Shokouhimehr, M.; Hong, K.; Lee, T.H.; Moon, C.W.; Hong, S.P.; Zhang, K.; Suh, J.M.; Choi, K.S.; Varma, R.S.; Jang, H.W. Magnetically retrievable nanocomposite adorned with Pd nanocatalysts: efficient reduction of nitroaromatics in aqueous media. *Green Chem.* **2018**, *20*, 3809–3817.
37. Muñoz-Batista, M.J.; Rodríguez-Padrón, D.; Puente-Santiago, A.R.; Luque, R. Mechanochemistry: toward sustainable design of advanced nanomaterials for electrochemical energy storage and catalytic applications. *ACS Sustainable Chem. Eng*. **2018**, *6*, 9530-9544.
38. Ouyang, W.; Yépez, A.; Romero, A.A.; Luque, R. Towards industrial furfural conversion: Selectivity and stability of palladium and platinum catalysts under continuous flow regime. *Catal. Today.* **2018**, *308*, 32–37.
39. Pineda, A.; Balu, A.M.; Campelo, J.M.; Romero, A.A.; Carmona, D.; Balas, F.; Santamaria, J.; Luque, R. A Dry Milling Approach for the Synthesis of Highly Active Nanoparticles Supported on Porous Materials. *ChemSusChem*. **2011**, *4*, 1561–1565.
40. Linares, N.; Silvestre-Albero, A.M.; Serrano, E.; Silvestre-Albero, J.; García-Martínez, J. Mesoporous materials for clean energy technologies. *Chem. Soc. Rev.* **2014**, *43*, 7681–7717.

41. Shokouhimehr, M.; Asl, M.S.; Mazinani, B. Modulated large-pore mesoporous silica as an efficient base catalyst for the Henry reaction. *Res. Chem. Intermed.* **2018**, *44*, 1617–1626.
42. Zhao, D.; Feng, J.; Huo, Q.; Melosh, N.; Fredrickson, G.H.; Chmelka, B.F.; Stucky, G.D. Triblock copolymer syntheses of mesoporous silica with periodic 50 to 300 angstrom pores. *Science.* **1998**, *279*, 548–552.
43. Peters, C.; Dekkers, M.J. Selected room temperature magnetic parameters as a function of mineralogy, concentration and grain size. *Phys. Chem. Earth, Parts A/B/C.* **2003**, *28*, 659–667.
44. Jia, C.; Sun, L.; Yan, Z.; You, L.; Luo, F.; Han, X.; Pang, Y.; Zhang, Z.; Yan, C. Single-crystalline iron oxide nanotubes. *Angew. Chemie.* **2005**, *117*, 4402–4407.
45. Park, J.; Lee, E.; Hwang, N.; Kang, M.; Kim, S.C.; Hwang, Y.; Park, J.; Noh, H.; Kim, J.; Park, J. One nanometer scale size controlled synthesis of monodisperse magnetic Iron oxide nanoparticles. *Angew. Chemie.* **2005**, *117*, 2932–2937.
46. Gregg, S.J.; Sing, K.S.W. A Surface Area and Porosity. *Academic Press*. **1982**.
47. Rajabi, F.; Fayyaz, F.; Luque, R. Cytosine-functionalized SBA-15 mesoporous nanomaterials: Synthesis, characterization and catalytic applications. *Microporous Mesoporous Mater.* **2017**, *253*, 64–70.
48. Yépez, A.; De, S.; Climent, M.S.; Romero, A.A.; Luque, R. Microwave-assisted conversion of levulinic acid to γ-valerolactone using low-loaded supported iron oxide nanoparticles on porous silicates. *Appl. Sci.* **2015**, *5*, 532–543.
49. Wagner, C.D.; Riggs, W.M.; Davis, L.E.; Moulder, J.F. Handbook of X-ray Photoemission Spectra. *Perkin-Elmer*, Minnesota, **1976.**

50. Rodríguez-Padrón, D.; Puente-Santiago, A.R.; Caballero, A.; Balu, A.M.; Romero, A.A.; Luque, R. Highly efficient direct oxygen electro-reduction by partially unfolded laccases immobilized on waste-derived magnetically separable nanoparticles. *Nanoscale.* **2018**, *10*, 3961–3968.
51. Rodríguez-Padrón, D.; Puente-Santiago, A.R.; Balu, A.M.; Romero, A.A.; Luque, R. Solventless mechanochemical preparation of novel magnetic bioconjugates. *Chem. Commun.* **2017**, *53*, 7635–7637.
52. Balu, A.M.; Pineda, A.; Yoshida, K.; Campelo, J.M.; Gai, P.L.; Luque, R.; Romero, A.A. Fe/Al synergy in Fe_2O_3 nanoparticles supported on porous aluminosilicate materials : excelling activities in oxidation reactions. *Chem. Commun*. **2010**, *46*, 7825–7827.
53. Mounzer, H. Heterogeneous oxidation of alcohols. Phd Thesis, University of Birmingham. **2009**.

catalysts

MDPI

Supporting Information

Mechanochemically synthesized supported magnetic Fe-nanoparticles as catalysts for efficient vanillin production.

M. Dolores Márquez-Medina[1], Daily Rodríguez-Padrón[1], Alina M. Balu[1], Antonio A. Romero[1], Mario J. Muñoz-Batista[1]*, Rafael Luque[1,2,]*

Table S1. Sumary of sinthesized samples and magnetic susceptibility measurments.

Catalyst	Precursor	Fe wt % (theorical)	Calcination Temperature (ºC)	Magnetic Susceptibility (m^3 K g^{-1})
10% FeMagC-300	ammonium iron (III) citrate	10	300	-
20% FeMagC-300		20		$52.0 \cdot 10^{-6}$
30% FeMagC-300		30		$85.6 \cdot 10^{-6}$
40% FeMagC-300		40		$116.5 \cdot 10^{-6}$
50% FeMagC-300		50		$135.0 \cdot 10^{-6}$
10% FeMagC-400		10	400	-
20% FeMagC-400		20		$63.3 \cdot 10^{-6}$
30% FeMagC-400		30		$96.1 \cdot 10^{-6}$
40% FeMagC-400		40		$140.1 \cdot 10^{-6}$
50% FeMagC-400		50		$186.1 \cdot 10^{-6}$
10% FeMagC-500		10	500	-
20% FeMagC-500		20		$31.2 \cdot 10^{-6}$
30% FeMagC-500		30		$50.0 \cdot 10^{-6}$
40% FeMagC-500		40		$97.2 \cdot 10^{-6}$
50% FeMagC-500		50		$135.4 \cdot 10^{-6}$
10% FeMagN-300	iron (III) nitrate	10	300	-
20% FeMagN-300		20		$55.2 \cdot 10^{-6}$
30% FeMagN-300		30		$152.0 \cdot 10^{-6}$
40% FeMagN-300		40		$233.2 \cdot 10^{-6}$
50% FeMagN-300		50		-

10% FeMagN-400		10	400	-
20% FeMagN-400		20		$68.6 \cdot 10^{-6}$
30% FeMagN-400		30		$164.3 \cdot 10^{-6}$
40% FeMagN-400		40		$271.6 \cdot 10^{-6}$
50% FeMagN-400		50		-
10% FeMagN-500		10	500	-
20% FeMagN-500		20		-
30% FeMagN-500		30		$178.9 \cdot 10^{-6}$
40% FeMagN-500		40		$254.5 \cdot 10^{-6}$
50% FeMagP-500		50		-
10% FeMagP-300	iron (III) perchlorate hydrate	10	300	-
20% FeMagP-300		20		-
30% FeMagP-300		30		-
40% FeMagP-300		40		-
50% FeMagP-300		50		-
10% FeMagP-400		10	400	-
20% FeMagP-400		20		-
30% FeMagP-400		30		-
40% FeMagP-400		40		-
50% FeMagP-400		50		-
10% FeMagP-500		10	500	-
20% FeMagP-500		20		-
30% FeMagP-500		30		-

40% FeMagP-500		40		-
50% FeMagP-500		50		-
10% FeMagCl-300	iron (III) chloride	10	300	-
20% FeMagCl-300		20		-
30% FeMagCl-300		30		-
40% FeMagCl-300		40		-
50% FeMagCl-300		50		-
10% FeMagCl-400		10	400	-
20% FeMagCl-400		20		-
30% FeMagCl-400		30		-
40% FeMagCl-400		40		-
50% FeMagCl-400		50		-
10% FeMagCl-500		10	500	-
20% FeMagCl-500		20		-
30% FeMagCl-500		30		-
40% FeMagCl-500		40		-
50% FeMagCl-500		50		-

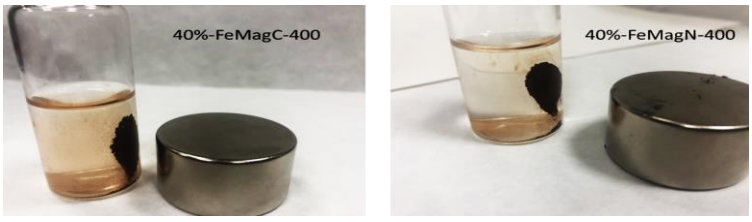

Figure S1. Magnetic separation of synthesized samples dispersed in the reaction media.

Table S2. Catalytic properties and reaction temperature of Fe-containing catalysts during isoeugenol and vanillin alchool oxidation reactions.

Sample	Conversion (%) isoeugenol oxidation/ Selectivity %	Conversion (%) vanillin alchool oxidation/ Selectivity (%)	Temperature (ºC)	Ref.
FeMagN-400	94/56	99/99	25	This work
Fe-Al-SBA-15	90/55	n.m.	90	12
Fe-Humins	91/63	n.m.	150	13
Fe-Graphene	62/52	n.m.	90	54
Fe-Al-SBA-15[a]	n.m.	63/99	25	19
Fe-Al-SBA-15[a]	n.m.	99/99	50	19

[a] Same synthetic protocol using propionic acid. n.m denote not measured.

III. 3. Post-synthetic mechanochemical incorporation of Al-species into the framework of porous materials: towards more sustainable redox chemistries.

Abstract.....152

Introduction.....152

Experimental Section.....154

Results and discussion......159

Conclusions.....171

Acknowledgments. 172

References.....172

Supporting Information……177

ACS Sustainable Chemistry & Engineering

Post-synthetic mechanochemical incorporation of Al-species into the framework of porous materials: towards more sustainable redox chemistries.

M. Dolores Marquez-Medina[a], Sareena Mhadmhan[a,b], Alina M. Balu[a], Antonio A. Romero[a], Rafael Luque[a,c*]

[a] Departmento de Quimica Organica, Facultad de Ciencias, Universidad de Cordoba, Campus de Rabanales, Edificio Marie Curie (C-3), Ctra Nnal IV-A, Km 396, E14014, Cordoba, Spain

[b] Petrochemistry and Polymer Science, Department of Chemical Technology, Faculty of Science, Chulalongkorn University, 10330, Bangkok, Thailand

[c] Peoples Friendship University of Russia (RUDN University), 6 Miklukho-Maklaya str., 117198, Moscow, Russia

Corresponding Author: q62alsor@uco.es (R. Luque)

DOI: 10.1021/acssuschemeng.9b00912

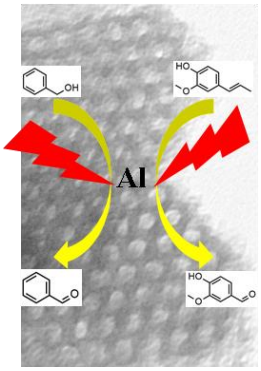

Abstract

The mechanochemical incorporation of catalytically active Al species in low loadings was successfully accomplished into the framework of mesoporous silica (SBA-15 and MCM-41) materials using a simple wet milling approach (with aluminum isopropoxide as source of aluminum) and a dry milling approach (using low quantities of Al-containing MOF materials). Characterization data pointed to the successful incorporation of Al species (typically with loadings of ca. 0.2-0.4 wt.%) mostly tetrahedrically coordinated. Despite such extremely low loadings, the isolated aluminum oxide species exhibited promising activities and stability in selective mild oxidations under various conditions (microwave irradiation and mechanochemistry) including the selective oxidation of benzyl alcohol to benzaldehyde, isoeugenol to vanillin and diphenyl sulfide to diphenyl sulfoxide as compared to similarly synthesized impregnated catalysts.

Introduction

The incorporation of functional and active sites into porous materials for catalytic applications still remains a challenge in the field, particularly aiming to highly active and stable systems at low loadings.[1,2] Conventional methodologies (i.e. impregnation, deposition-precipitation, anchoring/immobilization, etc.) were generally proved to provide active materials but the possibility to control the loading and localization of active sites as well as their stability is often compromised.[3,4] Alternative protocols have paved the way to a more controllable and reproducible materials functionalization.

Mechanochemistry emerged as one of such promising alternative methodologies to provide a simple and rapid but efficient, highly active, stable and reproducible access to advanced functional materials for

various applications.[5-7] We have extensively demonstrated that a wide range low loaded highly active supported nanoparticle systems including iron, cobalt, nickel, palladium, ruthenium and various other metal and metal oxides could be designed under wet/dry milling conditions for catalytic applications.[8-10] In these methodologies, metal precursors (both solid and/or liquid) were ground under optimized conditions towards the generation of mechanochemical nanomaterials. However, the possibility to utilize MOFs in low quantities as seeds to generate active species on porous materials has not been explored to date. In principle, the presence of organic linkers and various metals in MOFs makes them a potentially interesting platform to design homogeneously distributed and most importantly highly isolated nanoparticles (quasi-single atom) on various supports.

The selective oxidation of alcohols and sulfides to aldehydes and sulfoxides are among two most relevant chemistries in organic synthesis to provide access to useful compounds with extensive applications in herbicides, pharmaceuticals, fragrances and related industries.[11,12] Such chemistries (e.g. benzyl alcohol oxidation to benzaldehyde; diphenyl sulfide to diphenyl sulfoxide) have been extensively reported using a range of nanoparticle systems (mostly noble metals with only very few examples of transition metals as well as noble metal-containing mesoporous materials).[13-17] However, despite some examples on certain catalytic systems based on cheap and sustainable transition metals (Fe, W, Cu, etc.),[14-17] there are no reports on the utilization of Al-containing mesoporous materials in mild selective oxidations of alcohols or sulfides. Our group just recently reported the first available report on designed hierarchical Al-containing zeolites for mild oxidation reactions,[18] following a simple and environmentally friendly protocol for benzyl alcohol oxidation using alkali-treated ZSM-5 zeolites.[19] The possibility to catalyze redox chemistries using Al-containing materials

can be highly attractive as compared to conventional metals, taking into account the environmentally friendly and cheap nature as well as wide availability of Al including in waste (e.g. mining kaolin waste).

Based on these premises, the present contribution reports for the first time that a simple mechanochemical milling step allows the possibility of aluminum incorporation into the framework of mesoporous silica (SBA-15 and MCM-41) materials even at low loadings, with functionalized materials exhibiting promising catalytic activities with respect to analogous conventionally impregnated materials in the selective oxidations of benzyl alcohol to benzaldehyde, isoeugenol to vanillin and sulfides (diphenyl sulfide) to sulfoxides.

Experimental Section

Materials synthesis

Two types of mesoporous silica (SBA-15 and MCM-41) were synthesized by using a previously reported literature protocol.[20,21] Al was incorporated into mesoporous silica SBA-15 and MCM-41 by using incipient wetness impregnation and mechanochemical ball milling procedures. The details of the synthesis method were given below.

Incipient wetness impregnation method (I)

Aluminum isopropoxide (Sigma-Aldrich, Madrid, Spain) as source of aluminum (up to 1 wt.% theoretical Al loading) was dissolved in 1 molar ratio of water/ethanol mixture (5 mL). The silica support was then added in the solution under stirring for 2 h. The catalyst was then dried at 100 ºC for 24 h and finally calcined at 550ºC for 4 h under air. The catalysts were named as SBA-15-Al-I and MCM-41-Al-I.

Mechanochemical planetary ball milling method (M)

2 g of silica support (SBA-15 or MCM-41) and 1 wt.% of the desired aluminum source (Aluminum isopropoxide; Al or Al-MIL-53 MOF; AlMOF as the Al source) were laid in a 125 mL stainless steel jar from a PM-100 Retsch planetary ball mill containing 18 stainless steel balls (Ø10 mm, 4 g each ball). Al-MIL-53 MOF was synthesized by using a previously reported literature protocol.[22] The planetary ball milling was carried on at 350 rpm for 10 min (optimum mechanochemical conditions).[9,22,23] After that the catalysts were calcined at 550 ºC for 4 h under air. The catalysts obtained in this protocol were identified as SBA-15-Al-M, MCM-41-Al-M, SBA-15-AlMOF-M and MCM-41-AlMOF-M respectively.

Characterization

X-Ray Diffraction (XRD) measurements were performed in a Bruker D8 Discover Vario X-ray diffractometer equipped with a Brentano Bragg θ/2θ goniometer to work in reflection mode, a Cu X-ray tube, rotating platform, primary beam monochromator and detector ultra-fast high sensitivity. Diffractometers were collected at the step size of 0.02º and counting per step of 1.2 s, over a 2θ range from 1 to 80º.

Surface area (BET) and pore volume were obtained from the adsorption/desorption isotherms of nitrogen. Nitrogen adsorption measurements were carried out at -196ºC, temperature of the liquid nitrogen, using an automatic analyzer Micromeritics ASAP 2000. The weight of the sample used for the adsorption measurements of N_2 desorption is approximately 0.20 g. Samples were degassed for 24 hours at 100 °C under vacuum ($P < 10^{-2}$ Pa) and subsequently analyzed. The linear part of the BET equation (relative pressure between 0.05 and 0.30) was used for the determination of the specific surface area. The pore size distribution was calculated using the adsorption branch of the adsorption-

desorption isotherm of N_2, applying the method of Barret, Joyner and Halenda (BJH).

Elemental analysis of the materials was carried out using a JEOL JSM 6300 Scanning Electron Microscope equipped with an Inca Energy 250 microanalysis system, Si/Li type window detector (ATW2), detection range: from boron to uranium, resolution: 137 eV to 5.9 KeV. The software allows the qualitative and semiquantitative analysis, mapping of elements, elementary distribution in a sweep line.

Inductive coupling plasma mass spectrometry technique (ICP-MS) was employed for a quantitative metal analysis of the synthesized nanomaterials, using an Elan DRC-e ICP-MS (PerkinElmer SCIEX) located in the Central Service of Research Support (SCAI).

Magic Angle Spinning (MAS) ^{27}Al solid state NMR experiments of hydrated samples were recorded on a Bruker ACP-400 multinuclear spectrometer at 104.26 MHz. ^{27}Al spectra were recorded at 1 μs pulse with a recycle delay of 0.3 s. The chemical shifts are given in ppm from $Al(H_2O)_6^{3+}$ as external reference as in previous work by the group.[24]

Samples containing silica (~ 25 mg) were previously digested using a mixture of 1:1:1 HF: HNO_3: HCl acids. The solutions were made with milliQ water up to a maximum content of 1% HF, since HF is the only acid that dissolves the silicates and in acid solution has a low boiling point. This makes it easily volatilizable. If digestion becomes open, SiF_4 (boiling point = -86 ° C) can be lost volatilizing during digestion.

The determination of the surface acidity of the different catalysts, pyridine (PY) and 2,6-dimethylpyridine (DMPY) were chosen as titrating bases, since they are essentially adsorbed on both types of acidic centers, Brönsted and Lewis, and on Brönsted acid centers, respectively. PY, due to its low steric hindrance, is unspecifically adsorbed on both

types of centers, whereas DMPY is specifically adsorbed on Brönsted type acid centers, due to the high steric hindrance of the methyl groups.[24] This procedure has been carried out at a temperature of 250 °C (50 °C below the temperature of the final heat treatment in the synthesis of the nanomaterials). The pulses were carried out by means of a microinjector, in the catalytic bed, from a cyclohexane solution of the titrant (0.989 M in PY and 0.686 M in DMPY). The catalyst is standardized at each titration in a dehydrated and deoxygenated nitrogen flow (50 mL min^{-1}) (99.999% purity) at 250 °C. The catalyst used (~ 0.03 g) is fixed by means of Pyrex glass wool stoppers, inside a stainless-steel tubular microreactor of 4 mm internal diameter. The injected base is analyzed by gas chromatography with flame ionization detector (FID), using an analytical column of 0.5 m in length, containing 5% by weight of polyphenylether in Chromosorb AW-MCS 80/100.[24]

Catalytic activity

Selective oxidation of benzyl alcohol to benzaldehyde

Tests carried out were carried out in a focused microwave CEM-Discover monowave model, controlled and monitored by a computer in standard mode ("Discover") under pressure that allows us to control the power of irradiation, temperature and pressure. Typically, 1 mmol of benzyl alcohol (0.2 mL, assay >99%), 2.9 mmol of 30% (w/w) H_2O_2 in H_2O as oxidant (0.3 mL) and 0.35 mol % catalyst (0.05 g) were mixed with 1.25 mmol of acetonitrile as solvent (2 mL) and microwaved for 3 minutes at 90 °C (300 W power). The product was analyzed by using GC-FID equipped with a Supelco 2-8047-U capillary column.

Recycle experiments were carried out under identical conditions unless otherwise stated. After reaction, the catalyst was filtered off, washed with acetonitrile and dried at 100 ºC prior to its reuse in another reaction run.

Regeneration of the spent catalyst was performed by re-calcination after reaction under identical conditions to those employed in their synthesis (550 ºC, air, 4 h).

Oxidation of isoeugenol to vanillin

The reaction was conducted in a microwave CEM-Discover monowave model under identical reaction conditions and similar parameters. Typically, 1.2 mmol of isoeugenol (0.2 mL, assay 98%), 2.9 mmol 30% (w/w) H_2O_2 in H_2O (0.3 mL) and 0.35 mol % of catalyst (0.05 g) in 1.25 mmol acetonitrile (2 mL), at 90 ° C and 300 W for 3 minutes. The products were analyzed by using GC-FID equipped with a capillary column Petrocol 100 x 0.25 nm x 0.5 µm. Recycle experiments were carried out under identical conditions unless otherwise stated. After reaction, the catalyst was filtered off, washed with acetonitrile and dried at 100 ºC prior to its reuse in another reaction run.

Regeneration of the spent catalyst was performed by recalcination after reaction under identical reaction conditions to those employed in their synthesis (500 ºC, air, 4 h).

Mechanochemical oxidation of diphenyl sulfide to diphenyl sulfoxide

The oxidation reaction of diphenyl sulfide was studied under ball milling. In a typical procedure, 0.5 mmol diphenyl sulfide (0.083 mL, assay 98%), 30% (w/w) H_2O_2 in H_2O (8 equiv., 0.4074 mL) and 0.04 mol %, catalyst (0.005 g) were added to a 25 mL jar from a PM-100 Retsch planetary ball mill with eight stainless steel balls (Ø10 nm, 4 g each ball). Then, the mechanochemical reaction was performed at 350 rpm for 25 min. The crude reaction was recovered from the jar by using 0.5 mL toluene. The resulting liquid phase was analyzed by GC-FID equipped with a Supelco 2-8047-U capillary column. All results were finally confirmed by GC-MS. The reaction mixture was carefully analyzed for

potential traces of Fe (from the stainless steel balls), confirming by ICP-MS no measurable Fe quantities (<0.5 ppm) into solution. For the recycling step, the chamber of the ball mill containing the catalyst was dried at 100°C after the liquid phase of the first run was taken from the jar, followed by catalyst recovery and reusing for the next run.

Results and Discussion

Characterization of the Catalysts

Materials were characterized using different techniques including XRD, N_2 physisorption, SEM and EDX mapping as well as MAS ^{27}Al NMR and surface acid properties based. XRD patterns provided the typical long range hexagonally arrayed mesoporous structure for SBA-15.[25] No clear evidence of the presence of Al in the materials could be observed from XRD patterns (Figure 1), as expected due to the low quantity of Al (<1 wt.%) present. Interestingly, MAS ^{27}Al NMR could provide useful information of Al environments within the materials.

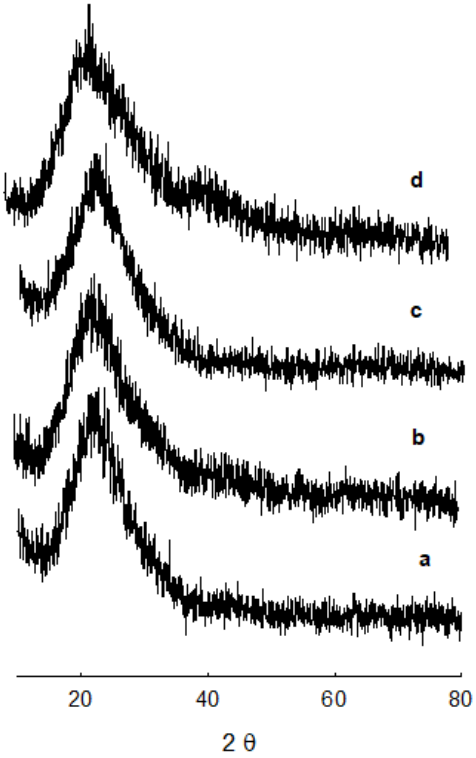

Figure 1. XRD patterns of (a) SBA-15-Al-I, (b) SBA-15-Al-M, (c) SBA-15-AlMOF-M and (d) SBA-15 samples.

Figure 2 depicts the different coordination of Al species within the synthesized materials measured by ^{27}Al MAS NMR spectra of the hydrated samples. A remarkable contribution of tetrahedrically coordinated Al (54.4 ppm) was found in all mechanochemically synthesized materials which correspond to framework Al species in good agreement with previous reports.[24,26] These results indicate that the mechanochemical approach was able to introduce post-synthesis Al species within the SBA-15 framework at low Al loadings, being the first literature report on such post-synthetic framework incorporation.[9] In general, this method can avoid the use of toxic organic solvents that

could be released to the environment and increase the effectiveness and reproducibility in materials synthesis (as well as catalytic reactions). Mechanochemistry has become a promising alternative for the synthesis and design of advanced heterogeneous catalysts.[27]

Interestingly, the presence of octahedrically coordinated Al species (ca. 0 ppm, Figure 2) in the materials was rather low after the mechanochemical step as compared for instance with the analogous Al impregnated SBA-15 via wetness impregnation (Figure 2a). Such effect was particularly remarkable for the mechanochemical framework Al incorporation of an Al-containing MOF material (Al-MIL-53) used as aluminium source into the silica SBA-15 (Figure 2c, NMR contribution at 54.4 ppm corresponding to tetrahedrically coordinated Al-ca. 75% from all incorporated Al).

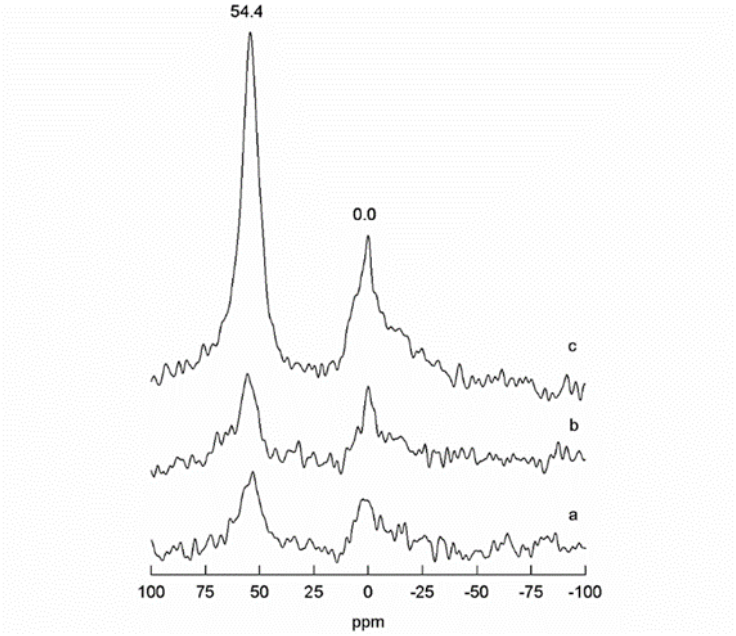

Figure 2. MAS ^{27}Al NMR spectra of (a) SBA-15-Al-I, (b) SBA-15-Al-M and (c) SBA-15-AlMOF-M catalysts.

A similar behavior was observed for the use of MCM-41 as mesoporous support (results not shown). These findings were found to have important consequences in the catalytic activity of Al-containing materials but most importantly provide unambiguous results, for the first time, on the possibility to post-synthetically incorporate catalytically active species within the framework of porous materials via mechanochemistry (even at low loadings) to generate catalytically active materials.

Table 1. Porosity analysis and acidity determination of synthesized materials.

Samples	S_{BET} [a] (m^2g^{-1})	D_p [b] (nm)	V_p [c] (mLg^{-1})	Al content (wt.%)	Acidity ($\mu molg^{-1}$)	
					PY	DMPY
SBA-15	800	7.6	0.8	-	<10	<10
SBA-15-Al-I	739	6.1	0.7	0.25	31	26
SBA-15-Al-M	419	5.9	0.6	0.30	30	18
SBA-15-AlMOF-M	466	5.9	0.7	0.38	22	21
MCM-41-AlMOF-M	456	4.7	0.6	0.40	23	20

[a] S_{BET}: specific surface areas was calculated by the Brunauer-Emmett-Teller (BET) equation.

[b] D_p: mean pore size diameter was calculated by the Barret-Joyner-Halenda (BJH) equation.

[c] V_p: pore volumes were calculated by the Barret-Joyner-Halenda (BJH) equation.

In addition to this, the surface properties of the materials were also characterized using N_2 physisorption, with Al-containing materials preserving most mesoporosity with a reduced surface area and pore diameters as compared to the parent (SBA-15 and MCM-41) as a consequence of the mechanochemical treatment (Table 1, Figure 3). Importantly, pore volumes remained almost unchanged, a clear

indication that all changes in textural properties were rather originated by 1) a degradation of the mesoporous structure upon milling and 2) the observed framework Al incorporation in mechanochemically synthesized nanomaterials.

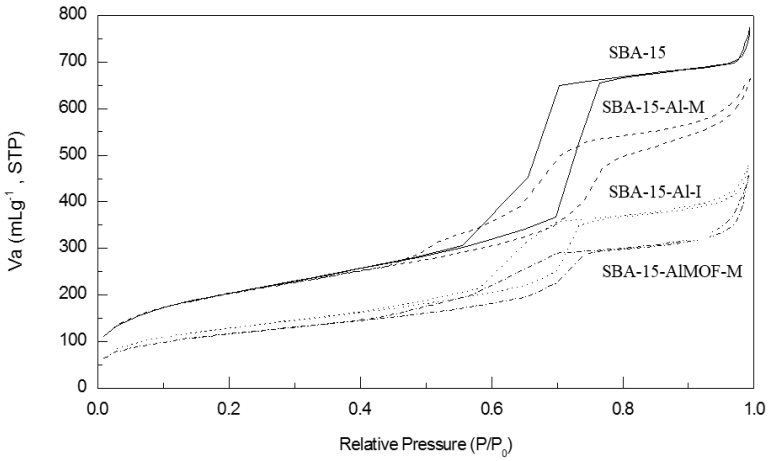

Figure 3. N_2 Physisorption profiles of synthesized materials

Surface acid properties measured by pyridine (PY) and 2,6-dimethylpyridine (DMPY) titration using a previously reported gas-phase approach [24] also pointed out a very mild acidity of the materials that did not appreciably change after the mechanochemical Al incorporation (Table 1). The average Al content measured by EDX and ICP-MS was ca. 0.2-0.4 wt.%, reduced as compared to the theoretical aimed content in the synthesis (1 wt.%, Table 1, contents measured by ICP-MS). Nevertheless, such Al content despite the low acidity was sufficient to improve the catalytic activity of the synthesized materials as compared to purely siliceous SBA-15 as demonstrated in a number of oxidation reactions.

Al-containing materials are generally inactive in redox reactions. However, we recently reported that the presence of isolated Al sites in aluminosilicates (hierarchical zeolites) could lead to promising mild redox activities.[18] Based on these previous results, materials were subsequently tested in three simple mild oxidations (benzyl alcohol to benzaldehyde, isoeugenol to vanillin and diphenyl sulfide to diphenyl sulfoxide) to further see the influence of the Al content in the synthesized materials.

The activity of Al-containing materials was firstly screened in the microwave assisted oxidation of benzyl alcohol to benzaldehyde (Table 2).

Table 2. Activity of post-synthetically functionalized Al-containing mesoporous silica in the microwave-assisted oxidation of benzyl alcohol to benzaldehyde

Samples	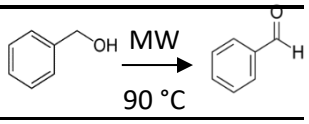
	Conversion (%)
Blank	<10
SBA-15	10
SBA-15-Al-I	11
SBA-15-Al-M	18
SBA-15-AlMOF-M	20
MCM-41	10
MCM-41-Al-I	7
MCM-41-Al-M	17
MCM-41-AlMOF-M	14

Reaction condition: 1 mmol (0.2 mL) benzyl alcohol, 2.9 mmol (0.3 mL) of 30% (w/w) H_2O_2 in H_2O, 0.35 mol % catalyst, 2 mL acetonitrile, 90ºC (300 W), 3 min reaction.

Blank and reaction runs using mesoporous silica (SBA-15 and MCM-41) provided identical low conversion (<10%) in the selective oxidation of benzyl alcohol under the investigated reaction conditions. These results were also similarly obtained over SBA-15-Al-I and MCM-41-Al-I catalysts (see experimental, Table 2). Remarkably, mechanochemically synthesized Al-containing mesoporous silica provided an interesting increase in conversion (almost double) despite the extremely low measured Al content in the materials (typically 0.2-0.4 wt.%, almost equal to the impregnated sample) and the short times of reaction (ca. 3 minutes). These results relate to a mechanochemically improved catalytic performance by creating defective sites on the surface as well as the presence of tetrahedrically coordinated Al framework species (as opposed to octahedrically coordinated extraframework species observed in impregnated materials), thus increasing activity.[27] Indeed, it seemed to be sufficient to improve benzyl alcohol conversion in the systems under the investigated reaction conditions. A complete selectivity to benzaldehyde was observed in all cases.

Similarly, the results obtained for all Al-containing materials in the oxidation of isoeugenol to vanillin pointed out to such enhanced catalytic activity for mechanochemically synthesized systems even at low Al loadings (Table 3), over two times as compared to SBA-15 and MCM-41. In this case, not only the conversion but importantly the selectivity to vanillin (even if still low, ca. 15-27%) was remarkably improved for Al-containing mechanochemically synthesized mesoporous silica materials, particularly when AlMOF was employed as source of Al in the mechanochemical synthesis. Mechanochemical materials were also highly stable under the investigated conditions for both reactions, with the possibility to be reused several times (up to five reuses tested in this work for both reactions, see supporting information)

without any observable decrease in catalytic activity conversion ca. 17-20 mol%.

Table 3. Comparison of catalytic activity in the microwave-assisted oxidation of isoeugenol

Samples	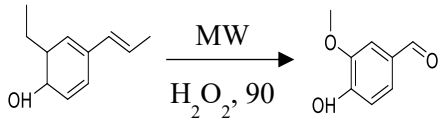		
	Conversion	**Selectivity (%)**	
	(%)	**Vanillin**	**Others**
Blank	<10	<5	>95
SBA-15	<10	<5	>95
SBA-15-Al-I	18	7	93
SBA-15-Al-M	25	16	84
SBA-15-AlMOF-M	27	27	73
MCM-41	15	8	92
MCM-41-Al-I	17	15	85
MCM-41-Al-M	22	21	79
MCM-41-AlMOF-M	19	27	73

Reaction condition: 1.2 mmol (0.2 mL) isoeugenol, 2.9 mmol (0.3 mL) of 30% (w/w) H_2O_2 in H_2O, 0.35 mol % catalyst, 2 mL acetonitrile, 90ºC (300 W), 3 min reaction.

Only a small decrease was observed in reuses for the isoeugenol to vanillin reaction due to previously reported formation of oligomeric lignin-like compounds that seem to partially block some of the Al active sites.[28] Regeneration of the materials at high temperature (400ºC, for just 2 h under air) restored the initial activity of the Al-containing SBA-15 catalysts to 25-30 mol.%. These findings also further confirmed the stability of the synthesized systems in good agreement with

previously reported similar mechanochemically synthesized nanomaterials.[22,28,29]

Additionally, results of the mechanochemically assisted oxidation of diphenyl sulfide have been summarized in Table 4. The catalysts tests were performed at 25 ºC under solvent free condition by using 30% (w/w) H_2O_2 in H_2O hydrogen peroxide as oxidant. As a result, the reaction of both absence catalyst and mesoporous silica SBA-15 exhibited low conversion as compared to Al incorporated mesoporous silica catalysts. Impregnated materials did not provide any improvements in catalytic activity, with values close to those of the blank/purely siliceous materials. Remarkably, mechanochemically synthesized exhibited significantly improved activities (almost double, Table 4). For the catalysts prepared by mechanochemical method, SBA-15-AlMOF-M provided the highest conversion of 39%, being however poorly selective to sulfoxide production (Table 4). Comparatively, a remarkable selectivity (70%) at comparable conversion (37%) was observed for MCM-41-AlMOF-M.

Table 4. Comparison of catalytic activity in the oxidation of diphenyl sulfide under ball milling.

Catalysts	Conversion (%)	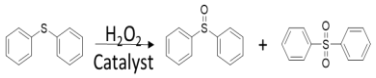	
		Selectivity (%)	
		Diphenyl sulfoxide	Diphenyl sulfone
Blank (no catalyst)	<15	29	71
SBA-15	17	28	72
SBA-15-Al-I	19	38	62
SBA-15-Al-M	35	50	50
SBA-15-AlMOF-M	39	25	75
MCM-41-Al-I	21	57	43
MCM-41-Al-M	33	57	43
MCM-41-AlMOF-M	37	70	30

Reaction condition: 0.5 mmol of diphenyl sulfide (0.083 mL), 8 equiv of 30% (w/w) H_2O_2 in H_2O (0.41 mL), 0.04 mol % catalyst, 25 stainless steel mL jar containing 8 balls (Ø 10 mm, 4 g each ball), 350 rpm, 25 min, ball milling.

The use of an AlMOF as Al source could in principle enhance the dispersion of Al incorporated into the framework of the mesoporous material, as a general improvement was observed for all investigated reactions in mechanochemically synthesized materials employing low quantities of Al-MIL-53 as source of Al. The interestingly observed different selectivity to diphenyl sulfoxide (Table 4) between MCM-41-AlMOF-M and SBA-15-AlMOF-M (70 vs 25%) may be a good indication that MCM-41 with a slightly reduced pore size (ca. 4.7 nm) is an optimum system to avoid overoxidation to the corresponding sulfone taking place on larger modified-SBA-15 pore size catalyst (ca. 5.9 nm), see Table 1.

Based on the observed selectivity, MCM-41-AlMOF-M catalyst was selected to optimize the mechanochemical conditions for the oxidation

of diphenyl sulfide. The effect of different amounts of catalyst and hydrogen peroxide were investigated under neat grinding conditions (Table 5). Almost negligible conversion was observed in the absence of catalyst (entry 1) as compared to the catalyzed reactions (entries 4, 9 and 13). These results further supported the claim that the synthesized catalysts are promoting chemical oxidations, particularly those performed under ball milling. Comparing results of entry 2-14 showed that increasing in the amount of hydrogen peroxide enhanced conversion. However, using higher amount of hydrogen peroxide increased over oxidation to diphenyl sulfone. The conversion of entry 10 (44%) was higher than other conditions. However, this condition was not selective to diphenyl sulfoxide. Optimum conditions, namely 0.04 mol% catalyst (0.005 g), 8 equiv. 30% (w/w) H_2O_2 in H_2O (0.407 mL) and 25 min reaction, provided 37% conversion with 70% selectivity to diphenyl sulfoxide. Longer reaction times (over 25 mins) or higher concentration hydrogen peroxide and catalyst contents originated a significant decrease in sulfoxide selectivity.

The reported results constitute the first literature report of the proved activity and stability of mechanochemically incorporated Al on mesoporous materials in a variety of oxidation reactions under various conditions (microwave irradiation, ball milling) using extremely low catalyst loadings (typically 0.04 mol %).

Table 5. Optimum amount of catalyst and hydrogen peroxide in the oxidation of diphenyl sulfide.

Entry	Catalyst loading (%mol)	H_2O_2 (equiv)	Conversion (%)	Selectivity (%)	
				Sulfoxide	Sulfone
1	-	8	<15	29	71
2	0.018	3	<15	65	35
3		5	16	54	46
4		8	23	37	63
5		10	37	26	74
6	0.042	1	<10	85	15
7		3	<15	74	26
8		5	23	68	32
9		8	37	70	30
10		10	44	54	46
11	0.084	3	<10	56	44
12		5	19	58	42
13		8	36	33	67
14		10	37	16	84

Reaction condition: 0.5 mmol of diphenyl sulfide, 25 stainless steel mL jar containing 8 balls (Ø 10 mm, 4 g), catalyst loading 0.02 to 0.08 mol% (0.002 to 0.01 g), 30% (w/w) H_2O_2 in H_2O content from 1 to 10 equiv. (0.05 to 0.50 mL), 350 rpm, 25 min, ball milling.

The recovery and reuse of MCM-41-AlMOF-M as catalyst for the oxidation of diphenyl sulfide was subsequently evaluated under optimum conditions. Upon reaction completion, the crude reaction mixture was recovered from the jar by using 0.5 mL of toluene. The chamber containing the catalyst was dried at 100 °C for 10 min and the catalyst was reused for the next run. As shown in Figure 4, MCM-41-AlMOF-M could be recovered and reused several times (4 runs) without any appreciable loss of its catalytic activity. No Al leaching was also

observed into solution as measured by ICP-MS (<0.5 ppm), further confirming the stability of the synthesized materials.

Figure 4. Recyclability of MCM-41-AlMOF-M in the oxidation of diphenyl sulfide with 30% (w/w) H_2O_2 in H_2O under mechanochemical solvent-free conditions.

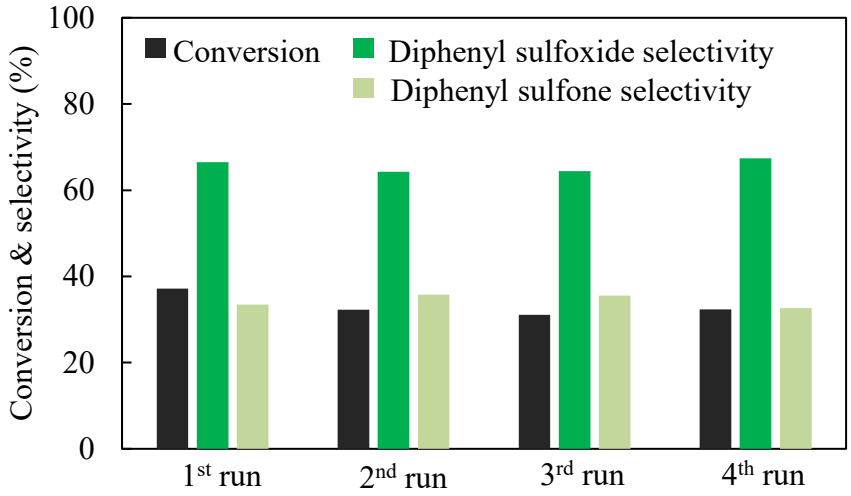

Reaction conditions: 0.5 mmol of diphenyl sulfide (0.08 mL), 25 stainless steel mL jar containing 8 balls (Ø 10 mm), 0.04 mol % catalyst (0.005 g), 8 equiv. 30% (w/w) H_2O_2 in H_2O (0.41 mL), 350 rpm, 25 min, ball milling.

Conclusions

The present work reports the unprecedented possibility to post-synthetically introduce metal species into the framework of mesoporous materials via mechanochemistry to render active catalysts for mild oxidation reactions. Even at very low loadings, typically 0.2-0.4 wt.% Al, mechanochemically synthesized Al-containing mesoporous silica (SBA-15 and MCM-41) provided unprecedented catalytic activities in mild selective oxidations and short times of reaction, both under microwave irradiation, conventional heating and mechanochemistry. The present methodology will pave the way to future post-synthetically

framework functionalized catalytically active additional materials even at low loadings that will be reported in due course.

Acknowledgments.

Rafael Luque gratefully acknowledges financial support from MINECO under project CTQ-201678289-P, co-financed with FEDER funds. The publication was prepared with support of RUDN University Program 5-100.

References

[1] Linares, N.; Silvestre-Albero, A. M.; Serrano, E.; Silvestre-Albero, J.; García-Martínez, J. Mesoporous materials for clean energy technologies. *Chem. Soc. Rev.*, **2014**, *43*, 7681–7717. https://doi.org/10.1039/C3CS60435G.

[2] Opanasenko, M.; Stepnicka, P.; Cejka, J. Heterogeneous Pd catalysts suppoorted on silica matrices. *RSC Adv.*, **2014**, *4*, 65137–65162. https://doi.org/10.1039/C4RA11963K.

[3] Rahemi, N.; Haghighi, M.; Babaluo, A.; Fallah, M.; Estifaee, P. Synthesis and physicochemical characterizations of Ni/Al_2O_3–ZrO_2 nanocatalyst prepared via impregnation method and treated with non-thermal plasma for CO_2 reforming of CH_4. *JIEC.,* **2013**, *19*, 1566-1576. https://doi.org/ 10.1016/j.jiec.2013.01.024.

[4] Putluru, S. S. R.; Schill, L.; Jensen, A. D.; Siret, B.; Tabaries, F.; Fehrmann, R. Mn/TiO_2 and Mn–Fe/TiO_2 catalysts synthesized by deposition precipitation—promising for selective catalytic reduction of NO with NH_3 at low temperatures. *Applied Catalysis B: Environ.,* **2015**, *165*, 628-635. https://doi.org/10.1016/j.apcatb.2014.10.060.

[5] Do, J. L.; Friš. ić, T. Mechanochemistry: a force of synthesis. *ACS Central Sci.,* **2016**, *3*, 13-19. https://doi.org/10.1021/acscentsci.6b00277.

[6] Xu, C.; De, S.; Balu, A. M.; Ojeda, M.; Luque, R. Mechanochemical synthesis of advanced nanomaterials for catalytic applications. *Chem. Commun.,* **2015**, *51*, 6698-6713. https://doi.org/10.1039/C4CC09876E.

[7] Muñoz-Batista, M. J.; Rodríguez-Padrón, D.; Puente-Santiago, A. R.; Luque, R. Mechanochemistry: toward sustainable design of advanced nanomaterials for electrochemical energy storage and catalytic applications. *ACS Sustainable Chem. Eng.*, **2018**, *6*, 9530–9544. https://doi.org/10.1021/acssuschemeng.8b01716.

[8] García-Espejo, G.; Rodríguez-Padrón, D.; Pérez-Morales, M.; Luque, R.; de Miguel, G.; Camacho, L. Mechanochemical synthesis of one-dimensional (1D) hybrid perovskites incorporating polycyclic aromatic spacers: highly fluorescent cation-based materials. *J. Mater. Chem. C.*, **2018**, *28*, 7677-7682. https://doi.org/10.1039/C8TC02169D.

[9] Franco, A.; De, S.; Balu, A. M.; Romero, A. A.; Luque, R. Selective oxidation of isoeugenol to vanillin over mechanochemically synthesized aluminosilicate supported transition metal catalysts. *Chem. Select*., **2017**, *29*, 9546-9551. https://doi.org/10.1002/slct.201701273.

[10] Al-Naji, M.; Balu, A. M.; Roibu, A.; Goepel, M.; Einicke, W.D.; Luque, R.; Gläser, R. Mechanochemical preparation of advanced catalytically active bifunctional Pd-containing nanomaterials for aqueous phase hydrogenation. *Catal. Sci. Technol.* **2015**, *5*, 2085-2091. https://doi.org/10.1039/C4CY01174K.

[11] Hazra, C. K.; Dherbassy, Q.; Wencel-Delord, J.; Colobert, F. Synthesis of axially chiral biaryls through sulfoxide-directed asymmetric

mild C-H activation and dynamic kinetic resolution. *Angew. Chem. Int. Ed*. **2014**, 53, 13871- 13875.

[12] Fioroni, G.; Fringuelli, F.; Pizzo, F.; Vaccaro, L. Easy and environmentally friendly uncatalyzed synthesis of β-hydroxy arylsulfides by thiolysis of 1,2-epoxides in water. *Green Chem*. **2003**, 5, 436–440.

[13] Wilde, C.A.; Ryabenkova, Y.; Firth, I.M.; Pratt, L.; Railton, J.; Bravo-Sanchez, M.; Sano, N.; Cumpson, P.J.; Coates, P.D.; Liu, X.; Conte, M. Novel rhodium on carbon catalysts for the oxidation of benzyl alcohol to benzaldehyde: A study of the modification of metal/support interactions by acid pre-treatments. *Appl. Catal. A* **2019**, 570, 2171-282.

[14] Amini, M.; Najafpour, M. M.; Salimi, S.; Ramezani, S.; Ashouri, F.; Mahmoudi, G. Iron oxide on carbon-based supports as efficient catalysts for organic compounds oxidation. *Appl. Organomet. Chem*. **2017**, 31, 3892-3902. b) Balu, A.M.; Pineda, A.; Yoshida, K.; Campelo, J.M.; Gai, P.L.; Luque, R.; Romero, AA. Fe/Al synergy in Fe_2O_3 nanoparticles supported on porous aluminosilicate materials: excelling activities in oxidation reactions. *Chem. Commun.,* **2010**, 41, 7825-7827.

[15] Rajabi, F.; Naresian, S.; Primo, A.; Luque, R. Aqueous selective oxidation of sulfides to sulfoxides at room temperature using supported iron oxide nanoparticles on SBA-15.*Adv. Synth. Catal.,* 2011, 353, 2060-2066.

[16] Karimi, B.; Ghoreishi-Nezhad, M.; Clark, J.H. Selective oxidation of sulfides to sulfoxides using 30% hydrogen peroxide catalyzed with a recoverable silica-based tungstate interphase catalyst. *Org. Lett.* **2005**, *7*, 625-628.

[17] Gamez, P.; Arends, I.W.C.E.; Shledon, R.A.; Reedijk, J. Room Temperature Aerobic Copper–Catalysed Selective Oxidation of Primary

Alcohols to Aldehydes. *Adv. Synth. Catal.* **2004**, *346*, 805-811. https://doi.org/10.1002/adsc.200404063

[18] Ojeda, M.; Grau-Atienza, A.; Campos, R.; Romero, A. A.; Serrano, E.; Marinas, J.M.; Martinez, J. G.; Luque, R. Hierarchical zeolites and their catalytic performance in selective oxidative processes. *ChemSusChem*, **2015**, *8*, 1328-1333.

[19] Jia, A.; Lou, L-L.; Zhang, C.; Zhang, Y.; Liu, S. Selective oxidation of benzyl alcohol to benzaldehyde with hydrogen peroxide over alkali-treated ZSM-5 zeolite catalyst. *J. Mol. Catal. A: Chem.* 2009, *306*, 123-129.

[20] Huo, Q.; Margolese, D. I.; Stucky, G. D. Surfactant control of phases in the synthesis of mesoporous silica-based materials. *Chem. Mater.,* **1996**, *8*, 1147. https://doi.org/10.1021/cm960137h.

[21] Steel, A.; Carr, S. W.; Anderson, M. W. J. Chem. Soc. ^{14}N NMR study of surfactant mesophases in the synthesis of mesoporous silicates. *Chem. Commun*., **1994**, *13*, 1571–1572. https://doi.org/10.1039/C39940001571.

[22] Pineda, A.; Balu, A. M.; Campelo, J. M.; Romero, A. A.; Carmona, D.; Balas, F.; Santamaria, J.; Luque, R. A dry milling approach for the synthesis of highly active nanoparticles supported on porous materials. *ChemSusChem.,* **2011**, *4*, 1561-1565. https://doi.org/10.1002/cssc.201100265.

[23] Yepez, A.; Prinsen, P.; Pineda, A.; Balu, A. M.; Garcia, A.; Lam, F.L.Y.; Luque, R. A comprehensive study on the continuous flow synthesis of supported iron oxide nanoparticles on porous silicates and their catalytic applications. *React. Chem. Eng.,* **2018**, *3*, 757-768. https://doi.org/10.1039/C8RE00063H.

[24] Campelo, J. M.; Luna, D.; Luque, R.; Marinas, J. M.; Romero, A. A.; Calvino, J. J.; Rodriguez-Luque, M. P. Synthesis of acidic Al-MCM-48: influence of the Si/Al ratio, degree of the surfactant hydroxyl exchange, and post-treatment in NH_4F solution. *J. Catal.,* **2005**, *230*, 327-338. https://doi.org/10.1016/j.jcat.2004.12.004.

[25] Zhao, D.; Feng, J.; Huo, Q.; Melosh, N.; Fredrickson, G. H.; Chmelka, B. F.; Stucky, G. D. Triblock copolymer syntheses of mesoporous silica with periodic 50 to 300 angstrom pores. *Science*, **1998**, *279*, 548-542. https://doi.org/10.1126/science.279.5350.548.

[26] Balu, A. M.; Pineda, A.; Yoshida, K.; Campelo, J. M.; Gai, P. L.; Luque, R.; Romero, A. A. Fe/Al synergy in Fe_2O_3 nanoparticles supported on porous alumiosilicate materials: execelling activities in oxidation reactions. *Chem. Commun.,* **2010**, 46, 7825-7827. https://doi.org/10.1002/cssc.201500124.

[27] Muñoz-Batista, M. J.; Rodríguez-Padrón, D.; Puente-Santiago, A. R.; Luque, R. Mechanochemistry: toward sustainable design of advanced nanomaterials for electrochemical energy storage and catalytic applications. *ACS Sustainable Chem. Eng*., **2018**, 6, 9530-9544. https://doi.org/10.1021/acssuschemeng.8b01716.

[28] Marquez-Medina, M. D.; Prinsen, P.; Li, H.; Shih, K.; Romero, A. A.; Luque**,** R. Continuous-Flow Synthesis of Supported Magnetic Iron Oxide Nanoparticles for Efficient Isoeugenol Conversion into Vanillin. *ChemSusChem.* **2018**, *11*, 389-396. https://doi.org/10.1002/cssc.201701884.

[29] Franco, A.; De, S.; Balu, A. M.; Garcia, A.; Luque, R. Selective oxidation of isoeugenol to vanillin over mechanochemically synthesized aluminosilicate supported transition metal catalysts. *Beilstein J. Org. Chem.,* **2017**, *13*, 1439-1443. https://doi.org/10.1002/slct.201701273.

ACS Sustainable Chemistry & Engineering

Supporting Information

Post-synthetic mechanochemical incorporation of Al-species into the framework of porous materials: towards more sustainable redox chemistries

M. Dolores Marquez-Medina[a], Sareena Mhadmhan[b], Alina M. Balu[a], Antonio A. Romero[a], Rafael Luque[a,c*]

[a] Departmento de Quimica Organica, Facultad de Ciencias, Universidad de Cordoba, Campus de Rabanales, Edificio Marie Curie (C-3), Ctra Nnal IV-A, Km 396, E14014, Cordoba, Spain

[b] Petrochemistry and Polymer Science, Department of Chemical Technology, Faculty of Science, Chulalongkorn University, 10330, Bangkok, Thailand

[c] Peoples Friendship University of Russia (RUDN University), 6 Miklukho-Maklaya str., 117198, Moscow, Russia

Table S1. Reuse of post-synthetically functionalized Al-containing mesoporous silica in the microwave-assisted oxidation of benzyl alcohol to benzaldehyde

Catalyst	1st Reaction	1st Reuse	2nd Reuse	3rd Reuse	4th Reuse	5th Reuse
SBA-15-Al-M	18	17	16	16	16	15
SBA-15-AlMOF-M	20	19	19	19	18	18
MCM-41-Al-M	17	17	16	16	15	14

Table S2. Reuse of catalysts on microwave-assisted oxidation of isoeugenol.

Catalyst	1st Reaction	1st Reuse	2nd Reuse	3rd Reuse	4th Reuse	5th Reuse
SBA-15-Al-M	25	23	22	22	21	20
SBA-15-AlMOF-M	27	26	25	25	24	23
MCM-41-Al-M	22	20	19	19	18	17

Conclusiones

CAPÍTULO IV

IV. 1. Conclusiones.

Las investigaciones llevadas a cabo en la presente Memoria de Tesis Doctoral nos han llevado a concluir que:

1. Se han sintetizado nanomateriales mediante un procedimiento simple y reproducible en flujo continuo, utilizando el aluminosilicato Al-SBA-15 como soporte de nanopartículas de óxido de hierro en nuestros materiales.

2. Los nanocomposites sintetizados muestran propiedades magnéticas adecuadas cuando la temperatura de síntesis se mantiene por debajo de 195 ºC.

3. La utilización de dichos materiales magnéticos en procesos catalíticos ha sido prometedora, en particular, para la reacción de conversión del isoeugenol a vainillina llevada a cabo a temperatura

ambiente en fase líquida mediante calefacción convencional, donde los materiales presentaron conversiones en el intervalo del 80 al 90% molar, con selectividades ≥ 50% molar a vainillina utilizando peróxido de hidrógeno como oxidante. El resultado óptimo se obtuvo con un 50% de conversión de isoeugenol 0,5 M con una selectividad a vainillina de 57% (24 h de reacción).

4. Las reacciones de conversión del isoeugenol llevadas a cabo mediante irradiación asistida por microondas reducen drásticamente los tiempos de reacción (a 5-15 min), sin embargo, dicha irradiación por microondas influye negativamente en la reutilización del catalizador. La desactivación del catalizador se ha relacionado con procesos de adsorción superficial, recuperándose el 80% de la actividad catalítica inicial del catalizador mediante regeneración térmica a 300 ºC.

5. Por otra parte, se han sintetizado nanocatalizadores separables magnéticamente, incorporando nanopartículas de hierro sobre la superficie de un aluminosilicato (Al-SBA-15) mediante un procedimiento de molienda mecanoquímica en una única etapa. La utilización de residuos derivados de la biomasa ha permitido obtener materiales con propiedades magnéticas destacables, que permiten su fácil separación del medio de reacción.

6. La obtención de vainillina mediante la oxidación del isoeugenol y del alcohol vainillínico, utilizando estos nanomateriales magnéticos como catalizadores, ha permitido demostrar su rendimiento catalítico con resultados prometedores para la producción selectiva de vainillina. En este sentido, se han obtenido conversiones en el intervalo del 80 al 90% molar y selectividades a vainillina ≥ 50% molar.

7. Además, los resultados obtenidos sugieren que las interacciones Al-Fe unidas al incremento de la acidez de tipo Lewis, así como, un

mayor número de especies de óxido de hierro superficial disponibles para los procesos de oxidación, son los factores que determinan la obtención de una actividad y selectividad más elevadas cuando se utiliza el nitrato de hierro (III) como sal precursora en la síntesis de los materiales.

8. La utilización de la metodología mecanoquímica ha permitido la incorporación directa de especies Al estructural (Al coordinado tetraédricamente) en silicatos mesoporosos del tipo SBA-15 y MCM-41 con contenidos de aproximadamente el 0,2-0,4% en peso de Al. Además, se han empleado, por primera vez, materiales Al-MOFs como fuente de aluminio.

9. A pesar del bajo contenido en Al (0,2-0,4% en peso), estos materiales poseen actividades catalíticas sin precedentes en reacciones de oxidación selectivas, a tiempos de reacción cortos, tanto en condiciones de reacción inducidas mediante irradiación con microondas como mediante molienda mecanoquímica.

10. Finalmente, la metodología mecanoquímica se propone como una novedosa opción para la funcionalización postsintética para el desarrollo de nuevos materiales catalíticamente activos.

IV. 2. Conclusions.

The research carried out in this Doctoral Thesis manuscript can be summarized into the following conclusions:

1. A range of nanomaterials have been synthesized using a simple and reproducible continuous flow method, employing the aluminosilicate Al-SBA-15 as support for the deposition of iron oxide nanoparticles.

2. The nanocomposites synthesized, besides structural and textural properties, feature magnetic characteristics which endow the materials with suitable properties as a catalyst with an optimum separation, where the temperature synthesis was a determining factor to achieve optimised nanomaterials below 195ºC.

3. The catalytic activity of synthesized magnetic materials has been promising, especially the isoeugenol conversion to vanillin at room

temperature in the liquid phase, where the material reached 80-90% molar conversion with selectivities ≥ 50% molar to vanillin using hydrogen peroxide as green oxidant. Optimum results provided a 50% conversion of 0.5 M isoeugenol with a vanillin selectivity of 57% (24 h reaction).

4. The reaction times in the isoeugenol conversion to vanillin can be drastically reduced (to 15 minutes) when the reaction is carried out under microwave-assisted irradiation. However, the use of microwaves has a negative effect on the reuse of the catalyst. Deactivation of the catalyst was found to be related to surface adsorption. Recovering 80% of the initial catalyst activity of the catalyst was only possible by thermal regeneration at 300 °C.

5. On the other hand, magnetically separable nanocatalysts have been synthesized incorporating iron nanoparticles on the surface of an aluminosilicate (Al-SBA-15) by means of a one-step mechanochemical milling process. The use of biomass-derived feedstocks allowed the possibility to obtain materials with remarkable magnetic properties, which allow a simple separation from the reaction medium.

6. Vanillin production via oxidation of isoeugenol and vanillin alcohol, using these magnetic nanomaterials as catalysts, was successfully achieved with promising results including conversions in the range of 80 to 90 mol% and selectivities to vanillin ≥ 50 mol%.

7. In addition, the results obtained suggested that Al-Fe interactions linked to the increase in Lewis acidity, as well as a greater number of surface iron oxide species available for oxidation processes, are determining factors to achieve a higher activity and selectivity when iron (III) nitrate is used as iron precursor.

8. The use of the mechanochemical methodology has allowed the direct incorporation of structural Al species (Al tetrahedrally coordinated) into mesoporous silicates of the type SBA-15 and MCM-41 with contents of ca. 0.2-0.4% by weight of Al. In addition, Al-MOFs have been used as the source of aluminium for the first time.

9. Despite the low Al content (0.2-0.4% by weight), these materials exhibited unprecedented catalytic activities in mild and selective oxidation reactions, at short reaction times, both under reaction conditions induced by microwave-assisted irradiation as well as by mechanochemical grinding.

10. Finally, the mechanochemical methodology is proposed as a novel promising alternative for the structural postsynthetic functionalization of new catalytically active materials.

Resumen

CAPÍTULO V

V. 1. Resumen.

Los artículos que componen la presente Memoria de Tesis Doctoral forman parte de las principales líneas de investigación actualmente en desarrollo en el Grupo de Investigación FQM-383, Nanoquímica y Valorización de Biomasa y Residuos (NANOVAL), asumiendo como objetivos fundamentales el uso de materiales eficientes y procesos más selectivos para la implementación procesos sostenibles en la industria química, farmacéutica, etc.

En esta Memoria de Tesis Doctoral, se expone el potencial que presentan los materiales mesoporosos en el ámbito de catálisis heterogénea, permitiendo ser funcionalizados por síntesis directa o mediante procesos post-sintéticos. La funcionalización de los materiales mesoporosos ha permitido el uso de éstos como catalizadores en diferentes reacciones químicas de interés industrial.

En el primer trabajo descrito en la memoria (Capítulo III.1), titulado "Continuous flow synthesis of supported magnetic iron oxide nanoparticles for efficient isoeugenol conversion to vanillin", se ha procedido a la síntesis de nuevos catalizadores magnéticos, incorporando nanopartículas de hierro sobre un soporte mesoporoso (Al-SBA-15) utilizando un sistema de flujo continuo, en un único paso "one pot". El proceso en flujo continuo nos ha permitido obtener nanocatalizadores magnéticos gracias al paso de una disolución etanólica de la sal de hierro precursora que se hace fluir a través de un reactor en el cual se encuentra empaquetado el material mesoporoso empleado como soporte a una temperatura controlada. Dicho procedimiento es por tanto simple, innovador y eficiente, permitiéndonos investigar la influencia de la velocidad de flujo de la disolución que contiene el precursor metálico y la temperatura de síntesis de los materiales.

Los valores de susceptibilidad magnética mostrados por los nanocatalizadores están en el intervalo de 70 a 210 10^{-6} m^3 K g^{-1}, hecho consistente con el contenido de maghemita en el soporte, ya que las nanopartículas de maghemita pura generalmente muestran susceptibilidades magnéticas de aproximadamente 500 10^{-6} m^3 K g^{-1}. Dichos valores de susceptibilidad son suficientemente elevados para que estos materiales sean separables magnéticamente de la mezcla de reacción utilizando un simple imán.

La utilización de estos materiales magnéticos en procesos catalíticos ha sido prometedora, en particular, para la reacción de conversión del isoeugenol a vainillina, mostrando una alta actividad catalítica, selectividad y estabilidad química, así como la ventaja de una fácil separación, eliminando la necesidad de procedimientos poco prácticos para el reciclado de los catalizadores.

En el trabajo "*Mechanochemically synthesized supported magnetic Fe-nanoparticles as catalysts for efficient vanillin production"* (Capítulo III.2), se ha estudiado la preparación de materiales magnéticos mediante molienda mecanoquímica empleando como soporte el material mesoporoso Al-SBA-15, un material orgánico de desecho como activador de la fase magnética y una sal precursora de hierro para generar la funcionalidad en el material (fase activa-magnetismo). Además, en el trabajo se optimiza el proceso de síntesis de los nanomateriales, empleando distintas sales precursoras de nanopartículas de hierro (citrato amónico de hierro, nitrato de hierro, perclorato de hierro y cloruro de hierro), diferentes temperaturas de calcinación (300, 400 y 500 ºC) e incorporando en el soporte diferentes contenidos en peso de hierro.

De todos los materiales obtenidos a lo largo de dichas investigaciones, solo aquellos preparados con citrato amónico de hierro y nitrato de hierro han mostrado propiedades magnéticas, siendo los materiales con mayor magnetismo los calcinados a una temperatura de 400 ºC.

Los materiales han sido caracterizados mediante distintas técnicas como son la adsorción/desorción de N_2, difracción de rayos-X (XRD), espectroscopía fotoelectrónica de rayos-X (XPS), microscopía electrónica de barrido acoplada a análisis elemental (SEM-EDX), microscopía electrónica de transmisión (TEM) y susceptibilidad magnética.

Los nanocatalizadores magnéticos han demostrado una elevada actividad catalítica y estabilidad química, destacando su capacidad de separación/reusabilidad en las reacciones de oxidación selectivas del isoeugenol (ruptura oxidativa) y del alcohol vainillínico (oxidación) a vainillina. El origen de sus propiedades catalíticas se ha relacionado con la concentración superficial de nanopartículas de hierro y con la interacción Al-Fe.

Por último, el estudio de la reutilización de estos nanocatalizadores ha demostrado la estabilidad de estos sistemas bajo las condiciones de reacción de investigadas, exhibiendo actividades catalíticas similares tras cinco usos.

Finalmente, en el trabajo "*Post-synthetic mechanochemical incorporation of Al species into the framework of porous materials: towards more sustainable redox chemistries*" (Capítulo III.3) se han sintetizado diferentes nanomateriales incorporando, mediante molienda mecanoquímica e impregnación, especies de aluminio en proporciones muy bajas (0,2-0,4% en peso) en materiales de sílice mesoporos (SBA-15 y MCM-41). Concretamente, la incorporación del aluminio se ha llevado a cabo utilizando como precursores isopropóxido de aluminio y, por primera vez, materiales MOFs conteniendo Al.

Las propiedades físico-químicas de los materiales sintetizados se han caracterizado mediante técnicas como la difracción de rayos-X (XRD), adsorción-desorción de N_2, microscopía electrónica de barrido acoplada a análisis elemental (SEM-EDX), espectrometría de masas acoplada a plasma de acoplamiento inducido (ICP/MS), cromatografía de pulsos utilizando piridina y dimetilpiridina como bases valorantes, resonancia magnética nuclear (NMR) y susceptibilidad magnética.

Los resultados obtenidos mediante RMN-MAS del Al^{27} nos indican que la técnica mecanoquímica ha sido capaz de introducir especies de aluminio estructural (Al tetraédrico) en los silicatos SBA-15 y MCM-41 con contenidos de Al muy bajos, siendo la primera vez que se publica dicha incorporación de tipo post-sintético mediante el procedimiento mecanoquímico.

A pesar de los contenidos extremadamente bajos en Al (0,2-0,4% en peso) las especies aisladas de óxido de aluminio muestran actividades

catalíticas prometedoras en reacciones de oxidación selectiva, utilizando condiciones de reacción suaves (irradiación asistida mediante microondas y molienda mecanoquímica), que incluyen las reacciones de oxidación de alcohol bencílico a benzaldehído, isoeugenol a vainillina y sulfuro de difenilo a sulfóxido de difenilo.

II. Summary.

The scientific contributions in the present Doctoral Thesis have principal research objectives related to the platform technologies from our research Group FQM-383, Nanochemistry and biomass valorisation and waste (NANOVAL), assuming as fundamental objectives the benign-by-design preparation of advanced materials for more selective processes to be potentially implemented into more sustainable processes in the chemical, pharmaceutical and related industries.

Research studies from the Doctoral Thesis illustrate the potential of mesoporous materials in the field of heterogeneous catalysis, with promising possibilities for their functionalization by direct synthesis or post-synthetic processes. The functionalization of mesoporous materials

allowed their use as catalysts in a wide range of reactions such as those catalysed by acid and redox sites and/or biomass conversion processes.

In the first work described in the manuscript (chapter III.1) entitled "*Continuous flow synthesis of supported magnetic iron oxide nanoparticles for efficient isoeugenol conversion to vanillin*", the synthesis of new magnetic catalysts was successfully accomplished, incorporating iron oxide nanoparticles on a mesoporous aluminosilicate support (Al-SBA-15) using a continuous flow system in a single step "one pot" reaction. The continuous flow process allowed us to obtain magnetic nanocatalysts in a simple system by pumping an ethanolic solution containing the dissolved iron salt precursor through a reactor in which the mesoporous material used as support at a controlled temperature is placed in a fixed bed reactor. The synthetic procedure is therefore simple, innovative and efficient, allowing us to investigate the influence of the flow rate of the solution containing the metallic precursor and the synthesis temperature.

The values of magnetic susceptibility shown by the nanocatalysts oscillate in the range from 70 to 210 10^{-6} m^3 K g^{-1}, consistent with the maghemite content in the support, due to the fact that pure maghemite has susceptibility values of ca. 500 10^{-6} m^3 K g^{-1}. These susceptibility values endow nanocatalysts with iron oxide nanoparticles with magnetic separation features for a simple nanomaterials recovery from the reaction mixture.

The use of magnetic materials in the catalytic process has been promising, especially, in the conversion reaction of isoeugenol to vanillin, where high catalytic activity and stability were observed together with the advantage of simple separation, eliminating the need for impractical procedures for catalysts recycling.

The manuscript "*Mechanochemically synthesized supported magnetic Fe-nanoparticles as catalysts for efficient vanillin production*" (Chapter III.2) proposes a simple and innovative mechanochemical methodology for the preparation of magnetic materials using Al-SBA-15 as mesoporous material support, a waste-derived organic material as an activator of the magnetic phase and iron precursors as the active phase (iron oxide nanoparticles) in the material. Practically, the nanomaterials synthesis was optimised using different iron precursor salts (ammonium iron (III) citrate, Iron (III) nitrate, Iron (III) perchlorate hydrate and iron (III) chloride), different calcination temperatures (300, 400 y 500 ºC) and incorporating different iron content

The materials were characterised using different techniques including N_2 adsorption/desorption, X-ray diffraction (XRD), X-ray photoelectronic spectroscopy (XPS), Scanning Electron Microscopy coupled with energy dispersive X-ray analysis for elemental analysis (SEM-EDX), Transmission Electron Microscopy (TEM) and magnetic susceptibility.

The magnetic nanocatalysts have demonstrated a high catalytic activity and chemical stability, highlighting their separation/reusability capacity in the selective oxidation reactions of isoeugenol (oxidative rupture) and vanillin alcohol (oxidation) to vanillin. The origin of its catalytic properties has been related to the surface concentration of iron nanoparticles and the Al-Fe interaction in the materials.

Finally, a reuse study of the nanocatalysts has been carried out, demonstrating the stability of these systems under the investigated reaction conditions exhibiting similar catalytic activities after five uses.

Lastly, the paper "*Post-synthetic mechanochemical incorporation of Al species into the framework of porous materials: towards more sustainable redox chemistries*" (Chapter III.3), different nanomaterials

have been synthesized incorporating low aluminium contents (typically 0.2-0.4 wt.%) via mechanochemical milling and impregnation on mesoporous materials. Specifically, the incorporation of aluminium species was carried out using different sources such as aluminium isopropoxide and aluminium-containing MOFs materials.

The physico-chemical properties of all materials were studied using characterization techniques including X-ray diffraction (XRD), adsorption-desorption of N_2, scanning electron microscopy coupled with energy dispersive X-ray analysis for elemental analysis (SEM-EDX), inductively coupled plasma mass spectrometry (ICP-MS), pulse chromatography with pyridine and dimethyl pyridine as titration bases, magnetic nuclear resonance (NMR) and magnetic susceptibility studies.

Solid state NMR studies pointed to different aluminium coordination states in the synthesised material, including framework aluminium species which strongly suggested that the mechanochemical procedure was able to introduce aluminium species within SBA-15 and MCM-41 post-synthetically with low Al content, being the first literature report on such post-synthetic mechanochemically assisted framework incorporation of catalytically active species in mesoporous materials.

Despite the extremely low contents in Al (0.2-0.4% by weight), the isolated species of aluminum show promising catalytic activities in selective oxidation reactions using mild reaction conditions (microwave irradiation and mechanochemical milling) including the oxidations of benzyl alcohol to benzaldehyde, isoeugenol to vanillin and diphenyl sulfide to diphenyl sulfoxide.

Indicios de Calidad

CAPÍTULO VI

Clave	Artículo
Título	Continuous flow synthesis of supported magnetic iron oxide nanoparticles for efficient isoeugenol conversion to vanillin
Autores	M. Dolores Márquez-Medina, Pepijn Prinsen, Hangkong Li, Kaimin Shih, Antonio A. Romero y Rafael Luque
Nombre de la revista	ChemSusChem
Año, volumen, página	2018, 11, 389-396
Editorial	Wiley-VCH Verlag GmbH & Co
Revista incluida en Journal Citations Reports (JCR)	Si Base de datos SCI, 2017
Índice de impacto	7,411
Categoría	Chemistry, Multidisciplinary
Lugar que ocupa la revista en la categoría	24 de 171
Cuartil	Q1

Clave	Artículo
Título	Mechanochemically synthesized supported magnetic Fe-nanoparticles as catalysts for efficient vanillin production.
Autores	M. Dolores Márquez-Medina, Daily Rodríguez-Padrón, Alina M. Balu, Antonio A. Romero, Mario J. Muñoz-Batista y Rafael Luque.
Nombre de la revista	Catalysts
Año, volumen, página	2019
Editorial	MDPI AG
Revista incluida en Journal Citations Reports (JCR)	Sí Base de datos SCI, 2017
Índice de impacto	3,465
Categoría	Chemistry, Physical
Lugar que ocupa la revista en la categoría	55 de 147
Cuartil	Q2

Clave	Artículo
Título	Post-synthetic mechanochemical incorporation of Al-species into the framework of porous materials: towards more sustainable redox chemistries
Autores	M. Dolores Márquez-Medina, Sareena Mhadmha, Alina M. Balu, Antonio A. Romero, Rafael Luque
Nombre de la revista	ACS Sustainable Chemistry & Engineering
Año, volumen, página	2019
Editorial	American Chemical Society
Revista incluida en Journal Citations Reports (JCR)	Si Base de datos SCI, 2017
Índice de impacto	6,14
Categoría	Engineering, Chemical
Lugar que ocupa la revista en la categoría	10 de 137
Cuartil	Q1

Otras Aportaciones Científicas

CAPITULO VII

Comunicaciones a Congresos

Durante los años de formación del doctorando se han producido otras aportaciones a congresos, que no forman parte de esta Memoria de Tesis Doctoral, que se citan a continuación:

1. Síntesis de nanocomposites magnéticamente separables mediante procesos de flujo continuo. Exposición oral: Mª Dolores Márquez Medina; V congreso jóvenes investigadores. Córdoba (España), 30 Noviembre - 1 Diciembre, 2016.

2. Síntesis de nanocomposites mediante procesos de flujo continuo. Exposición Póster: Mª Dolores Márquez Medina, Ana Franco, Alfonso Yépez, Alina Mariana Balu, Antonio Ángel Romero Reyes y Rafael Luque; VI Encuentro de nanociencia y

nanotecnología de jóvenes investigadores (Nanouco VI). Córdoba (España), 25-26 Enero, 2017.

3. Isoeugenol conversion to vanillin using separable magnetic materials. Exposition Poster: Mª Dolores Márquez Medina, Daily Rodríguez Padrón, Alina Mariana Balu, Antonio Ángel Romero Reyes y Rafael Luque; Fourth MC Meeting & Third Workshop (LIGNOVAL). Torremolinos, Málaga (España), 27-28 Marzo, 2017.

4. Catalyzed microwave assisted synthesis of carbon quantum dots from lignocellulosic residues. Exposition Poster: Mª Dolores Márquez Medina, Daily Rodríguez Padrón, Alina Mariana Balu, Antonio Ángel Romero Reyes y Rafael Luque; Fith MC Meeting & Fourth Workshop (LIGNOVAL). Thessaloniki (Grecia), 12-14 Marzo, 2018.

5. Incorporación de aluminio en materiales mesoporosos mediante procesos mecanoquímicos. Exposición Póster: Mª Dolores Márquez Medina, Alina Mariana Balu, Antonio Ángel Romero Reyes y Rafael Luque; VII Encuentro de nanociencia y nanotecnología de jóvenes investigadores (Nanouco VI). Córdoba (España), 21-22 Enero, 2019.

6. Post-synthetic mechanochemical incorporation of Al species into the framework of porous materials. Exposición oral: Mª Dolores Márquez Medina; VII congreso jóvenes investigadores. Córdoba (España), 6-7 Enero, 2019.

ANEXO I

Materiales y Métodos

Anexo I. Materiales y Método.

Preámbulo……..215

A. I. 1. Métodos de síntesis de nanopartículas soportadas 217

A. I. 1. 1. Molienda meconoquímica 217

A. I. 1. 2. Deposición de nanopartículas metálicas mediante flujo continuo 222

A. I. 1. 3. Impregnación hasta humedad incipiente o impregnación capilar 224

A. I. 2. Técnicas de caracterización 225

A. I. 2. 1. Porosimetría de adsorción/desorción de nitrógeno 225

A. I. 2. 2. Método cromatográfico de pulsos para la determinación de las propiedades ácidas superficiales 229

A. I. 2. 3. Técnicas de rayos-X 232

A. I. 2. 3. 1. Difracción de rayos-X (XRD) 232

A. I. 2. 3. 2. Espectroscopía fotoelectrónica de rayos-X (XPS) 233

A. I. 2. 4. Análisis térmico gravimétrico y térmico diferencial (ATG/ATD) 235

A. I. 2. 5. Microscopía electrónica 236

A. I. 2. 5. 1. Microscopía electrónica de barrido/ Análisis de energía dispersiva de Rayos-X (SEM/EDX) 236

A. I. 2. 5. 2. Microscopía electrónica de transmisión (TEM/HRTEM). 237

A. I. 2. 6. Espectrometría de masas con acoplamiento inductivo (ICP-MS) 239

A. I. 2. 7. Resonancia magnética nuclear (RMN) 240

A. I. 2. 8. Susceptibilidad magnética 243

A. I. 3. Actividad catalítica 245

A. I. 3. 1. Actividad catalítica asistida por microondas 245

A. I. 3. 2. Actividad catalítica mediante calefacción convencional 246

A. I. 3. 3. Actividad catalítica mediante molienda mecanoquímica 246

Bibliografía 249

Preámbulo.

El siguiente Anexo de la memoria de esta Tesis Doctoral tiene la finalidad de presentar y explicar brevemente las distintas técnicas que se han empleado en la síntesis de los materiales y determinación de sus propiedades físico-químicas. De igual manera, se describen los diferentes equipos y condiciones experimentales empleadas con sus respectivos modelos matemáticos, que nos han permitido utilizar los parámetros óptimos.

Los nanocatalizadores obtenidos han sido caracterizados empleando varias técnicas instrumentales entre las que se incluyen adsorción-desorción de N_2, el método cromatográfico de pulsos para la determinación de las propiedades ácidas superficiales, la difracción de rayos-X (DRX), la espectroscopía fotoelectrónica de rayos-X (XPS), análisis termogavimétrico y térmico diferencial (ATG-ATD), microscopía electrónica de barrido (SEM), microscopía electrónica de

transmisión (TEM), espectrometría de masas con plasma acoplado inductivamente (ICP-MS), resonancia magnética nuclear (RMN), susceptibilidad magnética, etc.

Del mismo modo, la actividad catalítica de los materiales se investigado para distintas reacciones químicas aplicando procedimientos de calefacción convencional, irradiación por microondas y molienda mecanoquímica. Los productos de reacción obtenidos se han analizado por cromatografía de gases (GC) y/o cromatografía de gases acoplada a espectrometría de masas (GC-MS).

A. I. 1. Métodos de síntesis de nanopartículas soportadas.

Las diferentes técnicas experimentales empleadas para llevar a cabo la síntesis de los nanomateriales investigados son: (i) el método de molienda meconoquímica, (ii) el sistemas de flujo continuo, y (iii) el método de impregnación hasta humedad incipiente.

A. I. 1. 1. Molienda meconoquímica.

Los procesos de molienda mecanoquímica se emplean desde hace décadas en el ámbito de química, no obstante, su uso en la estabilización de sistemas porosos donde se incorporan nanopartículas metálicas está suponiendo un avance respecto de otras técnicas. La aplicación de la fuerza mecánica para obtener nuevos materiales se ha vuelto una opción cada vez más atractiva debido a que no requieren el empleo de disolventes y permite reducir el número de etapas en la síntesis de nanomateriales ("Química Sostenible").

Esta metodología de síntesis se basa en energía mecánica para producir reacciones químicas a temperatura ambiente, en lugar de altas temperaturas. Los productos finales obtenidos mediante los procesos de mecanoquímicos son polvos ultrafinos con intervalos de distribución de tamaño de partícula amplios, que van desde una micra a la escala nanométrica [1].

Los choques entre partículas pueden ser bola-polvo-bola o bola-polvo-pared interna del contenedor; en ambos casos el choque modifica la morfología del polvo sólido. Por un lado, cuando las partículas del material están siendo aplastadas, se están produciendo uniones frías, formándose partículas nuevas que están constituidas por combinación de constituyentes o de materia prima iniciales. Los constituyentes más frágiles tienden a unirse con los más dúctiles y la soldadura en frío lleva consigo la deformación plástica y la aglomeración de partículas, mientras que la fractura conlleva una reducción del tamaño de partícula. La interacción de los dos fenómenos conduce a un refinamiento y homogeneización de los constituyentes. Habitualmente, hay una etapa del proceso en la que se produce un equilibrio entre los dos fenómenos, actuando cada uno sobre el otro y obteniéndose materiales de microestructura muy homogénea. La evolución particular de cada proceso depende de sus características y de los precursores (por ejemplo: precursores dúctiles y/o frágiles). En la Figura A. I. 1. se muestra el mecanismo de colisión bola-polvo-bola en un proceso de molienda de alta energía [2,3].

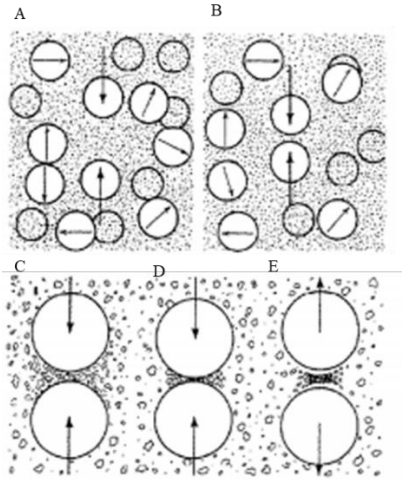

Figura A. I. 1. Mecanismo de colisión bola-polvo-bola en un proceso de molienda mecanoquímica. A) y B) Aproximación de las bolas, C) Atrapado y compactación de las bolas, D) Aglomeración, E) Abandono del aglomerado por energía elástica [3].

El molino de bolas planetario (Figura A. I. 2.), empleado para la síntesis de nuestros nanomateriales, recibe su nombre debido al movimiento que describe el recipiente donde tiene el proceso de molienda mecanoquímica es similar al de un planeta, es decir, realiza movimientos de rotación y translación. En el contenedor, tanto la carga como las bolas giran alrededor de un eje central, y giran sobre sí mismas muy rápidamente. El sentido de giro del eje central y de los contenedores es opuesto, y la composición de fuerzas inerciales superpuestas que derivan de estos movimientos de rotación hace que la carga del contenedor se separe de las paredes del mismo. Las fuerzas centrífugas actúan en un mismo sentido y en sentido contrario. Hay un rozamiento de las bolas en las paredes internas del contenedor (efecto abrasión), y un desprendimiento y proyección libre de las bolas y del producto en la pared contraria del contenedor (efecto de percusión). Gracias a los fenómenos de abrasión y percusión, y al gran intercambio

de energía entre bolas y polvos, se consigue un producto final homogéneo con un rendimiento de molienda muy alto.

Figura A. I. 2. Esquema del movimiento de las bolas dentro del molino planetario RESTCH modelo PM-100 empleado en la Memoria de Tesis Doctoral.

En cuanto al mecanismo por el cual se produce el proceso, éste no es claro debido a la diversidad de tipos de reacción, condiciones y materiales que se emplean. La naturaleza heterogénea de las reacciones sólido-sólido, la dificultad para observar directamente los materiales que están sufriendo el proceso mecanoquímico a nivel microscópico o molecular, así como la falta de estudios de algunos tipos de reacciones son algunos de los principales factores que complican el conocimiento avanzado de este tipo de procesos con claridad [4].

La molienda mecanoquímica se ha utilizado en la presente Tesis Doctoral para incorporar nanopartículas metálicas sobre materiales del tipo SBA-15 y MCM-41. El posible mecanismo que ha tenido lugar en esta deposición, supone una activación de los grupos silanoles que se encuentran en la superficie de los materiales silíceos (deshidroxilación) durante el proceso de molienda, produciendo moléculas de agua en el medio de reacción. En presencia de agua el precursor metálico podría

ser hidrolizado a especies hidróxido, que posteriormente se descompone en minúsculas cantidades de nanopartículas de óxido metálico, debido a las altas temperaturas que se alcanzan exclusivamente en lugares localizados durante el proceso de molienda. Tras la calcinación, las especies intermedias de hidróxido metálico también se convierten en nanopartículas de óxido metálico. La reacción mecanoquímica propuesta para la deposición de las nanopartículas de óxido metálico sobre los materiales mesoporosos tipo SBA-15 y MCM-41, se ha confirmado en diferentes publicaciones de nuestro grupo de investigación [5].

En nuestro procedimiento experimental, la preparación de los materiales por molienda mecanoquímica se llevó a cabo en un molino planetario de bolas Restch, modelo PM-100. Este modelo permite variar la velocidad de giro, tiempo de molienda, así como invertir la dirección de giro. La capacidad del recipiente de la molienda empleado es de 125 mL y el diámetro de las bolas empleadas es 1 cm. Tanto las bolas como el recipiente donde se llevó a cabo la molienda son de acero inoxidable.

Para la preparación de los nanomateriales soportados se añaden al recipiente de la molienda el soporte y el precursor del metal y se muelen conjuntamente a 350 r.p.m. durante 10 minutos. Una vez finalizado el proceso de molienda el material obtenido se somete a diferentes tratamientos térmicos de estandarización.

A. I. 1. 2. Deposición de nanopartículas metálicas mediante flujo continuo.

La síntesis de nanomateriales con nanopartículas soportadas mediante sistemas de flujo continuo está sufriendo un desarrollo exponencial, desbancando a la técnica convencional empleada (procesos batch). Esto se debe a las ventajas que posee la síntesis mediante flujo continuo en comparación con los sistemas batch [6]:

a) Mayor control de las condiciones de reacción, productividad y simplicidad en la preparación y operación del proceso. Además, dicho proceso nos permite modificar las condiciones de reacción durante el transcurso de la síntesis.
b) Permiten la obtención de una mayor cantidad de nanomateriales en una única síntesis, mejorando de esta forma la reproducibilidad de los mismos.

Gracias a esta técnica hemos podido llevar a cabo la síntesis de nanomateriales, donde se han soportado nanopartículas de hierro sobre aluminosilicatos del tipo SBA-15. Dicho proceso de síntesis se ha optimizado atendiendo a la concentración de la sal precursora en la disolución que pasara a través del lecho del soporte, tiempos de residencia, temperatura, etc.

Como punto de partida hemos utilizado los parámetros operacionales y de síntesis descritos por Luque y col. [7]. Entre dichos parámetros se encuentra el estudio del soporte utilizado, el empleo de la sal de hierro precursora, la concentración del metal y el empleo de diferentes flujos de alimentación, el tiempo de reacción en flujo para cada operación y la temperatura de trabajo. Este último parámetro ha sido identificado como crítico tanto en la cantidad de óxido de hierro depositado como en el magnetismo del nanomaterial obtenido.

El sistema utilizado, Figura A. I. 3, consta de una bomba peristáltica, que hace fluir la disolución etanólica de hierro, un reactor de lecho fijo de acero inoxidable, donde se empaqueta el material Al-SBA-15 utilizado como soporte, un horno para el calentamiento del reactor con un control de la temperatura mediante un termopar insertado directamente en el lecho catalítico y un total de dos válvulas de tres vías, que nos permitirán cambiar de disolución en cualquier momento y el paso de un flujo de aire en la etapa final de la síntesis [8].

Este procedimiento de preparación de nanocomposites magnéticos en flujo continuo consta de varias etapas que se describirán a continuación. En primer lugar, se rellena el reactor de acero inoxidable con el aluminosilicato Al-SBA-15 (~3 g) utilizado como soporte y se fija entre dos topes de lana de cuarzo en los extremos para evitar el desplazamiento del material. El reactor está dotado con dos filtros de acero inoxidable uno en la entrada y otro en la salida de este para evitar obstrucciones en el conjunto del sistema.

Una vez montado el sistema, la síntesis comienza inyectando un flujo de 0,5 mL/min de etanol durante 45 min al tiempo que se alcanza la temperatura de síntesis. Transcurrido este tiempo y con nuestro sistema a la temperatura de síntesis deseada, actuamos sobre una de las válvulas de tres vías que nos permite cambiar el flujo de etanol por el de una disolución saturada de $Fe(NO_3)_2 \cdot 9H_2O$ (sal precursora) en etanol, aplicando un flujo de 0,5 mL/min durante 1 hora. Seguidamente, volvemos a actuar sobre la válvula de tres vías para hacer pasar a través del lecho catalítico un flujo de 0,5 mL/min de ácido propiónico durante 45 min.

Transcurrido este tiempo se detiene la bomba peristáltica y se actúa sobre una segunda válvula de tres vías para inyectar un flujo de aire de

30 mL/min durante 3 h, aproximadamente, al tiempo que se ejecuta una rampa de temperatura programada de 5ºC/min hasta una temperatura final de 300ºC, manteniéndose constante durante 1 h.

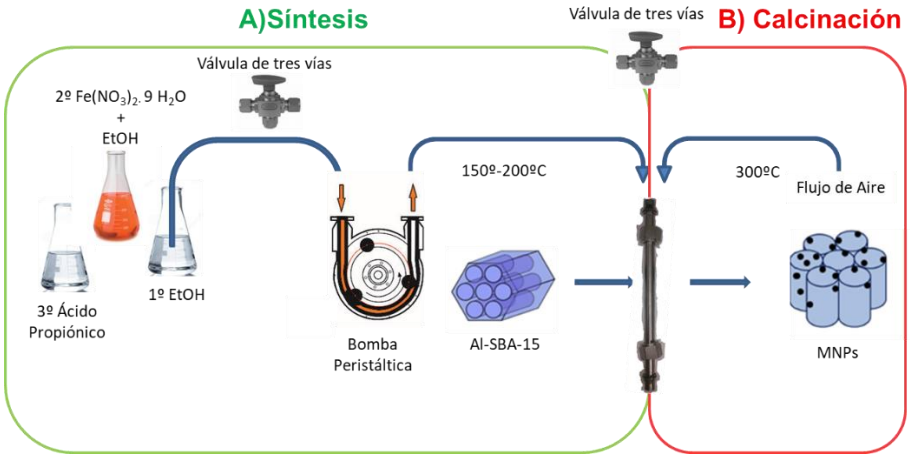

Figura A. I. 3. Esquema de síntesis de nanopartículas metálicas soportadas sobre material Al-SBA-15 mediante flujo continuo. Adaptado [8].

A. I. 1. 3. Impregnación hasta humedad incipiente o impregnación capilar.

El máximo de disolvente (agua, etanol, etc.) retenido por el soporte es la medida de disolvente necesario en la impregnación hasta humedad incipiente. Este volumen es determinado mediante la adición de disolvente lentamente al soporte hasta que esté saturado, lo que se hace evidente por el disolvente sobrenadante. La sal precursora es, posteriormente, disuelta en una cantidad igual de disolvente. Una vez seco, la estructura porosa del soporte contiene, ciertamente, la cantidad precisa de especies catalíticas (ventaja).

A. I. 2. Técnicas de caracterización.

A. I. 2. 1. Porosimetría de adsorción/desorción de nitrógeno.

La utilización de materiales mesoporosos del tipo SBA-15 y MCM-41 como soportes hace totalmente necesaria la determinación de las propiedades texturales, mediante porosimetría de N_2, de todos los nanomateriales estudiados en esta Memoria de Tesis Doctoral.

La representación de la cantidad de nitrógeno adsorbida frente a la presión relativa a temperatura constante se denomina isoterma de adsorción. La existencia de características particulares ha permitido su clasificación en seis tipos distintos (Figura A. I. 4) [9]. La interpretación de las isotermas de adsorción/desorción de N_2 mediante distintos modelos permite la caracterización de la textura porosa de los sólidos estudiados [10]. Atendiendo a la clasificación realizada en función del tamaño de poro, según la IUPAC, pueden distinguirse tres tipos de materiales porosos: materiales microporosos

(diámetro de poro inferior a 2 nm), mesoporosos (diámetro de poro entre 2 y 50 nm) y macroporosos (diámetro de poro mayor de 50 nm).

El primer paso en la interpretación de una isoterma de adsorción es la identificación del tipo de isoterma y, así, la naturaleza del proceso de adsorción: en monocapa-multicapa, condensación capilar o adsorción en los microporos. Está perfectamente establecido en la bibliografía los seis tipos de isotermas representadas en la Figuna A. I. 4, [9,10].

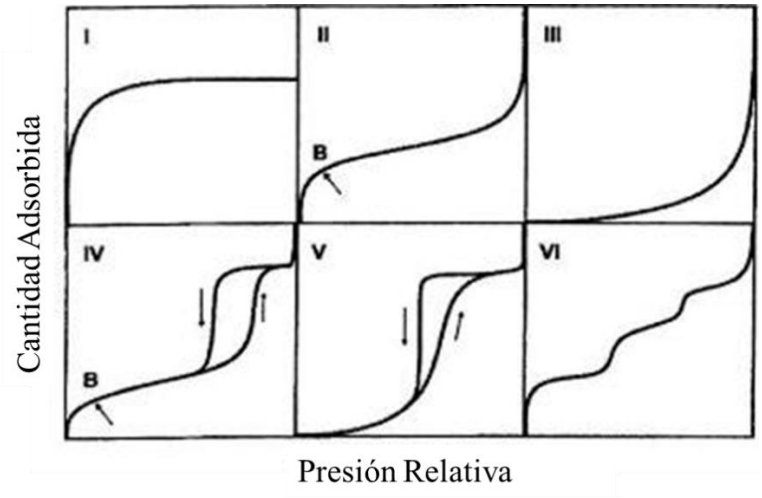

Figura A. I. 4. Clasificación de la IUPAC de los diferentes tipos de isotermas [9].

Todos nuestros materiales muestran isotermas del tipo IV, estas están asociadas a materiales mesoporosos. El ciclo de histéresis está asociado a la condensación capilar en los mesoporos del sólido. La parte inicial de la isoterma del tipo IV se atribuye a la adsorción en monocapa-multicapa ya que, a bajos valores de P/P_0, la forma de la isoterma es similar al tipo II.

La *superficie específica* se define como el número de m^2 que ocuparía la proyección del recubrimiento de los poros de un gramo de catalizador. El

método de Brunauer-Emmett-Teller (BET) es el más utilizado como procedimiento estándar para la determinación del área superficial de materiales porosos, a pesar de la simplificación del modelo en el cual se basa la teoría.

La ecuación de BET, en su forma lineal, se expresa como:

$$P / [V (P_0 – P)] = 1 / (V_m C) + (C - 1) P / (V_m C P_0)$$

Siendo:

V, el volumen de N_2 adsorbido, en condiciones normales de presión p;

V_m, el volumen requerido para cubrir la superficie del adsorbente con una capa monomolecular de adsorbato;

P, la presión de equilibrio;

P_0, la presión de saturación del adsorbato líquido utilizado;

C, una constante relacionada con el calor de adsorción de la primera capa.

El valor C puede utilizarse para determinar, en el intervalo de aplicabilidad de la ecuación BET, mostrándonos la magnitud de la interacción adsorbato-adsorbente. Así, valores altos de C superiores a 200 están asociados con la adsorción en microporos mientras que valores de C inferiores a 20 implican la imposibilidad de identificar el punto B (Figura A. I. 4). Por tanto, los valores de C entre estos dos puntos (≈100) son indicativos de un punto B bien definido.

Por otra parte, la ecuación BET necesita una relación lineal entre $P / [V (P_0 - P)]$ y P/P_0 limitado a una parte de la isoterma, normalmente, en el intervalo de presiones relativas $P/P_0 = 0,05 - 0,30$.

Otras características fundamentales son: *forma, tamaño y distribución de poros* ya que de ellas dependen los fenómenos de difusión que hacen que las moléculas de los reaccionantes accedan a los denominados "centros activos" del sólido poroso, cuando éste actúa como catalizador de un determinado proceso. Asimismo, estas características son las responsables de la difusión de los productos.

La caracterización de los materiales porosos se completa aplicando el método desarrollado por Barrett, Joyner y Halenda (BJH), por el cual se calcula el diámetro y el volumen de los poros presentes en los sólidos, así como la distribución de tamaño de poros del material en estudio. Estos parámetros se pueden determinar a partir de las isotermas de adsorción-desorción de nitrógeno empleando dicho método. El cálculo del tamaño de poros y de la distribución de los mismos se basa en la ecuación de Kelvin:

$$\ln P / P_0 = (- 2 \sigma V_m \cos \theta) / (r_k R T)$$

Siendo:

σ, la tensión superficial del adsorbato líquido;

V_m, el volumen molar del adsorbato líquido;

θ, el ángulo de contacto entre el líquido y la superficie;

r_k, el radio de curvatura o radio de Kelvin (positivo para una superficie cóncava).

Cuando la distribución del tamaño de poro que posee un sólido no es muy amplia, presenta gran utilidad el concepto de radio medio de poro, r_p, que se define como:

$$r_p = 2 V_g / S_g$$

Siendo:

V_g, el volumen de poro por gramo de sólido;

S_g, la superficie específica por gramo de sólido.

En la presente Memoria de Tesis Doctoral, el área superficial (BET) y el volumen de poro se han obtenido a partir de las isotermas de adsorción/desorción de N_2. Las medidas de adsorción de nitrógeno se llevaron a cabo a -196ºC, temperatura del nitrógeno líquido, utilizando un analizador automático Micromeritics ASAP 2000. El peso de la muestra utilizado para las medidas de adsorción-desorción de N_2 es aproximadamente de 0,20 g. Las muestras han sido desgasificadas durante 24 horas a 100ºC a vacío ($P < 10^{-2}$ Pa) y se analizaron posteriormente. La parte lineal de la ecuación de BET (presión relativa entre 0,05 y 0,30) se utilizó para la determinación del área superficial específica. La distribución del tamaño de poro se ha calculado utilizando la rama de adsorción de la isoterma de adsorción-desorción de N_2, aplicando el método de Barret, Joyner y Halenda (BJH) [11].

A. I. 2. 2. Método cromatográfico de pulsos para la determinación de las propiedades ácidas superficiales.

La aplicación del método cromatográfico de pulsos permite conocer la acidez de nuestros materiales gracias a la adsorción de diferentes moléculas sonda. Además, este método dinámico nos permite conocer las propiedades ácidas de los nanomateriales en condiciones semejantes a las que transcurren las reacciones catalíticas [12,13].

Dichas propiedades son de gran interés debido a la correlación que puede existir entre éstas y su actividad catalítica. Un material sólido ácido no tiene una sola clase de centros ácidos, sino que muestra una amplia distribución de

fuerzas de centros ácidos, resultado de la no homogeneidad en la composición del sólido, la existencia de interacciones de corto alcance y/o de estructuras superficiales diferenciadas. No obstante, en la mayoría de los casos, coexisten en la superficie de un sólido tanto centros ácidos de tipo Brönsted como de Lewis.

Para la determinación de la acidez superficial de los diferentes catalizadores con nanopartículas soportadas y sus respectivos soportes, se han elegido como bases valorantes a la piridina (PY) y a la 2,6-dimetilpiridina (DMPY), ya que se adsorben, esencialmente, sobre ambos tipos de centros ácidos, de Brönsted y de Lewis, y sobre centros ácidos de Brönsted, respectivamente. La PY, debido a su bajo impedimento estérico, se adsorbe inespecíficamente sobre ambos tipos de centros, mientras que, la DMPY, se adsorbe de forma selectiva sobre centros ácidos de tipo Brönsted, debido al impedimento estérico de los grupos metilo.

El método empleado para llevar a cabo esta técnica, desarrollado por nuestro grupo de investigación, se puede dividir en dos etapas:

i) Saturación de la muestra. La saturación de la muestra se lleva a cabo inyectando volúmenes idénticos de una disolución de la molécula sonda en ciclohexano hasta alcanzar un valor constante en el área integrada correspondiente al pico de la molécula sonda (PY o DMPY).
ii) Calibración de la respuesta del detector. Una vez saturada la muestra se procede a la inyección de pulsos de distintos volúmenes, de la base, obteniéndose una respuesta lineal del detector respecto de la base valorante, en el intervalo de pulso elegido (con coeficientes de correlación superiores al 0,997).

La determinación de la cantidad de base adsorbida de forma irreversible por la muestra se lleva a cabo por la diferencia entre la cantidad total de base

inyectada y la cantidad de base detectada (no adsorbida) hasta la saturación de la muestra. La cantidad de base adsorbida hasta alcanzar la saturación se determina gracias a las áreas de los picos integrados y la calibración de la respuesta del detector.

Los cálculos se han llevado a cabo empleando la siguiente ecuación:

$$C_a = \frac{\sum_{i-0}^{n} C_0 - C}{m}$$

Donde:

C_a, cantidad de base adsorbida de forma irreversible por gramo de catalizador (µmol g^1);

n, número de pulsos hasta alcanzar la saturación de la muestra;

C_0, cantidad de base inyectada en cada pulso (µmol);

C, cantidad de base no adsorbida en cada pulso (µmol);

m, masa del catalizador (g).

Este procedimiento se ha realizado durante el trabajo de Tesis Doctoral por debajo de la temperatura del tratamiento térmico final en la síntesis de los nanomateriales. Los pulsos se han efectuado por medio de un microjeringa sobre el lecho catalítico a partir de una disolución ciclohexánica del agente valorante (0,989 M en PY y 0,686 M en DMPY). El catalizador se estandariza en cada valoración en un flujo de nitrógeno (50 mL min^{-1}) deshidratado y desoxigenado (99,999% de pureza) a 250ºC. El catalizador utilizado (~ 0,03 g) se fija mediante topes de lana de vidrio Pyrex, en el interior de un microreactor tubular de acero inoxidable de 4 mm de diámetro interno. La base inyectada se analiza por cromatografía de gases con detector de

ionización de llama (FID), utilizando una columna analítica de 0,5 m de longitud, conteniendo un 5% en peso de polifeniléter en Chromosorb AW-MCS 80/100.

A. I. 2. 3. Técnicas de rayos-X.

La variedad e información que nos proporcionan las técnicas que emplean rayos-X son de gran importancia [14,15], haciéndolas así de unas de las técnicas de mayor peso en la presente Memoria de Tesis Doctoral. Dichas técnicas se clasifican según el fenómeno físico en el que se basan [16]:

- Absorción de rayos-X.
- Basada en el efecto fotoelectrónico.
- Difracción de rayos-X.

Para la caracterización de los materiales sintetizados en los trabajos de la Tesis Doctoral se han empleado dos de estas técnicas, difracción de rayos-X (XRD) y espectroscopía fotoelectrónica de rayos-X (XPS).

A. I. 2. 3. 1. Difracción de rayos-X (XRD).

La aplicación de la técnica de XRD a materiales mesoporosos permite la caracterización estructural de los mismos en términos de ordenamiento, distancia poro-poro, estimación del grosor de la pared del poro (complementada con las isotermas de adsorción-desorción de N_2 u otros gases), etc. Del mismo modo, en el caso de las nanopartículas, permite la identificación de las estructuras cristalinas de las mismas.

El equipo empleado es un difractómetro de rayos-X convencional, modelo Siemens D-5000 (40 kV, 30 mA) provisto de un goniómetro y registro de datos automatizado DACO-MP. La radiación utilizada ha sido la línea de Kα

del Cu (λ=1,54 Å). El difractómetro emplea un filtro de Ni y un monocromador de grafito.

En la Tabla A. I. 1. se muestran los parámetros utilizados en la adquisición de los DRX de las diferentes muestras investigadas en la presente Memoria de Tesis Doctoral.

Tabla A. I. 1. Parámetros utilizados en la adquisición de los difractogramas de rayos-X.

Materiales	Intervalo de barrido	Velocidad de barrido
SBA-15	$0,5^{o}<2\theta<5^{o}$	1,75 min^{-1}
MCM-41	$0,5^{o}<2\theta<5^{o}$	1,75 min^{-1}
Nanocatalizadores	$10^{o}<20\theta<80^{o}$	1,75 min^{-1}

A. I. 2. 3. 2. Espectroscopía fotoelectrónica de rayos-X (XPS).

El análisis de XPS más básico de una superficie puede proporcionar información cualitativa y cuantitativa de todos los elementos presentes, excepto H y He. Con aplicaciones más sofisticadas de la técnica, se obtiene información detallada de la química, organización y morfología de la superficie.

El principio de la espectroscopia XP es el siguiente: cuando se hace incidir radiación de rayos-X sobre una muestra, parte de la energía inicial se invierte en liberar electrones y darles la suficiente energía cinética para expulsarlos de los átomos, que quedan parcialmente ionizados. Este proceso se conoce como efecto fotoelectrónico [17]. El átomo así excitado recupera su estado fundamental cuando los electrones de las capas superiores pasan a ocupar los huecos dejados en las capas más internas. Para analizar el efecto

fotoelectrónico cuantitativamente es necesario plantear la siguiente ecuación, deducida por Einstein:

$$E_B = h\upsilon - KE$$

Siendo:

E_B, la energía de enlace del electrón en el átomo;

$h\upsilon$, la energía de la fuente de rayos-X;

KE, la energía cinética del electrón detectado que es medida por el espectrómetro del XPS.

En un espectro típico de XPS, se representa el número de electrones detectados frente a la energía de ligadura que poseen dichos electrones. Cada elemento produce un conjunto característico de picos XPS a unos valores determinados de energía de enlace, lo que permite identificar cada elemento que se encuentra en/sobre la superficie del material que se está analizando. Estos picos característicos corresponden a la configuración electrónica de los electrones en el interior de los átomos (1s, 2s, 2p,...). El número de electrones detectado en cada pico está relacionado directamente con la cantidad de este elemento que se encuentra en la zona irradiada. Para generar los porcentajes atómicos de los elementos presentes en la zona respectiva, la intensidad de cada señal XPS sin refinar (número de electrones detectados) debe dividirse por un factor denominado de sensibilidad relativa y normalizar de este modo todos los elementos detectados. Las medidas deben realizarse en ultra alto vacío para minimizar el porcentaje de error, al contar el número de electrones en cada valor de energía cinética.

La gran potencia de esta herramienta de trabajo se corrobora con las siguientes evidencias:

- Identificación de todos los elementos presentes (excepto H, He) en concentraciones mayores al 0,1 %.
- Determinación semicuantitativa de la composición elemental de la superficie (error ~10 %).
- Información acerca del entorno molecular: estado de oxidación, átomos enlazantes, orbitales moleculares, etc.

Es importante señalar que la espectroscopia fotoelectrónica de rayos-X detecta sólo los fotoelectrones que proceden de los 10-12 nm de la superficie del material ya que todos los fotoelectrones emitidos a mayor profundidad en la muestra quedan capturados o atrapados en los diversos estados excitados del material.

La caracterización por XPS de las superficies de los materiales preparados en esta memoria de Tesis Doctoral se llevó a cabo mediante un espectrómetro de ultra alto vacío (UHV) modelo SpecsTM, equipado con un analizador de electrones semiesférico y una fuente de radiación de rayos-X (XR-50, Specs, Mg-Kα (hν = 1253,6 eV, 1 eV = $1{,}603 \cdot 10^{-19}$ J) que funciona en modo "stop and go". Los materiales sólidos fueron preparados en pastillas y depositados sobre un portamuestras empleando una cinta adhesiva de doble cara, manteniéndose en una cámara de vacío ($<10^{-6}$ Torr) previamente a la adquisición de los espectros. Los espectros se tomaron a temperatura ambiente con una energía de paso de 10 eV.

A. I. 2. 4. Análisis térmico gravimétrico y térmico diferencial (ATG/ATD).

La termogravimetría (ATG) es una técnica en la que se determinan variaciones en el peso de una sustancia, en un ambiente específico, calentado o enfriado a velocidad controlada, que se registran en función del tiempo o de

la temperatura. Esta técnica suministra información de una amplia variedad de investigaciones químicas: calcinación, actividad catalítica, quimisorción, descomposición, desolvatación, higroscopicidad, cinéticas, reacciones en estado sólido, adsorción-desorción, estabilidad térmica, etc.

En el análisis térmico diferencial (ATD) la diferencia de temperatura entre la muestra y un material de referencia se registra mientras ambos son sometidos al mismo programa de calentamiento. Algunos de los procesos antes referidos son exotérmicos (ocurren con desprendimiento de calor) y otros son endotérmicos (ocurren con absorción de calor). En la gráfica de ATD se considera exotérmico un pico orientado en el sentido positivo del eje de flujo de calor y endotérmico al contrario, lo que permite identificar su naturaleza de forma muy sencilla, aunque no así la asignación a un determinado proceso [18].

El análisis termogravimétrico (ATG) y térmico diferencial (ATD) de los sólidos se ha llevado a cabo en presencia de aire como gas portador (40 mL min^{-1}), utilizando un sistema Setaram Setsys 12, con α-Al_2O_3 como material de referencia, y un termopar de Pt/Pt-Rh (10 %). La velocidad de calentamiento ha sido de 10 ºC min^{-1}, y el intervalo de temperatura de 30-1000 ºC.

A. I. 2. 5. Microscopía electrónica.

A. I. 2. 5. 1. Microscopía electrónica de barrido/ Análisis de energía dispersiva de rayos-X (SEM/EDX).

En microscopia electrónica de barrido (SEM) cuando un haz electrónico incide sobre la superficie de un sólido, tienen lugar varios fenómenos: reemisión de una parte de la radiación incidente, emisión de luz, electrones secundarios, electrones Auger, rayos-X, etc. Todas estas señales se pueden

emplear para obtener información sobre la naturaleza de la muestra (morfología, composición, etc.) y los equipos actuales disponen de detectores que permiten el análisis de la mayor parte de estas señales [19].

En nuestras investigaciones hemos utilizado dos de estos fenómenos que tienen lugar en la muestra bajo el impacto de los electrones: (1) el más importante en SEM es la emisión de electrones secundarios con energías de unas cuantas decenas de eV, seguido de la emisión de electrones retrodispersados con mayores energías. Hay detectores adecuados que discriminan los electrones en función de su energía permitiendo, por tanto, formar imágenes con ambos tipos que representan las características de la superficie de la muestra. (2) Otra emisión importante que tiene lugar cuando el haz de electrones interacciona inelásticamente con la muestra, tanto en SEM como en TEM, es la de fotones de rayos-X con energía y longitud de onda característica de los elementos que forman la muestra, permitiendo identificar y establecer la concentración de los elementos presentes.

Las imágenes de microscopía electrónica de barrido (SEM) de la presente Tesis Doctoral se han obtenido en un microscopio JEOL JSM-7800F con un detector detector de Si/Li tipo de ventana (ATW2), rango de detección: del boro al uranio, resolución: 137 eV a 5,9 KeV, permitiéndonos ver las imágenes de los nanocatalizadores gracias a la generación principalmente de electrones secundarios y retrodispersados generados mediante un haz de electrones. La composición elemental de los nanocatalizadores se obtuvo en el mismo equipo empleando análisis de dispersión de energía de rayos-X (EDX) a 20 kV.

A. I. 2. 5. 2. Microscopía electrónica de transmisión (TEM/HRTEM).

La microscopia electrónica de transmisión se ha convertido en una herramienta indispensable para el estudio de catalizadores basados en

nanopartículas metálicas dispersas sobre materiales porosos, puesto que permite observar las nanopartículas de forma directa evitando la imposición de hipótesis físicas y matemáticas. En principio, con TEM se puede medir visualmente el diámetro de partículas discretas y por tanto se puede calcular el tamaño de partícula promedio [17].

La técnica de microscopia electrónica de transmisión se basa en la irradiación de la muestra delgada con un haz de electrones con densidad de corriente uniforme, cuya energía está generalmente dentro del intervalo de 100-200 KeV. Una parte de estos electrones son transmitidos, otros son dispersados y, finalmente, otra parte da lugar a interacciones que producen distintos fenómenos tales como emisión de luz, electrones Auger, rayos-X, etc.

En esta técnica, se emplea la transmisión/dispersión de los electrones para generar imágenes, la difracción de los electrones para obtener información acerca de la estructura cristalina, así como la emisión de rayos-X característicos para conocer la composición elemental de la muestra (análisis EDX). Para que se pueda producir la transmisión de los electrones a través de la muestra es necesario que ésta sea preparada en una capa delgada, es decir, transparente a los electrones, normalmente de un grosor inferior a 100 nm (cuanto menor es el espesor de la muestra, mejor calidad de imágenes se puede obtener). Mediante la irradiación con electrones a la muestra se obtienen imágenes con alta resolución espacial, siendo la resolución que actualmente se puede alcanzar en TEM menor que 0,1 nm (empleando correctores de aberraciones en las imágenes).

La microscopia electrónica de transmisión de alta resolución (HRTEM) es un modo de imagen que permite la proyección de la estructura cristalina de una muestra a escala atómica. Debido a su alta resolución, es una herramienta muy valiosa para estudiar las propiedades a nanoescala de materiales cristalinos

como semiconductores y metales. En la actualidad, la resolución más alta alcanzada ha sido de 0,8 Å.

En el presente trabajo de investigación se han utilizado tanto la técnica TEM como la de HRTEM para estudiar la morfología, composición, dispersión de nanopartículas y estructura de los materiales preparados.

Las microfotografías de microscopía electrónica de transmisión (TEM) se han obtenido utilizando un sistema FEI Tecnai G2, equipado con una cámara CCD (*charge coupling device*) para una mayor facilidad y rapidez de uso.

A. I. 2. 6. Espectrometría de masas con acoplamiento inductivo (ICP-MS).

La técnica de espectrometría de masas con plasma de acoplamiento inductivo (ICP-MS, *Inductively Coupled Plasma - Mass Spectrometry*), es una variante de las técnicas de análisis por espectrometría de masas. Esta técnica de análisis inorgánico elemental e isotópico se ha desarrollado hasta convertirse en una de las técnicas más importantes en las últimas dos décadas para distintas aplicaciones en áreas como: química, biología, física de materiales, medioambiente y geoquímica [19–21]. Esto se debe principalmente a su capacidad de discriminar isótopos y a sus bajos límites de detección, que pueden llegar a ser inferiores a los 10^{-6} mg/L.

Por esta técnica pueden determinarse y cuantificarse la mayoría de los elementos de la tabla periódica (a excepción de H, C, N, O, F y los gases nobles) en un rango dinámico lineal de 8 órdenes de magnitud (ppt o ppm), lo que la hace ideal para el análisis de elementos traza. Además, dicha técnica presenta un alto grado de selectividad y una buena precisión y exactitud.

Las operaciones de preparación de las muestras dependen de su naturaleza sólida o líquida. Para la mayoría de las muestras sólidas es necesaria la disolución, siendo ésta una de las operaciones más comunes en laboratorios de Química Analítica. Se utilizan ácidos minerales fuertes combinados de forma apropiada para la digestión de la muestra. Generalmente, la digestión de la muestra se realiza en cápsulas que resisten los incrementos de presión, temperatura y el ataque de los ácidos.

Las muestras conteniendo sílice (~25 mg) se han digerido previamente empleando una mezcla de ácidos 1:1:1 HF: HNO_3: HCl. Las diluciones se hicieron con agua miliQ hasta un contenido máximo de 1% HF, ya que el HF es el único ácido que disuelve a los silicatos formando SiF_6^{2-} en solución ácida que tiene un bajo punto de ebullición. Esto hace que sea fácilmente volatilizable. Si la digestión se hace abierta, se puede perder el SiF_4 (punto de ebullición = -86 ºC) volatilizado durante la digestión. Por supuesto, otros fluoruros y cloruros también se pierden. Incluso a bajas concentraciones, el HF ataca el vidrio, haciendo preferible el uso de plástico o teflón. Cualquier residuo de HF en la muestra puede atacar a la parte interna del ICP ya que HF es muy corrosivo y tóxico, siendo uno de los ácidos más peligrosos que se utilizan en el laboratorio.

Para el análisis cuantitativo de metales en los distintos catalizadores sintetizados se ha empleado un ICP-MS Elan DRC-e (PerkinElmer SCIEX).

A. I. 2. 7. Resonancia magnética nuclear (RMN).

El fenómeno de la RMN se descubrió en 1946 y se convirtió rápidamente en una de las herramientas más poderosas para la resolución de estructuras y dinámicas moleculares, particularmente en Química Orgánica.

Desde 1950-1970, los estudios de RMN de alta resolución se dedicaron principalmente a líquidos, ya que los efectos de ciertas interacciones nucleares que pueden causar un ensanchamiento excesivo de la señal son promediadas a cero o a valores discretos debido al rápido movimiento al azar de las moléculas. Durante este periodo, particularmente importante para la técnica RMN, la mayoría de los estudios estuvieron relacionados, por razones de sensibilidad, a los núcleos que son más abundantes y fáciles de detectr (^{1}H, ^{19}F, ^{31}P,…).

En los años 1970-1990, se desarrollaron equipos con campos magnéticos muy altos (superconductores) y, especialmente, la utilización de la transformada de Fourier han hecho posible observar núcleos de abundancia baja y de baja sensibilidad de detección (por ejemplo, los isótopos de ^{13}C, ^{29}Si, etc.).

La aplicación de la RMN a sólidos durante este periodo fue muy limitada. La principal razón es que en sistemas rígidos (sólidos y también moléculas fuertemente adsorbidas químicamente) la interacción que puede causar un ensanchamiento considerable de las señales no puede promediarse a un valor pequeño por la movilidad de las especies.

El potencial de la espectroscopia de RMN es tal que es imposible no utilizar tal herramienta para el estudio de sistemas rígidos. El resultado ha sido el desarrollo, desde aproximadamente 1970, de técnicas experimentales sofisticadas para conseguir el estrechamiento de la señal hasta alcanzar resoluciones espectrales similares a las de los líquidos. Estas técnicas son principalmente [22,23]: (i) espín de ángulo mágico (MAS, “Magic Angle Spinning”); (ii) desacoplamientos dipolares heteronucleares y (iii) secuencias de multipulso apropiadas. Además, la técnica de polarización cruzada (CP, “Cross-Polarization”) se desarrolló para superar el problema de la baja sensibilidad en RMN del estado sólido de núcleos de abundancia baja [^{13}C (1,1%), ^{29}Si (4,67%), etc.].

En particular, la aplicación de la RMN de sólidos en catálisis heterogéneas da información esencial para avanzar en el diseño de nuevos catalizadores sólidos activos y selectivos en diferentes procesos químicos. Por sus características, esta técnica permite investigar aspectos diferentes de un sistema catalítico: i) caracterización estructural de los catalizadores, ii) interacción del catalizador con moléculas sonda y reactivos, y iii) estudio de mecanismos e intermedios de reacciones químicas.

La técnica MAS fue desarrollada por Low y Andrew como una forma mediante la cual los acoplamientos dipolo-dipolo pueden suprimirse en los espectros de RMN del estado sólido. La técnica MAS puede ser un método muy efectivo para la supresión de tales acoplamientos pero sólo en los casos donde la magnitud del acoplamiento sea menor que las velocidades de giro que puedan alcanzarse.

Además, la técnica MAS tiene efectos notables sobre otras interacciones de espín, de las cuales la más importante es el desplazamiento químico. Más específicamente, la técnica MAS estrecha la dispersión de los desplazamientos químicos, que es una propiedad inherente en los espectros RMN del estado sólido. En un sólido amorfo o cristalino en polvo, se observa una señal complicada en forma de banda ancha que surge de la suma de todos los desplazamientos químicos posibles.

Por ejemplo, los espectros de RMN del estado sólido de ^{13}C, donde el sólido está compuesto típicamente de una gran variedad de átomos de carbono diferentes químicamente, es espectro del ^{13}C es la suma de los diferentes patrones de desplazamiento químico anisotrópico, teniendo diferentes formas y diferentes centros isotrópicos. El ensanchamiento resultante surge de las restricciones que tienen lugar sobre la movilidad molecular del sólido.

Experimentalmente es posible restaurar parte de esta movilidad mediante la rotación/giro de la muestra. La anisotropía del desplazamiento químico (σ_{izz})

puede expresarse convenientemente en términos de ángulo de rotación de la muestra con respecto al campo magnético aplicado:

$$\sigma_{izz} = (3\,cos^2\,\beta - 1)\,(otros\ términos) + \left(\frac{3}{2}\,sen^2\,\beta\right)\sigma_i$$

Cuando β = 54,74º, 3 $\cos^2$ β – 1= 0, y σ_{izz}= σ_i, el desplazamiento químico anisotrópico se iguala al desplazamiento químico isotrópico, que es el que se observa en RMN de líquidos. Esto da lugar a espectros RMN de ^{13}C de sólidos de alta resolución y el ángulo β = 54.74º se le denomina "ángulo mágico". La técnica MAS promedia el efecto de las anisotropías locales, pero el desplazamiento químico de los diferentes centros nucleares se conserva.

En esta Memoria de Tesis Doctoral, se han determinado los espectros de RMN-MAS del ^{27}Al de muestras hidratadas de SBA-15 con nanopartículas de Al incorporadas mecanoquímicamente.

Los espectros RMN-MAS del ^{27}Al se han realizado a 104,26 MHz, con un espectrómetro multinuclear Bruker AVANCE ACP-400, con pulsos de excitación de 1μs y tiempos de retardo de 0,3 s. El desplazamiento químico se expresó en ppm, utilizando como referencia externa $Al(H_2O)_6^{+3}$ tal como se ha descrito en trabajos previos de nuestro grupo [24].

A. I. 2. 8. Susceptibilidad magnética.

El origen de las propiedades magnéticas macroscópicas observables experimentalmente de un sólido se encuentra, como bien es sabido, en el momento magnético de tipo electrónico asociado a sus átomos constituyentes. La susceptibilidad magnética constituye una medida cuantitativa de la respuesta del material al campo magnético aplicado [25]. De hecho, las sustancias diamagnéticas son ligeramente repelidas por dicho campo, mientras que las paramagnéticas experimentan una fuerza atractiva. Debido a que en

todos los átomos se genera un pequeño momento diamagnético mientras dure la presencia del campo aplicado, los valores experimentales obtenidos de la susceptibilidad magnética deben ser corregidos inicialmente con respecto a la contribución diamagnética.

La susceptibilidad magnética fue determinada mediante el uso a temperatura ambiente de un susceptibilímetro magnético MS2, Bartington Instruments Ltd., usando el sensor de laboratorio MS2B de doble frecuencia (470 y 4700 Hz).

A. I. 3. Actividad catalítica.

A. I. 3. 1. Actividad catalítica asistida por microondas.

Los ensayos realizados en fase líquida asistidos por la técnica de microondas han sido llevados a cabo en un microondas focalizado modelo CEM-Discover, controlado y monitorizado por un ordenador. En el dispositivo experimental se trabaja en el modo "Discover", empleando un dispositivo sensor de presión, controlando, en ambos casos la potencia de irradiación con microondas y la temperatura durante el desarrollo de la reacción.

En este método se han llevado a cabo las reacciones de oxidación del isoeugenol y alcohol vainillínico a vainillina, y la reacción de oxidación del alcohol bencílico a benzaldehído, lo que nos permite el seguimiento de la evolución de la presión generada a lo largo de la reacción.

Ambas reacciones se analizan por cromatografía de gases en un cromatógrafo Agilent Technologies 7890 A GC System equipado con una columna Petrol^{TM} DH (100 m x 0,25 mm x 0,50 µm) y un detector de ionización de llama (FID).

A. I. 3. 2. Actividad catalítica mediante calefacción convencional.

Las reacciones en fase líquida mediante calentamiento convencional desarrolladas en esta Memoria de Tesis Doctoral se han llevado a cabo empleando en un sistema de síntesis paralela múltiple modelo Carrusel Reaction Station TM (Radleys Discovery Technologies). El tubo de reacción, con un volumen de aproximadamente 45 mL, equipado de agitación magnética. Para la toma de muestra del medio, se ha utilizado una jeringa, tomando una pequeña cantidad de muestra a través de un filtro acoplado para minimizar la extracción de catalizador sólido.

Las reacciones llevadas a cabo empleando esta ha sido la ruptura oxidativa selectiva del isoeugenol a vainillina y la oxidación del alcohol vainillínico a vainillina a temperatura ambiente (20-25 ºC) y 90 ºC.

Las mezclas de ambas reacciones se analizan por cromatografía de gases en un cromatógrafo Agilent Technologies 7890 A GC System equipado con una columna Petrol^{TM} DH (100 m x 0,25 mm x 0,50 µm) y un detector de ionización de llama (FID).

A. I. 3. 3. Actividad catalítica mediante molienda mecanoquímica.

La molienda mecanoquímica además de ser un procedimiento de síntesis de materiales puede ser una técnica empleada para llevar a cabo reacciones sin la necesidad de emplear disolventes orgánicos.

En esta Tesis Doctoral se ha llevado a cabo la reacción de oxidación del sulfuro de difenilo bajo molienda mecanoquímica, sometiendo los reactantes a 350 rpm durante 25 minutos en un molino de bolas planetario RESTCH modelo PM-100.

Bibliografía

1. Palaniandy, S.; Azizli, K. A. M. Mechanochemical effects on talc during fine grinding process in a jet mill. *Int. J. Miner. Process.* **2009**, *92*, 22–33.

2. McCormick, P. G.; Froes, F. H. The fundamentals of mechanochemical processing. *J. Miner. Met. Mater. Soc.* **1998**, *50*, 61–65.

3. Suryanarayana, C. Powder metal technologies and applications. *ASM Handb.* **1998**, *7*, 80–90.

4. James, S. L.; Adams, C. J.; Bolm, C.; Braga, D.; Collier, P.; Friščić, T.; Grepioni, F.; Harris, K. D. M.; Hyett, G.; Jones, W. Mechanochemistry: opportunities for new and cleaner synthesis. *Chem. Soc. Rev.* **2012**, *41*, 413–447.

5. Pineda, A.; Balu, A. M.; Campelo, J. M.; Romero, A. A.; Carmona, D.; Balas, F.; Santamaria, J.; Luque, R. A Dry Milling Approach for the Synthesis of Highly Active Nanoparticles Supported on Porous Materials. *ChemSusChem.* **2011**, *4*, 1561–1565.

6. Jahn, A.; Reiner, J. E.; Vreeland, W. N.; DeVoe, D. L.; Locascio, L. E.; Gaitan, M. Preparation of nanoparticles by continuous-flow microfluidics. *J. Nanoparticle Res.* **2008**, *10*, 925–934.

7. Yépez, A.; Lam, F. L. Y.; Romero, A. A.; Kappe, C. O.; Luque, R. Continuous flow preparation of iron oxide nanoparticles supported on porous silicates. *ChemCatChem.* **2015**, *7*, 276–282.

8. Yépez, A. Nanopartículas soportadas sobre materiales SBA-15 para su aplicación a procesos de valorización de biomasa. Tesis Doctoral. *Universidad de Córdoba*. **2016**, 221-223.

9. Sing, K. S. W.; Everet, D. H.; Haul, R. A. W.; Moscou, L.; Pierotti, R. A.; Rouquerol, J.; Siemienwska, T. Reporting physisorption data for gas/solid systems with special reference to the determination of surface area and porosity. *Pure Appl. Chem.* **1985**, *57*, 603–619.

10. Rouquerol, J.; Rouquerol, F.; Llewellyn, P.; Maurin, G.; Sing, K. Adsorption by powders and porous solids: principles, methodology and applications. *Academic Press*. **2013**.

11. Barrett, E. P.; Joyner, L. G.; Halenda, P. P. The Determination of pore volume and area distributions in porous substances. I. Computations from Nitrogen Isotherms. *J. Am. Chem. Soc.* **1951**, *73*, 373–380.

12. Campelo, J. M.; Luna, D.; Luque, R.; Marinas, J. M.; Romero, A. A.; Calvino, J. J.; Rodríguez-Luque, M. P. Synthesis of acidic Al-MCM-48: Influence of the Si/Al ratio, degree of the surfactant

hydroxyl exchange, and post-treatment in NH_4F solution. *J. Catal.* **2005**, *230*, 327–338.

13. Paryjczak, T. Gas chromatography in adsorption and catalysis. *Halsted Press*. **1986**.

14. Cullity, B. D.; Stock, S. R. Elements of X-ray Diffraction. *Pearson Education*. **2014**.

15. Thibault, P.; Dierolf, M.; Menzel, A.; Bunk, O.; David, C.; Pfeiffer, F. High-resolution scanning X-ray diffraction microscopy. *Science.* **2008**, *321*, 379–382.

16. Goldstein, J. I.; Newbury, D. E.; Michael, J. R.; Ritchie, N. W. M.; Scott, J. H. J.; Joy, D. C. Scanning electron microscopy and X-ray microanalysis. *Springer*. **2017**.

17. Faraldos, M.; Goberna, C. Técnicas de análisis y caracterización de materiales. *CSIC*. **2002**.

18. Brown, M. E. Introduction to thermal analysis: Techniques and applications. *Mineral. Mag.* **1988**, *53*, 662.

19. Skoog, D. A.; Holler, F. J.; Nieman, T. A. Principios de análisis instrumental. *McGraw-Hill Interamericana de España*. **2001**.

20. Thomas, R. Practical guide to ICP-MS: a tutorial for beginners. *CRC press.* **2013**.

21. Mermet, J. M. Ionic to atomic line intensity ratio and residence time in inductively coupled plasma-atomic emission spectrometry. *Spectrochim. Acta Part B At. Spectrosc.* **1989**, *44*, 1109–1116.

22. Engelhardt, G.; Michel, D. High-resolution solid-state NMR of silicates and zeolites. *John Wiley & Sons*. **1987**.

23. Apperley, D. C.; Harris, R. K.; Hodgkinson, P. Solid-state NMR: Basic principles and practice. *Momentum Press.* **2012**.

24. Balu, A. M.; Pineda, A.; Yoshida, K.; Campelo, J. M.; Gai, P. L.; Luque, R.; Romero, A. A. Fe/Al synergy in Fe_2O_3 nanoparticles supported on porous aluminosilicate materials : excelling activities in oxidation reactions. *ChemComm.* **2010**, *46*, 7825–7827.

25. Mullins, C. E. Magnetic susceptibility of the soil and its significance in soil science – a Review. *J. Soil Sci.* **1977**, *28*, 223–246.

ANEXO II

Compendio de publicaciones

Home | Account Info | Help

Title:	Post-synthetic mechanochemical incorporation of Al-species into the framework of porous materials: towards more sustainable redox chemistries
Author:	M Dolores Marquez-Medina, Sareena Mhadmhan, Alina Mariana Balu, et al
Publication:	ACS Sustainable Chemistry & Engineering
Publisher:	American Chemical Society
Date:	Apr 1, 2019

Logged in as:
María Dolores Márquez-Medina
Universidad de Córdoba
Account #: 3001400331
LOGOUT

Quick Price Estimate

Permission for this particular request is granted for print and electronic formats, and translations, at no charge. Figures and tables may be modified. Appropriate credit should be given. Please print this page for your records and provide a copy to your publisher. Requests for up to 4 figures require only this record. Five or more figures will generate a printout of additional terms and conditions. Appropriate credit should read: "Reprinted with permission from {COMPLETE REFERENCE CITATION}. Copyright {YEAR} American Chemical Society." Insert appropriate information in place of the capitalized words.

I would like to...	reuse in a Thesis/Dissertation
Requestor Type	Author (original work)
Portion	Full article
Format	Print and Electronic
Will you be translating?	No
Select your currency	USD - $
Quick Price	Click Quick Price

QUICK PRICE CONTINUE

This service provides permission for reuse only. If you do not have a copy of the article you are using, you may copy and paste the content and reuse according to the terms of your agreement. Please be advised that obtaining the content you license is a separate transaction not involving Rightslink.

To request permission for a type of use not listed, please contact the publisher directly.

CHEMISTRY & SUSTAINABILITY

CHEMSUSCHEM

ENERGY & MATERIALS

Accepted Article

Title: Continuous flow synthesis of supported magnetic iron oxide nanoparticles for efficient isoeugenol conversion to vanillin

Authors: María Dolores Marquez, Pepijn Prinsen, Hangkong Li, Kaimin Shih, Antiono Ángel Romero Reyes, and Rafael Luque

To be cited as: *ChemSusChem* 10.1002/cssc.201701884

Link to VoR: http://dx.doi.org/10.1002/cssc.201701884

A Journal of

ChemPubSoc Europe

WILEY-VCH

www.chemsuschem.org

FULL PAPER WILEY-VCH

Continuous flow synthesis of supported magnetic iron oxide nanoparticles for efficient isoeugenol conversion to vanillin

M. Dolores Marquez-Medina,[a] Pepijn Prinsen,[a] Hangkong Li,[b] Kaimin Shih,[b] Antonio A. Romero,[a] and Rafael Luque[a]*

Abstract: This work presents the synthesis of iron oxide nanocatalysts supported on mesoporous Al-SBA-15 using a continuous flow set-up. The magnetic nanomaterials were tested as catalysts in the oxidative disruption of isoeugenol using hydrogen peroxide as green oxidant, featuring high activities (63-88 % conversion) and good selectivities to vanillin (44-68 %). The catalytic systems exhibited good magnetic properties when synthesized under continuous flow conditions at temperatures not exceeding 190 °C. The use of microwave irradiation significantly reduced times of reaction drastically, but exerted negative effects on catalyst re-usability.

Introduction

An important part of current research in green chemistry focus on the transition towards more sustainable manufacturing processes that efficiently utilize resources and raw feedstocks, reduce waste streams and avoid the use of toxic and hazardous materials. To bring this into practice, the use of recyclable catalysts has proven to be very useful for a wide range of chemical processes.[1-3] The deposition of highly active catalytic nanoparticles onto various organic or inorganic supports is probably the most efficient strategy to recover nanocatalysts. In this context, nanocatalysts recovery by magnetic fields could enable more efficient separation as compared to conventional decantation and filtration, especially when nanocatalysts are expensive (i.e. noble metals) and difficult to separate.[4,5] The incorporation of an iron oxide core in the nanocatalyst increases its density and thus also its recovery efficiency by conventional separation methods. The synthesis of magnetic nanoparticles (MNPs) was proposed for several applications being currently a hot topic in future catalyst design practises.[6-10] However, highly active MNPs are rather difficult to synthesize due to their tendency to aggregate and/or coalescence (sintering). This is important, because the nanosize of iron particles can have a significant impact on their catalytic activities. One way to overcome this problem is to support MNPs on mesoporous solids, which in turn also improve the stability of the metal or metal oxide nanoparticles.[11] In particular, mesoporous SBA-15 materials are attractive porous materials due to their hexagonally well-ordered mesopores with large specific surface areas (> 900 m^2 g^{-1}).[12,13] Recently, Gawande et al. reported a relatively simple protocol for the synthesis of MNPs using a continuous flow process in which Fe_2O_3 nanoparticles were deposited on aluminosilicates in a single step. This setup can provide greater process control, flexibility and productivity and has practical potential as an alternative to industrial scale synthesis processes based on traditional procedures.[14,15]

Vanillin can be isolated from natural source derived extracts, including vanilla beans and pods, pine woods (e.g. *Pinus tabuliformis*) and roasted coffee.[16] It can also be obtained from lignin fractions through depolymerization and subsequent conversion and/or isolation. The increasing global demand of vanillin cannot be met anymore by the supply of vanilla orchid pods as the sole source.[17] Only *ca.* 1 % of the global production of vanillin is derived from vanilla pods; the majority produced synthetically using e.g. lignin[18] and (iso)eugenol[19] as starting materials. The commercial value of vanillin extracted from vanilla pods varies between 1200-4000 USD kg^{-1}, excluding inflation.[20] Although the oxidative disruption of isoeugenol (**Scheme 1**) was already reported in literature, significant results were reported by Shimoni et al. using *Bacillus subtilis* sp. strains as biocatalysts,[21] resulting in vanillin production with 12-14 mol% yields (0.6-0.9 g L^{-1} after 24-48 h at 30 °C). Enzymatic conversion by lipoxygenases was also reported by Markus et al.,[22] with yields varying between 10 and 15 mol%. Major improvements (32.5 g L^{-1} vanillin after 72 h at 37 °C) were reported by Zhao et al. using *Bacillus fusiformis* strains.[23] Although these biocatalytic transformations are very attractive from an environmental point of view, they possess inherent drawbacks that include limited selectivity and stability in the systems, along with rather long reaction times and the need for nutrient media. Other catalytic systems were proposed by Herrmann et al. using 1 mol% methyltrioxorhenium at short reaction times (10 min). However, anhydrous hydrogen peroxide was required in 3:1 molar excess and MnO_2 was added to prevent further oxidation to vanillic acid.[24] More recently, Gusevskaya et al. reported the catalytic conversion of isoeugenol, with H_2O_2 as green oxidant in combination with $(n\text{-butyl})_4NVO_3$ and pyrazine-2-carboxylic acid, reaching 50 mol% yields in acetonitrile at 40 °C after 2 h.[25]

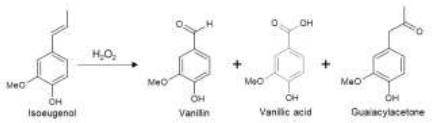

Scheme 1. Oxidative disruption of isoeugenol to vanillin and side-products.

[a] Bsc. M.D. Marquez Medina, Dr. P. Prinsen, Prof. A. A. Romero, Prof. R. Luque
Departamento de Química Orgánica
Universidad de Cordoba
Campus de Rabanales, Edificio Marie Curie (C-3), Ctra Nnal IV-A, Km 396, E-14014 Cordoba, Spain
E-mail: q62alsor@uco.es
[b] MSc. H. Li, Dr. K. Shih
Department of Civil Engineering,
The University of Hong Kong
Haking Wong Building, Pokfulam Road, Hong Kong HK 852, China

Supporting Information and the ORCID identification number(s) for the author(s) of this article can be found under

Results and Discussion

A series of magnetic nanoparticle (MNP) catalysts were synthesized in a continuous flow set up (**Scheme 2**) using iron oxide and Al-SBA-15 as support. This synthesis method promotes the deposition of iron oxide particles on the outer surface of Al-SBA-15 and promotes a close interaction of Fe with Al, rather than forming iron oxide particles within Al-SBA-15 pores. A catalyst prepared via deposition of iron oxide on Al-SBA-15 by classic wet impregnation (FeNMag-WI) was additionally synthesized for comparative purposes. MNP synthesis temperature was varied between 150 and 210 ºC to study its effect on the magnetic properties (**Table 1**) and the incorporation of iron (**Table 2**) in the final materials. FeNMag-WI was comparably non-magnetic (on a macroscopic basis) as classic wet impregnation proceeds at room temperature. The largest magnetic susceptibility was reached when the synthesis temperature was set at 170 ºC, while magnetic properties were lost at an apparent cut-off temperature of 195 ºC. The elemental composition results showed an iron (Fe) content in the whole materials in the range of 8 to 19 wt% (ICP-MS), while the Fe content at the surface was higher, with values ranging from 17 to 48 wt% (SEM/EDX). Fe content in the material prepared by classic wet impregnation (FeNMagWI), in contrast, did not show this surface enrichment effect. On the other hand, Fe content increased with higher synthesis temperatures, coinciding with the collapse of the SBA-15 structure in the materials synthesized at temperatures above 195 ºC.

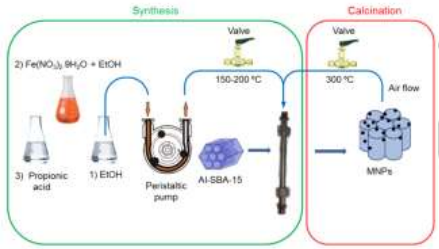

Scheme 2. Continuous flow synthesis of magnetic nanoparticles (MNPs).

Table 1. Magnetic properties of the synthesized MNPs.

Catalyst	Synthesis temperature (ºC)	Magnetic susceptibility χ_m ($\times 10^{-6}$ m^3 kg^{-1})
FeMag-150	150	73
FeMag-160	160	140
FeMag-170	170	206
FeMag-180	180	161
FeMag-190	190	190
FeNMag-195	195	[a]
FeNMag-200	200	[a]
FeNMag-205	205	[a]

[a] Non-magnetic.

Table 2. Elemental analysis (atomic percentages) according to SEM/EDX and ICP-MS.

Catalyst	SEM/EDX (%)			ICP-MS (%)		
	Al	Si	Fe	Al	Si	Fe
FeNMag-W[a]	0.8	40.7	4.9	0.8	22.3	13.3
FeMag-150	-	-	-	0,8	28.2	8.4
FeMag-160	1.0	23.6	21.4	0.8	22.2	11.7
FeMag-170	1.3	30.3	18.2	0.8	22.3	13.3
FeMag-180	1.1	28.9	17.1	-	-	-
FeMag-190	1.2	29.3	19.8	-	-	-
FeNMag-195	1.1	28.3	18.2	0.7	17.4	19.0
FeNMag-200	0.5	16.7	48.1	-	-	-

[a] Prepared by wet impregnation at 25 ºC with Fe loadings identical to those in FeMag-170.

The structure of the synthesized materials was studied by XRD. **Figure 1** shows the wide and low angle diffraction patterns of different temperature synthesized materials. Low angle diffractograms depict the presence of three peaks, one intense peak at low 2Θ values (reflection line d100) and two weaker peaks at higher angles (reflection lines d110 and d200), characteristic of SBA-15 structures.[26] The decrease in the intensity of these lines in FeNMag-200 indicates that Al-SBA-15 support underwent structural deterioration upon Fe incorporation. The high iron content in FeNMag-200 (Table 2) was most probably related to a partial collapse of the aluminosilicate SBA-15 as mesopores could be partly blocked by the high amount of iron oxide deposited on the aluminosilicate surface. These hypotheses were in good agreement with the wide angle XRD pattern in the materials in which the broad peak around 22° almost completely disappeared. Next to Al-SBA-15, peaks from Fe_2O_3 were also visible. Diffraction lines from iron oxide in FeNMagWI (**Figure S1** in the Supporting Information) were comparably hardly detectable, a most plausible indication of a highly dispersed iron oxide nanoparticles. The iron oxide diffraction pattern of FeNMag-200 could be indexed as a hematite crystal structure (α-Fe_2O_3, ICPDS No. 33-0,664) (Figure 1a), while XRD patterns of FeMag-190 and FeMag-170 are more difficult to assign. All diffraction peaks of maghemite and magnetite crystals are located within 1° difference.[27] The diffraction patterns of iron oxide in FeMag-190 and FeMag-170 samples (Figure 1b and 1c) are likely to be maghemite crystals (γ-Fe_2O_3, JCPDS No. 39-1346). However, the absence of magnetite cannot be excluded at the present signal-to-noise ratio and resolution since iron oxide nanoparticles typically exhibit noisy diffractograms,[28]. Crystal sizes of non-magnetic (FeNMag-200) vs magnetic samples (FeMag-190 and FeMag-170) were measured to be 30-40 nm and < 10 nm, respectively. FeNMag-200 and FeMag-170 samples were analyzed using a quantitative XRD technique, allowing the quantification of the amorphous material content. The content of the hematite phase in FeNMag-200 sample was 50 % by weight, while the content of the magnetic phase was less than 10 % by weight in FeMag-170.

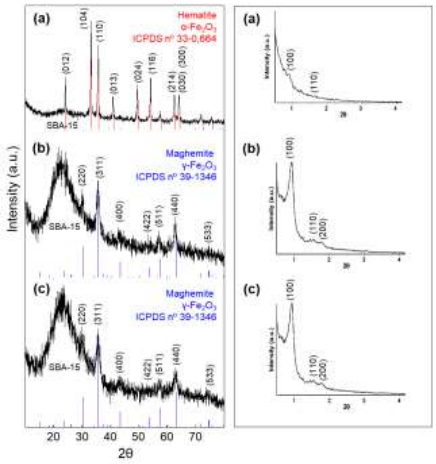

Figure 1. (Left) wide angle and (right) low angle XRD patterns of (a) FeNMag-200, (b) FeMag-190 and (c) FeMag-170.

The adsorption-desorption isotherms of SBA-15 aluminosilicate support and those of most representative synthesized nanocatalysts are of type IV (see **Figure S2** in the Supporting Information), characteristic of mesoporous materials. All synthesized solids exhibited relatively high specific surface areas (≥ 300 m^2 g^{-1}), with pore sizes in the 7-8 nm range (**Table 3**). FeNMag-WI prepared by wet impregnation showed a similar specific surface area and pore volume, but with a significantly reduced pore diameter. These results pointed to the deposition of a large part of the iron oxide nanoparticles into the pores of Al-SBA-15. Importantly, both the specific surface area and pore volume decreased with an increase of the temperature employed in the continuous flow synthesis, whereas the pore diameter was retained This fact can be explained by the increasing iron oxide content (see Table 2), which contributes in weight and partially obstructs the entrance to micropores in mesoporous void spaces. Surface acid properties (Table 3), as studied by the chromatographic pulse technique, pointed out no drastic differences in total acidity for the different synthesized nanocatalysts, whether magnetic or non-magnetic. In some cases, the number of BrØnsted acid centers exceeded the number of total acid centers, as DMPY is more basic than PY (pKb 7.4 and 8.8, respectively). The measured magnetic susceptibilities ranged between 70-210×10^{-6} m^3 kg^{-1} for magnetic nanocatalysts, consistent with the maghemite content in the materials (10-15 wt%). Pure magnetite nanoparticles generally show larger magnetic susceptibilities *ca.* 500×10^{-6} m^3 kg^{-1}.[29] These susceptibility values were large enough for the magnetic nanocatalysts to be magnetically recovered from reaction mixtures after reaction.

Table 3. Porosity analysis and acidity determination of synthesized (magnetic) nanoparticles.

Catalyst	S_{BET} (m^2 g^{-1})	Average pore diameter (nm)	Average pore volume (mL g^{-1})	Surface acidity (μmol g^{-1})[a]	
				BrØnsted	Total
Al-SBA-15	800	7.6	0.9	85	61
FeNMag-WI	450	0.3	0.5	-	-
FeMag-150	470	7.3	0.5	58	39
FeMag-160	470	7.8	0.5	36	30
FeMag-170	350	7.7	0.4	52	35
FeMag-180	310	7.5	0.4	40	40
FeMag-190	300	6.9	0.3	48	45
FeNMag-195	320	7.6	0.4	31	35

[a] As determined by titration with base probes pyridine and 2,6-dimethylpyridine for total and BrØnsted acidity, respectively.

Yepez et al. previously reported TEM images of pure Al-SBA-15.[30] In comparison, TEM images (**Figure 2**) of representative catalysts synthesized in the present study show that the ordered porous structure of the Al-SBA-15 support was preserved upon Fe incorporation in continuous flow. Hematite (FeNMag-200) and maghemite (FeMag-170) nanoparticles were homogeneously distributed on the aluminosilicate support. High resolution images of a single particle in the FeNMag-200 material along the plane zone (010) depict a periodic spacing of 0.368 nm, consistent with the "d" spacing corresponding to α-Fe_2O_3 planes, indicative of single crystals with good crystallinity. The periodic spacing between 0,489 nm bands in FeMag-170 sample is also consistent with the corresponding "d" spacing of the {111} plane of γ-Fe_2O_3.

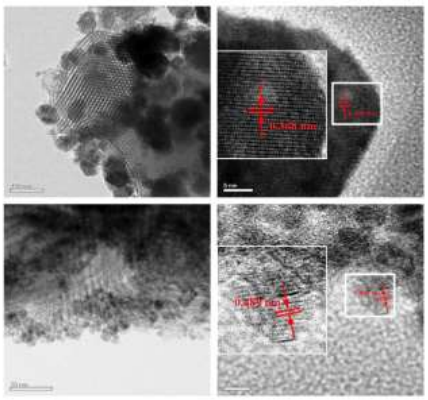

Figure 2. (Left) TEM and (right) HRTEM images of (up) FeNMag-200 and (bottom) FeMag-170 catalysts.

The synthesized MNPs were employed as heterogeneous catalyst in the selective oxidative disruption of isoeugenol in liquid phase using aqueous hydrogen peroxide as green oxidant, both at room temperature and 90 ºC (conventional heating). **Figure 3** depicts the conversion of isoeugenol and vanillin selectivity observed after 40 min and 24 h. Blank runs (no catalyst) and using Al-SBA-15 provided a very low total conversion (<20 %). The use of pure iron oxide nanoparticles (Fe) or a mixture of Fe with Al-SBA-15 comparatively led to significant conversions in the systems, pointing to iron oxide as catalytically active phase. The presence of Al-SBA-15 did not significantly influence final results as compared to Fe alone, with the exception of a higher selectivity to vanillin achieved at room temperature after 24 h. This may be the result of a caging effect of iron oxide and isoeugenol inside the Al-SBA-15 pores, leading to lower amounts of side products. GC/MS analysis of the products showed the presence of a diphenyl ether structure as main side product in all the experiments, produced by oxidative radical coupling of quinone methide tautomers of isoeugenol (or derivatives).

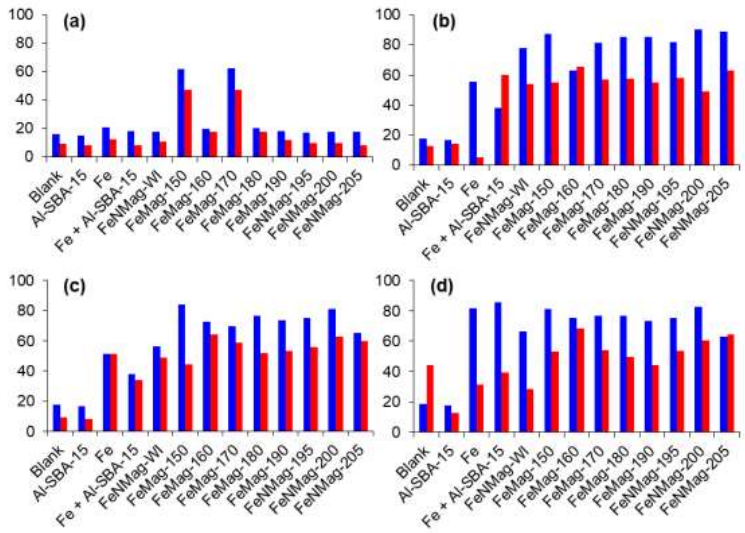

Figure 3. Isoeugenol conversion (blue, mol%) and selectivity to vanillin (red, mol%) without catalyst (blank), with Al-SBA-15, with pure iron oxide (Fe), with Al-SBA-15 + Fe (mix), with Fe deposited by wet impregnation (FeNMag-WI) and with Fe(N)Mag catalysts, at 20 °C after (a) 40 min. and (b) 24 h, and at 90 °C after (c) 40 min. and (d) 24 h.

As opposed to room temperature experiments, the advantage of heating related to an already close to the equilibrium conversion and selectivity after 40 min. (comparing with data after 24 h). Still, interesting results were obtained at room temperature after 24 h, with conversions ranging between 63 and 91 % at vanillin selectivities of ca. ≥ 50 %. Whereas the conversions increased consistently with reaction time up to 24 h, vanillin selectivity increased during the first 8 h of reaction, to then remain practically constant at ca. 50 %. At high temperatures, the selectivity was slightly reduced after 24 h as compared to 40 min. an indication that further oxidation to vanillic acid or other undesired processes took place. FeNMag-WI catalyst in contrast, prepared by wet impregnation, yielded vanillin amounts in the range of the results obtained with pure iron oxide (Fe) or with mixed Fe + Al-SBA-15 (Figure 3). No obvious relationship was found between Fe content and Fe_2O_3 phases present in materials (maghemite or hematite) when comparing conversion and selectivity obtained with all synthesized nanocatalysts under continuous flow conditions at different temperatures. The

catalytic activity was more related to their BrØnsted acidity. The fact that there was no direct relationship between catalytic activity and Fe_2O_3 phase together with the low selectivity to vanillin observed for Al-SBA-15 leads us to propose active centers similar to those described previously by our research group,[31] which showed a Fe-Al synergistic effect on Fe_2O_3 nanoparticles supported on SBA-15 type aluminosilicates, with excellent catalytic activities in oxidations of benzyl alcohol to benzaldehyde. This effect is most appreciable (Figure 3) comparing vanillin yields obtained for FeMag-170 and those obtained with physical mixtures of both compounds separately (Fe + Al-SBA-15) as catalyst. Next to conventional heating, microwave irradiation was also employed, showing beneficial effects (apart from faster and homogeneous heating). Outstandingly, the equilibrium seemed to be reached almost completely already after 5 min. when microwave heating was utilised (**Table 4**), (60-80 % conversion and 54-65 % selectivity). The differences with conventional heating after 24 h were small (< 10 %). Somewhat lower selectivity was observed after 15 min. due to possible side reactions.

Nanocatalysts presented in this work outperform previously reported results, at least in cost-effectiveness, when comparing results with previously reported data on the catalytic oxidation of vanillin using oxygen or hydrogen peroxide as oxidants (**Table 5)**. Still, the high amount of operational variables makes the comparison not straightforward. Gusevskaya et al. obtained similar vanillin yields (50 mol%) under comparable conditions, although they used a homogeneous and environmentally unfriendly catalyst in *ca.* 50 times less quantity (mol% of $(n\text{-Bu})_4NVO_3$ + pyrazine-2-carboxylic acid (PCA)).[25]

Finally, as the iron nanoparticles were recovered efficiently by activation in an external magnetic field, the re-usability of the magnetic catalysts was assessed (**Figure 4**). Although the magnetic properties were retained in the recovered catalysts, both conversion and selectivity significantly dropped, particularly after 4-5 uses. The spent FeMag-190 catalyst recovered after 4 cycles of 24 h at room temperature exhibited significantly lower porosity as compared to the fresh catalyst (Table 3), 150 $m^2\ g^{-1}$ specific surface area, 0.4 nm pore diameter and 0.3 mL g^{-1} pore volume. Comparably, vanillin yield was stable over 3 re-utilization experiments using conventional heating (90 ºC) while the yield dropped drastically when using microwave irradiation. This indicates that, although beneficial for the reactions kinetics, microwave irradiation had detrimental effects on catalyst performance (both activity and selectivity). In an attempt to provide further insights into catalyst deactivation, the reused catalyst was analyzed by TG-DTA and ATR (**Figure 5).** ATR spectrum showed absorption bands characteristic of vanillin-like aromatics including O-H stretching (3330 cm^{-1}), C=O stretching (1675 cm^{-1}), and the characteristic stretching vibration absorption of benzene ring corresponding to three bands at 1513, 1432 and 797 cm^{-1}. The band originated from the bending vibrations of phenolic OH around 1250 cm^{-1} was more difficult to appreciate as it was partially overlapped with the broad band from Si-O bonds (1062 cm^{-1}) in Al-SBA-15. Although the small band at 1600 cm^{-1} is representative of C=C stretching in isoeugenol, the amount adsorbed is negligible as any other bands arising from isoeugenol are hardly observable. In addition to these results, TG-DTA experiments (**Figure 5A,** see also supporting information**)** showed a significant mass loss (ca. 4-10%) in the 200-400ºC range accompanied by an endothermic peak in the DTA spectra, plausibly related to the observed aromatic compounds in ATR experiments. Importantly, a second small mass loss at higher temperatures (400-500ºC, **Figure S3**) is also present and likely to be due to the formation of heavier molecular weight aromatics as side products from the oxidation reaction.

It can be thus concluded that the observed deactivation in the catalytic experiments is mostly due to adsorption of aromatics-including vanillin and heavier molecular weight compounds-on the catalyst surface (**fouling**). FeMag-190 spent catalyst (after 5 reuses) was regenerated by recalcination at 300 ºC (in air, 2 h). XRD analysis (**Figure S4**, Supporting Information) pointed out the presence of the key diffraction lines corresponding to the iron oxide phase with the inherently amorphous nature of the aluminosilicate material. Interestingly, catalytic experiments of regenerated spent catalysts at 300ºC (e.g. FeMag-190) showed a remarkable recovery in the initial catalytic activity after regeneration (**Figure 4**), which in principle may be fully recovered upon thermal treatment at 550-600ºC (according to TG-DTA results, Figure 5A, a temperature at which all organics are fully removed). However, thermal regeneration was not conducted at such a high temperature to preserve the magnetic properties of the materials. Nevertheless, the regeneration studies clearly evidenced that the catalytic activity drop due to surface fouling could be solved by thermal treatment of the catalysts (300ºC) after which most of the initial catalytic activity in the systems was recovered. These findings also pointed out the strong deactivating role of adsorbed aromatic compounds on the surface after subsequent reuses, a phenomenon that also supports the observed strong deactivation of Fe-containing systems under microwave irradiation.

Table 4. Fe(N)Mag catalyzed isoeugenol conversion and selectivity to vanillin using microwave irradiation.

Catalyst	Conversion (mol%)		Selectivity (mol%)	
	5 min.	15 min.	5 min.	15 min.
Blank	18	19	10	17
Al-SBA-15	15	16	10	9
FeMag-150	73	75	59	58
FeMag-160	77	75	65	64
FeMag-170	80	81	56	57
FeMag-180	69	70	61	57
FeMag-190	68	70	58	54
FeNMag-195	68	67	62	56
FeNMag-200	60	61	59	65
FeNMag-205	62	57	54	55

Table 5. Comparison of catalytic performance of FeMag200 catalyst with previously reported ones for the selective oxidation of isoeugenol to vanillin.

Catalyst	Conversion (mol%)	Selectivity (mol%)	Yield (mol%)	Ref.
$PhI(OAc)_2$-NaY[a]	-	-	43	[32]
Nocardia iowensis whole cells[b]	-	-	60	[33]
TiO_2 (P25 Degussa)[c]	84	9	8	[34]
CoTPyP/TN[d]	99	72	71	[35]
$(n\text{-}Bu)_4NVO_3$ + PCA[e]	71	70	50	[25]
FeMag-180[f]	85	57	49	This work

[a] 0.3 M isoeugenol in 6 mL acetonitrile, 2 eq. of catalyst, 130 °C, 5 min. [b] 0.01 M isoeugenol in 2 mL aqueous buffer, 40 g L^{-1} cells, 130 °C 32 h. [c] 0.5 mM isoeugenol in 150 mL aqueous phase, 0.8 g L^{-1} catalyst, 20 °C, 2 h. [d] 0.03 mM isoeugenol in 10 mL acetonitrile, 1 mol% cobalt (as cobalt porphyrin/lithium taeniolite), 50 °C, 24 h, 3 bars pure O_2. [e] 0.2 M isoeugenol in 0.9 mL acetonitrile, 2 eq. H_2O_2, 0.025 mol% $(n\text{-}Bu)_4NVO_3$ + 0.05 mol% PCA, 80 °C, 2 h. [f] 0.5 M isoeugenol in 8 mL acetonitrile, 2.3 eq. H_2O_2, 12.5 mol% catalyst, 20 °C, 24 h.

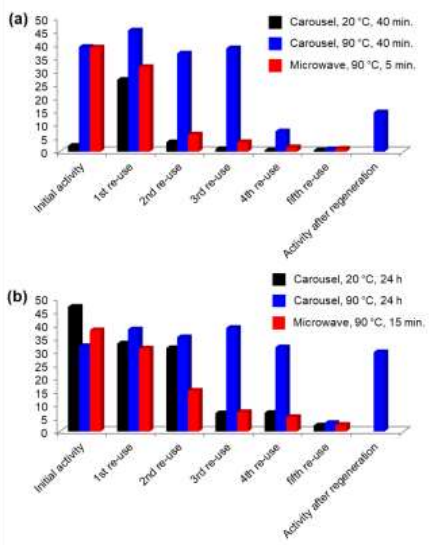

Figure 4. Vanillin yield (mol%) obtained with FeMag-190 catalyst over 5 re-utilization experiments for the catalytic oxidation of isoeugenol at 20 ºC and at 90 ºC (using both conventional heating and microwave irradiation). The activity after regeneration (300ºC, under air, 2h) is also included showing the almost complete regeneration of the initial catalytic activity upon calcination, particularly for the bottom plot (time extended reactions, 24 h).

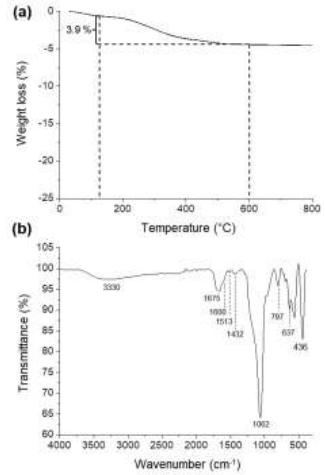

Figure 5. (a) TGA analysis and (b) ATR analysis of deactivated FeMag-190 catalyst recovered after 5 catalytic reuses.

Conclusions

The synthesis of iron nanoparticles supported on Al-SBA-15 has been successfully performed using a simple and reproducible continuous flow method. Synthesized nanomaterials exhibited suitable good magnetic properties when the synthesis temperature stayed below an apparent cut-off temperature of 195 °C. Nanocatalysts obtained provided excellent catalytic activities and promising selectivities (>50%) to vanillin in the selective oxidation of isoeugenol using hydrogen peroxide as green oxidant. Optimum results pointed to an 85 % conversion of 0.5 M isoeugenol with 57 % selectivity to vanillin after 24 h at room temperature. Reaction times were drastically reduced to 5-15 min under microwave irradiation, however with negative effects on catalyst re-usability. The catalyst deactivation was related with surface fouling, with thermally-treated regenerated catalysts (300ºC) able to recover over 80% of the initial catalytic activity of fresh catalysts.

Experimental Section

The synthesis of the mesoporous aluminosilicate Al-SBA-15 was carried out following the procedure described by Stucky and co-workers.[36] The triblock co-polymer Pluronic P123 was used as directing agent and dissolved in aqueous HCl (2M, pH 1.5) for 2 h at room temperature. After complete dissolution, tetraethyl

orthosilicate (25 mmol) was used as the silica source and the corresponding amount of aluminum isopropoxide (10 mmol) was slowly added. The mixture was stirred for 24 h at room temperature. Subsequently, the mixture was submitted to hydrothermal treatment in an oven at 100 °C for 24 h. The obtained solid was filtered off, dried and subsequently calcined under nitrogen atmosphere at 600 °C for 2 h, and then under air atmosphere for 4 h. The obtained SBA solids (Si/Al molar ratio 20) were recovered and stored.

The preparation of magnetic nanoparticles (MNPs) was carried using a continuous flow setup (**Scheme 2**). First, a stainless steel reactor (15 cm × 1 cm i.d.) was filled with Al-SBA-15 support (*ca.* 3.0 g) and fixed between two quartz wool stoppers above and beneath to prevent the displacement of the solids. The reactor was equipped with two stainless steel filters, one at the entrance and another one at the exit to avoid obstructions. The synthesis started by injecting ethanol at 0.5 mL $min.^{-1}$ during 45 min. while reaching the desired synthesis temperature. Subsequently, the ethanol flow was changed to a saturated solution of $Fe(NO_3)_2.9H_2O$ (precursor salt, Sigma Aldrich) in ethanol, at 0.5 mL $min.^{-1}$ during 1 h. After completion, propionic acid was pumped at a flow of 0.5 mL $min.^{-1}$ during 45 min. Then, after closing the valve in this loop, an air flow of 30 mL $min.^{-1}$ was injected for approximately 3 h while the reactor was submitted to a programmed temperature ramp of 1 °C $min.^{-1}$ to reach a final temperature of 300 °C, which then was kept constant for 1 h. FeNMag-WI was prepared by wet impregnation at room temperature using an Fe_2O_3 load corresponding with the same Fe content as determined by ICP-MS analysis in the FeMag-170 catalyst. We assumed that in wet impregnation 100 % of the iron was retained in the FeNMag-WI material. The Fe_2O_3, Al-SBA-15 and the FeNMag-WI materials were also treated with propionic acid which was added dropwise in batch, followed by calcination in air using an oven at the same temperature program as used in the continuous flow synthesis.

MNP solids obtained were characterized by X-ray diffraction (XRD), nitrogen adsorption-desorption porosimetry, magnetic susceptibility, scanning electron microscopy (SEM), inductively coupled plasma mass spectroscopy (ICP-MS), (high resolution) transmission electron microscopy and pulse chromatography (to study the surface acid properties). XRD spectra were recorded on a Bruker D8 X-ray diffractometer (10-80° 2θ range) in the Bragg-Brentano geometry and in reflection mode, using a Cu X-ray tube, a rotating platform, a monochromatic primary beam and a high sensitivity detector. In addition, some samples were analyzed using an advanced D8 X-ray diffractometer (Bruker AXS GmbH, Germany) with a LYNXEYE detector and Cu Kα irradiation at 40 kV and 40 mA, using a count time of 1 second for phase identification and 1 second for phase quantification. The quantitative analysis (QXRD) was carried out using TOPAS 4.2 software (Bruker AXS). All samples were mixed with 20 wt% CaF_2 (Merck, Germany) as internal standard for the quantification of the amorphous content. The elemental composition of the synthesized materials was studied in two ways. First, the surface of the solids was analyzed with an Inca Energy 250 microanalysis system using an JEOL JSM 6300 Scanning Electron Microscope equipped with a window type Si/Li detector (ATW2), in the boron to uranium detection range (137 eV to 5.9 keV). Secondly, the quantitative elemental analysis of the solids was determined with ICP-MS, using an Elan DRC-e equipment (Perkin Elmer SCIEX, Waltham, USA). The surface morphologies of the particles were examined by TEM and HRTEM using FEI Tecnai G2 20 S-TWIN and 2010F JEOL electron microscopes, respectively. The nitrogen adsorption-desorption isotherms were recorded at -196 °C using a Micromeritics ASAP 2000 automatic analyzer. The samples were degassed for 24 h at 100 °C under vacuum (p < 10-20 Pa) prior to analysis. The linear part of the Brunauer–Emmett–Teller (BET) equation (relative pressure between 0.05 and 0.30) was used to determine the specific surface area. The pore size distribution was calculated using the adsorption branch of the adsorption-desorption isotherm, applying the method of Barrett, Joyner and Halenda (BJH).[37] The magnetic susceptibility χm was determined at room temperature using an MS2 magnetic susceptibility meter (Bartington Instruments Ltd., UK) equipped with a MS2B dual-frequency (470 and 4700 Hz) laboratory sensor. χ_m is equal to the ratio of the magnetization M within the material to the applied magnetic field strength H. This ratio, strictly speaking, is the volumetric susceptibility, because magnetization essentially involves a certain measure of magnetism (dipole moment) per unit volume. It is a measure of the magnetic response of a material to an external magnetic field. The determination of the surface acidity was carried out at 250 °C, with pyridine (PY) and 2,6-dimethylpyridine (DMPY) as titration bases for total and BrØnsted acidity, respectively. The bases were introduced (2, 3, 4, 5 and 6 µL) in a GC injector coupled to a stainless steel column (10 cm × i.d. 2 mm) packed with the analyte (40-70 mg), which in turn was coupled to a 50 cm chromatographic column containing 5 wt% polyphenylether in Chromosorb AW-MCS 80/100. The bases remaining after elution through the packed column were quantified by gas chromatography equipped with a flame ionization detector (GC-FID). Thermogravimetric analysis (TGA) was carried out in equipment using *ca.* 15 mg sample under dynamic air atmosphere (10 mL min^{-1}). Attenuated total reflectance infrared Fourier transform spectroscopy (ATR-IR) spectra were recorded using a Spectrum Two™ instrument (Perkin Elmer, Waltham, USA), from 4000 to 450 cm^{-1} with a resolution of 4 cm^{-1}.

The reactions with isoeugenol were carried out by conventional heating at one hand and by microwave heating at the other hand. The conventional heated reactions were performed using a multiple parallel synthesis system (Carrusel Reaction Station™, Radleys Discovery Technologies Ltd., UK) equipped with magnetic stirring at 1000 rpm. The experiments were run at 20 and at 90 °C, using 5 mmol isoeugenol and 11.7 mmol hydrogen peroxide (1.2 mL of 33 % w/v H_2O_2 in water) in 8 mL acetonitrile with 100 mg catalyst, which were added when the desired reaction temperature was reached (time = 0). For the

experiments with Al-SBA-15+Fe_2O_3-170, the corresponding amounts of Al-SBA-15 (56.7 mg) and Fe_2O_3-170 (43.3 mg) were used (to reach an equal Fe content in the reaction as compared to the experiment with FeMag-170 catalyst, based on the Fe content according to the ICP-MS analysis in Table 2). The experiments with FeNMag-WI were carried out with 100 mg catalyst, as it contained the same amount of Fe as in FeMag-170. The reactions using microwave heating were carried out in a CEM-Discover focused microwave, controlled and monitored by a computer in standard mode ("Discover") under pressure which allows control of the irradiation power, temperature and pressure. The reactants used were 1.25 mmol isoeugenol and 2.9 mmol H_2O_2 in 2 mL acetonitrile, with 25 mg catalyst at 90 °C, using 300 W irradiation power. In all experiments the reaction temperature was reached after *ca.* 1 min without any significant overheating. The reaction mixture was analyzed before, during and after the reaction by gas chromatography on an Agilent Technologies 7890 A GC System equipped with a Petrocol™ DH column (100 m x 0.25 mm x 0.50 µm i.d.) and a FID detector. The temperature of the column was set at 200 ºC (70 min. hold time) and the temperature of the injector and detector at 300 ºC. The nitrogen gas flow was set at 3 mL min^{-1}. The retention times of isoeugenol and vanillin were 33.4 and 30.2 min., respectively. Isoeugenol calibration was carried out in the 2.00-60.00 g L^{-1} range (r^2 0.98). The reaction mixture was also analyzed with GC/MS, The standard deviation on conversion and selectivity, as determined from two independent experiments with catalyst FeNMag-200 at 90 ºC was 7 and 2 % after 40 min. and 24 h, respectively. The corresponding deviations on selectivity were 3 and 8 %, respectively. The recycle experiments were carried out identically. The catalyst was recovered with a hand magnet, washed with acetonitrile and dried at 100 ºC. Regeneration of the spent catalyst was performed by recalcination under identical conditions as used in their synthesis (300 ºC, air, 2 h).

Acknowledgements

R.L. gratefully acknowledges MINECO as well as FEDER funds for funding under project CTQ2016-78289-P and financial support from Programa Propio at University of Cordoba (Spain).

Keywords: Isoeugenol • Oxidation • Vanillin • Magnetic • Nanoparticles

[1] F. Lu, J. Ruiz, D. Astruc, *Tetrahedron Lett.* **2004**, *45*, 9443–9445.
[2] D. Astruc, F. Lu, J. Ruiz, *Angew. Chem. Int. Ed.* **2005**, *44*, 7852–77872.
[3] D. Astruc, *Transition-metal nanoparticles in catalysis*, Wiley-VCH, Weinheim, Germany**, 2008**.
[4] M. Iranmanesha J. Hulliger, *Chem. Soc. Rev.* **2017**, Advance Article, DOI: 10.1039/C7CS00230K.
[5] Q. M. Kainz, O. Reiser, *Acc. Chem. Res.* **2014**, *47*(2), 667–677.
[6] A. H. Lu, E. L. Salabas, F. Schüth, *Angew. Chem. Int. Ed*. **2007**, *46*, 1222-1244.
[7] S. Shylesh, V. Schünemann, W. R. Thiel, *Angew. Chem. Int. Ed.* **2010**, *49*, 3428–3459.
[8] Y. Zhu, L. P. Stubbs, F. Ho, R. Liu, C. P. Ship, J. A. Maguire, N. S. Hosmane, *ChemCatChem* **2010**, *2*, 365–374.
[9] V. Polshettiwar, R. Luque, A. Fihri, H. Zhu, M. Bouhrara, J. M. Basset, *Chem. Rev.* **2011**, *111*, 3036–3075.
[10] R. B. N. Baig, R. S. Varma, *Chem. Commun*. **2013**, *49*, 752–770.
[11] N. I. Cuello, V. R. Elías, E. Winkler, G. Pozo-López, M. I. Oliva, G. A. Eimer, *J. Magn. Magn. Mater.* **2016**, *407*, 299–307.
[12] C. T. Kresge, M. E. Leonowicz, W. J. Roth, J. C. Vartuli, J. S. Beck, *Nature* **1992**, *359*, 710–712.
[13] J. S. Beck, J. C. Vartuli, W. J. Roth, M. E. Leonowicz, C. T. Kresge, K. D. Schmitt, C. T.-W. Chu, D. H. Olson, E. W. Sheppard, S. B. McCullen, J. B. Higgins, J. L. Schlenkert, *J. Am. Chem. Soc.* **1992**, *114*, 10834–10843.
[14] M. B. Gawande, Y. Monga, R. Zboril, R. K. Sharma, *Coord. Chem. Rev.* **2015**, *288*, 118–143.
[15] M. B. Gawande, R. Luque, R. Zboril, *ChemCatChem* **2014**, *6*, 3312–3313.
[16] M. J. W. Dignum, J. Kerler, R. Verpoorte, *Food Rev. Int.* **2001**, *17*, 119-120.
[17] N. J. Walton, A. Narbad, C. B. Faulds, G. Williamson, *Curr. Opin. Biotechnol*. **2000**, *11*, 490–496.
[18] M. Fache, B. Boutevin, S. Caillol, *ACS Sustainable Chem. Eng.* **2016,** *4*(1), 35–46.
[19] A. Franco, S. De, A. M. Balu, A. Garcia, R. Luque, *Beilstein J Org. Chem.* **2017**, *13*, 1439-1445.
[20] N. J. Walton, M. J. Mayer, A. Narbad, *Phytochemistry* **2003**, *63*, 505–515.
[21] E. Shimoni, U. Ravid, Y. Shoham, *J. Biotechnol*. **2000**, *78*, 1-9.
[22] P. H. Markus, A. L. J. Peters, R. Roos, Process for the preparation of phenylaldehydes. European patent EP 542348 (1992).
[23] L. Q. Zhao, Z. -H. Sun, P. Zheng, L. -L. Zhu, *Biotechnol. Lett.* **2005**, *27*, 1505–1509.
[24] W. A. Herrmann, T. Weskamp, J. P. Zoller, R. W. Fischer, *J. Mol. Catal. A.-Chem.* **2012**, *363-364*, 140-147.
[25] E. V. Gusevskaya, L. Menini, L. A. Parreira, R. A. Mesquita, Y. N. Kozlov, G. B. Shul'pin, *J. Mol. Catal. A.-Chem.* **2012**, *363-364*, 140-147.
[26] L. Y. Shi, Y. M. Wang, A. Ji, L. Gao, Y. Wang, *J. Mater. Chem.* **2005**, *15*, 1392–1396.
[27] F. Fajaroh, H. Setyawan, A. Nur, I. W. Lenggor, *Adv. Powder Technol.* **2013**, *24*, 507-511.
[28] G. C. Papaefthymou, E. Devlin, A. Simopoulos, D. K. Yi, S. N. Riduan, S. S. Lee, J. Y. Ying, J. Physical Review B **2009**, *80*, 024406, 1-9.
[29] C. Peters, M. J. Dekkers, *Phys. Chem. Earth* **2003**, *28*, 659-665.
[30] A. Yepez, J. M. Hidalgo, A. Pineda, R. Černý, P. Jíša, A. Garcia, A. A. Romero, R. Luque, *Green Chem.* **2015**, 17, 565-572.
[31] A. M. Balu, A. Pineda, K. Yoshida, J. M. Campelo, P. L. Gai, R. Luque, A. A. Romero, *Chem. Commun.* **2010**, *46*, 7825–7827.
[32] H. Marquez Alvarez, D. P. Barbosa, A. Tinoco Fricks, D. A. G. Aranda, R. H. Valdés, O. A. C. Antunes, *Org. Process Res. Dev.* **2006**, *10*, 941-943.
[33] R. Seshadri, A. S. Lamm, A. Khare, J. P.N. Rosazza, *Enzyme Microb. Technol.* **2008**, *43*, 486–494.
[34 V. Augugliaro, G. Camera-Roda, V. Loddo, G. Palmisano, L. Palmisano, F. Parrino, M. A. Puma, *Appl. Catal., B* **2012**, *111–112*, 555– 561.
[35] I. Badria Adilina, T. Hara, N. Ichikuni, S. Shimazu, *J. Mol. Catal. A: Chem.* **2012**, *361–362*, 72–79.
[36] D. Zhao, J. Feng, Q. Huo, N. Melosh, G. H. Fredrickson, B. F. Chmelka, G. D. Stucky, *Science* **1998**, *279*, 548-542.
[37] E. P. Barrett, L. G. Joyner, P. P. Halenda, *J. Am. Chem. Soc.* **1951**, *61*, 373-380.

FULL PAPER

Magnetic iron oxide nanoparticles supported on Al-SBA-15, prepared under continuous flow, are highly active and selective for the disruptive oxidation of isoeugenol to vanillin using hydrogen peroxide as green oxidant.

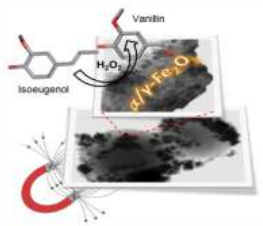

*María Dolores Marquez, Pepijn Prinsen, Hangkong Li, Kaimin Shih, Antonio Angel Romero, Rafael Luque**

Page No. – Page No.

Continuous flow synthesis of supported magnetic iron oxide nanoparticles for efficient isoeugenol conversion to vanillin

CHEMISTRY & SUSTAINABILITY
CHEMSUSCHEM
ENERGY & MATERIALS

Supporting Information

Continuous-Flow Synthesis of Supported Magnetic Iron Oxide Nanoparticles for Efficient Isoeugenol Conversion into Vanillin

M. Dolores Marquez-Medina,[a] Pepijn Prinsen,[a] Hangkong Li,[b] Kaimin Shih,[b] Antonio A. Romero,[a] and Rafael Luque*[a]

cssc_201701884_sm_miscellaneous_information.pdf

Author Contributions

M.M. Investigation: Lead; Writing – original draft: Equal
P.P. Data curation: Lead; Investigation: Supporting; Supervision: Supporting; Validation: Equal; Visualization: Lead; Writing – review & editing: Lead
H.L. Data curation: Equal; Formal analysis: Equal; Methodology: Supporting
K.S. Data curation: Equal; Formal analysis: Equal; Methodology: Supporting
A.R. Methodology: Supporting; Project administration: Lead; Resources: Lead; Supervision: Lead.

Supporting Information

Figure S1 shows the XRD pattern of FeWI, prepared by wet impregnation of Fe on Al-SBA-15 at room temperature.

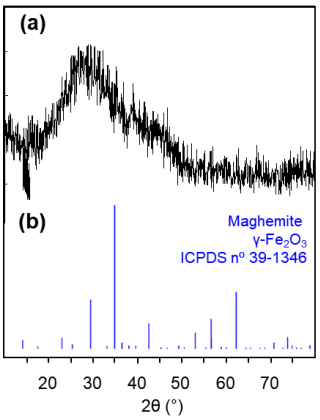

Figure S1. XRD patterns of (a) FeWI and (b) pure maghemite.

Figure S2 shows the nitrogen adsorption-desorption isotherms of the mesoporous support (Al-SBA-15) and the samples FeMag-150, FeMag-180 and FeMag-195 (iron oxide particles supported on Al-SBA-15 synthesized at 150, 180 and 195 °C).

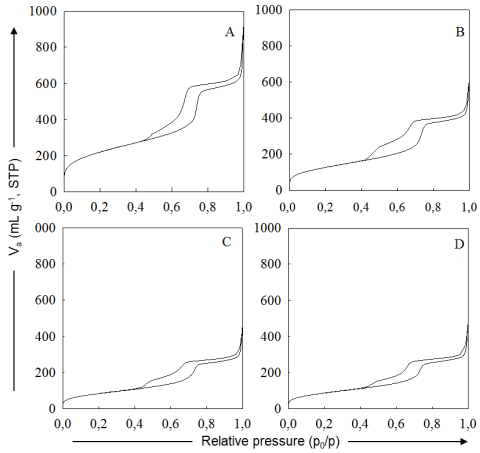

Figure S2. Nitrogen adsorption-desorption isotherms of (a) Al-SBA-15, (b) FeMag-150, (c) FeMag-180 and (d) FeMag-195.

Figure S3 shows a detailed TG-DTA spectra of FeMag-190 where the corresponding mass losses explained in the manuscript can be clearly seen.

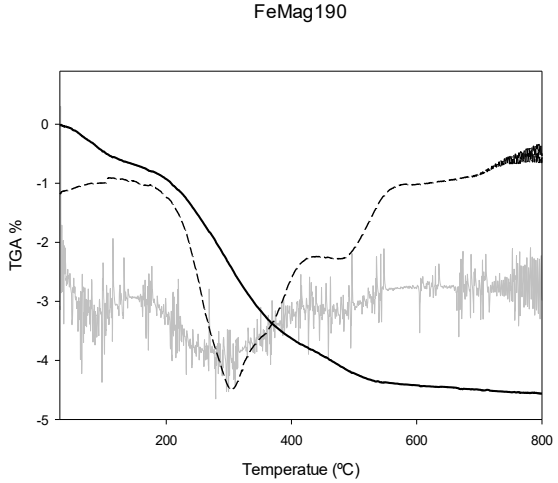

Figure S3. TG-DTA pattern of FeMag-190.

Figure S4 depicts the XRD pattern of the FeMag-190 catalyst recovered after 24 h reaction at 90 °C and regenerated by recalcination at 300° C.

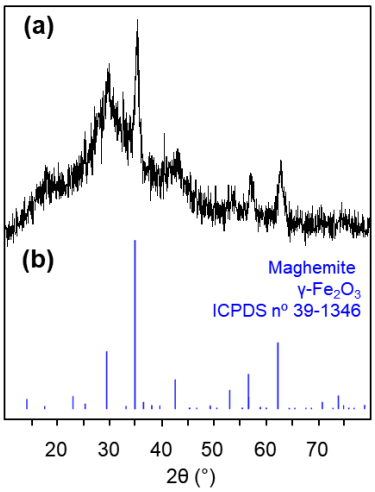

Figure S4. XRD patterns of (a) regenerated FMag-190 catalyst and (b) pure maghemite.

Volume 9, Issue 3

Catalysts 2019, *9*(3), 290; https://doi.org/10.3390/catal9030290 Open Access Article

Mechanochemically Synthesized Supported Magnetic Fe-Nanoparticles as Catalysts for Efficient Vanillin Production

María Dolores Márquez-Medina [1], Dailly Rodríguez-Padrón [1], Alina M. Balu [1], Antonio A. Romero [1], Mario J. Muñoz-Batista [1,*] and Rafael Luque [1,2,*]

[1] Departamento de Química Orgánica, Universidad de Córdoba, Campus de Rabanales, Edificio Marie Curie (C-3), Ctra Nnal IV-A, Km 396, E14014 Cordoba, Spain
[2] Scientific Center for Molecular Design and Synthesis of Innovative Compounds for the Medical Industry, People's Friendship University of Russia (RUDN University), 6 Miklukho-Maklaya str., Moscow 117198, Russia
* Authors to whom correspondence should be addressed.

Received: 15 February 2019 / Revised: 12 March 2019 / Accepted: 15 March 2019 / Published: 21 March 2019

Full-Text | PDF [3254 KB, uploaded 28 March 2019] | Figures

Abstract

Magnetically separable nanocatalysts were synthesized by incorporating iron nanoparticles on a mesoporous aluminosilicate (Al-SBA-15) through a mechanochemical grinding pathway in a single step. Noticeably, magnetic features were achieved by employing biomass waste as a carbon source, which additionally may confer high oxygen functionalities to the resulting material. The resulting catalysts were characterized using X-ray diffraction, X-ray photoelectron spectroscopy, transmission electron microscopy, scanning electron microscopy, porosimetry, and magnetic susceptibility. The magnetic nanocatalysts were tested in the selective oxidative cleavage reaction of isoeugenol and vanillyl alcohol to vanillin. As a result, the magnetic nanocatalysts demonstrated high catalytic activity, chemical stability, and enormous separation/reusability qualities. The origin of catalytic properties and its relationship with the iron oxide precursor were analyzed in terms of the chemical, morphological, and structural properties of the samples. Such analysis allows, thus, to highlight the superficial concentration of the iron entities and the interaction with Al as key factors to obtain a good catalytic response. View Full-Text

Keywords: magnetic nanoparticles; mechanochemistry; iron oxides; Al-SBA-15; vanillin

▼ Figures

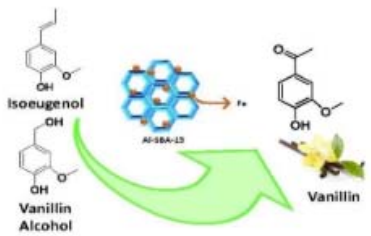

Graphical abstract

catalysts

MDPI

Article

Mechanochemically Synthesized Supported Magnetic Fe-Nanoparticles as Catalysts for Efficient Vanillin Production

María Dolores Márquez-Medina [1], Daily Rodríguez-Padrón [1], Alina M. Balu [1], Antonio A. Romero [1], Mario J. Muñoz-Batista [1,*] and Rafael Luque [1,2,*]

[1] Departamento de Química Orgánica, Universidad de Córdoba, Campus de Rabanales, Edificio Marie Curie (C-3), Ctra Nnal IV-A, Km 396, E14014, Cordoba, Spain; q92mamem@uco.es (M.D.M.-M.); dailydggs@gmail.com (D.R.-P.) qo2balua@uco.es (A.M.B.); qo1rorea@uco.es (A.A.R.)

[2] Scientific Center for Molecular Design and Synthesis of Innovative Compounds for the Medical Industry, People´s Friendship University of Russia (RUDN University), 6 Miklukho-Maklaya str., 117198 Moscow, Russia

* Correspondence: rafael.luque@uco.es (R.L.), qo2mubam@uco.es (M.J.M.-B.)

Received: 15 February 2019; Accepted: 18 March 2019; Published: 21 March 2019

Abstract: Magnetically separable nanocatalysts were synthesized by incorporating iron nanoparticles on a mesoporous aluminosilicate (Al-SBA-15) through a mechanochemical grinding pathway in a single step. Noticeably, magnetic features were achieved by employing biomass waste as a carbon source, which additionally may confer high oxygen functionalities to the resulting material. The resulting catalysts were characterized using X-ray diffraction, X-ray photoelectron spectroscopy, transmission electron microscopy, scanning electron microscopy, porosimetry, and magnetic susceptibility. The magnetic nanocatalysts were tested in the selective oxidative cleavage reaction of isoeugenol and vanillyl alcohol to vanillin. As a result, the magnetic nanocatalysts demonstrated high catalytic activity, chemical stability, and enormous separation/reusability qualities. The origin of catalytic properties and its relationship with the iron oxide precursor were analyzed in terms of the chemical, morphological, and structural properties of the samples. Such analysis allows, thus, to highlight the superficial concentration of the iron entities and the interaction with Al as key factors to obtain a good catalytic response.

Keywords: magnetic nanoparticles; mechanochemistry; iron oxides; Al-SBA-15; vanillin

1. Introduction

Currently, environmental issues related to global warming [1], which can have a negative impact on human safety, together with the limited reserves of crude oil, motivated the scientific community in the design of sustainable alternatives for materials, chemicals, energy, and fuel production [2,3]. A change is required from the traditional concept of process efficiency focused on chemical performance, considering the premises of sustainable development for the replacement of fossil resources by renewable raw materials. In this regard, biomass valorization represents an attractive option to supply the chemical demand by using an abundant and renewable source [4,5]. Lignocellulosic biomass, mainly composed of lignin, cellulose, and hemicellulose, can lead to terpenes, carbohydrates, fatty esters, and aromatics. In this sense, biomass was recently subject of numerous studies, attracting great interest as the most abundant renewable raw material of organic carbon available on the planet and as a perfect substitute for oil in the production of fuels and chemical products [6–8]. These facts represent at the same time an interesting and challenging topic

for the chemical industry [9]. Therefore, the use of catalytic systems can pave the way for an optimum biomass valorization [10,11].

In particular, the catalytic valorization of biomass-derived compounds such as eugenol, isoeugenol, and ferulic acid was broadly studied through the past few years [12–15]. The molecules may replace petrol-based intermediates, such as guaiacol and glyoxylic acid, for the synthesis of vanillin [16]. The latter compound is a well-known flavoring agent, popular in the food, cosmetic, and pharmaceutical industries. Several catalytic strategies, employing different transition metal oxides, were explored for the conversion of isoeugenol and vanillyl alcohol to vanillin [17,18]. In particular, supported and non-supported iron oxides were extensively applied to isoeugenol valorization [19–21]. However, much more effort should be devoted in order to optimize the catalytic systems and, in turn, to enhance the catalytic performance in terms of conversion, selectivity, and stability.

Nanostructured heterogeneous catalysts possess advantages related to their recovery and reuse, thus contributing to increasing the sustainable credentials of chemical processes [22,23]. In this regard, the use of stable, active, and recyclable materials proved to be very useful for a wide range of chemical processes [24–26]. The deposition of highly active nanoparticles on various organic or inorganic supports is probably the most effective strategy for the reuse of nanocatalysts [27]. The design of magnetic nanocatalyts facilitates a more efficient separation by using a magnetic field, compared to conventional decanting and filtration techniques [28–34].

Iron oxide-based nanomaterials may possess different magnetic features depending on their crystalline phase (e.g., hematite, maghemite, and magnetite) [35]. Magnetic iron oxides are generally obtained by liquid-phase methods, which involve additional solvents and reagents [36]. A novel technique for the synthesis of magnetic nanocatalysts is mechanical grinding (mechanochemistry). In general, this method can avoid the use of toxic organic solvents that could be released to the environment and increase the effectiveness and reproducibility in the synthesis of the materials. Mechanochemistry is a promising alternative for the synthesis of heterogeneous catalysts [37]. Regarding the synthesis of magnetic iron oxide, mechanochemical methods require the use of propionic acid, as previously described by our research group [38,39]. Propionic acid, together with the iron precursor, gives rise to an iron carboxylate compound, which can be further converted via calcination into crystalline magnetic iron-oxide phases. Replacement of such a reagent by a lignocellulosic residue not only results in the desired iron oxide phase, but could also represent a sustainable alternative for these type of materials. Also, textural properties constitute a key factor for a good catalytic performance, such as porosity. Therefore, employing silica mesoporous supports including MCM-41 (Hexagonal), MCM-48 (Cubic pore morphology), SBA-15 (Hexagonal pore morphology), and Al-SBA-15 (Hexagonal pore morphology) for transition-metal oxides can provide access to advanced systems with optimum porosity for catalytic applications [40-42]. Through this work, two strategies are explored for biomass valorization, namely chemical and materials, revealing the underexploited potential of such types of residues to ameliorate the environmental impact of chemical processes.

2. Results and Discussion

The proposed methodology resulted to be effective for the preparation of such catalytic systems, pointing out that mechanochemical protocols represent a green and remarkable pathway to synthesize advanced nanomaterials. Table S1 (Supplementary Materials) summarizes the materials synthesized. In particular, the employment of biomass residue as a carbon source presents outstanding advantages, since it allows the formation of a magnetic phase without employing other chemicals, such as propionic acid, commonly used for the synthesis of magnetic iron oxide [17]. Nanomaterials synthesized employing iron perchlorate and iron chloride did not show magnetic susceptibility. On the other hand, concentrations higher than 40% for iron citrate and higher than 30% for iron nitrate showed remarkable magnetic features. Magnetic susceptibility values were found in the range of 70–210 × 10^{-6} $m^3 \cdot kg^{-1}$ (Table S1, Supplementary Materials). These values are consistent with the content of maghemite in the support since the pure maghemite nanoparticles generally show

magnetic susceptibilities of approximately 500 × 10^{-6} $m^3 \cdot kg^{-1}$ [43]. These susceptibility values allow the magnetic separation from the reaction mixture.

After functionalization with iron oxide, X-ray diffraction (XRD) analysis of the samples prepared with iron citrate (FeMagC) showed a typical diffraction pattern that could be correlated with a mixture of hematite (as the major component) and maghemite phases (Figure 1). The diffraction peaks at 2θ = 30.2°, 33.2°, 35.7°, 40.9°, 49.5°, 54.1°, 57.3°, 62.4°, and 64.1° correspond to (200), (104), (110), (113), (024), (116), (112), (214), and (300) crystallographic planes of hematite phase, respectively [41]. In addition, maghemite-related peaks were observed at 2θ = 24.2° and 43.3°, suggesting the presence of both crystalline phases with a marked hematite prominence. Remarkably, the employment of iron nitrate (FeMagN) resulted in (a) formation of pure maghemite (2θ = 30.2°, 35.5°, 43.5°, 57.5°, and 63.0° associated with (200), (311), (400), (511) and (440)), and (b) loss of crystallinity [44,45]. The presence of the maghemite phase in the samples facilitates further recovery and reuse of the synthesized catalytic systems.

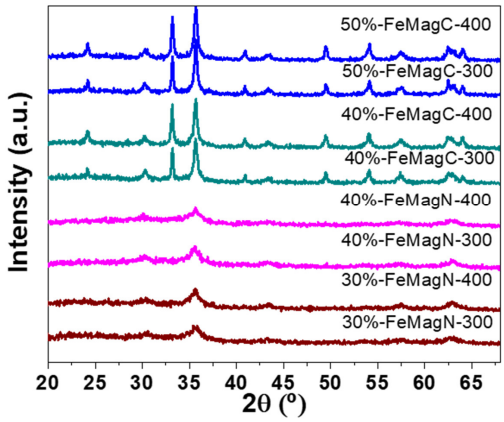

Figure 1. X-ray diffraction (XRD) patterns of selected samples.

Nitrogen adsorption–desorption analysis of selected materials displayed a mesoporous structure in all cases, as can be observed in Figure 2A and B, corresponding to type IV isotherms, according to the International Union of Pure and Applied Chemistry (IUPAC) classification, showing an acute inflection in the P/P_0 range of 0.5–0.8 [46]. A decrease of surface area was observed after incorporation of iron oxide nanoparticles. Brunauer–Emmett–Teller (BET) surface areas around 240–340 $m^2 \cdot g^{-1}$ were obtained (Table 1). Such values are in good agreement with those previously reported for functionalized Al-SBA-15 samples.[47]. In addition, pore diameters and pore volume also showed a decrease of around 50% after functionalization (Table 1). These results can be understood from a partial occlusion of Al-SBA-15 pores in presence of the Fe-oxide co-catalyst. Elemental information about the components of samples was obtained with the help of SEM and energy-dispersive X-ray spectroscopy (EDX). EDX analysis (Table 1) corroborated the presence of the expected elements Al, Si, and Fe, and no significant differences were observed among the studied samples, as may be envisaged by their similar chemical composition (for same iron salt concentration) when different precursors were used. EDX analysis also allowed the identification of bulk N concentration in the samples; however, very low concentrations (in comparison to superficial concentration obtained by X-ray photoelectron spectroscopy (XPS)) and, consequently, high standard errors prevented the analysis of this data. This is an expected result considering that a sacrificial template

mechanochemical-based method was used, in which the waste feedstock is almost completely removed during the calcination process.

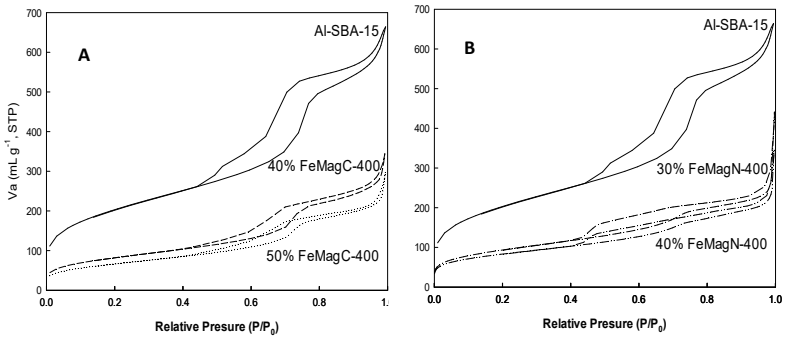

Figure 2. N_2 adsorption–desorption isotherms of **(A)** FeMagC at 400 °C, and **(B)** FeMagN at 400 °C.

Table 1. Textural properties of the obtained materials. BET—Brunauer–Emmett–Teller; EDX—energy-dispersive X-ray spectroscopy.

Catalyst	S_{BET} ($m^2 \cdot g^{-1}$)	Average Pore diameter (nm)*	Average pore volume ($mL \cdot g^{-1}$)	SEM–EDX		
				%Al	%Si	%Fe
Al-SBA-15	736	8.5	0.8	-	-	-
40% FeMagC-400	297	7.5	0.4	3.0	76.1	20.9
50% FeMagC-400	242	7.6	0.3	2.5	70.7	26.8
30% FeMagN-400	339	6.3	0.2	2.6	72.3	25.1
40% FeMagN-400	300	6.4	0.2	2.3	70.6	27.1

Morphological differences between the samples obtained using iron citrate and iron nitrate were further investigated through a TEM study, using 40% FeMagC at 400 °C and 30% FeMagN at 400 °C as representative samples. TEM images of 40% FeMagC at 400 °C and 30% FeMagN at 400 °C (Figures 3A,B) depicted that iron-oxide nanoparticles were successfully incorporated on the Al-SBA-15 surface. In both cases, the Al-SBA-15 support displays its characteristic well-crystallized and porous structure [48]. Also, in both examples, several darker areas, which can be clearly associated with the iron-oxide counterpart, were observed. EDX and TEM analyses support the idea that very close contact between the Al-SBA-15 support and iron-oxide component both at the surface and trapped in the porous structure was generated; however, a heterogeneous distribution of iron-oxide agglomerates also seemed to be present.

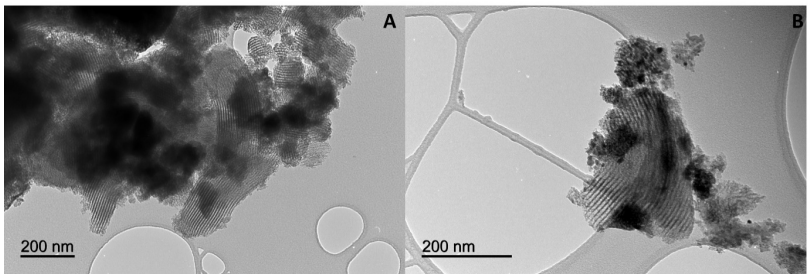

Figure 3. TEM images of (**A**) 40% FeMagC at 400 °C, and (**B**) 40% FeMagN at 400 °C.

In order to provide insight into species at the surface of the material and elucidate their relationship with the precursor used, as well as their influence on the reactions, XPS analysis of the same representative samples (40% FeMagC at 400 °C and 40% FeMagN at 400 °C) was performed. Curve fitting was carried out using the carbon C 1*s* peak (284.6 eV) as a reference for binding energy calibration. The deconvoluted C 1*s* XPS spectra of the obtained materials exhibited three different contributions associated to the presence of C–C/C=C, C–N, and C–O bonds. In particular, the C–N signal detected can be understood most likely due to the presence of nitrogen-containing compounds in the utilized biomass source. In both samples, the presence of Fe^{3+} species could be also inferred from the Fe $2p_{3/2}$ and Fe $2p_{1/2}$ peaks around 710 eV and 725 eV, respectively (Figures 4A,D). XPS spectra did not show the characteristic peaks associated with Fe(II), 709.6 eV or Fe(0), 706.7 eV species [49]. The absence of Fe(II) in the samples, especially, confirmed the formation of maghemite as a magnetic phase instead of magnetite, where both Fe(III) and Fe(II) species are presented [50,51]. Additionally, O 1*s* XPS spectra displayed three different peaks attributed to O–C, O–Fe, and O–Si. In addition, the typical signals of Si 2*p* in SiO_2 were observed at 103.0 eV for both materials. Calculation of Fe/Si ratio was carried out using XPS (Table 2). Interestingly, a comparison with the Fe/Si ratio obtained by EDX (bulk) provides evidence that remarkable superficial differences were obtained using nitrate and citrate precursors. While Fe/Si ratios of the bulk obtained by EDX were essentially unchanged (enhancement factor of 1.4: $(Fe/Si)_{EDX}$ 40% FeMagN at 400 °C/$(Fe/Si)_{EDX}$ 40% FeMagC at 400 °C), the superficial ratio calculated by XPS shows an enhancement factor of 6.2 $(Fe/Si)_{XPS}$ 40% FeMagN at 400 °C/$(Fe/Si)_{XPS}$ 40% FeMagC at 400 °C).

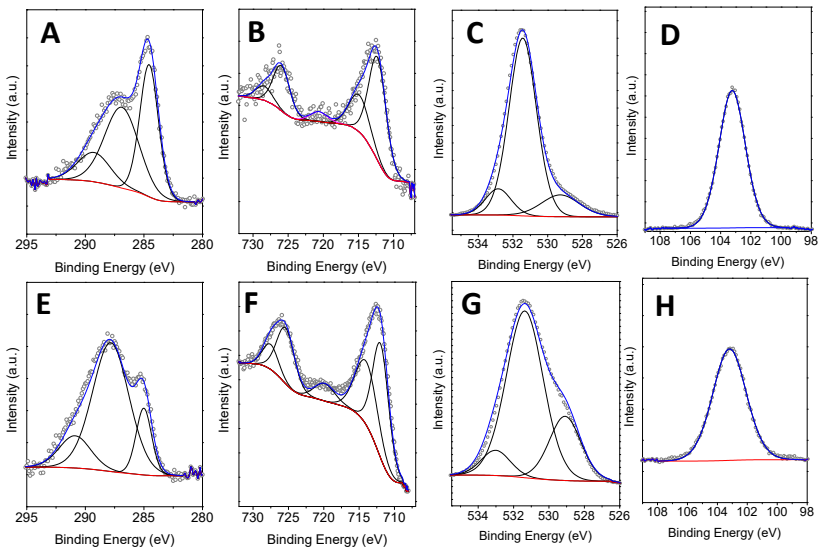

Figure 4. Deconvoluted X-ray photoelectron spectroscopy (XPS) spectra of 40% FeMagC at 400 °C and 40% FeMagN at 400 °C for (**A,E**) C 1*s*, (**B,F**) Fe 2*p*, (**C,G**) O 1*s*, and (**D,H**) Si 2*p*.

Table 2. Fe/Si atomic ratio obtained by chemical analysis and X-ray photoelectron spectroscopy (XPS).

Sample	$(Fe/Si)_{XPS}$	$(Fe/Si)_{EDX}$	$(Fe/Si)_{XPS}/(Fe/Si)_{EDX}$
40% FeMagC at 400 °C	0.03	0.3	0.1
40% FeMagN at 400 °C	0.19	0.4	0.5

The catalytic properties of the samples were investigated during the oxidation of isoeugenol and vanillyl alcohol toward the selective production of vanillin (Scheme 1).

Scheme 1. Reaction scheme. (**A**) Oxidation of isoeugenol; (**B**) oxidation of vanillyl alcohol.

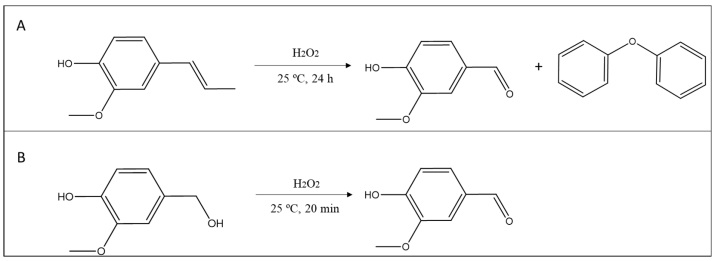

Firstly, control experiments were performed in the absence of the catalysts (blank) and employing Al-SBA-15 as a reference. These control reactions showed negligible activity in the absence of an effective catalytic system (see blank vs. Al-SBA-15 in Figure 5A) for isoeugenol oxidation, obtaining diphenyl structures as the main product. In addition, the vanillyl alcohol oxidation reaction to vanillin showed fair conversions after 2 h of reaction without catalyst and relatively low values when the reference support Al-SBA-15 was used (Figure 5B). The Al-SBA-15 reference is active in the vanillyl alcohol oxidation reaction under used experimental conditions but displays a rather modest activity in comparison with samples containing iron oxide. Under optimized reaction conditions for isoeugenol oxidation [17], prepared nanomaterials showed remarkable differences as a function of the iron precursor. A similar situation was acquired using vanillyl alcohol as a reagent, for which 20 min was settled on as the final reaction time. In both reactions, samples obtained using iron nitrate provided significantly improved conversions in comparison to the series of samples synthesized from iron citrate. In the case of isoeugenol oxidation, the addition of the iron oxide obtained from iron(III) nitrate drove to the highest positive impact in the conversion (more than 80%) regardless of the calcination temperature. As can be seen in Figure 5A, the optimum value of activity was reached using the 40% FeMagN at 400 °C sample. On the other hand, significantly lower conversion values were obtained using ammonium iron(III) citrate as an iron source (~40%). Focusing on selectivity, higher selectivity toward the desired vanillin product was detected for the series FeMagN which confirms the advantages of the use of nitrate instead of the other inorganic salt (Figure 5A). Note that selectivity to vanillin is higher than 70% for the catalyst 30$ MagN at 300 °C and higher than 50% for all samples prepared from nitrate, being higher than previously reported for Fe-containing samples and similar SBA-15-based samples (see Table S2, Supplementary Materials) [19,20]. Diphenylether was the other dominant product of this reaction from which a carbon balance above 95% was obtained for all runs. As presented in Figure 5B, rather similar behavior in terms of activity as a function of the iron precursor was obtained during the vanillyl alcohol oxidation. In this case, full selectivity to vanillin was achieved. Catalysts obtained from nitrate salt showed conversions greater than 99% in the reaction while a worsening of activity was detected using citrate. In addition, calcination temperature modulated the catalytic response of the solid, causing more activity at higher calcination temperature, which does not seem related to the crystallinity of samples (Figure 1). No easy comparison between sample obtained using nitrate or citrate was possible. We, however, previously demonstrated by ^{27}Al NMR that Al-SBA-15 suffers a considerable transformation in contact with Fe_2O_3 entities, which clearly indicates a strong interaction between Fe and Al elements

[52]. In fact, the enhancement of surface acidities presented in Table 3 for Fe-containing samples, measured using pyridine and 2,6-dimethylpyridine, could be associated with Al–Fe interaction. Note that a siliceous sample (Si-SBA-15) did not show measurable acidity properties. Just as important, higher Lewis acidity was obtained when iron nitrate was used as an iron source (while both catalysts synthesized, 40% FeMagN at 400 °C and 40% FeMagN at 400 °C, presented similar Brønsted acid sites), which would favor an enhanced activity.

Table 3. Surface acidity measured at 300 °C as μmol adsorbed of pyridine (PY) or 2,6-dimethylpyridine (DMPY) per gram of sample.

Sample	Surface acidity at 300 °C/μmol·g^{-1}	
	PY (Total acidity)	DMPY (Brønsted acidity)
Si-SBA-15	-	-
Al-SBA-15	82	61
40% FeMagN at 400 °C	290	143
40% FeMagC at 400 °C	155	164

In fact, Al/Fe reduces the binding energy of the Fe–O bond, which, as demonstrated [53], generates more flexible lattice oxygen and reactivity during oxidation reactions [52]. To further analyze the activity of the samples and its relationship with the iron precursor, differences of Fe/Si bulk and superficial ratios can be compared. Data presented in Table 2 clearly describe a correlation in the behavior of the activity (see activity data for 40% FeMagC at 400 °C and 40% FeMagN at 400 °C in Figures 5A,B) and superficial iron entities exposed (measured as Fe/Si ratio obtained by XPS) for the catalytic process using the 40% FeMagC at 400 °C and 40% FeMagN at 400 °C samples. This means that, although the use of nitrate instead of citrate seems to produce slightly better interaction with the porous structure of the Al-SBA-15, these differences cannot be considered significant (see Tables 1 and 2). On the other hand, the Fe/Si ratio obtained by XPS indicates a significant increase of the superficial concentration of iron oxide of the nitrate series in comparison with samples obtained from citrate, which, according to activity data of Figure 4, would define the differences between both groups of catalysts (FeMagN vs. FeMagC).

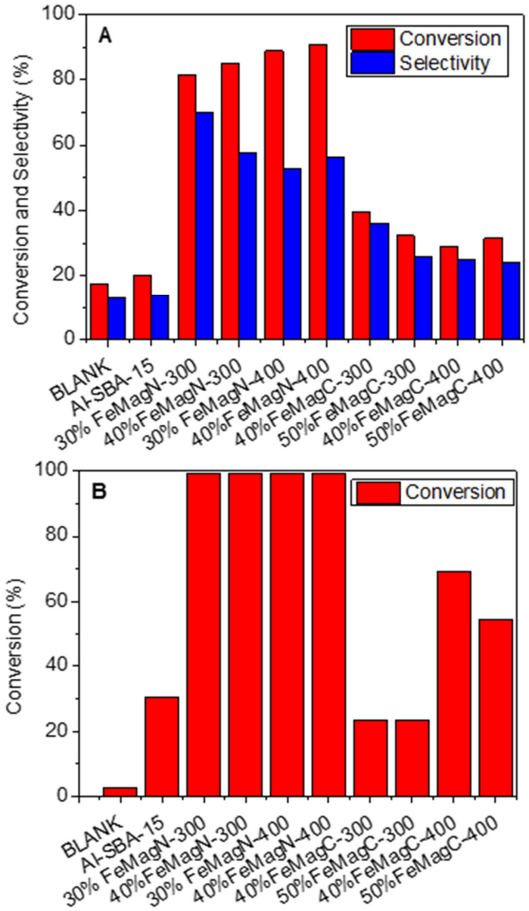

Figure 5. Catalytic conversion and vanillin selectivity (for isoeugenol reaction) for both oxidation reactions at 25 °C, 1 atm. (**A**) Oxidation of isoeugenol at 24 h; (**B**) oxidation of vanillyl alcohol at 20 min. The blank was measured after 2 h of reaction.

A reusability study of representative samples suggested a relatively high stability of the synthesized catalysts obtained by mechanochemistry. These measurements were performed employing one of the most active catalytic systems, namely 30% FeMagN at 400 °C (Figures 6A, B) and cycles of 24 h and 20 min for isoeugenol and vanillyl alcohol, respectively. For the isoeugenol oxidation reaction (Figure 6A), after a decrease of the activity (from 77% to 53% conversion), the catalytic properties remained essentially unchanged. As shown in Figure 6A, after the first cycle (24 h of reaction), approximately 25% conversion was lost. However, a reactivation of the activity can be easily obtained by calcinating the catalyst at 400 °C. A very similar conversion and selectivity, in comparison with the first use of the catalyst, was obtained after the calcination treatment (80% and

60% conversion and selectivity to vanillin, respectively), suggesting that deactivation of the sample was not due to potential iron-oxide leaching, but to the presence of poisoning surface compounds, which is a common phenomenon under batch conditions and long reaction times. Furthermore, much less catalytic deactivation was observed during the oxidation of vanillyl alcohol under the used experimental conditions (Figure 6B, see caption for details), which can also be understood taking into account that significantly shorter reaction times were used. Similarly, a simple calcination post-treatment (400 °C) was demonstrated to be an effective process to reactivate the catalyst (Figure 6B).

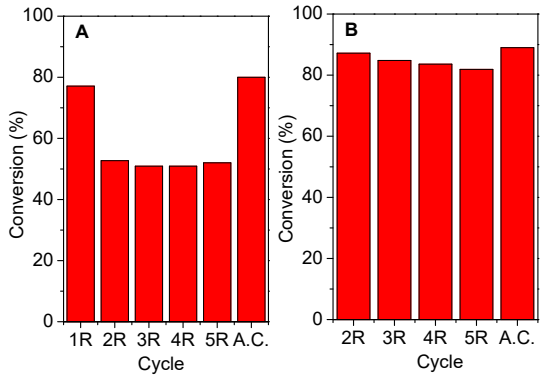

Figure 6. Reuses of the 30% FeMagN at 400 °C for both oxidation reactions at 25 °C, 1 atm. (**A**) Oxidation of isoeugenol; each cycle was 24 h of reaction; (**B**) oxidation of vanillyl alcohol; each cycle was 20 min of reaction. A.C.: reused catalyst after calcination.

3. Materials and Methods

3.1. Synthesis of Al-SBA-15

The preparation of the mesoporous aluminosilicate (Al-SBA-15, molar ratio Si/Al = 20) was carried out according to a procedure reported by Stucky et al. [42]. In particular, Pluronic, P123 triblock copolymer, Sigma-Aldrich, Madrid, Spain (20.6 g) was dissolved in 750 mL of HCl (Panreac, Barcelona, Spain) solution (0.2 M, pH = 1.5), by stirring at 40 °C for 2 h. Tetraethyl orthosilicate (TEOS), Sigma-Aldrich, Madrid, Spain (25 mmol) and aluminum isopropoxide, Sigma-Aldrich, Madrid, Spain (10 mmol) were then added to the mixture and further stirred for 24 h at 40 °C. Subsequently, the solution was transferred to a 100-mL autoclave at 100 °C for 24 h. The obtained material was filtered, dried at 60 °C, and finally calcined at 600 °C for 2 h.

3.2. Synthesis of Catalysts

The synthesis of the nanocatalysts was carried out by means of a mechanochemical milling process using Al-SBA-15 as the support, biomass (a lignocellulosic-derived residue) as the carbon source, and different iron precursors (ammonium iron(III) citrate (Sigma-Aldrich, Madrid, Spain), iron(III) nitrate (Sigma-Aldrich, Madrid, Spain), iron(III) perchlorate hydrate (Panreac, Barcelona, Spain), and iron(III) chloride, (Sigma-Aldrich, Madrid, Spain). For the catalyst preparation, Al-SBA-15 support (2 g) and organic waste (1 g) were introduced into the planetary ball mill jar, where the different iron salts used in percentages by weight of 10, 20, 30, 40, and 50 were introduced. The synthesis mixture was ground for 10 min at 350 rpm using 18 stainless-steel balls of 10 mm × 1 cm. The material obtained after the grinding process was calcined at three different temperatures, namely

300, 400, and 500 °C. The nanomaterials obtained were denoted as X-FeMagY-Z, where X = theoretical content by weight of iron present, Y = iron precursor salt (C = ammonium iron(III) citrate, N = iron(III) nitrate, P = iron(III) perchlorate hydrate, and Cl = iron(III) chloride), and Z = calcination temperature.

3.3. Characterization Techniques

Nanocatalysts were characterized by several techniques, including X-ray diffraction (XRD), X-ray photoelectron spectroscopy (XPS), scanning electron microscopy with energy-dispersive X-ray spectroscopy (SEM-EDX), transmission electron microscopy (TEM), and N_2 physisorption. Additionally, magnetic susceptibility values were additionally determined, in order to confirm the magnetic properties of the prepared materials. X-ray diffraction analysis was carried out on a Bruker D8-Advanced Diffractometer (40 kV, 40 mA) with a Cu X-ray tube (λ = 0.15406) and a goniometer Bragg Bretano θ/θ (Bruker AXS, Karlsruhe, Germany). XRD patterns were acquired in a 10–80° range, at a step size of 0.02° with a counting time per step of 20 s. XPS experiments were carried out in an ultra-high vacuum (UHV) multipurpose surface analysis system Specs™, equipped with the Phoibos 150-MCD energy detector (Berlin, Germany). The sample was previously evacuated overnight under vacuum ($<10^{-6}$ torr). The measurement was accomplished at pressures $<10^{-10}$ mbar, employing a conventional X-ray source (XR-50, Specs (Berlin, Germany), Mg-Kα, hv = 1253.6 eV, 1 eV = 1.603×10^{-19} J) in a "stop and go" mode. The XPS CASA program (Casa Software Ltd., Cheshire, UK) was used to obtain the deconvolution of the curves and the element quantification. TEM micrographs were acquired in a FEI Tecnai G2 system, equipped with a charge-coupled device (CCD) camera. Samples were previously suspended in ethanol and subsequently deposited on a copper grid. Element quantification of the catalysts was obtained using a JEOL JSM 7800F (JEOL Ltd., Akishima, Tokyo, Japan) scanning electron microscope equipped with an Inca Energy 250 microanalysis system, Si/Li type window detector (ATW2), detection range from boron to uranium, and resolution of 137 eV to 5.9 keV. The adsorption/desorption isotherms of N_2 were determined in the Micromeritics automatic analyzer ASAP 2000 (Micromeritics Instrument Corp., Norcross, GA, USA). at −196 °C. Samples were previously degassed overnight at 130 °C under vacuum ($P < 10^{-2}$ Pa). The linear determination of the BET equation was carried out to obtain specific surface areas. Magnetic susceptibility of samples was determined by using a MS2 magnetic susceptibiliser, (Bartington Instruments Ltd., Witney, UK), at room temperature using the dual frequency MS2B (Bartington Instruments Ltd., Witney, UK) laboratory sensor (470 and 4700 Hz). Surface acidity of the samples was measured using pyridine (PY) and 2,6-dimethylpyridine (DMPY) as titrant bases, since they are essentially adsorbed on both types of acidic sites, Brønsted and Lewis and Brønsted acid sites, respectively, at 250 °C (50 °C below the calcination temperature during the synthesis of the samples). The pulses were carried out by means of a microinjector, in the catalytic bed, from a cyclohexane solution of the titrant (0.989 M PY and 0.956 M DMPY). The catalyst was standardized at each titration in a dehydrated and deoxygenated nitrogen flow (50 mL·min^{-1}) (99.999% purity) at 250 °C. The catalyst used (~0.03 g) was fixed by means of Pyrex glass wool stoppers, inside a stainless-steel tubular microreactor of 4 mm internal diameter. The injected base was analyzed by gas chromatography with a flame ionization detector (FID), using an analytical column 0.5 m in length, containing 5% by weight of polyphenylether in Chromosorb AW-MCS 80/100 (Supelco Analytical, Bellefonte, PA, USA).

3.4. Catalytic Activity

The production of vanillin was carried out by conventional heating using isoeugenol and vanillyl alcohol as reagents. The selective oxidative cleavage of isoeugenol to vanillin was carried out using a multiple parallel reaction system (Carrusel Reaction Station™, Radleys Discovery Technologies Ltd., Saffron Walden, United Kingdom) at 25 °C, employing isoeugenol (0.8 g, 5 mmol), 33% hydrogen peroxide (1.2 mL, 11.7 mmol) as an oxidant agent, acetonitrile as a solvent (8 mL, 153 mmol), and 10 mol.% catalyst. In addition, oxidation of vanillyl alcohol to vanillin was carried out, using vanillyl alcohol (0.8 g, 5 mmol), hydrogen peroxide, 30 wt.% in water (1.2 mL, 11.7 mmol), acetonitrile (8 mL, 153 mmol), and 10 mol.% catalyst.

The progress of the reaction was evaluated by gas chromatography (GC) employing an Agilent Technologies 7890 A GC System (Madrid, Spain) equipped with a Petrocol™ DH column (100m×0.25mm×0.50 μm) and a flame ionization detector (FID).

4. Conclusions

A simple and reproducible process for the synthesis of iron nanoparticles deposited on Al-SBA-15 using biomass waste was developed. The nanomaterials possess suitable structural and textural properties for their subsequent use as catalysts, as well as magnetic properties that allow easy separation from the reaction media. The catalytic performance of such noncatalytic systems shows promising results for the selective production of vanillin toward isoeugenol and vanillyl alcohol oxidation at room temperature in conventional liquid phase. Conversions in the range of 80% to 90% molar, with selectivities ≥50% molar were achieved. Results suggested that the Al–Fe interaction and the subsequent enhancement of Lewis acid sites, as well as more iron-oxide species superficially available for the oxidation process, are the most important factors to obtain high activity and vanillin selectivity using the nitrate salt.

Acknowledgments: The authors gratefully acknowledge support from MINECO under project CTQ2016-78289-P, co-financed with FEDER funds. Mario J. Munoz-Batista gratefully acknowledges MINECO for a JdC contract (Ref. FJCI-2016-29014). This publication was prepared with support from RUDN University Program 5-100.

Funding: This research was funded by MINECO, CTQ2016-78289-P, FJCI-2016-29014 and RUDN University Program 5-100.

Conflicts of Interest: The authors declare no conflict of interest.

References

1. Sang, W.; Bai, F. Vascular diversity patterns of forest ecosystem before and after a 43-year interval under changing climate conditions in the Changbaishan Nature Reserve, northeastern China. In *Forest Ecology*; Springer: Berlin, Germany, 2008; Volume 201, pp. 115–130.
2. Clark, J.H.; Luque, R.; Matharu, A.S. Green chemistry, biofuels, and biorefinery. *Annu. Rev. Chem. Biomol. Eng.* **2012**, *3*, 183–207.
3. Liao, S.; Wang, F.; Wu, T.; Pan, W. Crude oil price decision under considering emergency and release of strategic petroleum reserves. *Energy* **2016**, *102*, 436–443.
4. Tuck, C.O.; Pérez, E.; Horváth, I.T.; Sheldon, R.A.; Poliakoff, M. Valorization of biomass: Deriving more value from waste. *Science* **2012**, *337*, 695–699.
5. Ragauskas, A.J.; Beckham, G.T.; Biddy, M.J.; Chandra, R.; Chen, F.; Davis, M.F.; Davison, B.H.; Dixon, R.A.; Gilna, P.; Keller, M. Lignin valorization: Improving lignin processing in the biorefinery. *Science* **2014**, *344*, 1246843.
6. Corma, A.; Iborra, S.; Velty, A. Chemical routes for the transformation of biomass into chemicals. *Chem. Rev.* **2007**, *107*, 2411–2502.
7. Ragauskas, A.J.; Williams, C.K.; Davison, B.H.; Britovsek, G.; Cairney, J.; Eckert, C.A.; Frederick, W.J.; Hallett, J.P.; Leak, D.J.; Liotta, C.L. The path forward for biofuels and biomaterials. *Science* **2006**, *311*, 484–489.
8. Stöcker, M. Biofuels and biomass to liquid fuels in the biorefinery: Catalytic conversion of lignocellulosic biomass using porous materials. *Angew. Chem. Int. Ed.* **2008**, *47*, 9200–9211.
9. Filiciotto, L.; Luque, R. Biomass Promises: A Bumpy Road to a Renewable Economy. *Curr. Green Chem.* **2018**, *5*, 47–59.
10. Rodríguez-Padrón, D.; Puente-Santiago, A.R.; Balu, A.M.; Muñoz-Batista, M.J.; Luque, R. Environmental Catalysis: Present and Future. *ChemCatChem* **2018**, *11*, 18–38.
11. Polshettiwar, V.; Varma, R.S. Green chemistry by nano-catalysis. *Green Chem.* **2010**, *12*, 743–754.
12. Franco, A.; De, S.; Balu, A.M.; Romero, A.A.; Luque, R. Selective oxidation of isoeugenol to vanillin over mechanochemically synthesized aluminosilicate supported transition metal catalysts. *ChemistrySelect* **2017**, *2*, 9546–9551.
13. Filiciotto, L.; Balu, A.M.; Romero, A.A.; Rodríguez-Castellón, E.; van der Waal, J.C.; Luque, R. Benign by design preparation of humin-based iron oxide catalytic nanocomposites. *Green Chem.* **2017**, *19*, 4423–4434.

14. Chen, C.L.; Chang, H.M.; Kirk, T.K. Aromatic acids produced during degradation of lignin in spruce wood by Phanerochaete chrysosporium. *Holzforsch. Int. J. Biol. Chem. Phys. Technol. Wood* **1982**, *36*, 3–9.
15. Gallage, N.J.; Møller, B.L. Vanillin–bioconversion and bioengineering of the most popular plant flavor and its de novo biosynthesis in the vanilla orchid. *Mol. Plant* **2015**, *8*, 40–57.
16. Lampman, G.M.; Sharpe, S.D. A phase transfer catalyzed permanganate oxidation: Preparation of vanillin from isoeugenol acetate. *J. Chem. Educ.* **1983**, *60*, 503.
17. Márquez-Medina, M.D.; Prinsen, P.; Li, H.; Shih, K.; Romero, A.A.; Luque, R. Continuous-Flow Synthesis of Supported Magnetic Iron Oxide Nanoparticles for Efficient Isoeugenol Conversion into Vanillin. *ChemSusChem* **2018**, *11*, 389–396.
18. Geng, L.; Zheng, B.; Wang, X.; Zhang, W.; Wu, S.; Jia, M.; Yan, W.; Liu, G. Fe_3O_4 nanoparticles anchored on carbon serve the dual role of catalyst and magnetically recoverable entity in the aerobic oxidation of alcohols. *ChemCatChem* **2016**, *8*, 805–811.
19. Saberi, F.; Rodríguez-Padrón, D.; Doustkhah, E.; Ostovar, S.; Franco, A.; Shaterian, H.R.; Luque, R. Mechanochemically modified aluminosilicates for efficient oxidation of vanillyl alcohol. *Catal. Commun.* **2019**, *118*, 65–69.
20. Saberi, F.; Rodriguez-Padrón, D.; Garcia, A.; Shaterian, H.R.; Luque, R. Unprecedented Proline-Based Heterogeneous Organocatalyst for Selective Production of Vanillin. *Catalysts* **2018**, *8*, 167.
21. Fache, M.; Boutevin, B.; Caillol, S. Vanillin production from lignin and its use as a renewable chemical. *ACS Sustain. Chem. Eng.* **2015**, *4*, 35–46.
22. Zhang, K.; Hong, K.; Suh, J.M.; Lee, T.H.; Kwon, O.; Shokouhimehr, M.; Jang, H.W. Facile synthesis of monodispersed Pd nanocatalysts decorated on graphene oxide for reduction of nitroaromatics in aqueous solution. *Res. Chem. Intermed.* **2019**, *45*, 599–611.
23. Zhang, K.; Suh, J.M.; Choi, J.W.; Jang, H.W.; Shokouhimehr, M.; Varma, R.S. Recent Advances in the Nanocatalyst-Assisted NaBH4 Reduction of Nitroaromatics in Water. *ACS Omega* **2019**, *4*, 483–495.
24. Lu, F.; Ruiz, J.; Astruc, D. Palladium-dodecanethiolate nanoparticles as stable and recyclable catalysts for the Suzuki-Miyaura reaction of aryl halides under ambient conditions. *Tetrahedron Lett.* **2004**, *45*, 9443–9445.
25. Astruc, D. *Transition-Metal Nanoparticles in Catalysis: From Historical Background to the State of the Art*; Wiley-VCH Verlag Gmbh & Co.: Weinheim, Germany, 2008, Volume 1, pp. 1–48.
26. Shokouhimehr, M.; Shin, K.-Y.; Lee, J.S.; Hackett, M.J.; Jun, S.W.; Oh, M.H.; Jang, J.; Hyeon, T. Magnetically recyclable core–shell nanocatalysts for efficient heterogeneous oxidation of alcohols. *J. Mater. Chem. A* **2014**, *2*, 7593–7599.
27. Alamgholiloo, H.; Zhang, S.; Ahadi, A.; Rostamnia, S.; Banaei, R.; Li, Z.; Liu, X.; Shokouhimehr, M. Synthesis of bimetallic 4-PySI-Pd@ Cu (BDC) via open metal site Cu-MOF: Effect of metal and support of Pd@ Cu-MOFs in H2 generation from formic acid. *Mol. Catal.* **2019**, *467*, 30–37.
28. Iranmanesh, M.; Hulliger, J. Magnetic separation: Its application in mining, waste purification, medicine, biochemistry and chemistry. *Chem. Soc. Rev.* **2017**, *46*, 5925–5934.
29. Kainz, Q.M.; Reiser, O. Polymer and dendrimer coated magnetic nanoparticles as versatile supports for catalysts, scavengers, and reagents. *Acc. Chem. Res.* **2014**, *47*, 667–677.
30. Shokouhimehr, M. Magnetically separable and sustainable nanostructured catalysts for heterogeneous reduction of nitroaromatics. *Catalysts* **2015**, *5*, 534–560.
31. Choi, K.H.; Shokouhimehr, M.; Sung, Y.E. Heterogeneous Suzuki cross-coupling reaction catalyzed by magnetically recyclable nanocatalyst. *Bull. Korean Chem. Soc.* **2013**, *34*, 1477–1480.
32. Jun, S.W.; Shokouhimehr, M.; Lee, D.J.; Jang, Y.; Park, J.; Hyeon, T. One-pot synthesis of magnetically recyclable mesoporous silica supported acid–base catalysts for tandem reactions. *Chem. Commun.* **2013**, *49*, 7821–7823.
33. Shokouhimehr, M.; Lee, J.E.; Han, S.I.; Hyeon, T. Magnetically recyclable hollow nanocomposite catalysts for heterogeneous reduction of nitroarenes and Suzuki reactions. *Chem. Commun.* **2013**, *49*, 4779–4781.
34. Rafiaei, S.M.; Kim, A.; Shokouhimehr, M. Gadolinium triflate immobilized on magnetic nanocomposites as recyclable Lewis acid catalyst for acetylation of phenols. *Nanosci. Nanotechnol. Lett.* **2014**, *6*, 309–313.
35. Rodríguez-Padrón, D.; Balu, A.M.; Romero, A.A.; Luque, R. New bio-nanocomposites based on iron oxides and polysaccharides applied to oxidation and alkylation reactions. *Beilstein J. Org. Chem.* **2017**, *13*, 1982.
36. Shokouhimehr, M.; Hong, K.; Lee, T.H.; Moon, C.W.; Hong, S.P.; Zhang, K.; Suh, J.M.; Choi, K.S.; Varma, R.S.; Jang, H.W. Magnetically retrievable nanocomposite adorned with Pd nanocatalysts: Efficient reduction of nitroaromatics in aqueous media. *Green Chem.* **2018**, *20*, 3809–3817.

37. Muñoz-Batista, M.J.; Rodríguez-Padrón, D.; Puente-Santiago, A.R.; Luque, R. Mechanochemistry: Toward sustainable design of advanced nanomaterials for electrochemical energy storage and catalytic applications. *ACS Sustain. Chem. Eng.* **2018**, *6*, 9530–9544.
38. Ouyang, W.; Yépez, A.; Romero, A.A.; Luque, R. Towards industrial furfural conversion: Selectivity and stability of palladium and platinum catalysts under continuous flow regime. *Catal. Today* **2018**, *308*, 32–37.
39. Pineda, A.; Balu, A.M.; Campelo, J.M.; Romero, A.A.; Carmona, D.; Balas, F.; Santamaria, J.; Luque, R. A Dry Milling Approach for the Synthesis of Highly Active Nanoparticles Supported on Porous Materials. *ChemSusChem* **2011**, *4*, 1561–1565.
40. Linares, N.; Silvestre-Albero, A.M.; Serrano, E.; Silvestre-Albero, J.; García-Martínez, J. Mesoporous materials for clean energy technologies. *Chem. Soc. Rev.* **2014**, *43*, 7681–7717.
41. Shokouhimehr, M.; Asl, M.S.; Mazinani, B. Modulated large-pore mesoporous silica as an efficient base catalyst for the Henry reaction. *Res. Chem. Intermed.* **2018**, *44*, 1617–1626.
42. Zhao, D.; Feng, J.; Huo, Q.; Melosh, N.; Fredrickson, G.H.; Chmelka, B.F.; Stucky, G.D. Triblock copolymer syntheses of mesoporous silica with periodic 50 to 300 angstrom pores. *Science* **1998**, *279*, 548–552.
43. Peters, C.; Dekkers, M.J. Selected room temperature magnetic parameters as a function of mineralogy, concentration and grain size. *Phys. Chem. Earth Parts A/B/C* **2003**, *28*, 659–667.
44. Jia, C.; Sun, L.; Yan, Z.; You, L.; Luo, F.; Han, X.; Pang, Y.; Zhang, Z.; Yan, C. Single-crystalline iron oxide nanotubes. *Angew. Chem.* **2005**, *117*, 4402–4407.
45. Park, J.; Lee, E.; Hwang, N.; Kang, M.; Kim, S.C.; Hwang, Y.; Park, J.; Noh, H.; Kim, J.; Park, J. One nanometer scale size controlled synthesis of monodisperse magnetic Iron oxide nanoparticles. *Angew. Chem.* **2005**, *117*, 2932–2937.
46. Gregg, S.J.; Sing, K.S.W. *A Surface Area and Porosity*; Academic Press: Cambridge, MA, USA, 1982.
47. Rajabi, F.; Fayyaz, F.; Luque, R. Cytosine-functionalized SBA-15 mesoporous nanomaterials: Synthesis, characterization and catalytic applications. *Microporous Mesoporous Mater.* **2017**, *253*, 64–70.
48. Yépez, A.; De, S.; Climent, M.S.; Romero, A.A.; Luque, R. Microwave-assisted conversion of levulinic acid to γ-valerolactone using low-loaded supported iron oxide nanoparticles on porous silicates. *Appl. Sci.* **2015**, *5*, 532–543.
49. Wagner, C.D.; Riggs, W.M.; Davis, L.E.; Moulder, J.F. *Handbook of X-ray Photoemission Spectra*; Perkin-Elmer: Waltham, MA, USA, 1976.
50. Rodríguez-Padrón, D.; Puente-Santiago, A.R.; Caballero, A.; Balu, A.M.; Romero, A.A.; Luque, R. Highly efficient direct oxygen electro-reduction by partially unfolded laccases immobilized on waste-derived magnetically separable nanoparticles. *Nanoscale* **2018**, *10*, 3961–3968.
51. Rodríguez-Padrón, D.; Puente-Santiago, A.R.; Balu, A.M.; Romero, A.A.; Luque, R. Solventless mechanochemical preparation of novel magnetic bioconjugates. *Chem. Commun.* **2017**, *53*, 7635–7637.
52. Balu, A.M.; Pineda, A.; Yoshida, K.; Campelo, M.; Gai, P.L.; Angel, A. Fe/Al synergy in Fe_2O_3 nanoparticles supported on porous aluminosilicate materials : Excelling activities in oxidation reactions. *Chem. Commun.* **2010**, *46*, 7825–7827.
53. Mounzer, H. Heterogeneous Oxidation of Alcohols. Ph.D. Thesis, University of Birmingham, Birmingham, UK, 2009.

Supporting Information

Mechanochemically synthesized supported magnetic Fe-nanoparticles as catalysts for efficient vanillin production

María Dolores Márquez-Medina,[a] Daily Rodríguez-Padrón,[a] Alina M. Balu,[a] Antonio A. Romero,[a] Mario J. Muñoz-Batista,[a]* Rafael Luque[a,b]*

[a]Departamento de Química Orgánica, Universidad de Córdoba, Campus de Rabanales, Edificio Marie Curie (C-3), Ctra Nnal IV-A, Km 396, E14014, Cordoba, Spain. M.J.M-B qo2mubam@uco.es, R.L. rafael.luque@uco.es

[b]Scientific Center for Molecular Design and Synthesis of Innovative Compounds for the Medical Industry, People´s Friendship University of Russia (RUDN University), 6 Miklukho-Maklaya str., 117198 Moscow, Russia.

Table S1. Sumary of sinthesized samples and magnetic susceptibility measurments.

Catalyst	Precursor	Fe wt % (theorical)	Calcination Temperature (ºC)	Magnetic Susceptibility ($m^3\ K\ g^{-1}$)
10% FeMagC-300	ammonium iron (III) citrate	10	300	-
20% FeMagC-300		20		$52.0 \cdot 10^{-6}$
30% FeMagC-300		30		$85.6 \cdot 10^{-6}$
40% FeMagC-300		40		$116.5 \cdot 10^{-6}$
50% FeMagC-300		50		$135.0 \cdot 10^{-6}$
10% FeMagC-400		10	400	-
20% FeMagC-400		20		$63.3 \cdot 10^{-6}$
30% FeMagC-400		30		$96.1 \cdot 10^{-6}$
40% FeMagC-400		40		$140.1 \cdot 10^{-6}$
50% FeMagC-400		50		$186.1 \cdot 10^{-6}$
10% FeMagC-500		10	500	-
20% FeMagC-500		20		$31.2 \cdot 10^{-6}$
30% FeMagC-500		30		$50.0 \cdot 10^{-6}$
40% FeMagC-500		40		$97.2 \cdot 10^{-6}$
50% FeMagC-500		50		$135.4 \cdot 10^{-6}$
10% FeMagN-300		10	300	-
20% FeMagN-300		20		$55.2 \cdot 10^{-6}$

30% FeMagN-300	iron (III) nitrate	30		$152.0 \cdot 10^{-6}$
40% FeMagN-300		40		$233.2 \cdot 10^{-6}$
50% FeMagN-300		50		-
10% FeMagN-400		10	400	-
20% FeMagN-400		20		$68.6 \cdot 10^{-6}$
30% FeMagN-400		30		$164.3 \cdot 10^{-6}$
40% FeMagN-400		40		$271.6 \cdot 10^{-6}$
50% FeMagN-400		50		-
10% FeMagN-500		10	500	-
20% FeMagN-500		20		-
30% FeMagN-500		30		$178.9 \cdot 10^{-6}$
40% FeMagN-500		40		$254.5 \cdot 10^{-6}$
50% FeMagP-500		50		-
10% FeMagP-300	iron (III) perchlorate hydrate	10	300	-
20% FeMagP-300		20		-
30% FeMagP-300		30		-
40% FeMagP-300		40		-
50% FeMagP-300		50		-
10% FeMagP-400		10	400	-
20% FeMagP-400		20		-
30% FeMagP-400		30		-
40% FeMagP-400		40		-
50% FeMagP-400		50		-
10% FeMagP-500		10	500	-
20% FeMagP-500		20		-
30% FeMagP-500		30		-
40% FeMagP-500		40		-
50% FeMagP-500		50		-
10% FeMagCl-300	iron (III) chloride	10	300	-
20% FeMagCl-300		20		-
30% FeMagCl-300		30		-
40% FeMagCl-300		40		-
50% FeMagCl-300		50		-
10% FeMagCl-400		10	400	-
20% FeMagCl-400		20		-
30% FeMagCl-400		30		-
40% FeMagCl-400		40		-
50% FeMagCl-400		50		-
10% FeMagCl-500		10	500	-
20% FeMagCl-500		20		-
30% FeMagCl-500		30		-
40% FeMagCl-500		40		-
50% FeMagCl-500		50		-

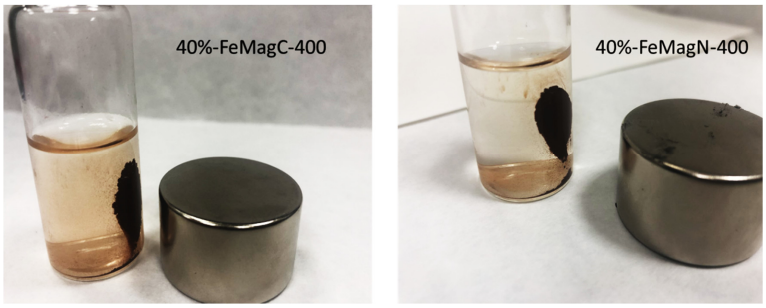

Figure S1. Magnetic separation of synthesized samples dispersed in the reaction media.

Table S2. Catalytic properties and reaction temperature of Fe-containing catalysts during isoeugenol and vanillin alchool oxidation reactions.

Sample	Conversion (%) isoeugenol oxidation/ Selectivity %	Conversion (%) vanillin alchool oxidation/ Selectivity (%)	Temperature (ºC)	Ref.
FeMagN-400	94/56	99/99	25	This work
Fe-Al-SBA-15	90/55	n.m.	90	12
Fe-Humins	91/63	n.m.	150	13
Fe-Graphene	62/52	n.m.	90	54
Fe-Al-SBA-15[a]	n.m.	63/99	25	19
Fe-Al-SBA-15[a]	n.m.	99/99	50	19

[a] Same synthetic protocol using propionic acid. n.m denote not measured.

Title: Post-synthetic mechanochemical incorporation of Al-species into the framework of porous materials: towards more sustainable redox chemistries

Author: M Dolores Marquez-Medina, Sareena Mhadmhan, Alina Mariana Balu, et al

Publication: ACS Sustainable Chemistry & Engineering

Publisher: American Chemical Society

Date: Apr 1, 2019

Logged in as:
María Dolores Márquez-Medina
Universidad de Córdoba
Account #: 3001400331

LOGOUT

PERMISSION/LICENSE IS GRANTED FOR YOUR ORDER AT NO CHARGE

This type of permission/license, instead of the standard Terms & Conditions, is sent to you because no fee is being charged for your order. Please note the following:

- Permission is granted for your request in both print and electronic formats, and translations.
- If figures and/or tables were requested, they may be adapted or used in part.
- Please print this page for your records and send a copy of it to your publisher/graduate school.
- Appropriate credit for the requested material should be given as follows: "Reprinted (adapted) with permission from (COMPLETE REFERENCE CITATION). Copyright (YEAR) American Chemical Society." Insert appropriate information in place of the capitalized words.
- One-time permission is granted only for the use specified in your request. No additional uses are granted (such as derivative works or other editions). For any other uses, please submit a new request.

BACK CLOSE WINDOW

Article

Post-synthetic mechanochemical incorporation of Al-species into the framework of porous materials: towards more sustainable redox chemistries

M Dolores Marquez-Medina, Sareena Mhadmhan, Alina Mariana Balu, Antonio A. Romero, and Rafael Luque

ACS Sustainable Chem. Eng., **Just Accepted Manuscript** • DOI: 10.1021/acssuschemeng.9b00912 • Publication Date (Web): 22 Apr 2019

Post-synthetic mechanochemical incorporation of Al-species into the framework of porous materials: towards more sustainable redox chemistries

*M. Dolores Marquez-Medina[a], Sareena Mhadmhan[a,b], Alina M. Balu[a], Antonio A. Romero[a], Rafael Luque[a,c]**

[a]Departmento de Quimica Organica, Facultad de Ciencias, Universidad de Cordoba, Campus de Rabanales, Edificio Marie Curie (C-3), Ctra Nnal IV-A, Km 396, E14014, Cordoba, Spain

[b]Petrochemistry and Polymer Science, Department of Chemical Technology, Faculty of Science, Chulalongkorn University, 10330, Bangkok, Thailand

[c]Peoples Friendship University of Russia (RUDN University), 6 Miklukho-Maklaya str., 117198, Moscow, Russia

Corresponding Author: q62alsor@uco.es (R. Luque)

KEYWORDS: Mechanochemistry, Mesoporous materials, Aluminium, Framework incorporation, Selective oxidations

ABSTRACT

The mechanochemical incorporation of catalytically active Al species in low loadings was successfully accomplished into the framework of mesoporous silica (SBA-15 and MCM-41) materials using a simple wet milling approach (with aluminum isopropoxide as source of aluminum) and a dry milling approach (using low quantities of Al-containing MOF materials). Characterization data pointed to the successful incorporation of Al species (typically with loadings of ca. 0.2-0.4 wt.%) mostly tetrahedrically coordinated. Despite such extremely low loadings, the isolated aluminum oxide species exhibited promising activities and stability in selective mild oxidations under various conditions (microwave irradiation and mechanochemistry) including the selective oxidation of benzyl alcohol to benzaldehyde, isoeugenol to vanillin and diphenyl sulfide to diphenyl sulfoxide as compared to similarly synthesized impregnated catalysts.

INTRODUCTION

The incorporation of functional and active sites into porous materials for catalytic applications still remains a challenge in the field, particularly aiming to highly active and stable systems at low loadings.[1,2] Conventional methodologies (i.e. impregnation, deposition-precipitation, anchoring/immobilization, etc.) were generally proved to provide active materials but the possibility to control the loading and localization of active sites as well as their stability is often compromised.[3,4] Alternative protocols have paved the way to a more controllable and reproducible materials functionalization.

Mechanochemistry emerged as one of such promising alternative methodologies to provide a simple and rapid but efficient, highly active, stable and reproducible access to advanced functional materials for various applications.[5-7] We have extensively demonstrated that a wide range low loaded highly active supported nanoparticle systems including iron, cobalt, nickel, palladium, ruthenium and various other metal and metal oxides could be designed under wet/dry milling conditions for catalytic applications.[8-10] In these methodologies, metal

precursors (both solid and/or liquid) were ground under optimized conditions towards the generation of mechanochemical nanomaterials. However, the possibility to utilize MOFs in low quantities as seeds to generate active species on porous materials has not been explored to date. In principle, the presence of organic linkers and various metals in MOFs makes them a potentially interesting platform to design homogeneously distributed and most importantly highly isolated nanoparticles (*quasi*-single atom) on various supports.

The selective oxidation of alcohols and sulfides to aldehydes and sulfoxides are among two most relevant chemistries in organic synthesis to provide access to useful compounds with extensive applications in herbicides, pharmaceuticals, fragrances and related industries.[11,12] Such chemistries (e.g. benzyl alcohol oxidation to benzaldehyde; diphenyl sulfide to diphenyl sulfoxide) have been extensively reported using a range of nanoparticle systems (mostly noble metals with only very few examples of transition metals as well as noble metal-containing mesoporous materials).[13-17] However, despite some examples on certain catalytic systems based on cheap and sustainable transition metals (Fe, W, Cu, etc.),[14-17] there are no reports on the utilization of Al-containing mesoporous materials in mild selective oxidations of alcohols or sulfides. Our group just recently reported the first available report on designed hierarchical Al-containing zeolites for mild oxidation reactions,[18] following a simple and environmentally friendly protocol for benzyl alcohol oxidation using alkali-treated ZSM-5 zeolites.[19] The possibility to catalyze redox chemistries using Al-containing materials can be highly attractive as compared to conventional metals, taking into account the environmentally friendly and cheap nature as well as wide availability of Al including in waste (e.g. mining kaolin waste).

Based on these premises, the present contribution reports for the first time that a simple mechanochemical milling step allows the possibility of aluminum incorporation into the

framework of mesoporous silica (SBA-15 and MCM-41) materials even at low loadings, with functionalized materials exhibiting promising catalytic activities with respect to analogous conventionally impregnated materials in the selective oxidations of benzyl alcohol to benzaldehyde, isoeugenol to vanillin and sulfides (diphenyl sulfide) to sulfoxides.

EXPERIMENTAL

Materials synthesis

Two types of mesoporous silica (SBA-15 and MCM-41) were synthesized by using a previously reported literature protocol.[20,21] Al was incorporated into mesoporous silica SBA-15 and MCM-41 by using incipient wetness impregnation and mechanochemical ball milling procedures. The details of the synthesis method were given below.

Incipient wetness impregnation method (I)

Aluminum isopropoxide (Sigma-Aldrich, Madrid, Spain) as source of aluminum (up to 1 wt.% theoretical Al loading) was dissolved in 1 molar ratio of water/ethanol mixture (5 mL). The silica support was then added in the solution under stirring for 2 h. The catalyst was then dried at 100ºC for 24 h and finally calcined at 550ºC for 4 h under air. The catalysts were named as SBA-15-Al-I and MCM-41-Al-I.

Mechanochemical planetary ball milling method (M)

2 g of silica support (SBA-15 or MCM-41) and 1 wt.% of the desired aluminum source (Aluminum isopropoxide; Al or Al-MIL-53 MOF; AlMOF as the Al source) were laid in a 125 mL stainless steel jar from a PM-100 Retsch planetary ball mill containing 18 stainless steel balls (Ø10 mm, 4 g each ball). Al-MIL-53 MOF was synthesized by using a previously reported literature protocol.[22] The planetary ball milling was carried on at 350 rpm for 10 min (optimum mechanochemical conditions).[9,22,23] After that the catalysts were calcined at 550ºC for 4 h under air. The catalysts obtained in this protocol were identified as SBA-15-Al-M, MCM-41-Al-M, SBA-15-AlMOF-M and MCM-41-AlMOF-M respectively.

Characterization

X-Ray Diffraction (XRD) measurements were performed in a Bruker D8 Discover Vario X-ray diffractometer equipped with a Brentano Bragg θ/2θ goniometer to work in reflection mode, a Cu X-ray tube, rotating platform, primary beam monochromator and detector ultra-fast high sensitivity. Diffractometers were collected at the step size of 0.02º and counting per step of 1.2 s, over a 2θ range from 1 to 80º.

Surface area (BET) and pore volume were obtained from the adsorption/desorption isotherms of nitrogen. Nitrogen adsorption measurements were carried out at -196ºC, temperature of the liquid nitrogen, using an automatic analyzer Micromeritics ASAP 2000. The weight of the sample used for the adsorption measurements of N_2 desorption is approximately 0.20 g. Samples were degassed for 24 hours at 100 ° C under vacuum ($P < 10^{-2}$ Pa) and subsequently analyzed. The linear part of the BET equation (relative pressure between 0.05 and 0.30) was used for the determination of the specific surface area. The pore size distribution was

calculated using the adsorption branch of the adsorption-desorption isotherm of N_2, applying the method of Barret, Joyner and Halenda (BJH).

Elemental analysis of the materials was carried out using a JEOL JSM 6300 Scanning Electron Microscope equipped with an Inca Energy 250 microanalysis system, Si/Li type window detector (ATW2), detection range: from boron to uranium, resolution: 137 eV to 5.9 KeV. The software allows the qualitative and semiquantitative analysis, mapping of elements, elementary distribution in a sweep line.

Inductive coupling plasma mass spectrometry technique (ICP-MS) was employed for a quantitative metal analysis of the synthesized nanomaterials, using an Elan DRC-e ICP-MS (PerkinElmer SCIEX) located in the Central Service of Research Support (SCAI).

Magic Angle Spinning (MAS) ^{27}Al solid state NMR experiments of hydrated samples were recorded on a Bruker ACP-400 multinuclear spectrometer at 104.26 MHz. ^{27}Al spectra were recorded at 1 μs pulse with a recycle delay of 0.3 s. The chemical shifts are given in ppm from $Al(H_2O)_6^{3+}$ as external reference as in previous work by the group.[24]

Samples containing silica (~ 25 mg) were previously digested using a mixture of 1:1:1 HF: HNO_3: HCl acids. The solutions were made with milliQ water up to a maximum content of 1% HF, since HF is the only acid that dissolves the silicates and in acid solution has a low boiling point. This makes it easily volatilizable. If digestion becomes open, SiF_4 (boiling point = -86 ° C) can be lost volatilizing during digestion.

The determination of the surface acidity of the different catalysts, pyridine (PY) and 2,6-dimethylpyridine (DMPY) were chosen as titrating bases, since they are essentially adsorbed on both types of acidic centers, Brönsted and Lewis, and on Brönsted acid centers, respectively.

PY, due to its low steric hindrance, is unspecifically adsorbed on both types of centers, whereas DMPY is specifically adsorbed on Brönsted type acid centers, due to the high steric hindrance of the methyl groups.[24] This procedure has been carried out at a temperature of 250 °C (50 °C below the temperature of the final heat treatment in the synthesis of the nanomaterials). The pulses were carried out by means of a microinjector, in the catalytic bed, from a cyclohexane solution of the titrant (0.989 M in PY and 0.956 M in DMPY). The catalyst is standardized at each titration in a dehydrated and deoxygenated nitrogen flow (50 mL min^{-1}) (99.999% purity) at 250 °C. The catalyst used (~ 0.03 g) is fixed by means of Pyrex glass wool stoppers, inside a stainless-steel tubular microreactor of 4 mm internal diameter. The injected base is analyzed by gas chromatography with flame ionization detector (FID), using an analytical column of 0.5 m in length, containing 5% by weight of polyphenylether in Chromosorb AW-MCS 80/100.[24]

Catalytic activity

Selective oxidation of benzyl alcohol to benzaldehyde

Tests carried out were carried out in a focused microwave CEM-Discover monowave model, controlled and monitored by a computer in standard mode ("Discover") under pressure that allows us to control the power of irradiation, temperature and pressure. Typically, 1 mmol of benzyl alcohol (0.2 mL, assay >99%), 2.9 mmol of 30% (w/w) H_2O_2 in H_2O as oxidant (0.3 mL) and 0.35 mol % catalyst (0.05 g) were mixed with 1.25 mmol of acetonitrile as solvent (2 mL) and microwaved for 3 minutes at 90 °C (300 W power). The product was analyzed by using GC-FID equipped with a Supelco 2-8047-U capillary column.

Recycle experiments were carried out under identical conditions unless otherwise stated. After reaction, the catalyst was filtered off, washed with acetonitrile and dried at 100 ºC prior to its reuse in another reaction run.

Regeneration of the spent catalyst was performed by re-calcination after reaction under identical conditions to those employed in their synthesis (550 ºC, air, 4 h).

Oxidation of isoeugenol to vanillin

The reaction was conducted in a microwave CEM-Discover monowave model under identical reaction conditions and similar parameters. Typically, 1.2 mmol of isoeugenol (0.2 mL, assay 98%), 2.9 mmol 30% (w/w) H_2O_2 in H_2O (0.3 mL) and 0.35 mol % of catalyst (0.05 g) in 1.25 mmol acetonitrile (2 mL), at 90 ° C and 300 W for 3 minutes. The products were analyzed by using GC-FID equipped with a capillary column Petrocol 100 x 0.25 nm x 0.5 µm. Recycle experiments were carried out under identical conditions unless otherwise stated. After reaction, the catalyst was filtered off, washed with acetonitrile and dried at 100 ºC prior to its reuse in another reaction run.

Regeneration of the spent catalyst was performed by recalcination after reaction under identical reaction conditions to those employed in their synthesis (500 ºC, air, 4 h).

Mechanochemical oxidation of diphenyl sulfide to diphenyl sulfoxide

The oxidation reaction of diphenyl sulfide was studied under ball milling. In a typical procedure, 0.5 mmol diphenyl sulfide (0.083 mL, assay 98%), 30% (w/w) H_2O_2 in H_2O (8 equiv., 0.4074 mL) and 0.04 mol %, catalyst (0.005 g) were added to a 25 mL jar from a PM-100 Retsch planetary ball mill with eight stainless steel balls (Ø10 nm, 4 g each ball). Then, the mechanochemical reaction was performed at 350 rpm for 25 min. The crude reaction was recovered from the jar by using 0.5 mL toluene. The resulting liquid phase was analyzed by GC-FID equipped with a Supelco 2-8047-U capillary column. All results were finally confirmed by GC-MS. The reaction mixture was carefully analyzed for potential traces of Fe (from the

stainless steel balls), confirming by ICP-MS no measurable Fe quantities (<0.5 ppm) into solution. For the recycling step, the chamber of the ball mill containing the catalyst was dried at 100°C after the liquid phase of the first run was taken from the jar, followed by catalyst recovery and reusing for the next run.

RESULTS AND DISCUSSION

Characterization of the Catalysts

Materials were characterized using different techniques including XRD, N_2 physisorption, SEM and EDX mapping as well as MAS ^{27}Al NMR and surface acid properties based. XRD patterns provided the typical long range hexagonally arrayed mesoporous structure for SBA-15.[25] No cle aterials could be observed from XRD patterns (Figure tity of Al (<1 wt.%) present. Interestingly, MAS ^{27}A of Al environments within the materials.

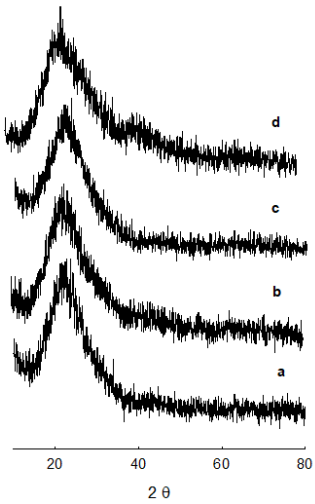

Figure 1. XRD patterns of (a) SBA-15-Al-I, (b) SBA-15-Al-M, (c) SBA-15-AlMOF-M and (d) SBA-15 samples.

Figure 2 depicts the different coordination of Al species within the synthesized materials measured by ^{27}Al MAS NMR spectra of the hydrated samples. A remarkable contribution of tetrahedrically coordinated Al (54.4 ppm) was found in all mechanochemically synthesized materials which correspond to framework Al species in good agreement with previous reports.[24,26] These results indicate that the mechanochemical approach was able to introduce post-synthesis Al species within the SBA-15 framework at low Al loadings, being the first literature report on such post-synthetic framework incorporation.[9] In general, this method can avoid the use of toxic organic solvents that could be released to the environment and increase the effectiveness and reproducibility in materials synthesis (as well as catalytic reactions). Mechanochemistry has become a promising alternative for the synthesis and design of advanced heterogeneous catalysts.[27]

Interestingly, the presence of octahedrically coordinated Al species (ca. 0 ppm, Figure 2) in the materials was rather low after the mechanochemical step as compared for instance with the analogous Al impregnated SBA-15 via wetness impregnation (Figure 2a). Such effect was particularly remarkable for the mechanochemical framework Al incorporation of an Al-containing MOF material (Al-MIL-53) used as aluminium source into the silica SBA-15 (Figure 2c, NMR contribution at 54.4 ppm corresponding to tetrahedrically coordinated Al-ca. 75% from all incorporated Al).

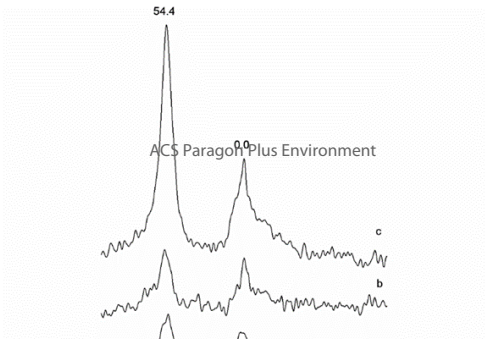

Figure 2. MAS ^{27}Al NMR spectra of (a) SBA-15-Al-I, (b) SBA-15-Al-M and (c) SBA-15-AlMOF-M catalysts.

A similar behavior was observed for the use of MCM-41 as mesoporous support (results not shown). These findings were found to have important consequences in the catalytic activity of Al-containing materials but most importantly provide unambiguous results, for the first time, on the possibility to post-synthetically incorporate catalytically active species within the framework of porous materials via mechanochemistry (even at low loadings) to generate catalytically active materials.

Table 1. Porosity analysis and acidity determination of synthesized materials.

Samples	S_{BET} [a]	D_p [b]	V_p [c]	Al content	Acidity (μmolg^{-1})	
	(m^2g^{-1})	(nm)	(mLg^{-1})	(wt.%)	PY	DMPY
SBA-15	800	7.6	0.8	-	<10	<10
SBA-15-Al-I	739	6.1	0.7	0.25	31	26
SBA-15-Al-M	419	5.9	0.6	0.30	30	18

SBA-15-AlMOF-M	466	5.9	0.7	0.38	22	21
MCM-41-AlMOF-M	456	4.7	0.6	0.40	23	20

[a] S_{BET}: specific surface areas was calculated by the Brunauer-Emmett-Teller (BET) equation.

[b] D_p: mean pore size diameter was calculated by the Barret-Joyner-Halenda (BJH) equation.

[c] V_p: pore volumes were calculated by the Barret-Joyner-Halenda (BJH) equation.

In addition to this, the surface properties of the materials were also characterized using N_2 physisorption, with Al-containing materials preserving most mesoporosity with a reduced surface area and pore diameters as compared to the parent (SBA-15 and MCM-41) as a consequence of the mechanochemical treatment (Table 1, Figure 3). Importantly, pore volumes remained almost unchanged, a clear indication that all changes in textural properties were rather originated by 1) a degradation of the mesoporous structure upon milling and 2) the observed framework Al incorporation in mechanochemically synthesized nanomaterials.

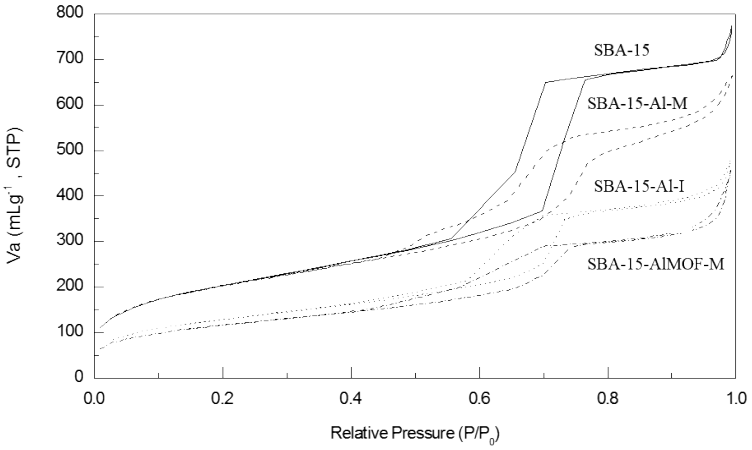

Figure 3. N_2 Physisorption profiles of synthesized materials

Surface acid properties measured by pyridine (PY) and 2,6-dimethylpyridine (DMPY) titration using a previously reported gas-phase approach [24] also pointed out a very mild acidity of the materials that did not appreciably change after the mechanochemical Al incorporation (Table 1). The average Al content measured by EDX and ICP-MS was ca. 0.2-0.4 wt.%, reduced as compared to the theoretical aimed content in the synthesis (1 wt.%, Table 1, contents measured by ICP-MS). Nevertheless, such Al content despite the low acidity was sufficient to improve the catalytic activity of the synthesized materials as compared to purely siliceous SBA-15 as demonstrated in a number of oxidation reactions.

Al-containing materials are generally inactive in redox reactions. However, we recently reported that the presence of isolated Al sites in aluminosilicates (hierarchical zeolites) could lead to promising mild redox activities.[18] Based on these previous results, materials were

subsequently tested in three simple mild oxidations (benzyl alcohol to benzaldehyde, isoeugenol to vanillin and diphenyl sulfide to diphenyl sulfoxide) to further see the influence of the Al content in the synthesized materials.

The activity of Al-containing materials was firstly screened in the microwave assisted oxidation of benzyl alcohol to benzaldehyde (Table 2).

Table 2. Activity of post-synthetically functionalized Al-containing mesoporous silica in the microwave-assisted oxidation of benzyl alcohol to benzaldehyde

Samples	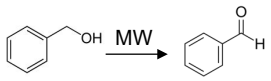 **Conversion (%)**
Blank	<10
SBA-15	10
SBA-15-Al-I	11
SBA-15-Al-M	18
SBA-15-AlMOF-M	20
MCM-41	10
MCM-41-Al-I	7
MCM-41-Al-M	17
MCM-41-AlMOF-M	14

Reaction condition: 1 mmol (0.2 mL) benzyl alcohol, 2.9 mmol (0.3 mL) of 30% (w/w) H_2O_2 in H_2O, 0.35 mol % catalyst, 2 mL acetonitrile, 90ºC (300 W), 3 min reaction.

Blank and reaction runs using mesoporous silica (SBA-15 and MCM-41) provided identical low conversion (<10%) in the selective oxidation of benzyl alcohol under the investigated reaction conditions. These results were also similarly obtained over SBA-15-Al-I and MCM-41-Al-I catalysts (see experimental, Table 2). Remarkably, mechanochemically synthesized Al-containing mesoporous silica provided an interesting increase in conversion

(almost double) despite the extremely low measured Al content in the materials (typically 0.2-0.4 wt.%, almost equal to the impregnated sample) and the short times of reaction (ca. 3 minutes). These results relate to a mechanochemically improved catalytic performance by creating defective sites on the surface as well as the presence of tetrahedrically coordinated Al framework species (as opposed to octahedrically coordinated extraframework species observed in impregnated materials), thus increasing activity.[27] Indeed, it seemed to be sufficient to improve benzyl alcohol conversion in the systems under the investigated reaction conditions. A complete selectivity to benzaldehyde was observed in all cases.

Similarly, the results obtained for all Al-containing materials in the oxidation of isoeugenol to vanillin pointed out to such enhanced catalytic activity for mechanochemically synthesized systems even at low Al loadings (Table 3), over two times as compared to SBA-15 and MCM-41. In this case, not only the conversion but importantly the selectivity to vanillin (even if still low, ca. 15-27%) was remarkably improved for Al-containing mechanochemically synthesized mesoporous silica materials, particularly when AlMOF was employed as source of Al in the mechanochemical synthesis. Mechanochemical materials were also highly stable under the investigated conditions for both reactions, with the possibility to be reused several times (up to five reuses tested in this work for both reactions, see supporting information) without any observable decrease in catalytic activity conversion ca. 17-20 mol%.

Table 3. Comparison of catalytic activity in the microwave-assisted oxidation of isoeugenol

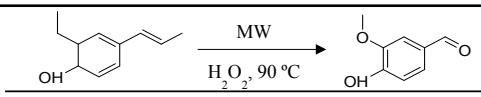

Samples	Conversion (%)	Selectivity (%)	
		Vanillin	Others
Blank	<10	<5	>95
SBA-15	<10	<5	>95
SBA-15-Al-I	18	7	93
SBA-15-Al-M	25	16	84
SBA-15-AlMOF-M	27	27	73
MCM-41	15	8	92
MCM-41-Al-I	17	15	85
MCM-41-Al-M	22	21	79
MCM-41-AlMOF-M	19	27	73

Reaction condition: 1.2 mmol (0.2 mL) isoeugenol, 2.9 mmol (0.3 mL) of 30% (w/w) H_2O_2 in H_2O, 0.35 mol % catalyst, 2 mL acetonitrile, 90ºC (300 W), 3 min reaction.

Only a small decrease was observed in reuses for the isoeugenol to vanillin reaction due to previously reported formation of oligomeric lignin-like compounds that seem to partially block some of the Al active sites.[28] Regeneration of the materials at high temperature (400ºC, for just 2 h under air) restored the initial activity of the Al-containing SBA-15 catalysts to 25-30

mol.%. These findings also further confirmed the stability of the synthesized systems in good agreement with previously reported similar mechanochemically synthesized nanomaterials.[22,28,29]

Additionally, results of the mechanochemically assisted oxidation of diphenyl sulfide have been summarized in Table 4. The catalysts tests were performed at 25 ºC under solvent free condition by using 30% (w/w) H_2O_2 in H_2O hydrogen peroxide as oxidant. As a result, the reaction of both absence catalyst and mesoporous silica SBA-15 exhibited low conversion as compared to Al incorporated mesoporous silica catalysts. Impregnated materials did not provide any improvements in catalytic activity, with values close to those of the blank/purely siliceous materials. Remarkably, mechanochemically synthesized exhibited significantly improved activities (almost double, Table 4). For the catalysts prepared by mechanochemical method, SBA-15-AlMOF-M provided the highest conversion of 39%, being however poorly selective to sulfoxide production (Table 4). Comparatively, a remarkable selectivity (70%) at comparable conversion (37%) was observed for MCM-41-AlMOF-M.

Table 4. Comparison of catalytic activity in the oxidation of diphenyl sulfide under ball milling.

Catalysts	Conversion (%)	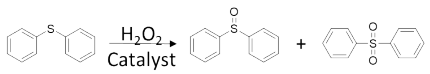	
		Selectivity (%)	
		Diphenyl sulfoxide	Diphenyl sulfone
Blank (no catalyst)	<15	29	71
SBA-15	17	28	72
SBA-15-Al-I	19	38	62
SBA-15-Al-M	35	50	50
SBA-15-AlMOF-M	39	25	75
MCM-41-Al-I	21	57	43
MCM-41-Al-M	33	57	43
MCM-41-AlMOF-M	37	70	30

Reaction condition: 0.5 mmol of diphenyl sulfide (0.083 mL), 8 equiv of 30% (w/w) H_2O_2 in H_2O (0.41 mL), 0.04 mol % catalyst, 25 stainless steel mL jar containing 8 balls (Ø 10 mm, 4 g each ball), 350 rpm, 25 min, ball milling.

The use of an AlMOF as Al source could in principle enhance the dispersion of Al incorporated into the framework of the mesoporous material, as a general improvement was observed for all investigated reactions in mechanochemically synthesized materials employing low quantities of Al-MIL-53 as source of Al. The interestingly observed different selectivity to diphenyl sulfoxide (Table 4) between MCM-41-AlMOF-M and SBA-15-AlMOF-M (70 vs 25%) may be a good indication that MCM-41 with a slightly reduced pore size (ca. 4.7 nm) is an optimum system to avoid overoxidation to the corresponding sulfone taking place on larger modified-SBA-15 pore size catalyst (ca. 5.9 nm), see Table 1.

Based on the observed selectivity, MCM-41-AlMOF-M catalyst was selected to optimize the mechanochemical conditions for the oxidation of diphenyl sulfide. The effect of different amounts of catalyst and hydrogen peroxide were investigated under neat grinding conditions (Table 5). Almost negligible conversion was observed in the absence of catalyst (entry 1) as compared to the catalyzed reactions (entries 4, 9 and 13). These results further supported the claim that the synthesized catalysts are promoting chemical oxidations, particularly those performed under ball milling. Comparing results of entry 2-14 showed that increasing in the amount of hydrogen peroxide enhanced conversion. However, using higher amount of hydrogen peroxide increased over oxidation to diphenyl sulfone. The conversion of entry 10 (44%) was higher than other conditions. However, this condition was not selective to diphenyl sulfoxide. Optimum conditions, namely 0.04 mol% catalyst (0.005 g), 8 equiv. 30% (w/w) H_2O_2 in H_2O (0.407 mL) and 25 min reaction, provided 37% conversion with 70% selectivity to diphenyl sulfoxide. Longer reaction times (over 25 mins) or higher concentration hydrogen peroxide and catalyst contents originated a significant decrease in sulfoxide selectivity.

The reported results constitute the first literature report of the proved activity and stability of mechanochemically incorporated Al on mesoporous materials in a variety of oxidation reactions under various conditions (microwave irradiation, ball milling) using extremely low catalyst loadings (typically 0.04 mol %).

Table 5. Optimum amount of catalyst and hydrogen peroxide in the oxidation of diphenyl sulfide.

Entry	Catalyst loading (%mol)	H_2O_2 (equiv)	Conversion (%)	Selectivity (%)	
				Sulfoxide	Sulfone
1	-	8	<15	29	71
2	0.018	3	<15	65	35
3		5	16	54	46
4		8	23	37	63
5		10	37	26	74
6	0.042	1	<10	85	15
7		3	<15	74	26
8		5	23	68	32
9		8	37	70	30
10		10	44	54	46
11	0.084	3	<10	56	44
12		5	19	58	42
13		8	36	33	67
14		10	37	16	84

Reaction condition: 0.5 mmol of diphenyl sulfide, 25 stainless steel mL jar containing 8 balls (Ø 10 mm, 4 g), catalyst loading 0.02 to 0.08 mol% (0.002 to 0.01 g), 30% (w/w) H_2O_2 in H_2O content from 1 to 10 equiv. (0.05 to 0.50 mL), 350 rpm, 25 min, ball milling.

The recovery and reuse of MCM-41-AlMOF-M as catalyst for the oxidation of diphenyl sulfide was subsequently evaluated under optimum conditions. Upon reaction completion, the crude reaction mixture was recovered from the jar by using 0.5 mL of toluene. The chamber containing the catalyst was dried at 100 °C for 10 min and the catalyst was reused for the next run. As shown in Figure 4, MCM-41-AlMOF-M could be recovered and reused several times

(4 runs) without any appreciable loss of its catalytic activity. No Al leaching was also observed into solution as measured by ICP-MS (<0.5 ppm), further confirming the stability of the synthesized materials.

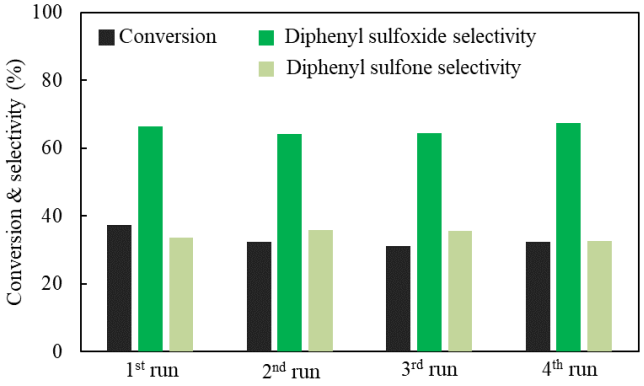

Figure 4. Recyclability of MCM-41-AlMOF-M in the oxidation of diphenyl sulfide with 30% (w/w) H_2O_2 in H_2O under mechanochemical solvent-free conditions. Reaction conditions: 0.5 mmol of diphenyl sulfide (0.08 mL), 25 stainless steel mL jar containing 8 balls (Ø 10 mm), 0.04 mol % catalyst (0.005 g), 8 equiv. 30% (w/w) H_2O_2 in H_2O (0.41 mL), 350 rpm, 25 min, ball milling.

CONCLUSIONS

The present work reports the unprecedented possibility to post-synthetically introduce metal species into the framework of mesoporous materials via mechanochemistry to render active catalysts for mild oxidation reactions. Even at very low loadings, typically 0.2-0.4 wt.% Al,

mechanochemically synthesized Al-containing mesoporous silica (SBA-15 and MCM-41) provided unprecedented catalytic activities in mild selective oxidations and short times of reaction, both under microwave irradiation, conventional heating and mechanochemistry. The present methodology will pave the way to future post-synthetically framework functionalized catalytically active additional materials even at low loadings that will be reported in due course.

ACKNOWLEDGMENTS

Rafael Luque gratefully acknowledges financial support from MINECO under project CTQ-201678289-P, co-financed with FEDER funds. The publication was prepared with support of RUDN University Program 5-100.

Supporting Information

Results for reuses in the microwave-assisted oxidation of benzyl alcohol to benzaldehyde and isoeugenol to vanillin

REFERENCES

[1] Linares, N.; Silvestre-Albero, A. M.; Serrano, E.; Silvestre-Albero, J.; García-Martínez, J. Mesoporous materials for clean energy technologies. *Chem. Soc. Rev.*, **2014**, *43*, 7681–7717. https://doi.org/10.1039/C3CS60435G.

[2] Opanasenko, M.; Stepnicka, P.; Cejka, J. Heterogeneous Pd catalysts suppoorted on silica matrices. *RSC Adv.*, **2014**, *4*, 65137–65162. https://doi.org/10.1039/C4RA11963K.

[3] Rahemi, N.; Haghighi, M.; Babaluo, A.; Fallah, M.; Estifaee, P. Synthesis and physicochemical characterizations of $Ni/Al_2O_3–ZrO_2$ nanocatalyst prepared via impregnation method and treated with non-thermal plasma for CO_2 reforming of CH4. *JIEC.,* **2013**, *19*, 1566-1576. https://doi.org/ 10.1016/j.jiec.2013.01.024.

[4] Putluru, S. S. R.; Schill, L.; Jensen, A. D.; Siret, B.; Tabaries, F.; Fehrmann, R. Mn/TiO_2 and $Mn–Fe/TiO_2$ catalysts synthesized by deposition precipitation—promising for selective catalytic reduction of NO with NH_3 at low temperatures. *Applied Catalysis B: Environ.,* **2015**, *165*, 628-635. https://doi.org/10.1016/j.apcatb.2014.10.060.

[5] Do, J. L.; Friščić, T. Mechanochemistry: a force of synthesis. *ACS Central Sci.,* **2016**, *3*, 13-19. https://doi.org/10.1021/acscentsci.6b00277.

[6] Xu, C.; De, S.; Balu, A. M.; Ojeda, M.; Luque, R. Mechanochemical synthesis of advanced nanomaterials for catalytic applications. *Chem. Commun.,* **2015**, *51*, 6698-6713. https://doi.org/10.1039/C4CC09876E.

[7] Muñoz-Batista, M. J.; Rodríguez-Padrón, D.; Puente-Santiago, A. R.; Luque, R. Mechanochemistry: toward sustainable design of advanced nanomaterials for electrochemical energy storage and catalytic applications. *ACS Sustainable Chem. Eng.*, **2018**, *6*, 9530–9544. https://doi.org/10.1021/acssuschemeng.8b01716.

[8] García-Espejo, G.; Rodríguez-Padrón, D.; Pérez-Morales, M.; Luque, R.; de Miguel, G.; Camacho, L. Mechanochemical synthesis of one-dimensional (1D) hybrid perovskites incorporating polycyclic aromatic spacers: highly fluorescent cation-based materials. *J. Mater. Chem. C.*, **2018**, *28*, 7677-7682. https://doi.org/10.1039/C8TC02169D.

[9] Franco, A.; De, S.; Balu, A. M.; Romero, A. A.; Luque, R. Selective oxidation of isoeugenol to vanillin over mechanochemically synthesized aluminosilicate supported transition metal catalysts. *Chem. Select*., **2017**, *29*, 9546-9551. https://doi.org/10.1002/slct.201701273.

[10] Al-Naji, M.; Balu, A. M.; Roibu, A.; Goepel, M.; Einicke, W.D.; Luque, R.; Gläser, R. Mechanochemical preparation of advanced catalytically active bifunctional Pd-containing nanomaterials for aqueous phase hydrogenation. *Catal. Sci. Technol.* **2015**, *5*, 2085-2091. https://doi.org/10.1039/C4CY01174K.

[11] Hazra, C. K.; Dherbassy, Q.; Wencel-Delord, J.; Colobert, F. Synthesis of axially chiral biaryls through sulfoxide-directed asymmetric mild C-H activation and dynamic kinetic resolution. *Angew. Chem. Int. Ed*. **2014**, 53, 13871- 13875.

[12] Fioroni, G.; Fringuelli, F.; Pizzo, F.; Vaccaro, L. Easy and environmentally friendly uncatalyzed synthesis of β-hydroxy arylsulfides by thiolysis of 1,2-epoxides in water. *Green Chem*. **2003**, 5, 436–440.

[13] Wilde, C.A.; Ryabenkova, Y.; Firth, I.M.; Pratt, L.; Railton, J.; Bravo-Sanchez, M.; Sano, N.; Cumpson, P.J.; Coates, P.D.; Liu, X.; Conte, M. Novel rhodium on carbon catalysts for the oxidation of benzyl alcohol to benzaldehyde: A study of the modification of metal/support interactions by acid pre-treatments. *Appl. Catal. A* **2019**, *570*, 2171-282.

[14] Amini, M.; Najafpour, M. M.; Salimi, S.; Ramezani, S.; Ashouri, F.; Mahmoudi, G. Iron oxide on carbon-based supports as efficient catalysts for organic compounds oxidation. *Appl. Organomet. Chem*. **2017**, 31, 3892-3902. b) Balu, A.M.; Pineda, A.; Yoshida, K.; Campelo, J.M.; Gai, P.L.; Luque, R.; Romero, AA. Fe/Al synergy in Fe_2O_3 nanoparticles supported on porous aluminosilicate materials: excelling activities in oxidation reactions. *Chem. Commun.,* **2010**, 41, 7825-7827.

[15] Rajabi, F.; Naresian, S.; Primo, A.; Luque, R. Aqueous selective oxidation of sulfides to sulfoxides at room temperature using supported iron oxide nanoparticles on SBA-15. *Adv. Synth. Catal.,* 2011, 353, 2060-2066.

[16] Karimi, B.; Ghoreishi-Nezhad, M.; Clark, J.H. Selective oxidation of sulfides to sulfoxides using 30% hydrogen peroxide catalyzed with a recoverable silica-based tungstate interphase catalyst. *Org. Lett.* **2005**, *7*, 625-628.

[17] Gamez, P.; Arends, I.W.C.E.; Shledon, R.A.; Reedijk, J. Room Temperature Aerobic Copper–Catalysed Selective Oxidation of Primary Alcohols to Aldehydes. *Adv. Synth. Catal.* **2004**, *346*, 805-811. https://doi.org/10.1002/adsc.200404063

[18] Ojeda, M.; Grau-Atienza, A.; Campos, R.; Romero, A. A.; Serrano, E.; Marinas, J.M.; Martinez, J. G.; Luque, R. Hierarchical zeolites and their catalytic performance in selective oxidative processes. *ChemSusChem*, **2015**, *8*, 1328-1333.

[19] Jia, A.; Lou, L-L.; Zhang, C.; Zhang, Y.; Liu, S. Selective oxidation of benzyl alcohol to benzaldehyde with hydrogen peroxide over alkali-treated ZSM-5 zeolite catalyst. *J. Mol. Catal. A: Chem.* **2009**, *306*, 123-129.

[20] Huo, Q.; Margolese, D. I.; Stucky, G. D. Surfactant control of phases in the synthesis of mesoporous silica-based materials. *Chem. Mater.,* **1996**, *8*, 1147. https://doi.org/10.1021/cm960137h.

[21] Steel, A.; Carr, S. W.; Anderson, M. W. J. Chem. Soc. ^{14}N NMR study of surfactant mesophases in the synthesis of mesoporous silicates. *Chem. Commun*., **1994**, *13*, 1571–1572. https://doi.org/10.1039/C39940001571.

[22] Pineda, A.; Balu, A. M.; Campelo, J. M.; Romero, A. A.; Carmona, D.; Balas, F.; Santamaria, J.; Luque, R. A dry milling approach for the synthesis of highly active nanoparticles supported on porous materials. *ChemSusChem.,* **2011**, *4*, 1561-1565. https://doi.org/10.1002/cssc.201100265.

[23] Yepez, A.; Prinsen, P.; Pineda, A.; Balu, A. M.; Garcia, A.; Lam, F.L.Y.; Luque, R. A comprehensive study on the continuous flow synthesis of supported iron oxide nanoparticles on porous silicates and their catalytic applications. *React. Chem. Eng.,* **2018**, *3*, 757-768. https://doi.org/10.1039/C8RE00063H.

[24] Campelo, J. M.; Luna, D.; Luque, R.; Marinas, J. M.; Romero, A. A.; Calvino, J. J.; Rodriguez-Luque, M. P. Synthesis of acidic Al-MCM-48: influence of the Si/Al ratio, degree of the surfactant hydroxyl exchange, and post-treatment in NH_4F solution. *J. Catal.,* **2005**, *230*, 327-338. https://doi.org/10.1016/j.jcat.2004.12.004.

[25] Zhao, D.; Feng, J.; Huo, Q.; Melosh, N.; Fredrickson, G. H.; Chmelka, B. F.; Stucky, G. D. Triblock copolymer syntheses of mesoporous silica with periodic 50 to 300 angstrom pores. *Science*, **1998**, *279*, 548-542. https://doi.org/10.1126/science.279.5350.548.

[26] Balu, A. M.; Pineda, A.; Yoshida, K.; Campelo, J. M.; Gai, P. L.; Luque, R.; Romero, A. A. Fe/Al synergy in Fe_2O_3 nanoparticles supported on porous alumiosilicate materials: execelling activities in oxidation reactions. *Chem. Commun.,* **2010**, 46, 7825-7827. https://doi.org/10.1002/cssc.201500124.

[27] Muñoz-Batista, M. J.; Rodríguez-Padrón, D.; Puente-Santiago, A. R.; Luque, R. Mechanochemistry: toward sustainable design of advanced nanomaterials for electrochemical energy storage and catalytic applications. *ACS Sustainable Chem. Eng.*, **2018**, 6, 9530-9544. https://doi.org/10.1021/acssuschemeng.8b01716.

[28] Marquez-Medina, M. D.; Prinsen, P.; Li, H.; Shih, K.; Romero, A. A.; Luque**,** R. Continuous-Flow Synthesis of Supported Magnetic Iron Oxide Nanoparticles for Efficient Isoeugenol Conversion into Vanillin. *ChemSusChem.* **2018**, *11*, 389-396. https://doi.org/10.1002/cssc.201701884.

[29] Franco, A.; De, S.; Balu, A. M.; Garcia, A.; Luque, R. Selective oxidation of isoeugenol to vanillin over mechanochemically synthesized aluminosilicate supported transition metal catalysts. *Beilstein J. Org. Chem.,* **2017**, *13*, 1439-1443. https://doi.org/10.1002/slct.201701273.

For Table of Contents Use Only

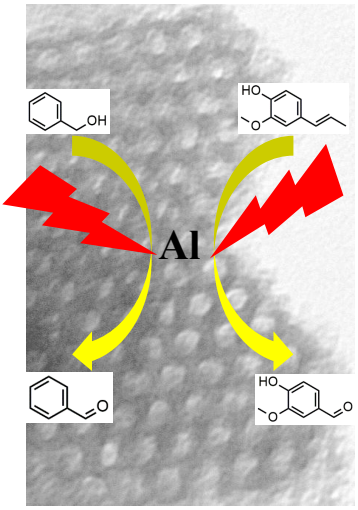

Mechanochemical post-synthetic incorporation of Al species within mesoporous silica materials rendered unprecedented catalytically active materials for more sustainable transition metal-catalysed oxidation reactions